University of Technology, Sydney

Centre for Intelligent Mechatronic Systems

Faculty of Engineering and Information Technology

Investigation into Dynamics of a Rolling Body-Bearing-Support System in a Cold Rolling Stand

by

Yoo Shin, Kim

A thesis submitted for fulfilment of requirements for the degree of

Doctor of Philosophy

August 2012

Certificate of Authorship/Originality

I certify that the work in this thesis has not previously been submitted for a degree nor has it been submitted as part of requirements for a degree except as fully acknowledged within the text.

I also certify that the thesis has been written by me. Any help that I have received in my research work and the preparation of the thesis itself has been acknowledged. In addition, I certify that all information sources and literature used are indicated in the thesis.

Production Note:
Signature removed prior to publication.

Yoo Shin, Kim

August 2012

Acknowledgments

This PhD research would not have been completed without the guidance, assistance and support of a number of individuals, whose contributions I would like to gratefully acknowledge here. I would especially like to thank Professor Nong Zhang, Dr. Daniel Yuen, Dr. Jin Chen Ji and Dr. William Hu, who have supervised me during this research over the last four years.

Professor Nong Zhang, who has been my principal supervisor for this research, has been instrumental in guiding me throughout this research. His constant supervision and encouragement have helped me fulfil the objectives of this research and to complete this thesis.

I would like to convey my thanks to Dr. Daniel Yuen of BlueScope Steel Research, BlueScope Steel Limited, for being like a mentor throughout this research. His guidance and advice have been very important in motivating me throughout the research. I would also like to thank him for always taking time out of his busy schedule on a short notice whether it was for discussing intellectual challenge or for sharing ideas.

I would like to extend my deepest appreciation to Dr. Jin Chen Ji for his pioneering work in nonlinear control. When I am in a cold case, it was Dr. Jin Chen Ji who is willingly to share innovative ideas and encourage my inspiration. His sincere contribution and invigoration will never be forgettable.

Dr. William Hu has been very helpful throughout this research especially with his expert advice on the journal bearing theory. His suggestions and guidance has been very helpful in properly controlling the mill vibration.

On the social side, sincere appreciation is directed toward my fellow colleagues, Dr. Paul David Walker, Dr. Salisa Abdulrahman and Mr. Robert Heal and many other students who work in our group, for their enthusiastic help, inspiration and support in various aspects of this study. I will always treasure the times in the early days, sitting

next to Paul and Salisa in the office. More importantly, Paul and Salisa provided great friendship at UTS offering valuable discussions and ideas throughout the research. Robert also inspired me throughout this research delivering many conceptions in a cold rolling mill. Furthermore, special thanks to Dr. Paul David Walker for reviewing and proofreading my work and encouraging me to establish the concrete knowledge. And if time allows us, I am enthusiastically looking forward to the weekend adventures with you all.

I would like to dedicate this work to my family, for their constant love, support and encouragement made my higher education possible. My mother Ms. Soon Ja Yoo, in particular, deserves special thanks for all her help over the decades. I also would like to dedicate this work to my sister Miss. Jee Young Kim for her encouragement and support. Finally, my wife Ms. Su Hee Yang, who stood by me all the time, I really appreciate her patience and understanding with sincere love.

The last four years have been a wonderful experience and will always be memorable. I learned a lot of new things but need to explore new areas.

I wish to gratefully acknowledge the financial support of this research by the Australian Research Council (ARC), University of Technology, Sydney and BlueScope Steel Limited through a Linkage Project (LP0776980).

Production Note:
Signature removed prior to publication.

Yoo Shin, Kim

Sydney, August 2012

Table of Contents

List of Figures

List of Tables

Nomenclature

ABBREVIATIONS USED IN THIS THESIS

AGC	—	Automatic Gauge Control
Assay's	—	Assembly
CRM	—	Cold Rolling Mill
BF	—	Bland and Ford
MBF	—	Modified Bland and Ford
BH	—	Bearing Housing Chock
BR	—	Backup Roll
WR	—	Work Roll
ODE	—	Ordinary Differential Equation
DDE	—	Delay Differential Equation
DOF	—	Degree Of Freedom
STC	—	Stability Threshold Curve
COP	—	Critical Operating Point
SSC	—	Steady State Condition
LQ	—	Linear Quadrant
ESO	—	Extended State Observer

CHAPTER 2 NOTATION

m_{BH}	—	Lumped mass of the bearing housing chock
m_{BR}	—	Lumped mass of the backup roll
m_{WR}	—	Lumped mass of the work roll
C_{yy}^{WR}	—	Equivalent damping component in the vertical direction
K_{yy}^{WR}	—	Equivalent stiffness component in the vertical direction
$F_{dyn,y}^{WR}$	—	Dynamic rolling force component in the vertical direction
y_{WR}, $\dot{y}_{WR}$, $\ddot{y}_{WR}$	—	Displacement, velocity and acceleration of the work roll, respectively
h_c	—	Roll gap spacing at the center plane of the roll gap
K_2, K_3	—	Elastic constant depending on the elastic contact between the backup roll and work roll, respectively
K_1, K_4	—	Elastic constant depending on the elastic deformation of the bearing housing chock and backup roll, respectively

K_0, K_5	—	Elastic constant depending on the elastic contact between the mill housing and mill foundation, respectively
K_6	—	Spring constant depending on the contact between the work roll and strip
K_{var}	—	Elastic deformation resistance in the roll gap
$C_0 - C_5$	—	Viscous damping coefficients
z_1, z_2	—	Displacements of the top and bottom surfaces of the strip, , respectively
$t_{e,var,i}$, $t_{x,var,i}$	—	Variation of tension at entry and exit side, respectively
$v_{e,var,i}$, $v_{x,var,i}$	—	Variation of rolling speed at entry and exit side, respectively
E	—	Young's modulus
D_i	—	Inter-stand distance at (i)th stand
s	—	Laplacian operator
Δ_i	—	Time delay at (i)th stand
f_y	—	Rolling force per unit width
I	—	Identity matrix
A	—	System matrix
x_{BH}, x_{BR}, x_{WR} y_{BH}, y_{BR}, y_{WR}	—	Coordinates of a rolling stand in cold rolling

Subscripts

BH	—	Bearing Housing Chock
BR	—	Backup Roll
WR	—	Work Roll
dyn	—	Dynamic component
var	—	Variable component
i	—	(i)th stand
e	—	Entry side
x	—	Exit side

CHAPTER 3 NOTATION

§ Any previously used terminology is not listed here.

v	—	Strip velocity at any arbitrary point in the roll gap
v_e, v_x	—	Strip velocity at entry and exit sides, respectively
v_R *or* v_n	—	Work roll velocity (Peripheral rolling speed)
$\overline{v}_R$	—	Average rolling speed
h	—	Strip thickness at any arbitrary point in the roll gap
h_e, h_x	—	Strip thickness at entry and exit sides, respectively
h_n	—	Strip thickness at the neutral point

h_c	—	Roll gap spacing
Δh	—	Reduction of the strip thickness
W	—	Strip width
R_{WR}	—	Undeformed roll radius
R_d	—	Deformed roll radius
L	—	Roll bite length
ϕ	—	Roll contact angle at any arbitrary point in the roll gap
v	—	Poisson's ratio
F_{sp}	—	Specific rolling force per unit width
c	—	Hitchcock constant
τ_s	—	Friction stress
μ	—	Coefficient of friction
p	—	Normal pressure
m	—	Friction factor
k	—	Material shear strength
α	—	Ratio of the real contact area to the apparent contact area
x	—	Location of the arbitrary point in the horizontal plane
x_n	—	Location of the neutral point in the horizontal plane
ω	—	Operating frequency in unit of *rad/s*
Q	—	Torque characteristics of the driving motor
G	—	Variation of the roll torque
$v_{R,\text{var}}$ or Δv_R	—	Variation of the rolling speed
S_f	—	Forward slip
S_b	—	Backward slip
l_0	—	Parallel line distance in the roll surface
l_1	—	Distance between two imprints by slip
σ_0	—	Base yield strength
σ_Y	—	Yield strength or flow stress of the work-piece
ε	—	Strain in the roll gap
$\dot{\varepsilon}$	—	Strain-rate
$\dot{\varepsilon}_{ref}$	—	Strain-rate reference
$\dot{\varepsilon}_{gap}$	—	Strain-rate in the roll gap
B	—	Material-dependent coefficients
T	—	Temperature
N	—	Peripheral rolling speed of the work roll in unit of *rev/s*
θ	—	Angle subtended by the actual work roll axis
$\dot{\theta}$	—	Angular velocity
X	—	Amplitude of the work roll
t	—	Time

ΔD_i	—	Variable amount of elongation at (i)th stand
t_e , t_x	—	Tension stress at entry and exit sides, respectively
t_{avg}	—	Average tension stress
A	—	Cross-sectional area of the roll gap

Superscripts

γ_1	—	Strain exponent (dimensionless)
γ_2	—	Strain-rate sensitivity exponent (dimensionless)

Subscripts

ref	—	Reference
gap	—	Roll Gap
avg	—	Average
Y	—	Yield
b	—	Backward
f	—	Forward

CHAPTER 4 NOTATION

§ Any previously used terminology is not listed here.

f	—	Horizontal rolling force
s	—	Normal pressure
s^- , s^+	—	Normal pressure at entry and exit sides, respectively
c	—	Constant determined by Bland and Ford model
H , H_e , H_n	—	Constant at any arbitrary, entry and neutral planes, respectively
p , q	—	Horizontal and vertical pressures, respectively
σ	—	Yield stress in uniaxial compression
σ_e , σ_x	—	Yield (Flow) stress at entry and exit sides, respectively
ϕ_n	—	Neutral point/angle
$\dot{\varepsilon}^*$	—	Dimensionless strain-rate
F_R	—	Resultant rolling force
F_H , F_V	—	Horizontal and vertical rolling forces, respectively
R_{BR}	—	Backup roll radius
r	—	Reduction rate
μ_{s0}	—	Friction coefficient at the steady-state rolling condition
μ_{sl}	—	Sliding friction coefficient
$\dot{h}_c$	—	Reduction rate with respect to time or rate of change in strip thickness

$F_{dyn,R}^{WR}$	—	Resultant component of dynamic rolling force
$F_{dyn,x}^{WR}$	—	Horizontal component of the dynamic rolling force
$F_{dyn,y}^{WR}$	—	Vertical component of the dynamic rolling force
K_{ij}^{var}	—	Stiffness coefficient components in the dynamic roll gap
C_{ij}^{var}	—	Damping coefficient components in the dynamic roll gap
α_s	—	Friction gradient (s/m)
v_{WR}	—	Work roll velocity
v_S	—	Strip velocity at the exit side
$C_{\text{var}\,0}$	—	Variation of rolling force to the change in friction coefficient
Q	—	Rolling force variation due to the change in exit strip thickness based on the strip plastic deformation
ΔS_0	—	Variation of the dynamic roll displacement
ΔM_m	—	Elastic mill modulus
Δv_H	—	Variation of the horizontal rolling speed
Δh_c	—	Variation of reduction rate (roll gap spacing)
$\Delta \dot{h}_c$	—	Variation of reduction rate with respect to time
$\dot{R}$	—	Time derivative of roll radius
$\dot{x}_n$	—	Time derivative of neutral position
$\dot{\phi}_n$	—	Time derivative of neutral point
$K_{\text{var}\,1}$	—	Stiffness component of the dynamic rolling force due to the variation of the vertical displacements
$C_{\text{var}\,1}$	—	Damping component of the dynamic rolling force due to the variation of the horizontal velocity
$C_{\text{var}\,2}$	—	Damping component of the dynamic rolling force due to the variation of the dynamic roll gap
$K_{ij}^{\text{var}\,1}$	—	Stiffness components in the dynamic roll gap due to the variation of the vertical displacements
$C_{ij}^{\text{var}\,1}$	—	Damping components in the dynamic roll gap due to the relative motion between the work roll and strip
$C_{ij}^{\text{var}\,2}$	—	Damping components in the dynamic roll gap due to the variation of the horizontal velocity
$C_{ij}^{\text{var}\,3}$	—	Damping components in the dynamic roll gap due to the variation of the reduction rate (with respect to time)
β	—	Tilted angle caused by offset
μ_c	—	Friction coefficient in metal-to-metal (between BR and WR)
F_{fc}	—	Friction force between the backup roll and work roll
F_{fw}	—	Friction force between the work roll and strip

Subscripts

ij	—	x- or y-directional components, respectively
$R1, R2, R3, R4$	—	First to fourth variable components in the dynamic roll gap

CHAPTER 5 NOTATION

§ Any previously used terminology is not listed here.

F_{HCH} , F_{HCV}	—	Reaction forces from the mill frame and Screw-down forces on top, respectively
F'_{JBH} , F'_{JBV} , F'_{RBH} , F'_{RBV}	—	Bearing force components resulted from support bearings
F_H , F_V	—	Horizontal and vertical rolling forces in the roll gap, respectively
F'_H , F'_V	—	Surface contact force components between BR and WR
F_R , F'_R	—	Resultant rolling force, respectively
F_{HCf}	—	Frictional force in the sliding surface of the housing chock
k_{ij}^n	—	Stiffness coefficients of the system resulted from the bearing housing, backup roll and work roll
c_{ij}^n	—	Damping coefficient of the system resulted from the bearing housing, backup roll and work roll
$[K_{BR}]$	—	Stiffness matrix for the backup roll
$[C_{BR}]$	—	Damping matrix for the backup roll
$[K_{WR}]$	—	Stiffness matrix for the work roll
F_{tot}	—	Frictional and dynamic rolling force components
R_{bb}	—	Journal bearing radius
L_{bb}	—	Journal bearing length
η	—	Dynamic viscosity in the journal bearing
C_{bb}	—	Journal bearing clearance
ε_{bb}	—	Eccentricity
ω_{bb}	—	Rotation speed (RPM)
R_{wb}	—	Tapered roller bearing radius
L_{wb}	—	Tapered roller bearing length
Z	—	Number of rolling element
C_{wb}	—	Tapered roller bearing clearance
n	—	Roller bearing exponent
K_n	—	Load deflection constant
α_0	—	Rolling element angle
ω_{wb}	—	Rotational speed (RPM)
δ_{im}	—	Mean displacement
δ_{Rm}	—	Resultant elastic deformation
ψ_j	—	Angular position of (j)th rolling element
Δ_{ij}	—	Relative displacement along the axis of loading of two points
f_{ij}	—	Compressive load per unit length
D_{BR}	—	Backup roll diameter
D_{WR}	—	Work roll diameter

F_{ij}	—	Rolling force component
k_{ij}^{C}	—	Stiffness component between two rolls
φ	—	Rotational angle
U_1, U_2, U_3	—	Transformation matrix

Superscripts

n	—	Refer to BH, BR and WR
ij	—	x- or y-directional components, respectively

Subscripts

HCH, HCV	—	Refer to the bearing housing chock in the horizontal and vertical directions, respectively
JBH, JBV	—	Refer to the journal bearing in the horizontal and vertical directions, respectively
RBH, RBV	—	Refer to the tapered roller bearing in the horizontal and vertical directions, respectively
H, V	—	Refer to the horizontal and vertical directions, respectively
R	—	Refer to the resultant component
HCf	—	Frictional component of the bearing housing chock
tot	—	Total
bb	—	Backup roll bearing (Journal bearing)
wb	—	Work roll bearing (Tapered roller bearing)

CHAPTER 6 NOTATION

§ Any previously used terminology is not listed here.

C_{Tlusty}^{1}	—	Damping component of a variable force component depending on the rolling speed by Tlusty
C_{Kimura}^{1}	—	Damping component of a variable force component depending on the rolling speed by Kimura
k_f	—	Deformation resistance of the material
C_{Tlusty}^{2}	—	Damping component of a variable force component due to negative damping effect by Tlusty
C_{Gap}	—	Positive damping component in the bearing support (resulted from the mill structure) and the roll gap
C_{var}	—	Negative damping component in the dynamic roll gap
K_{Tlusty}	—	Stiffness component of a variable force component presented by Tlusty
K_{Kimura}	—	Stiffness component of a variable force component presented by Kimura
K_{Gap}	—	Positive stiffness component in the bearing support (resulted from the mill structure) and the roll gap

K_{var}	—	Stiffness coefficient in the deformed strip
$[M]$	—	Mass matrix
$[K]$	—	Stiffness matrix
$[C]$	—	Damping matrix
0_6	—	6×6 zero matrix
I_{D6}	—	6×6 identity matrix
ζ	—	Damping ratio
f_i	—	Damped natural frequency (Hz)
X	—	Displacement vector of a rolling stand
$\dot{X}$	—	Velocity vector of a rolling stand
cSt	—	Kinematic viscosity ($1cSt = 1mm^2/s$)
η	—	Dynamic viscosity
η_0	—	Viscosity at ambient pressure and temperature
ρ	—	Fluid density
υ	—	Kinematic viscosity
$P_{\max}$	—	Oil-film pressure at a maximum
α	—	Pressure coefficient of viscosity

Subscripts

i	—	Refer to the first to sixth mode
JBH , JBV	—	Refer to the journal bearing in the horizontal and vertical direction

CHAPTER 8 NOTATION

§ Any previously used terminology is not listed here.

ΔL	—	Variation of length of arc contact in the roll gap)
y_i	—	Dynamic oscillation of the work roll
$t_{e,\text{var}}\big\|_{Tlusty}$	—	Tension variation at the entry side by Tlusty
$t_{e,\text{var}}\big\|_{Yun}$	—	Tension variation at the entry side by Yun
$t_{e,\text{var}}\big\|_{Dyn}$	—	Tension variation at the entry side by the current model
$\phi_{n,\text{var}}$	—	Variation of the neutral point

Subscripts

i	—	Refer to the work roll

Abstract

The objective of this thesis is to gain a good understanding of the chatter phenomenon incorporating the dynamic rolling model and mechanical system model of a rolling stand in cold rolling. Although such systems have received great attention in the academic literature, research to-date has not covered dynamic characteristics of the multiple rolling body-bearing-support system due to its complexity and nonlinearities.

In this thesis, a steady-state rolling process model that includes the work hardening and work roll flattening effect was developed based on the homogeneous deformation theory with the relaxation of conventional assumptions. A dynamic model of the rolling process was then formulated by taking into account multiple nonlinearities such as the change in friction coefficient, rolling speed, roll gap (strip thickness) reduction and reduction rate with respect to time. In linearisation of rolling force variations as stiffness and damping coefficients, negative gradient of friction coefficient was introduced to identify the negative damping effect in the dynamic roll gap. Also, dynamic rolling force components were included in the analysis by the linearisation of variations of the strip thickness and rolling speed at exit side and of variations of reduction rate with respect to time.

In addition, a mechanical system model was derived through the inclusion of the support bearings and surface contact between rolls. For the backup roll, a journal bearing model was introduced to examine oil-film thickness change and a tapered roller bearing model was adopted to model the work roll motion. In order to explain dynamics in the surface contact between the backup roll and work roll, Hertzian contact theory is incorporated into the mode-coupling theory. Finally, by coupling the dynamic rolling process model with a mechanical system model including support bearings and surface contact, a 6DOF mill vibration model for the analysis of vibrations symmetric to the roll gap was developed.

In determination of stability in the derived cold rolling stand chatter model, stability analyses were performed through the change in the friction coefficient and rolling speed at a given friction gradient. Many different aspects of stability threshold curves (STC)

have been obtained from the eigenvalues analysis of the system characteristic equation. Influences of 10 rolling parameters such as the friction gradient, strip width, roll radius, exit thickness, strain and strain-rate exponent, roll offset, bearing viscosity, length and clearance on mill stability were thoroughly investigated. With the linearised stiffness and damping coefficients at the given operating conditions, transient studies were executed to prove the validity of the presented model.

Finally, in order to understand the effects of tension variations from the adjacent mill stand, three different tension models were applied into the dynamic roll gap. By so doing, the mill stability has been determined through the inclusion of transient characteristics in the dynamic roll gap. In light of observation from the practical mill configuration, simulation results suggest that chatter arises as the rolling speed increases and friction coefficient decreases under the steady-state rolling conditions. When tension variation applied, instability occurs as the inter-stand distance decreases and a strip feed-in speed variation frequency matches to one of the system natural frequencies.

CHAPTER 1. INTRODUCTION

This thesis presents the detailed investigation into the dynamic response of a rolling stand in cold rolling to a variety of rolling conditions, and the study of the application of the coupled mill vibration model. To date the vast majority of mill vibration research has focused on the dynamic roll gap and simplified mill structure, with under- or over-estimated transient responses predicted by these investigations. Through these investigations nonlinearity inherent to a rolling mill stand is ignored and its respective influence on vibration response is neglected, with an over-simplified mill vibration model studying rolling force variations in the roll gap only.

With improved knowledge of the roll gap behaviour, the identification and investigation of many nonlinear characteristics are possible and provide more accurate prediction of the vibration behaviour of the tandem cold rolling mill. Research conducted herein fills the gap between industry and academic knowledge of the performance of a rolling stand through the application of multiple nonlinearities to the study of mill vibration response under transient conditions using the roll gap variations and simulation scheme for a rolling stand in cold rolling mill.

The impact of nonlinearities in cold rolling mill under various transient conditions – including the hydrodynamics of journal bearing and tapered roller bearing, surface contact mechanism between the backup roll and work roll, dynamic characteristics of the roll gap model – is the main feature of this study. Through the examination of roll gap response the most significant parameters to mill vibration during the rolling process will be identified.

1.1. PROJECT STATEMENT

- The development of mathematical models of identifying the nature of chatter for the prediction of its transient characteristics under the wide range of operating conditions, including the linearisation and analysis of bearings, contact surface and roll gap performance.

Over 100 million tons of cold rolled steels are produced annually worldwide on multi-stand rolling mills. These mills consist of a sequence of roll stands through which steel sheet is rolled, successively reducing its thickness to the desired gauge and imparting the desired surface finish. Modern application demands thinner gauge, greater gauge precision, higher production rates and higher strip flatness and surface quality. The prevention of rolling chatter becomes more and more crucial for rolling mills to produce thinner and thinner product efficiently.

Chatter results from the interaction between dynamics of the mill structure components and the dynamics of the rolling operation. Generally speaking, there are three types of chatter occurring on rolling mills referred to, in a comprehensive review by Roberts (1978), as "torsional", "third octave" and "fifth octave" chatter. Each type is characterised by the frequency associated with the dynamic mechanism involved. Among the three types of chatter, third octave mode chatter, in a frequency range of 120-300 Hz, occurs most suddenly with growing oscillations characteristic of a process instability. The third octave mode chatter is likely related to rolling force since the dynamic forces generated during the rolling process deform the mill structure, leading to variations in the roll gap, rolling speed, rolling forces and the operating points of supporting journal bearings. Consequently, under certain circumstances, particularly when rolling ultra thin gauge where the rolling force is very high, these variations will be exacerbated to cause mill system vibration. With the increasing rolling speed, the build-up of vibration at the natural frequency of the mill rapidly reaches destructive proportions. This self-excited chatter causes unacceptable gauge variations in the rolled strip and surface finish, and is particularly damaging on products which demand high surface quality and tight tolerances. As the mill speed increases, the vibrations and thickness variation become more severe and tension fluctuations between stands often result in strip rupture. Furthermore, associated sensitivity of the mill system to forced vibration necessitates costly maintenance programs to maintain desired equipment conditions, achieve high production level and required product quality. Therefore, the rolling mill chatter is a serious problem limiting the throughput of metal rolling operations, particularly thin strip rolling operation.

The prevention of rolling mill chatter requires an in-depth understanding of the mechanisms that lead to the dynamic instability of the rolling process, particularly the

mechanisms of coupled chatter in the vertical and horizontal directions of single-stand (a rolling stand), and between multi-stand cold rolling mills. A thorough investigation into the coupled chatter of single-stand mills needs to involve the modelling of major components and rolling processes that include mainly (a) modelling of the dynamic roll gap, lubrication and tension variations; (b) modelling of a rolling stand with support bearings and flexible supporting structure; and (c) the integration of the dynamic interactions between these sub-systems.

1.2. PROJECT OBJECTIVES

This project aims to develop comprehensive mathematical models for stability and transient analysis of self-excited chatter of a rolling stand in cold rolling. Numerical schemes will be developed for investigating thoroughly the roll gap model under a steady-state operating condition. The key aspects of this research include:

1. Modelling the rolling process for predicting dynamic forces applied to work rolls by strips taking into account variations in rolling friction, rolling speed, reduction, reduction rate and tension;
2. Modelling the highly nonlinear journal bearings, including the determination of the dynamic characteristics of the bearing housing support provided by the bearing housing chock;
3. Developing integrated models of a rolling stand in cold rolling and solution schemes for determining the stability regions of the systems under a wide range of operating conditions;
4. Investigation into the effects of key system parameters on the chatter transients with respect to the system dynamic states and operating condition variations;
5. Validating the developed mathematical models and numerical simulations from practical observations, both qualitatively and quantitatively, on BlueScope Steel's five-stand cold mills.

1.3. PROJECT SCOPE

The scope of this project is limited to the following:

1. Physical modelling of the major components of a rolling stand in cold rolling using conventional theories of the roll gap mechanism;
2. Free and forced vibration analysis of a coupled mill vibration model.
3. Time domain analysis of the rolling stand in relation to the symmetric roll gap and transient response;

Aspects of research beyond the scope of this research are:

1. The impacts of temperature in the roll gap and bearing supports during the rolling process;
2. Accurate friction model predicting and compensating dynamic characteristics of the roll gap;
3. Investigation of roll gap control mechanism;
4. Extensive experimental validation of simulation results.

1.4. SIGNIFICANCE AND INNOVATION

1.4.1. Significance

This project will significantly advance the knowledge on the dynamics of cold rolling mills and provide a theoretical base for improving the quality and productivity of flat strip rolling processes. It will achieve a thorough understanding of the chatter mechanism and its transient characteristics in a rolling stand in cold rolling mill under a wide range of operating conditions. The outcomes will enable engineers to control the cold rolling process with improved reliability, productivity, quality and capability.

The flat strip rolling process is widely used in the steel manufacturing industry. Technological advancement in this area will bring enormous economic gains in terms of improved productivity and reduced cost in equipment maintenance. The outcomes will assist the industry in improving greatly the existing technologies in cold rolling process

control and maintenance, and thus the productivity. The acquired knowledge and technologies are also readily applicable to many complex systems of heavy duty mechanical equipment, often seen in mining and transportation.

1.4.2. Innovation

The proposed integral model of the rolling stand in cold rolling mill is conceptually innovative because it overcomes the simplifications made in existing models for chatter studies. These simplifications include: (i) chatter in the direction perpendicular to strip only; (ii) linearised and un-coupled journal bearing stiffness and damping; (iii) linear stiffness and damping of the contact between backup and work rolls; and (iv) rigid support of journal bearings from stand chuck. The new model integrates the major sub-systems together through the nonlinear couplings between vibrations in the vertical and horizontal directions caused by journal bearings and that between inter-stands due to strip tension variation. The model makes it possible to investigate thoroughly the chatter transients caused by variations in operating conditions, strip specifications and equipment conditions.

The project is methodologically innovative because the proposed approaches include: modelling the highly nonlinear hydrodynamics of journal bearings using the Reynolds equation of lubrication; inclusion of the bearing support dynamic characteristics in terms of equivalent stiffness and damping coefficients; coupling the motions of top and bottom work rolls through the inclusion of the applied transient torque, forces in vertical and horizontal directions resulting from the rolling process; and a procedure for predicting the chatter stability of a rolling stand in cold rolling under a wide range of operating conditions. Another innovative aspect is to develop new methodologies and numerical solution schemes for formulation of the integrated system model, and the transient response analysis of the mills with multiple nonlinearities and time-dependent system configurations.

1.5. PRESENTATION OF THIS THESIS

The surface contact mechanism and hydrodynamic bearing characteristics resulted from the roll gap model are necessarily complex mechanical systems, detailed modelling and analysis in this thesis require the application of fluid and friction theories, and rigid and flexible multi-body mechanics to develop the coupled mill vibration dynamics. Specific modelling and analysis methods are therefore introduced in Chapters in which they are first applied, rather than as a methodology chapter so as to assist the reader in their understanding of the procedure applied, and provide clarity.

Figure 1-1 shows the main topics of this thesis and how each independent topic interacts with other aspects of research. It should be used to understand why this thesis is broken down into the chosen format. The main topics of each chapter are introduced in the following sections.

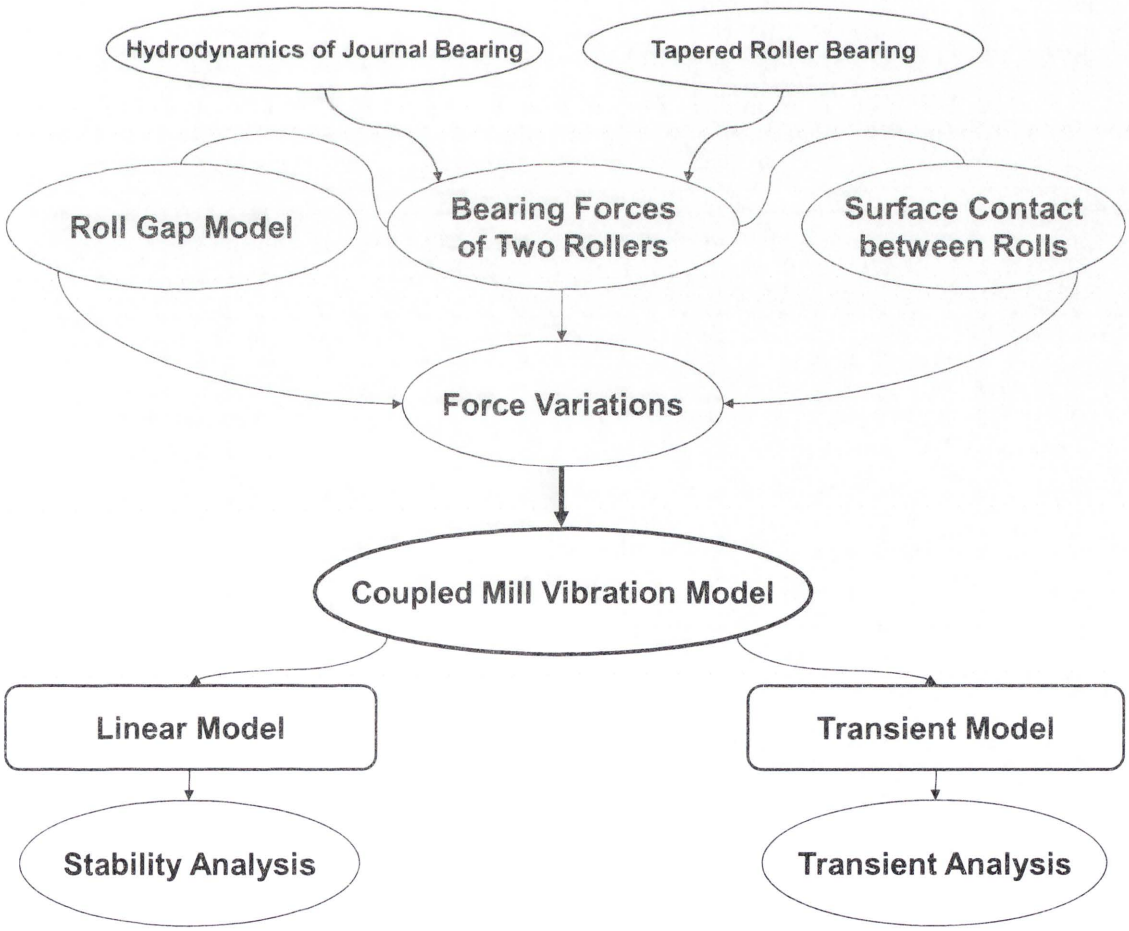

Figure 1-1: Overview for chapter descriptions in this thesis

Chapter 2

This chapter provides the framework for the research of this thesis. Initially the required background information on relevant aspects of roll gap model and mill vibration is presented to introduce topics for research. This is followed by a detailed literature search into all relevant aspects of chatter and its effect, identifying the state-of-the-art in rolling mill dynamics and major components. To complement this work brief exploration of literature is performed in each relevant chapter to identify important aspects of relevant research, as necessary.

Chapter 3

Effects of rolling parameters on cold rolling mill are presented in this chapter using conventional rolling theories and its limitation is described in order to develop the new dynamic model. Moreover, many different aspects of stress-strain curve are examined including the full-range of stress-strain curve as well as strain and strain-rate exponent. Tension variation models are introduced for the estimation of the rolling force and investigation of the influence of tension variation at entry side.

Chapter 4

Mathematical and analytical models of the roll gap dynamics for a rolling stand in cold rolling are developed in this chapter using conventional theories of the roll gap and deformation resistance of materials. These models are applied to Matlab environments to investigate the response to basic inputs for the characterisation of subsystem dynamics and force variations under the steady-state conditions. Furthermore, due to the offset between the backup roll and work roll, friction force components are defined by the assumption of metal-to-metal contact between two rolls and lubricated surface in the work roll.

Chapter 5

Chapter 5 is devoted to the development of a coupled mill vibration model with the general assumption symmetric in relation to the roll gap. This chapter specifically considers the influence of the dynamic roll gap model without the use of a tension variation model for determining stability through eigenvalue analysis. Simulations are then carried out under the steady-state operating conditions by identifying the dynamic

characteristics of support bearings and surface contact. Finally, rolling force in multi-stand tandem cold rolling mill is calculated under the given deformation profile.

Chapter 6

Stability analysis has been performed in the chapter, especially for the determination of stable and unstable region during the rolling process. Specifically, owing to relative motion between the work roll and strip, stability threshold curves (STC) have been determined through the change in the friction gradient in the dynamic roll gap. Many different aspects of stability threshold curve (STC) have been calculated from the small change in key rolling parameters which are significantly affecting mill stability.

Chapter 7

For the validity of the determined stability threshold curve (STC), Matlab programming codes have been modified to provide the transient responses under various operating conditions.

Chapter 8

In the final chapter the linear transient study of Chapter 7 is extended to include fully transient response with three different tension variation models. Mill stability is highly dependent on the dynamic characteristics of support bearings as well as the roll gap. In principle, stability needs to be determined from the fully transient responses as the states of support bearings and roll gap are varying with the rolling process. Therefore, this chapter introduces the tension variation models to the dynamic roll gap model and transient characteristics of a rolling stand are identified considering the oscillation of the neutral point and strip thickness at entry side. In this way, the limitation of linear stability analysis would be overcome although it costs too much time for a single calculation.

Chapter 9

The concluding chapter reviews and summarises each of these chapters, presenting important and novel results of this thesis as well as identifying the important areas for extending this research.

Chapter 2. BACKGROUND INFORMATION AND LITERATURE REVIEW

It is important to understand how mathematical models of a stand and dynamic rolling process are established. Chatter is generally understood to arise in high speed tandem cold rolling mills, not only as a result of the interaction between the mill structure and rolling process but also as a consequence of the dynamic relationship between the adjacent mass elements. As such, it is necessary that the dynamic behavior of the rolling stand and roll gap be determined in accordance with the resulting force variation. The dynamic chatter model is then created by coupling the established models taking into account associated variables. In this chapter, in order to understand the nature of mill chatter through the literature review, the background research into mill vibrations and its limitations of work done are extensively introduced.

2.1. INTRODUCTION

In past decades, chatter studies of cold rolling mills have been extensively performed in academic and industrial fields, covering many different types of roll gap models focusing on the plane deformation in the roll bite profile (Von Karman et al., 1925; Orowan, 1943; Bland and Ford, 1948). Only recently dynamic rolling models related to the study on the reduction of transient vibration during the rolling process have gained an intensive attention. In order to achieve the stable rolling during transient periods Arimura et. al. (1970) investigated the impact of nonlinearities affecting rolling force and torque as variables *i.e.* variations of thickness, rate of change of the roll spacing, roll bite length, and tension. The purpose of this survey is therefore to identify current trends in simulations and analysis of tandem cold rolling mills and respective components, exploring the background into each of these nonlinearities.

Modelling of cold rolling process – The models used to describe the cold rolling process have been developed and constantly improved during past decades. With the trend of rolling thinner and thinner strip, more accurate rolling models such as steady-state roll gap model, dynamic rolling process model and Automatic Gauge Control (AGC) mechanism have been developed to assist the rolling process. For instance, due

to higher rolling force with thin gauge rolling, the roll gap model under investigation needs to take into an account accurate friction model, yield stress model and roll flattening effect. A large amount of literature has been published these days, including the contributions made by many leading academic and industrial researchers. Many studies (Swift, 1952; Johnson et al., 1983; Wagoner and Wang, 1983; Smerd et al., 2005) investigated the deformation mechanism of the thin strip in cold rolling and discussed the effects of initial thickness and yield stress of rolled materials. Yuen et al., (1998; 1999; 2003) developed real time hybrid mathematical models for predicting accurately the rolling parameters, by considering the elastic and plastic deformation of the strip and the elastic deformation of work roll in the roll bite.

Dynamics of single stand mill and major components – Substantial research has been conducted and reported on the chatter of single-stand cold rolling. Tamiya et al., (1980), Tlusty et al., (1982), Pawelski et al., (1986) and Yun and Ehmann (1998) among others recognise that the roll bite geometry may vary from conventional models particularly when the chatter vibration period is close to the roll gap transit time. However, most studies modelled chatter in the vertical direction only, using lumped masses, linear springs and damping elements to represent the dynamic mill system, as evidenced by the work reported by Meehan (2002). Based on the simplified model and through analysis and experiment, Meehan developed a criterion that quantifies the third-octave rolling chatter stability and suggested that, in addition to low roll stand damping, low roll stand natural frequency, and low slip sensitivity to tension stress, the dominant factors for chatter also include high roll force sensitivity to tension stress and geometrically wider or thinner strips. In the last 10 years, attention has been paid to effects of nonlinearities on chatter within the dynamic system of cold rolling. Based on the results obtained by Yun et al., (1998), Hu and Ehmann (2006) considered the effect of plastic deformation of homogeneous and inhomogeneous strips on nonlinear chatter in rolling. Lin et al., (2003) developed a nonlinear model for describing the dynamic interaction between work rolls and strips and the initiation of fifth octave mode chatter. Previous studies show that the mill system modelled with four or five degrees of freedom provides very good quantitative prediction for frequencies of the first few modes of vibration in the vertical direction. However, these reported studies commonly use rather simple roll gap models and contact models to kinetically couple the work rolls and backup rolls. The journal bearings, which are most often used to support the

backup rolls in cold rolling mills, are also commonly modelled with linearised stiffness and damping coefficients, often only in the direction perpendicular to the rolled strip. Even more importantly, the nonlinearity and dynamic coupling between horizontal and vertical motions of journal bearings, and the dynamic compliance in the bearing housing chock supporting structures were not considered at all. As a result of this oversimplification in modelling, the nonlinear and coupled vibrations in both horizontal and vertical directions of cold rolling stands have been significantly overlooked.

Integrated dynamics of sub-systems of single- and/or multi-stand – In comparison to the above reviewed areas, far fewer thorough studies in this area were reported. As early as 1985, experimental studies reported by Paton and Critchley (1985) showed that the work rolls vibrate in the horizontal direction as well as in the vertical direction. Their work suggests that tension oscillations in the strip become large during chatter and have a relationship with the vertical motion of the roll stack due to roll force induced variations. Only in recent years, theoretical investigations (Yun et al., 1998; Hu et al., 2006) focused on the nonlinearities and coupled chatter that is caused mainly by tension variations. However, the nonlinear dynamics of supporting bearings and complex dynamic compliance of the mill stand were not considered in the presented studies.

In addition to the findings in Paton and Critchley (1985), vibration measurements taken at the five-stand cold mill of BlueScope Steel Research in 1991 provide strong evidence of the nonlinear and coupled chatter in both directions (Yuen et al., 1998). Vines (2005) recently reported that USS-POSCO Industries tandem cold mill experienced an abnormally high rate of roll changes due to "bearing-chatter" and the problem went away once the bad bearings were replaced. Other observations provide further evidence of the dynamic coupling. These include: (i) high variation in rolling forces; (ii) variation in friction in rolling and in strip tension; (iii) variation in rolling speed; (iv) lubrication; and (v) deflection of mill stand caused by about 10 MN rolling forces. All of these factors can be related to operating conditions in a highly nonlinear manner: the load (rolling force and work roll condition); backup roll speed (strip speed); backup rolls' positions relative to bearing housing (chatter itself); and bearing support motion (stand chock vibrations).

In order to gain an in-depth understanding of the effects of the above mentioned factors on the dynamics of tandem cold mills, it is in no doubt that new modelling methods need to be developed. The new model will take into account not only the dynamic coupling between mill stands caused by strip tension variation, the force coupling between driving systems and rolls, but also the dynamics of nonlinear journal bearings and mill stand structures. Hence, based on the determined initial conditions, the stability region and the chatter transients of a rolling stand in cold rolling under a wide range of operating conditions can then be investigated thoroughly using the new integrated system model.

This chapter therefore covers the state-of-the-art in tandem cold rolling mill literature, its components and applications. The primary sections of this chapter focus on introducing the mill structure and its major component before undertaking research into chatter simulations and control of the tandem cold rolling mill, and identification of limitations in current literature. From the identification of these limitations research is expanded into modelling of bearing supports, contact surface between the backup roll and work roll, studies of nonlinearities in the roll gap model and other relevant research into the current state-of-the-art for mill vibration modelling and control.

2.2. COLD ROLLING MILL MODELLING METHODS

Chatter phenomenon in cold rolling is a particular type of self-excited vibration as a result of the interactions between the rolling process and mechanical dynamics of the mill stand. Thus, a chatter model can be generally formulated as a consequence of the interactions between the dynamic model of the mill stand and rolling process. In this section, two mill mechanical models (Meehan, 2002; Kimura et al., 2003) for both single-stand and multi-stand rolling mills are introduced for identifying chatter characteristics.

Although there have been some work employing vibration modes to represent the mechanical dynamics in cold rolling, extensive studies of both mechanical and dynamic models still need more attention. Up to date, almost all models of the mill stand are linear lumped parameter systems with all the masses vibrating along the longitudinal direction only, which is perpendicular to the rolling direction of the material. In order to

further simplify complexity in analysing the coupling effect of mill stands, it is frequently assumed that the structure is symmetrical with respect to the strip so that the number of degrees of freedom of the model could be reduced by a factor of two.

Yun and Hu (2000) employed a new dynamic model by using the Tresca friction factor approach instead of Amontons-Coulomb friction law and developed a dynamic rolling process model to relax assumptions and simplifications made in many works. However, they ignored the interaction between the backup roll and work roll, and bearing supports and focused on the lumped mass on the work roll vibration.

Therefore, in order to relieve assumptions and simplifications made in many works, this research investigates the nature of chatter, which is related to vibrations in the horizontal and vertical direction, introducing the bearing dynamics and contact surface mechanism between the backup roll and work roll.

2.2.1. One DOF Mechanical Model

A spring-mass-damper model with one-degree-of freedom, which is the most widely adapted and simplest, is a very good example to represent the dynamics of the mill stand structure (Tamiya et al., 1980; Tlusty et al., 1982; Pawelski et al., 1986; Yun et al., 1998; Lin et al., 2003; Hu et al., 2006, etc). A main reason of utilising this simple system is due to the fact that the primary concern lies in the vertical vibration of the roll. Moreover, the horizontal vibration of the roll is ignored owing to the limitation of intensive calculations. In general, it is assumed that the system is symmetric with respect to the centre-plane of the roll gap. As shown in Figure 2-1, the strip continuously travels through the roll gap and the material deforms in a way that the work roll is assumed very rigid and squeezes the strip with plastic deformation. Therefore, the work roll shifts to upward and downward as rolling force is generated from the deformed strip and acts on the work roll.
This single degree-of-freedom system can be expressed by applying Newton's second law of motion in terms of the roll vibration as:

$$m_{WR}\ddot{y}_{WR} = -K_{yy}^{\text{var}} y_{WR} - C_{yy}^{\text{var}} \dot{y}_{WR} + F_{dyn,y}^{WR} \tag{2.1}$$

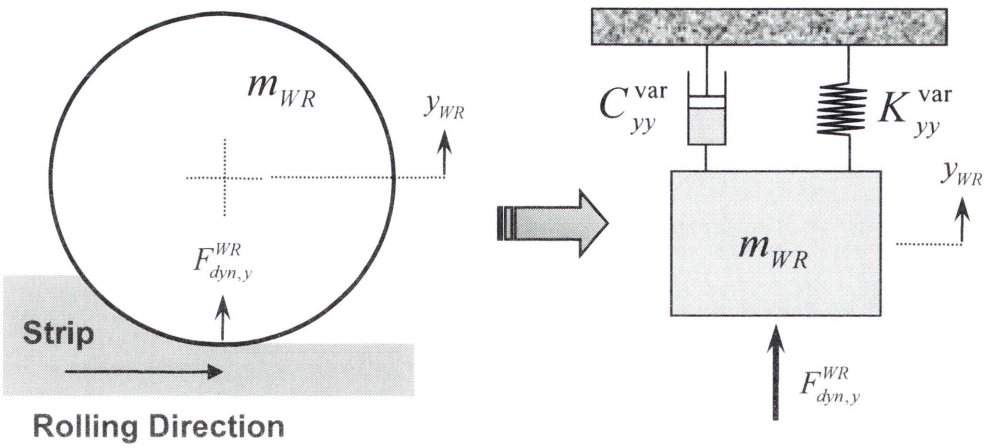

Figure 2-1: One DOF mechanical model

where m_{WR} is the lumped work roll mass, C^{var}_{yy} is the damping coefficient, and K^{var}_{yy} is the spring constant.

The dynamic rolling force $F^{WR}_{dyn,y}$ is used to express the force variation in the roll gap rather than the force variation per unit width. Since it is assumed that the structure is symmetrical with respect to the roll gap in the center plane of the strip, the vertical displacement of the roll, y_{WR}, is related to the roll gap spacing at the center line as:

$$y_{WR} = \frac{h_c}{2} \tag{2.2}$$

This single-stand model coupled with the dynamic rolling process can be used to identify the instability or chatter caused by the positive, negative damping and regenerative effects in the roll bite.

2.2.2. Multi-DOF Mechanical Model

With the help of fast computational methods, a vibration system with four or five degrees of freedom has been developed in order to represent a four-high tandem mill stand (Chefneux et al., 1984; Yarita, 1984; Johnson and Qi, 1994; Meehan, 2002; Chen et al., 2002; Kimura et al., 2003). It consists of five mass elements, including the top and bottom backup and work rolls in addition to the mill housing, as represented in

Figure 2-2. The spring constant K_{var} is linearised to represent the elastic deformation resistance of the work roll flattening when a rolling force variation is applied.

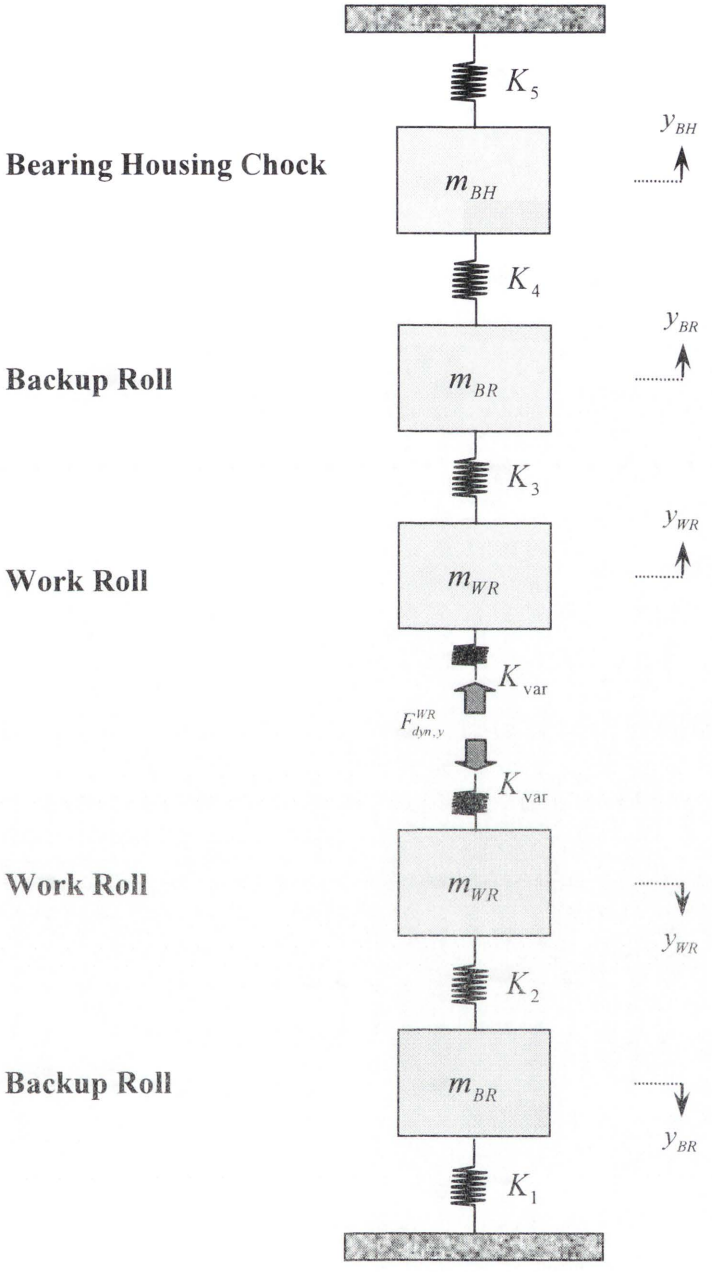

Figure 2-2: Model of a four-high mill (Five Degrees of Freedom)

As shown in Figure. 2-2, the displacements between mass elements are only free to the vertical direction when there is a dynamic force variation acting on the rolls. The relative motions between the mass elements and the force variation $F^{WR}_{dyn,y}$ can be expressed by a set of second order differential equations:

$$
\begin{aligned}
m_{BR}\ddot{y}_{BR} &= -K_1 y_{BR} - K_2\left(y_{BR} - y_{WR}\right) \\
m_{WR}\ddot{y}_{WR} &= -K_2\left(y_{WR} - y_{BR}\right) - K_{\text{var}} y_{WR} - F_{dyn,y}^{WR} \\
m_{WR}\ddot{y}_{WR} &= -K_3\left(y_{WR} - y_{BR}\right) - K_{\text{var}} y_{WR} + F_{dyn,y}^{WR} \\
m_{BR}\ddot{y}_{BR} &= -K_3\left(y_{BR} - y_{WR}\right) - K_4\left(y_{BR} - y_{BH}\right) \\
m_{BH}\ddot{y}_{BH} &= -K_5 y_{BH} - K_4\left(y_{BH} - y_{BR}\right)
\end{aligned}
\tag{2.3}
$$

The rolling force variation is directly applied as an external force to the system rather than a spring because of highly nonlinear characteristics between the work roll and strip. Thus, the mill system is significantly oversimplified as translational block rather than a roll vibration including cross-coupling rotations.

Also, as shown in Figure 2-3, Chen et al. (2002) developed asymmetrical mass-spring-damper system with six degrees of freedom in order to identify the regenerative chatter which is known as one of the most serious vibration phenomena. For brevity, equations of motions of the system are not listed in this section. However, it seems to the Author that stiffness and damping coefficients of the system have not been discussed enough to provide information where these are resulted from although equations of motion of the system are reasonable. On the other hand, damping coefficients are not listed how these significantly affect the mill stability even though the interaction of damping coefficients between the housing and work roll as well as between the backup roll and work roll exists. Also, in the z direction, the combination of the spring in the roll gap is not clear.

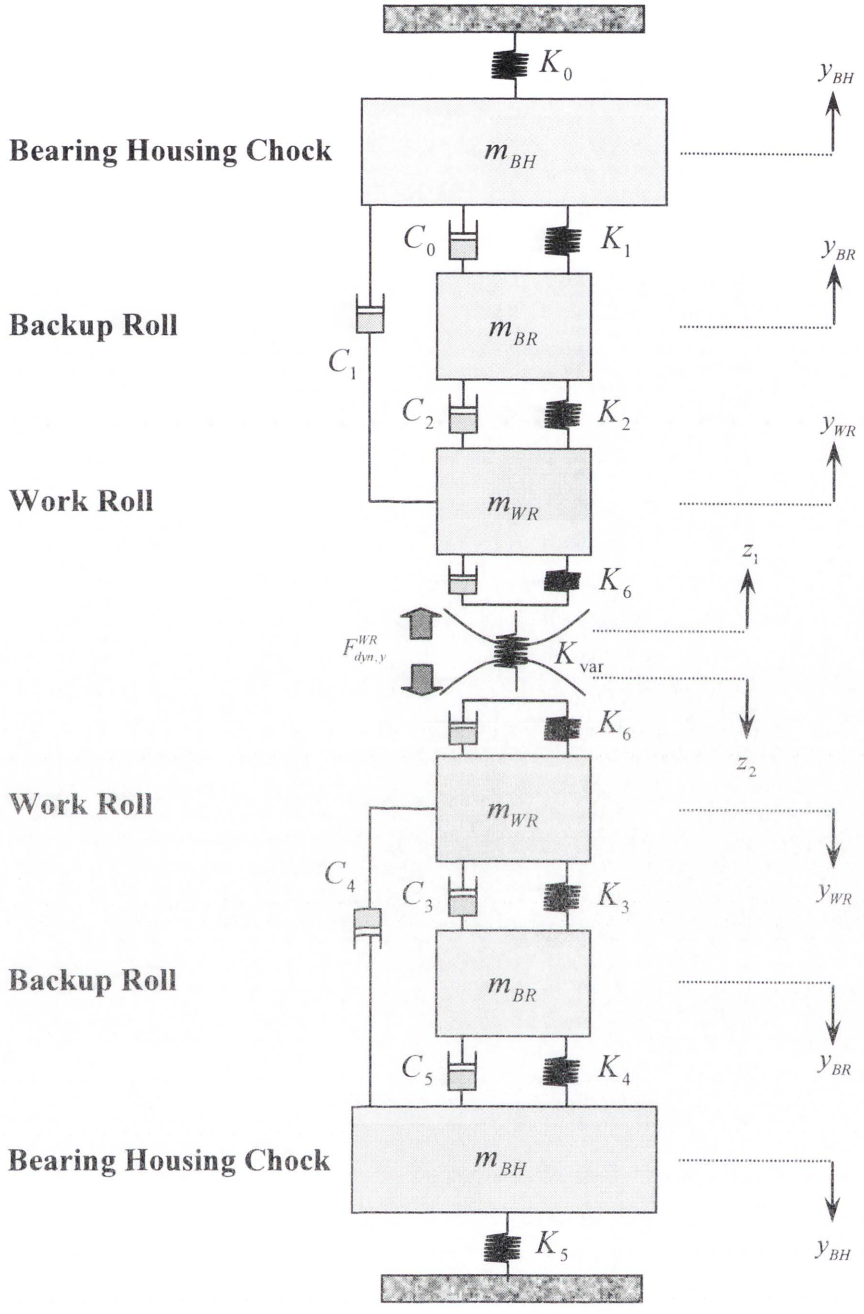

Figure 2-3: Asymmetrical mass-spring-damper system with six degrees of freedom

Almost all of the vibration analysis in rolling is focused on delivering the main cause of chatter but chatter is simply assumed to occur along the vertical direction, which is perpendicular to the mass flow direction of the strip. Even though these vertical vibration models have been adopted in many research fields, it is very limited because all the stiffness and damping coefficients do not result from the analysis of bearing supports and chatter is generally initiated with the close interaction between two translational motions.

Once the incorrect system coefficients are used to identify the chatter characteristics in the rolling process, the overall process would yield in inaccurate results. However, with particular care, it can be applied in a simulation program to study the dynamic response of the tandem cold rolling mill in the frequency domain. Here it should be mentioned that torsional vibration is not considered here as the torsional chatter occurs at the very low frequency range of 5-20Hz and rapidly dies out in high-speed rolling process (Yun et al. 1998).

2.3. RELATIONSHIPS BETWEEN INTERSTANDS

Arimura et al. (1970) considered that tension stresses at both entry and exit are the consequence of inter-stand interaction when each stand is connected in tandem configuration although there are independent variables influencing the single-stand mill. As shown in Figure 2-4, the variation of stress at entry of (i)th stand is proportional to the integral of the difference between the exit speed of (i-1)th stand and the entry speed of (i)th stand, according to Hook's law.

Yun et al. (1998) and Hu et al. (2006) suggested that the vibration at the current stand (Stand i) leads to a variation of the strip speed at entry through inter-stand interactions between (i)th stand and (i-1)th stand. This influences the forward tension of the upstream stand (Stand i-1) and causes gauge variations. After a small time delay, tension variations enter the current stand. Furthermore, the inter-stand interactions between (i)th stand and (i-1)th stand influence the dynamics of (i-1)th stand and cause a tension variations between (i-1)th stand and (i-2)th stand, which further affect the gauge variation in (i-2)th stand. The gauge variations of (i-2)th stand enter (i-1)th stand after a

time delay and (i)th stand after another time delay. These kinds of interactions can be traced back on and on and lead to a wave train effect.

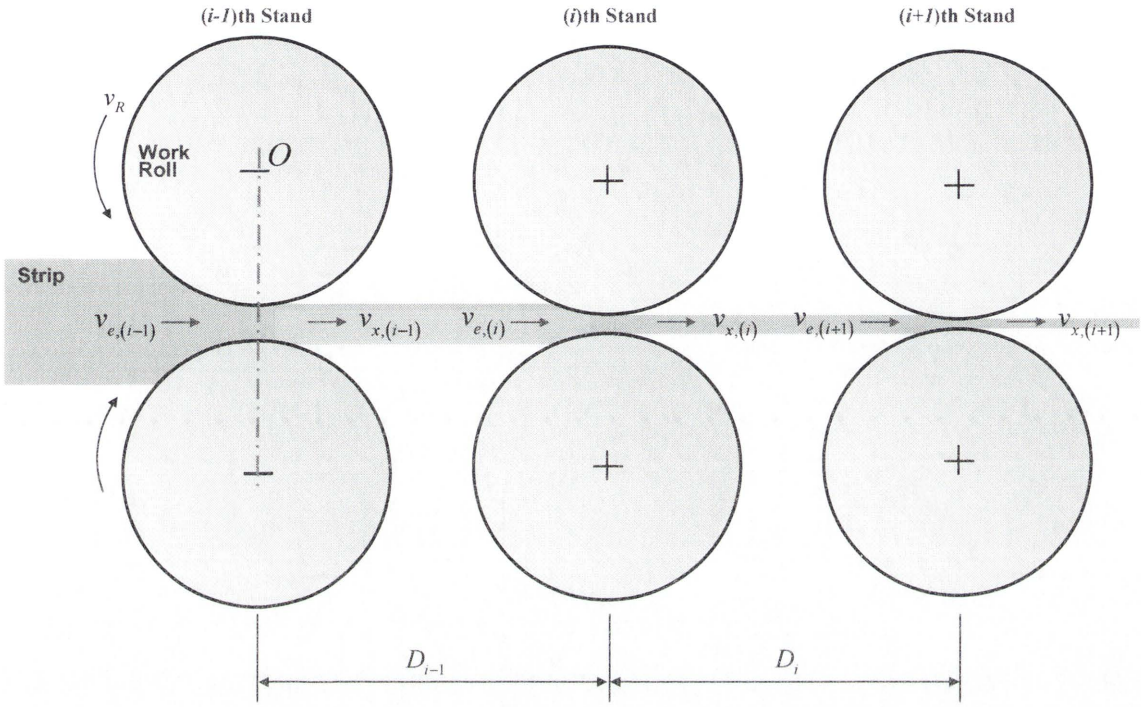

Figure 2-4: Relationship between inter-stands in the tandem cold rolling mill

That is,

$$t_{e,\mathrm{var},i} = \frac{E}{D_{i-1}} \int_0^t \left(v_{e,\mathrm{var},i} - v_{x,\mathrm{var},i-1} \right) dt \tag{2.4}$$

$$t_{x,\mathrm{var},i} = \frac{E}{D_i} \int_0^t \left(v_{e,\mathrm{var},i+1} - v_{x,\mathrm{var},i} \right) dt \tag{2.5}$$

where E is Young's modulus of the strip and $D_{i\text{-}1}$ is the distance between (i)th stand and (i-1) stand.

Another important relationship between consecutive stands is presented by Arimura et al. (1970) introducing the Laplacian operator s to identify how the strip thickness variation from one stand affects the next stand. This plays an important role in regenerative effects. The transfer function representation of the relationship between

strip thickness variations at entry of (i)th stand and that at exit of (i-1)th stand can be written as:

$$dh_{e,i} = e^{-s\Delta_i} dh_{c,i-1} \tag{2.6}$$

$$dh_{e,i-1} = e^{-s\Delta_{i-1}} dh_{c,i-2} \tag{2.7}$$

where Δi is the time delay that can be expressed as:

$$\Delta_i = \frac{D_{i-1}}{v_{e,i}} \tag{2.8}$$

2.4. CHATTER SIMULATIONS, MODELLING AND CONTROL

2.4.1. Types of Rolling Chatter

Based on the observation of unstable vibrations in the tandem cold rolling mill, it is well known that three typical types of chatter have been recognised. To effectively reduce or eliminate chatter or shudder in mill operations, it is first necessary to understand resonant frequencies and nature of chatter. As reported by Tamiya et al. (1980), Tlusty et al. (1982), Chefneux et al. (1984), Yun et al. (1998), Chen et al. (2002), Farley et al. (2006), there are three predominant types of mill vibrations, these can be classified as: torsional chatter, with a natural frequency lying in the 5-20 *Hz* range; third-octave mode, ranging from 125-300 *Hz*; and fifth-octave mode, with natural frequencies in the 500-1000 *Hz* range. Torsional chatter is associated with the drive system, while third-octave and fifth-octave mode chatter are related to the translational oscillations of the roll stack.

2.4.1.1. Torsional Chatter

In the main drive system of a tandem cold rolling mill, shaft torsional vibration is often generated when a motor and a roll are connected with a flexible shaft. In the high-speed mill operation, torsional vibration known as torsional chatter usually occurs only as a result of malfunctioning of motor speed-control circuits or as result of third-octave mode chatter. Torsional chatter associated with the drive train causes very small fluctuation in the gauge of the rolled strip and texture on the strip surface.

Belli et al. (2004) presented the model of the kinematic drive chain and that of the material deformation in the roll bite. They identified resonant natural frequency (16.7 *Hz* and 17.6 *Hz*) in terms of the torsional vibration. In order to reduce unstable vibration, they suggested that the kinematic chain needs to be modified by adopting a top spindle with a stiffness and inertia larger than the stiffness and inertia of the bottom spindle.Zhang and Tong (2006) proposed the linear quadrant (LQ) based speed controller including load compensation. In order to achieve vibration suppression and disturbance rejection, the extended state observer (ESO) is used to estimate not only the states but also load torque. They concluded that the proposed controller guarantees stability when mechanical parameters are changed and its validity and superiority is verified in comparison with the conventional PI controller and the state feedback controller based on a reduced-order state observer.

2.4.1.2. Third-Octave-Mode Chatter

Third-octave-mode chatter is the most destructive vibration problem encountered in the high-speed thin rolling mills. It occurs most suddenly and vibrations approach to instability reaching its maximum amplitude within just a few seconds. It results in severe and undesirable gauge variations of the rolled strip and very pronounced tension fluctuations between stands. In some extreme conditions, it may even lead to strip breakage and rolling mill damage.

Tamiya et al. (1980) have reported that this type of chatter phenomenon is a self-excited vibration, rather than externally excited, due to the phase difference of strip tension when the influence of change in tension on the change of the strip thickness becomes large. Based on their observation, Tamiya et al. (1980) suggested the following methods to avoid chatter: (*i*) increase the length between stands, and (*ii*) increase the damping effect in the screw-down system to reduce the strip variation. Tamiya et al. (1980) also recommended an alternative method which is to use lubricants that are scarcely affected by the fluctuation of tension. In light of this, the following considerations have been taken into consideration: (*i*) the ratio of hydrodynamic lubrication to boundary lubrication and (*ii*) the strength and stability of the boundary film.

Tlusty et al. (1982) developed a vertical mill vibration theory with two degrees of freedom incorporating the inter-stand tension to obtain rolling force components in cold rolling. In addition, they presented a standard for instability of the system and described the effects of the rolling speed, strip width, contact length and tuned dampers on the limit of stability as a means to identify self-excited vibration, as designated by a negative damping from the derived rolling force components. Due to the periodic variation of the inter-stand tension, they showed that the mill system experiences negative damping effects and causes vertical oscillations of the work roll, taking the variation of the rolling force by a 90 degree phase difference while the periodic variations of the contact length and rolling speed produce a positive damping effect. However, calculations used for determining variations of rolling force and tension in their study were oversimplified and can provide only the limited vibration modes.

Yarita et al. (1984) examined both a four DOF linear system and a one DOF system with a time dependent rolling stiffness. The four DOF system describes the motion of a four-high stand; the motion of the two work rolls and the two backup rolls. The natural frequencies of the four DOF systems were determined numerically. In addition, a heuristic model of a one DOF system with variable stiffness was introduced. This was transformed into a Mathieu's equation and a stability criterion was deduced using classical techniques. They further concluded that chatter occurs when the tension fluctuation frequency coincides with the system natural frequency or when coupled with inadequate lubrication.

In order to increase productivity and decrease in rejection due to chatter in 5-stand tandem Ferblatil mill, Chefneux et al. (1984) investigated third-octave-mode chatter by taking into account the successive engagement between inter-stands. Interactions between inter-stands where the exit thickness of the strip leaving the (i)th stand is the entry thickness of the strip at the (i+1)th stand after the appropriate transit time, and instantaneous interaction, where any disturbance altering the forward slip of the strip leaving a roll bite has an immediate effect on strip tensions at adjacent stands. The mill sensitivity they obtained are: (i) the tendency to chatter increases as the rolling speed increases, (ii) tension between the last two stands must be held at the lowest possible value, (iii) friction coefficient in the last stand must be not too low, (iv) rolls must be in good condition, (v) sudden changes in the mill during rolling process must be avoided.

According to experimental observation, this enabled a mill to safely increase its operating speed by 15 per cent without encountering chatter and resulted in an increase in mill productivity of 15%, a 38% decrease in chatter.

The vibrations of any oscillatory system may be reduced if sufficient damping exists, regardless of the mode of excitation. In this respect, Paton and Critchley (1985) developed methods for increasing damping in the case of third-octave mode chatter by using tuned dampers installed on the top backup roll chocks. They advocated that variation of inter-stand tension is the primary factor which induces variation of the vertical rolling force and therefore, the vertical oscillation of the roll stack.

Pawelski et al. (1986) also presented a vertical model which predicts the influence of the rolling parameters on the susceptibility of a mill to self-excited vibrations. This model treats the harmonic oscillation of the work rolls at given frequency and amplitude to calculate rolling force as functions of time, neglecting the dynamic characteristics of the mill stand.

In recent years, Yun et al. (1998) developed a new dynamic model taking into account both the variations of the roll gap and the rate of change of the roll gap. In order to find its effects on rolling process variables, the dynamic model employed the Amontons-Coulomb friction law for obtaining rolling force and toque as a function of the strip thickness, tension, friction and flow stress. Simulations to compare the measured rolling force to the predicted rolling force were performed for identifying the phase difference between the strip thickness and rolling force variations. They further developed a uni-modal chatter model and a multi-model caused by the tension variation at the entry side.

Kimura et al. (2003) attempted to understand how the rolling conditions can be related with vibration phenomena through numerical simulations. Firstly, they constituted a theoretical model to simulate the vibrational behaviour of a five-stand continuous rolling mill, and evaluated the stability of the mill vibration, introducing a disturbance to the static rolling conditions. The results of the calculation show that the vibration is greatly influenced by rolling speed and friction coefficient. With increase in rolling speed, the mill vibration tends to be self-excited. Also, the results have shown that optimal ranges of the friction coefficient exist in which the vibration is damped and the

mill is stable against the disturbance. Secondly, they proposed a simple self-exited vibration model and the stability index for further understanding of the phenomena. Thus, an analytic approach is made to predict the stability of the rolling process. With this model, they have shown that the rolling force and the delay of the response to the change in the roll gap have a major effect on self-excited vibration. These phenomena were explained using self-excitation model with a five degrees of freedom. The results indicated that the stability of a rolling mill system is affected by the phase difference between the vertical motion of rolls and the force response. Therefore, they thought that the stability of a tandem cold rolling mill is determined by the rolling conditions, especially the friction coefficient. Neither too high nor too low friction coefficient stabilises the self-excited vibration in a tandem cold rolling.

Hu et al. (2006) combined a linearized rolling process model and a mechanical dynamic model to study the third-octave and fifth-octave-mode chatter, which is a result of the relative motions between the work and backup rolls. The interaction between work and backup rolls was expressed in terms of the constant contact stiffness and damping coefficients. A unidirectional (vibrations allowed only perpendicular to the strip) two degree-of-freedom linear mechanical model was employed to represent the vibration of work and backup rolls. A stability criterion for the third-octave and fifth-octave mode chatter was given by analysing the characteristic equation contributed through the combination of the rolling process and mechanical model.

2.4.1.3. Fifth-Octave-Mode Chatter

Fifth-octave-mode chatter causes chatter marks on the backup roll barrel and prints via the work roll onto the strip surface with a spacing between 10 and 40*mm*. According to Farley (2006), the markings are generally parallel to the roll axis and often have uniform intensity across the backup roll barrel. The vibration frequency associated with fifth-octave chatter is usually in the range 500 to 1000 Hz and involves the two work rolls moving in-phase and vibrating between the two backup rolls. The backup rolls move in off-phase to the work rolls. The relative motion between the work roll and backup roll damages the backup roll surface during the rolling process. It is reported that this type of mode belongs to a family of fifth octave modes, all capable of

damaging the backup roll or leaving the chatter marks, through relative motion between the backup roll and work roll.

In previous study, Johnson and Qi (1994) formulated two and four DOF systems to examine chatter phenomenon. From the system matrix, they found the frequencies of the two modes which represent fifth-octave-mode chatter that produces sheet corrugations and the other two modes being third-octave-mode chatter that leads to gauge variations.

Fortunately or not, it is being understood that fifth-octave-mode chatter does not affect the variation of the rolled strip and is detrimental to the rolled products or mills. Furthermore, it is said that it is not generally difficult to suppress this mode of chatter. In order to suppress fifth-octave mode chatter, the effective method appears to be the removal of various sources of external forced vibrations, especially of damaged rotational parts of the rolling mill.

2.4.2. Single-Stand Chatter Model

Yun et al. (1998) formulated single-stand chatter model by coupling the rolling process model with the mechanical model (surface contact mechanism between the work roll and backup roll) and by considering the interactions between stands (roll gap variations), as shown in Figure 2-5. The inter-stand tension effect was included to incorporate the pay-off and pick-up reels. It was assumed that the pay-off and pick-up reels do not introduce any velocity variations, meaning that the exit velocity variation of the pay-off reel at (i-1)th stand and the entry velocity variation of the pick-up reel at (i+1)th stand disappear. In a single-stand chatter model, the inter-stand tension variations of 90 degrees were purely generated only by the entry and exit velocity variations by the stand itself.

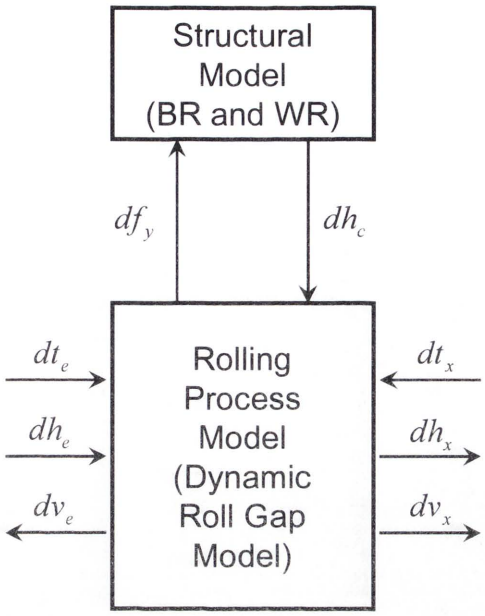

Figure 2-5: Single-stand chatter model

Variations of force components were represented by positive damping imposed by the plastic deformation of the strip in the roll gap and by negative damping introduced by the back tension variation, respectively. In addition, the rolling contact stiffness was also calculated by the strip deformation in the roll gap, which increases the natural frequency of the stand. Based on this chatter model, the single-stand negative damping effect and the effects of these quantities have been analysed by Hu et al. (2006) introducing a synthetic block diagram of tandem cold rolling mill.

2.4.3. Multi-Stand Chatter Model

Chatter phenomena are usually observed before and after final stages of the rolling process on tandem cold rolling mills. It is commonly understood by researchers that the tendency of chatter, which generally occurs at the fourth or fifth stand, is due to the instability caused by tension and force variations between inter-stands. So as to identify the influence of roll gap variations between inter-stands on overall system stability, a multi-stand chatter model (Yun et al., 1998; Hu et al., 2006) including dynamic roll gap variations, was established based on the single-stand chatter model, as shown in Figure 2-6. In order to identify the nature of chatter between inter-stands, the inter-stand tensile stress variation has been calculated by using equations (2.4) and (2.5).

The dynamic chatter model below consists of two stands and each stand has four state variables for a total of eight state variables. As the front tension variation of (i-1)th stand is equal to the back tension variation of (i)th stand, the number of independent state variables of the system have been reduced to seven. The same procedure can be applied to construct a state space model of a tandem cold rolling mill consisting of more than two stands. It has been noted that the time delay term, Δ_i, which plays a critical role in unstable vibration, appears in the square matrix of a state space model. In essence, this is a set of delay differential equations (DDE), which require much more complex stability criteria to perform stability analysis.

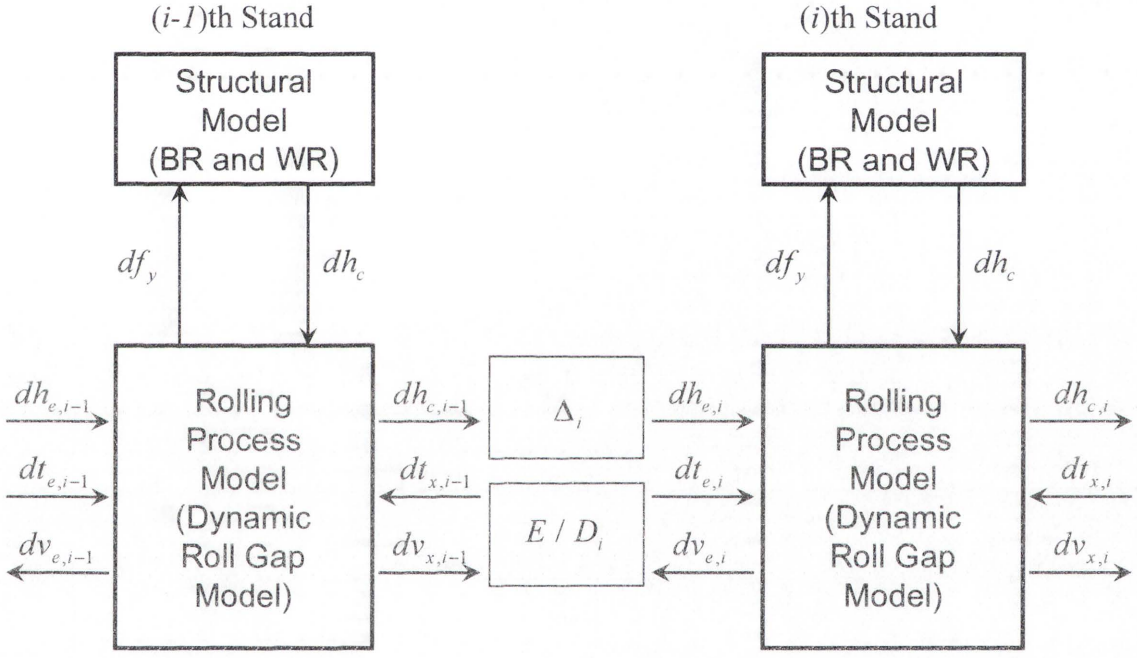

Figure 2-6: Multi-stand chatter model

These two chatter models are an excellent example to represent the synthetic block diagram of tandem cold rolling mills; the concept firstly introduced by Tamiya et al. (1980) is intended to identify the effect of inter-stand tension on self-excited vibration caused by phase difference of tension.

Therefore, this research will develop a new dynamic chatter model not only identifying the coupling effect between the associated variables in the roll gap but also investigating the effect of tension variation terms developed by Tlusty et al. (1980) and Yun et al. (1998). Also, considering the change in roll gap area, a new tension variation model and

its significant influence on mill stability will be discussed. The negative damping effect will then be investigated based on a rolling stand chatter model. Of course, if the tension variation terms are neglected between stands, two chatter models can be used to explore the single-stand negative damping mechanism due to the friction gradient as well.

2.4.4. Stability Analysis for Chatter Model

In determination of the onset of instability, stability analysis is often utilised to exhibit the system stability based on a given chatter model of the rolling process (Tamiya et al., 1980). It is a critical procedure to obtain the corresponding output (natural frequencies and mode shapes). A necessary and sufficient condition for the vibration system to be stable is that all the poles of the system transfer function must have negative real parts. In other words, all the poles should lie in the left-hand s-plane otherwise the system becomes unstable where all the roots are not in the left-hand plane.

The Routh stability criterion, one of the most popular techniques for assessing stability of a linear time invariant (LTI) system, has been employed to determine whether the presented model provides a stable solution or not. After examining Routh's array, stability is determined through examining the first column of the calculated array. For a stable system, the criterion requires that there be no changes in sign in the first column. Due to its simplicity, this method provides the number of roots of the characteristic equation in the right half plane without necessarily computing the values of the roots, and is valid for all types of bounded inputs such as impulse, step or harmonic disturbance.

For the system matrix described in a state space form, stability can be determined from the characteristic equation given by:

$$\det(s\mathrm{I} - \mathrm{A}) = 0 \tag{2.9}$$

where **I** is the identity matrix and **A** is the system matrix.

In order to determine stability of the presented system, Routh criterion can be applied to identify any unstable roots in equation (2.9), as demonstrated by Tamiya et al. (1980). Alternatively, the roots of the characteristic equation can be directly calculated by

computing the determinant. Unfortunately, system matrix (**A**) generally results in very complex function of the rolling process parameters due to its nonlinearities. This makes either calculating the eigenvalues or applying the Routh criterion impractical. On the other hand, in addition to the steady-state rolling condition, the system matrix can be evaluated for each setting of different rolling conditions as the positions of rolls and variations of the dynamic roll gap are varying with the rolling process. After that, the eigenvalues of the system matrix can be found numerically without any difficulty.

Initially, Tamiya et al. (1980) employed the Routh criterion to assess the stability of the characteristic equation from the chatter model. Tlusty et al. (1982) developed the second order characteristic polynomial to determine if the system is stable or not. The requirement for a stable second-order system is simply that all the coefficients of the damping and stiffness terms should be positive. They concluded that chatter is due to periodical variation of the inter-stand tension leading the variation of the rolling force by a 90 degrees phase. At this instant, the periodical tension variation represents negative damping and causes unacceptable gauge variation in the roll gap, while variations of the contact length produce a positive damping effect. In order to maintain the system as stable, positive damping is introduced by the periodic variation of the contact length. This should be larger than the negative damping initiated by the back tension variation at the entry side. As a result, they described the effects of various process parameters on the limit of stability.

In a similar way, Meehan (2002) presented a dynamic model for investigating third-octave-mode chatter. Based on a feedback mechanism incorporating simplified models for the roll stack dynamics, strip and inter-stand dynamics, a stability analysis was performed to obtain a criterion for the critical rolling speed at which chatter begins to grow.

Hu et al. (2001; 2006) established fifth-octave-mode and third-octave-mode chatter stability of single-stand and multi stand mills by formulating analytical stability criteria in terms of relevant rolling process parameters. For fifth-octave-mode chatter, it was shown that fifth-octave-mode chatter generates vibrations mostly on the backup rolls and thus the high-frequency between the backup roll and work roll produces an unpleasant noise when it occurs. They concluded that fifth-octave-mode chatter is not

directly related to the strip thickness variation but associated with the noise and the mill system will more likely becomes unstable due to third-octave-mode chatter. For third-octave-mode chatter, on the other hand, model matching and mode coupling mechanisms were analysed.

In stability analysis of a single-stand mill, the model matching effect was assessed by applying the Routh criterion on a second order linear system, which is similar to the work done by Tlusty (1982). In a similar way, the Routh criterion was applied on a fourth order system to access mode coupling stability. Sign changes in the Routh array elements were studied instead because of complexity of the coefficients of the characteristic equation. They pointed out that third-octave-mode chatter was initiated by the negative damping effect due to the existence of mode coupling at a higher operating speed.

In determination of stability in a multi-stand tandem mill, stability was calculated by applying strip tension variations caused by inter-stand interactions. In order to access the effect of the multi-stand negative damping on multi-stand mill stability, variations in Routh array elements were studied by investigating the first column of a sixth order polynomial. This mechanism explicitly provides the explanation of self-excitation in the tandem cold rolling mills and leads to the most detrimental effects associated with third-octave mode chatter. However, they failed to directly relate the rolling process parameters, such as the nominal tension variation setting, variations of the friction coefficient with respect to the rolling speed, equilibrium of support bearings, etc, to the instability of the mechanisms.

Nonetheless, the choice of the appropriate method is very case specific, and the analysis and evaluation of this type of characteristic equation is generally rather tedious. Zhao and Ehmann (2006) adopted the integral criterion because it offered slight advantages, such as numerical evaluation of the integral instead of symbolic evaluation. As a result, a stability chart, similar to stability threshold curve (STC) in this study, that relates the friction factor and the critical rolling speed was created. It demonstrated that vibrations in a tandem cold rolling mill can be unstable due to the regenerative effect, even if the individual stands are stable in the sense of negative damping.

2.5. DISCUSSION

The development of a single-stand chatter model is fundamental to investigate the negative damping mechanism in cold rolling, which is the consequence of the interactions between the rolling process and the mill structure. Although many chatter models have been formulated by coupling the dynamic model of the homogeneous rolling process and various mechanical models of the mill stand, the coupling relationship initiated from the mill structure such as hydrodynamics of support bearings has been consistently ignored.

Multi-stand chatter models, on the other hand, are more suitable for studying the multi-stand negative damping and the regenerative effects, since they take into account the interactions between two stands, such as tension variations and strip thickness delay transportation. The simplified multi-stand models, however, also does not take into account the mill structure borne vibration. Therefore, it may not be suitable for identifying the origin of unstable vibration, *i.e.*, the accurate prediction of resonant natural frequency range, which is often referred to as chatter or shudder.

In the modelling of the dynamics of mill vibration between the inter-stands, the rolling speed is assumed constant, which is the same as in the steady state condition. Yet, the entry and exit velocities of the strip change during the dynamics of the rolling process. So, the constant speed model may not be able to predict accurately the position of the entry point when the strip thickness varies. However, a roll gap model to form an analytical or numerical solution, which is capable of finding the position of the entry point in the deformed roll, would be the more reliable than any other.

Finally, the stability analysis of the negative damping or regenerative mechanism is required to be dependent on the state in order to obtain closed form solutions existing between the upstream and downstream stands. This means that tension between stands also changes with other associated variables. In order to model the chatter mechanism with more than 2 stands, additional state-dependent variables are needed. As such, it would be very difficult to model the chatter mechanism and the determination of stability analysis of such system would be too computationally intensive. Instead, in order to determine stability threshold regime based on the linear system, a single-stand

chatter model will be formulated by ignoring the tension variations between stands because tension variation model so far developed is assumed to be harmonic. Tension variation model will then be included in the fully transient study only as it is highly dependent on both the state and time during the rolling process. Also, so as to simulate a chatter model only in a single-stand cold rolling mill, especially at 4^{th} stand which chatter commonly takes place, a more feasible way will be presented comparing tension variation models to the current tension variation model since computational time can be reduced more efficiently than multi-stand chatter model scaled up to more than 2 stands.

CHAPTER 3. EFFECTS OF ROLLING PARAMETERS

3.1. INTRODUCTION

Many different models of the homogeneous or in-homogeneous rolling process, based on the roll gap profile, are presented in literature (Orowan, 1943; Bland and Ford, 1948; Yuen et al., Qiu et al., 1999; Tan et al., 2008, etc). Some models relax certain assumptions made in the simplified model, by considering the influence of the material strain hardening effect and the elastic deformation of the work roll. The simplified model needs to provide proper explanation of the physical and mechanical properties of materials being investigated. In order to formulate the explicit quasi-static or dynamic model of the rolling process, a fundamental understanding of rolling process for various parameters is required. Accordingly, all the factors of interest, which may affect system stability, need to be discussed so that the chatter model for a dynamic rolling process can be formulated.

3.2. ROLL BITE PROFILE (GEMETRY OF THE ROLL GAP)

Based on the equation of the mass conversation principle, which means the incoming mass flow of the being rolled material is all the time same as the outgoing mass flow of the strip, the mass flow through the roll gap may be represented by:

$$vh = v_e h_e = v_x h_x = v_R h_n \tag{3.1}$$

The basic rolling process is illustrated in Figure 3.1. A continuous strip with thickness h_e and width W passes through the roll gap between two work rolls with a velocity v_e, and exits with thickness h_x and velocity v_x. The radius of the undeformed work roll is R_{WR}, the strip thickness at the neutral point is h_n and the roll peripheral velocity is v_R. For the radius of the undeformed rolls of the order of one hundred times the strip thickness and for a W/h ratio greater than ten, it can be assumed that the exit width is also W. The plastic deformation thus becomes a plane strain problem.

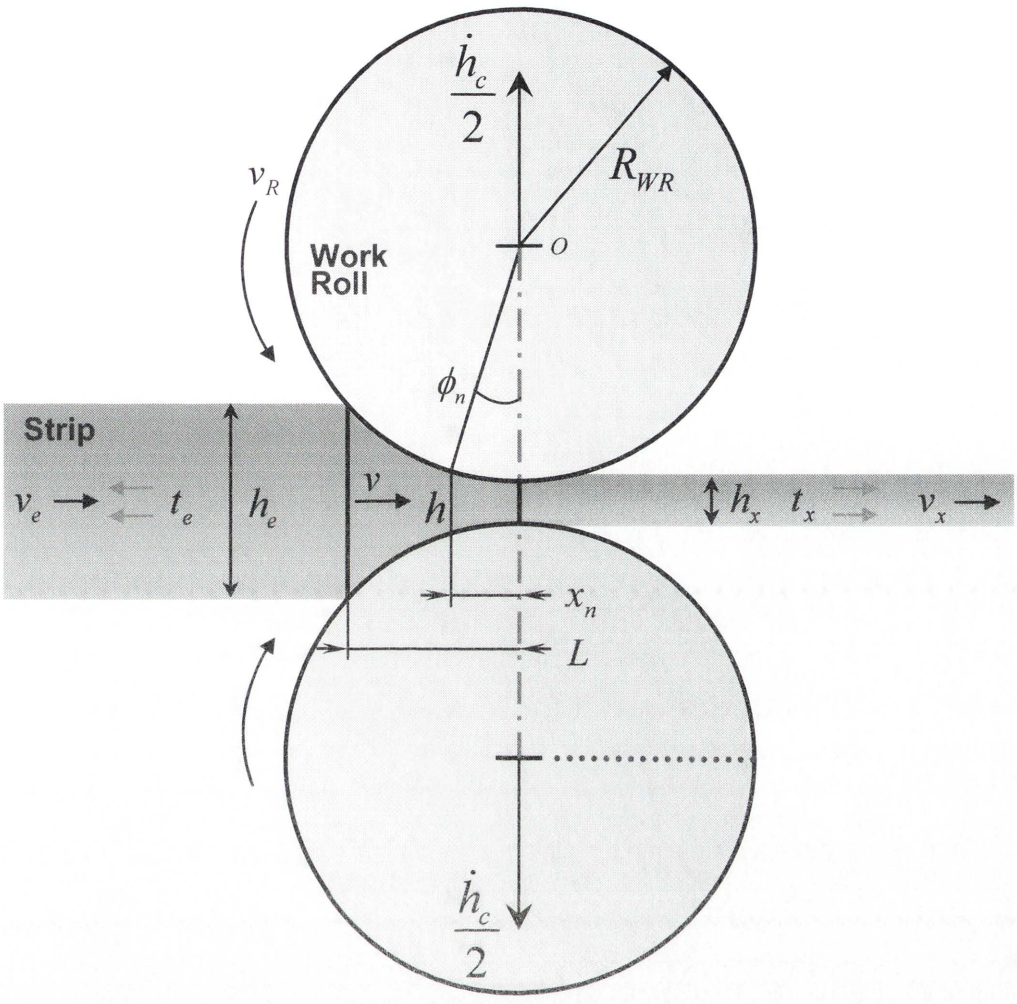

Figure 3-1: Roll bite profile during steady-state rolling process

When rolls are rotating in a steady-state condition, the x-axis can be defined to be along the line of symmetry and runs from the centerline of the rolls towards the entry. It was usually assumed that the exit plane coincides with the centerline of rolls, but this would become invalid once the rolls begin to vibrate. Based on the observation on industrial rolling mills, the work rolls can vibrate in both horizontal and vertical directions (Paton and Critchley, 1985) as the bearing oil film changes during the rolling process. It is then reasonable to take both vibrations into consideration when constructing the rolling process model. As shown in Figure 3-1, the top work roll may vibrate in both x and y directions with velocity of $\dot{x}$ and $\dot{y}$, respectively, while the bottom work roll vibrates in-phase along the x direction but opposite in y direction with top roll. "In-phase" vibrations in the y direction would have little effect on the force equilibrium of the deformation process (Tamiya et al., 1980), but would rather

move the strip up or down with the work roll pair. If the movements in the x direction are different at top and bottom, however, the deformation process will become too complicated for an analytical solution to be found.

In order to provide a suitable deformation process in the roll gap, this assumption can be regarded as valid since two work rolls (top and bottom) are the same and symmetric to the centre plane of the strip. Thus, the degrees of freedom of the work roll vibration can be reduced to a factor of 2 when ignoring torsional vibration.

It was usually assumed that the roll surface can be treated as a parabolic curve so the calculation can be simplified without losing much accuracy (Yun et al., 1995). With the two translational motions of the rolls, a parabolic approximation (Underwood, 1950) for the strip thickness within the roll bite may be represented as:

$$h(x) = h_c + \frac{x^2}{R_{WR}} \tag{3.2}$$

The approximate roll bite length may be formulated as:

$$L(x) = \sqrt{R_d (h_e - h_x)} = \sqrt{R_d \Delta h} \tag{3.3}$$

where $\Delta h = (h_e - h_x)$ is the reduction of the strip thickness with the deformed roll radius R_d of the work roll.

The parabolic approximation is more or less restricted to the case where the roll bite length is several times larger than its thickness. Under the condition referred to as "homogeneous deformation", the horizontal stresses and vertical stresses along the roll gap may be assumed constant. Also, the analysis is restricted to stable rolling where it is required that the magnitude of the surface velocity of the roll is greater than the entry speed of the strip but less than the exit speed of the strip. This ensures a 'neutral point', where the strip velocity equals to the roll surface velocity with respect to the roll gap. At the entry side prior to the neutral point, the work roll rotates faster than the strip velocity and friction tends to reject the material and prevent it from entering the roll gap. After

the neutral point the strip velocity moves faster than the roll surface and friction pulls the strip out of the roll gap, meaning that the direction of the friction is reversed.

Finally, under the steady-state rolling condition, strip thickness is determined by the trigonometry.

$$h = h_c + 2R_{WR}(1-\cos\phi) \tag{3.4}$$

3.3. ELASTIC FLATTENING OF THE WORK ROLL

In the conventional rolling theories, the work roll was assumed to remain rigid, or to undergo no elastic deformation. In the compressive rolling of relatively soft materials, the assumption of rigidity is reasonably valid but in the rolling of thin, hard strips, and in dry temper or lubricated cold rolling, the rolls are significantly flattened so that the arc of contact is considerably longer than that of rigid rolls through the roll gap.

Before Hitchcock (1935) developed the concept of the roll neck bearing, the roll flattening effect has been neglected due to the complexity of a varying roll radius. In an analytical model of the rolling process, the error generated by this simplification can be mostly corrected by using the effective radius of the roll R_d instead of the undeformed radius R_{WR}. The effective radius (deformed roll radius) changes over applied load along the arc of contact when the compressive pressure acting on the roll surface changes. This roll flattening model greatly reduces the complexity of the roll flattening model, yet it advances the accuracy of the estimation of rolling force without requiring too much additional effort.

In deriving the above equation, Hitchcock assumed that the pressure distribution between the roll and strip is of an elliptical form and thus the deformed roll profile still remains circular during the rolling process and the effective deformed roll radius can be expressed as:

$$R_d = R_{WR}\left(1+\frac{16(1-v^2)F_{sp}}{\pi E\Delta h}\right) = R_{WR}\left(1+\frac{cF_{sp}}{\Delta h}\right) \tag{3.5}$$

where c is the Hitchcock constant, R_{WR} is the undeformed roll radius, Δh is the reduction or draft of the strip and F_{sp} is the roll separating force (specific rolling force with unit of N/m). A simple estimation of roll flattening ratio is given in Figure 3-2. This model gives a rough estimation of the roll flattening and can be easily used in conjugation with the rolling process model to provide a more accurate calculation of rolling force.

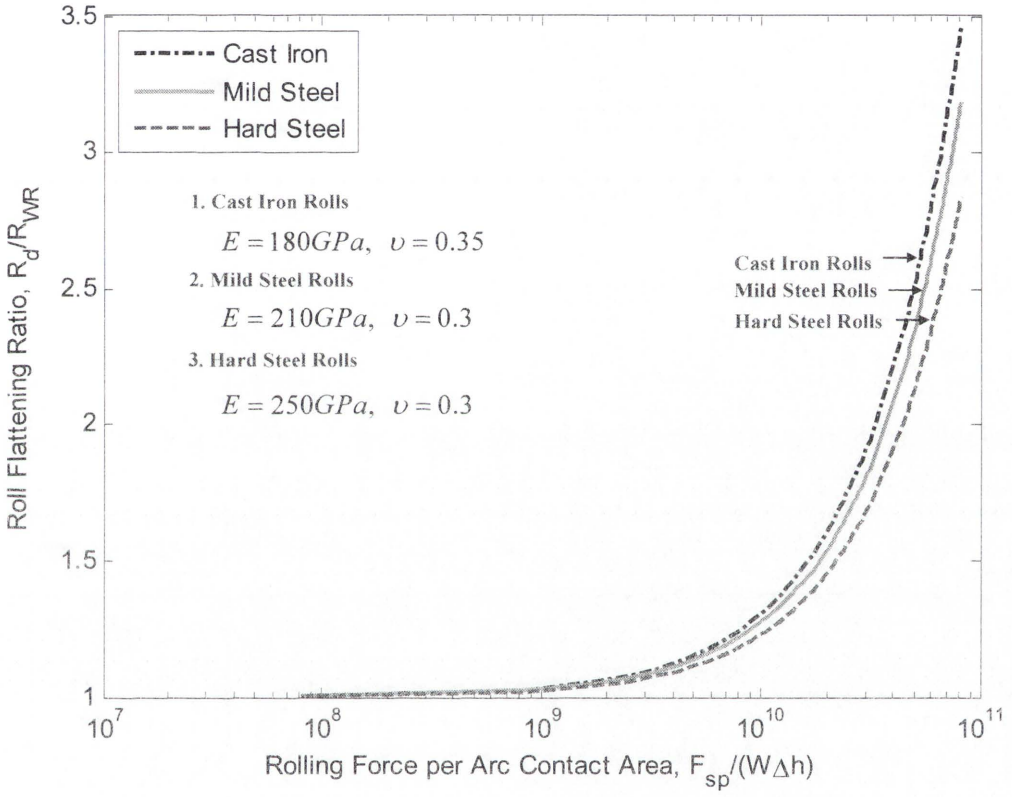

Figure 3-2: Roll flattening ratio $\left(R_d/R_{WR}\right)$ depending on materials used

However, it should be noted that Hitchcock theory unfortunately fails to estimate the deformed roll radius when its reduction and the coefficient of friction is very small because of inability to find exact solution for those conditions. Thus, it may need to be estimated correctly if one uses Hitchcock concept in very thin rolling such as foil rolling.

Bland (1950) proposed that Hitchcock's aforementioned assumption is reasonable and can be used with confidence only for the case of a thick strip rolling. When the strip thickness decreases, the rolling force required for attaining an exact reduction increases.

This is due to the increase of the yield stress in the roll gap which will be discussed next section. Also, with the increase of the strip thickness, required rolling force will be decreased. Therefore, it should be noted that rolls are deformed into a non-circular shape in case of rolling of a thin hard material, indicating that the use of Hitchcock's formula may cause unsatisfactory results.

In order to reduce the overestimation of the roll flattening, a more complicated and accurate model which takes the dynamic rolling condition into account is proposed by Gohar (1974). After that, Chang (1994) concluded that Gohar's model gives a better estimation of roll radius deflection than those calculated by Jortner et al. (1960) and other researchers.

Pawelski (1986) assumed that the effective radius of the work roll is constant along the contact arc between the work roll and the strip and remains the same even when the total rolling force changes to simplify the analysis of the rolling process. The work roll is assumed to be a very stiff spring in the mechanical model of the deformed roll profile. When rolling force increases or decreases, the strip thickness accordingly changes including the displacement caused by the movement of the work roll. Using these assumptions, the accuracy of the dynamic model of the rolling process is significantly improved, yet, still resulting in a solvable analytical model.

3.4. FRICTION MODEL

In general, friction is required for ensuring the surface contact in compressive rolling, in such a way that the work roll draws the strip into the roll bite by means of friction. However, friction has to be carefully controlled in the rolling process as the rolling force and torque rise with the increasing friction. In cold rolling, it is generally understood that the coefficient of friction usually ranges from 0.01 to 0.1, depending on the strip materials, surface finish of the rolls and lubricants applied.

As reported by Robert (1978), chatter typically occurs at the last few stands (4^{th} stand) in tandem cold rolling mills during high speed rolling of hard and thin strips. Generally, the friction coefficients for these stands are very small in modern production mills, around 0.01~0.03 (Meehan 2002 and Kimura et al., 2003), indicating extremely good

lubrication in the roll bite. In this case, friction force is far lower than the shear strength of the strip material. Some case studies show that the friction force is always less than the shear strength of the strip material when the friction coefficient is less than 0.1. It is important to make sure that the friction does not exceed the shear strength of the strip material. Since the traditional usage of the friction coefficient is widely adapted both in academy and industry, the friction coefficient model is employed to simplify the computation of the dynamics of the rolling process as well as to facilitate comparisons.

Tan (2008) summarised a number of friction models used in plasticity, such as the Amontons-Coulomb friction model (ACM) (e.g., applications by von Kármán, 1925 and Kudo, 1960), the constant friction model (e.g., reviewed by Schey, 1983), the general friction model by Wanheim and Bay, 1974 and Bay, 1987), the absolute constant friction stress model by e.g., Orowan (1946), Alexander (1955), Tan et al. (1998), Levanov friction model (Levanov, 1997), Anand friction model (Anand, 1993), the empirical model by Tan et al. (2002).

For some rigid contact bodies with elastic deformation, Amontons-Coulomb friction model can be modelled with extreme accuracy (reviewed by Dowson, 1979 and Bowden and Tabor, 1954). For plasticity problems, some friction models have been used to "successfully" evaluate applied loads, material flows and deformation, as reviewed by such as Schey (1983), Ginzburg (1985), Tan (2002). However, none of these friction models has been applied to satisfactorily predict the distribution of local contact stresses in flat rolling, especially for the neutral point/plane.

The accuracy of the conventional theory of rolling partly results from ignorance of the material velocity. Rolling speed affecting rolling forces has been experimentally observed by a number of researchers. Azushima (1978) examined coefficient of friction, surface qualities, and oil film thickness using a high-speed test mill, and observed that oil film thickness decreases with increasing reduction, but increases with increasing rolling speed; the magnitude of the coefficient of friction decreases with increasing rolling speed. Matsui et al. (1984) conducted high-speed rolling tests up to 1500m/min and pendulum type of friction test and showed that with increasing rolling speed, mean peak rolling pressure decreases, oil film thickness increases. Azushima and Miyagawa (1984) experimentally investigated lubricant behaviours in cold sheet rolling and

showed that the influence of the roll speed on the coefficient of friction is significant: values of the coefficient of friction decrease with increasing roll speed. Lin et al. (1991) conducted experiments in cold strip rolling and showed that with increasing rolling speed, the values of the forward slip increases, the friction coefficient decreases, whereas torque increases slightly. The effects of the reduction, roll speed, lubricant-type and viscosity on the roll separating forces, forward slip and resulting specimen surface roughness during the cold rolling of aluminium have been studied by Zhang and Lenard (1992). The forward slip, the friction coefficient and roll separating force decreased with increasing lubricant viscosity while increasing speed was found to lower the friction coefficient. The above paragraph mistakenly quoted by Tan et al. (2008), especially for the forward slip with the increasing rolling speed, is corrected by the Author.

Most recently, Tan (2007) has developed a new friction model – the dynamic friction model and has successfully applied it to establish solution to the plane-strain compression. The basis of this model was combination of sliding mechanics with fluid mechanics. In this hybrid model (a) Amontons-Coulomb friction model and the definition expression of viscosity have been jointly taken into account and (b) the friction stress is related to not only the flow stress and dimension of material, but also material velocity.

Friction in a real forming process depends on many parameters. However, the researchers have attempted to propose friction models by means of simple laws and relationships. The most common friction models employed in academic and industrial studies are the classical Amontons-Coulomb friction model and the friction factor model. The Amontons-Coulomb friction model assumes that friction stress increases in proportion to normal pressure with proportionality constant called the coefficient of friction. Amonton's law is one of important friction models that can mathematically be expressed as follows:

$$\tau_s = \mu p \tag{3.6}$$

where τ_s is the friction stress, μ is the coefficient of friction and p is the normal pressure. This law is valid for elastic contacts as well as for forming process with low interfacial pressures, i.e. $p/\sigma_Y < 1.5$ where σ_Y is the flow stress of the work-piece.

The friction factor model, on the other hand, assumes that the friction stress is a function of roll pressure and friction factor.

$$\tau_s = mk \tag{3.7}$$

where m is the friction factor and k is the material shear strength. It appears that this model is better suited for most metal forming process, and especially for the rolling process since it requires the conditions of high loading and plastic deformation of the strip. The value of m is generally less than 1 and is chosen from empirical data for a given process.

The general friction model, which is a combination of two models mentioned above, is stated by the following relationship:

$$\tau_s = m\alpha k \tag{3.8}$$

In this equation α is the ratio of the real contact area to the apparent contact area.

In addition, in order to explain the exact surface condition and overcome the limitation of friction model, several friction tests were also suggested for different bulk and sheet forming processes (Wanheim et al., 1974). However, due to the complex calculation of the abbreviations of certain quantities depending on sticking or slipping conditions, the most common friction models which are employed in mill industry are the Amontons-Coulomb friction model and the friction factor model as mentioned in the previous section.

3.5. ROLLING SPEED

Referring to equations (3.1) and (3.2) from Figure 3-1, the arbitrary strip velocity within the arc of contact may be represented as:

$$v = \frac{v_e h_e}{h_c + \frac{x^2}{R_{WR}}} \tag{3.9}$$

Likewise, the strip velocity at the neutral point may be expressed as:

$$v_n = v_R = \frac{v_e h_e}{h_c + \frac{x_n^2}{R_{WR}}} \tag{3.10}$$

Rearranging equation (3.10), and solving for the location of the neutral point yields the following expression:

$$x_n = \pm\sqrt{\frac{R_{WR}\left(v_e h_e - v_R h_c\right)}{v_R}} \tag{3.11}$$

where the negative sign is discarded as it indicates that the location of the neutral point is defined outside of the arc of contact.

Here, it needs to be mentioned that the difference between the strip speed and rolling speed through the roll bite causes slips in the roll gap to change the roll properties. If the work roll rotates with harmonic oscillations, the average rolling speed can be approximated to $\overline{v}_R$ as shown in Figure 3-3. Then rolling speed can be approximated as:

$$v_R \cong v_M \sin\left(\omega t\right) + \overline{v}_R \tag{3.12}$$

Throughout this study, however, the rolling speed v_R is used as an addition of an average rolling speed $\overline{v}_R$ and motor speed v_M instead.

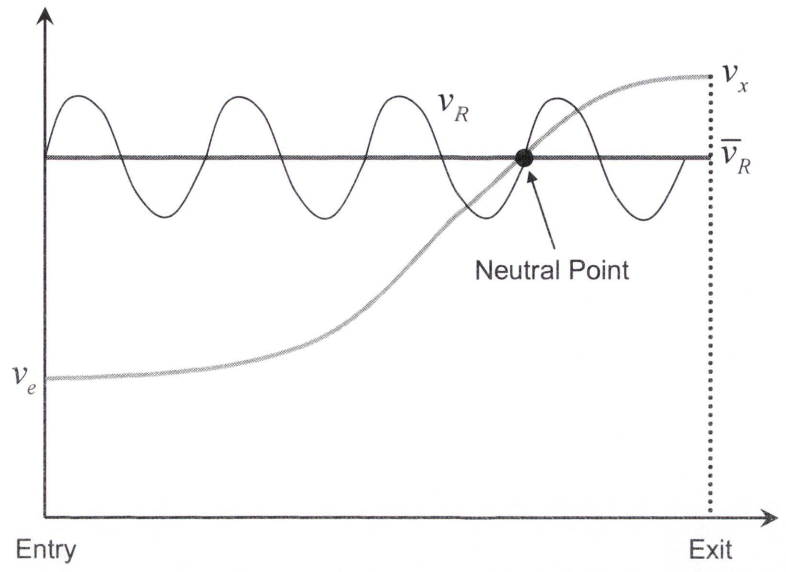

Figure 3-3: Rolling speed change in the roll gap

3.5.1. Variation of the Peripheral Rolling Speed of the Work Roll

According to Arimura et. al (1970), the variation of the rolling speed may be represented as a function of roll torque variation as follows:

$$v_{R,\mathrm{var}} = \Delta v_R = Q G_{\mathrm{var}} \tag{3.13}$$

where Q is the torque characteristics of the driving motor and G_{var} is the variation of the roll torque.

From equation above, the variation of the rolling speed causes torsional vibrations of the roll and motor spindles whose frequency ranges from 5 to 20 Hz as reported by Tamiya et al. (1980). However it is small compared with the frequency of third-octave-mode chatter as its resonant frequency generally falls within the range of the third musical octave (125 – 300 Hz). Its effect on the roll is negligible and has little loss of significance (Yun et al., 1998).

Therefore, it can be considered that variation of the peripheral roll speed is not significant during third- and fifth-octave mode chatter. Thus, the equation above becomes:

$$v_{R,\mathrm{var}} = 0 \tag{3.14}$$

3.5.2. Forward Slip

According to the principle of mass flow conservation, the speed of the incoming and outgoing strip is, respectively, slower and faster than the peripheral speed of the roll. For this reason, forward slip (Schey, 1983) is usually determined from experiment by first making scratch marks on the surface of the work rolls parallel with the roll axis at two different locations at a distance, l_0 apart, as shown in Figure 3-4. Therefore, forward slip during rolling can be defined in terms of exit speed of the strip and the surface speed of the roll as:

$$S_f = \frac{v_x - v_R}{v_R} \tag{3.15}$$

The usual and best way of monitoring forward slip is to mark the roll surface with two parallel lines a known distance (l_0) apart and measure the distance between the impressions of those lines of the rolled strip. The formula can be defined as:

$$S_f = \frac{l - l_0}{l_0} \tag{3.16}$$

where l is the distance between the two imprints, is then used to calculate S_f.

Thus, the relative velocity between the work roll and strip can be rewritten by using forward slip ratio.

$$\left(v_x - v_R\right) = S_f v_R \tag{3.17}$$

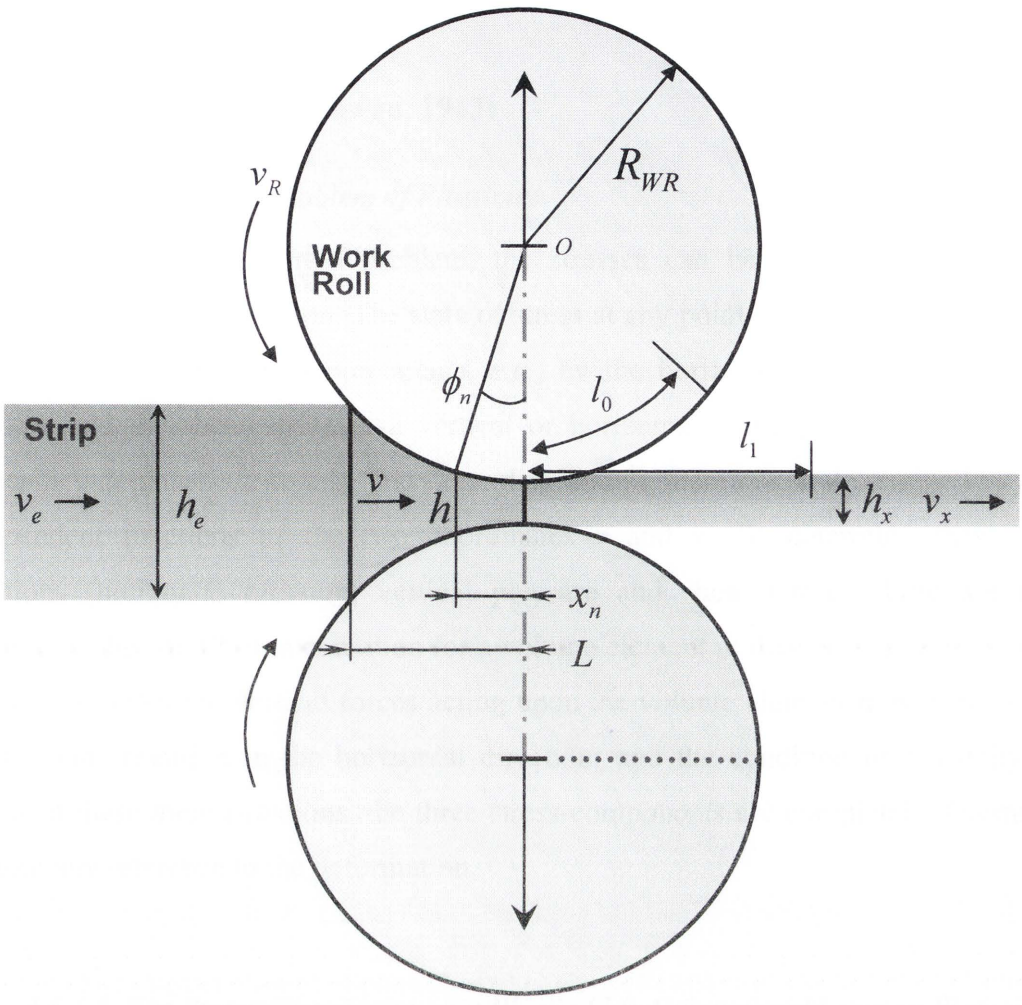

Figure 3-4: Measurement of forward slip

Similarly, the exit speed of the strip is faster than the strip entry speed due to the reduction in the roll bite. The effect of the backward slip on the roll gap can be expressed as:

$$v_e = (1 + S_b) v_R \tag{3.18}$$

where S_b is the backward slip.

3.6. FLOW STRESS

3.6.1. Yield Criterion (Orowan, 1943)

3.6.1.1. The Plane Problem of Plasticity

In the case of a plane-strain problem, the stresses can be calculated without any knowledge of the deformation. The state of stress at any point of the body is completely determined by three stress-components, *e.g.*, by the horizontal pressure, the vertical pressure and the shear stress in a vertical or horizontal plane (the shear stresses in perpendicular planes are equal). The stress distribution, therefore, is determined by three independent functions of the two coordinates x and y. To determine these three functions (horizontal pressure, vertical pressure and shear stress), there are three conditions: the equilibrium condition for a volume element in the vertical direction (*i.e.*, the condition that the vertical forces acting upon the volume element must vanish); the equilibrium condition in the horizontal direction; and the condition of plasticity. By means of these three equations, the three stress-components are completely determined without any reference to the deformation.

3.6.1.2. The Stress Distribution in a Plastic Slab Compressed between Plates

A fundamental theorem of the classical theory of plasticity, discovered by Hencky in 1923, presents that the stress distribution can be determined using a case of "plane problem" where there is a direction in the deformed body along which none of the variables (stresses and strains) changes. This is the case in rolling if there is no lateral spread. Soon after Hencky (1923) published his theorem, Prandtl (1923) found the mathematical solution of a two dimensional case of plastic deformation if the approximate distribution of stress over a cross-section of the rolled stock in flat rolling can be derived without spread.

The case treated by Prandtl is that of a plastic slab compressed between two parallel plates as shown in Figure 3-5. The problem being a plane one, we have to imagine the plastic slab and the compression plates extending into infinity in both directions perpendicular to the plane of the figure. Using rectangular coordinates x and y with the origin in the middle between the compression plates, let $s(x,y)$ be the vertical, $t(x,y)$

the horizontal pressure and $\tau(x, y)$ the shear stress in vertical and horizontal planes, h the distance between the plates, and k the yield stress in uniaxial constrained compression. c is a constant determined by boundary conditions and defined as $c^{\pm} = \pm k / h(L)$ where vertical pressure becomes zero for $x = \pm L$. According to Prandtl (1923), the stress distribution is then given by

$$s = c + \frac{k}{h}x \tag{3.19}$$

$$t = c + \frac{k}{h}x - k\sqrt{1 - 4y^2 / h^2} = s - k\sqrt{1 - 4y^2 / h^2} \tag{3.20}$$

$$\tau = \frac{k}{h}y \tag{3.21}$$

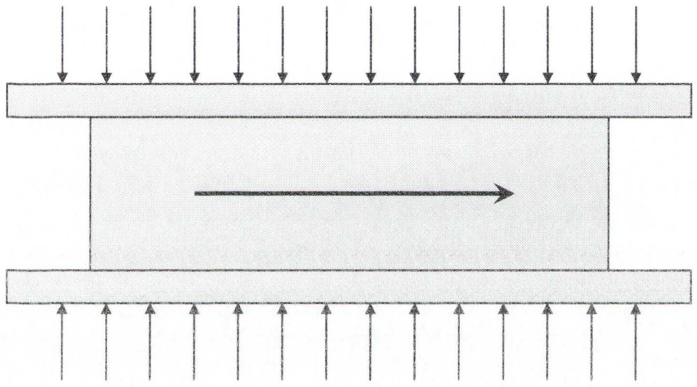

Figure 3-5: Plastic slab between parallel plates

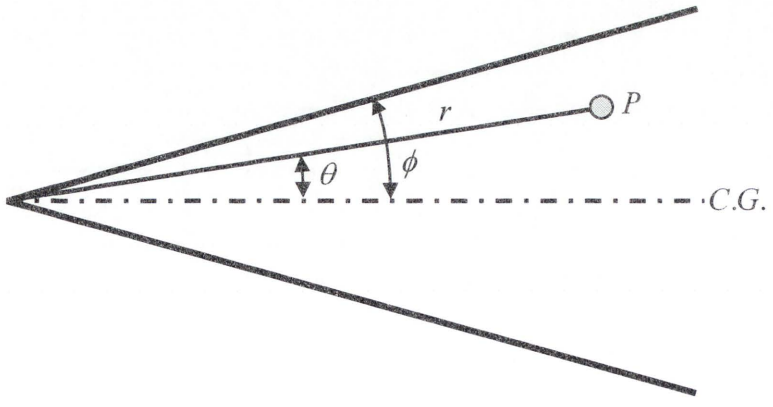

Figure 3-6: Non-parallel compression plates

However, the simple case treated by Prandtl differs in several respects from that of a material compressed between the rolls. The surfaces of the rolls are neither plane nor

parallel, and the being-rolled strip may slip on the rolls, instead of sticking in the roll gap. This problem has been treated by Nádai (1931) who applied Prandtl's mathematical method to polar coordinates, as shown in Figure 3-6.

As shown in Figure 3-7, replacing the rectangular coordinate (x, y) into the circular coordinate (ϕ, θ), *i.e.* y by θ and h by 2ϕ, the shear stress can further be defined by

$$\tau = \frac{\theta}{\phi}\mu s \tag{3.22}$$

where τ is the shear stress at the surface contact, ϕ is the angle of the arc of contact and θ is the subtended angle between the line connecting the point P and the plane of symmetry.

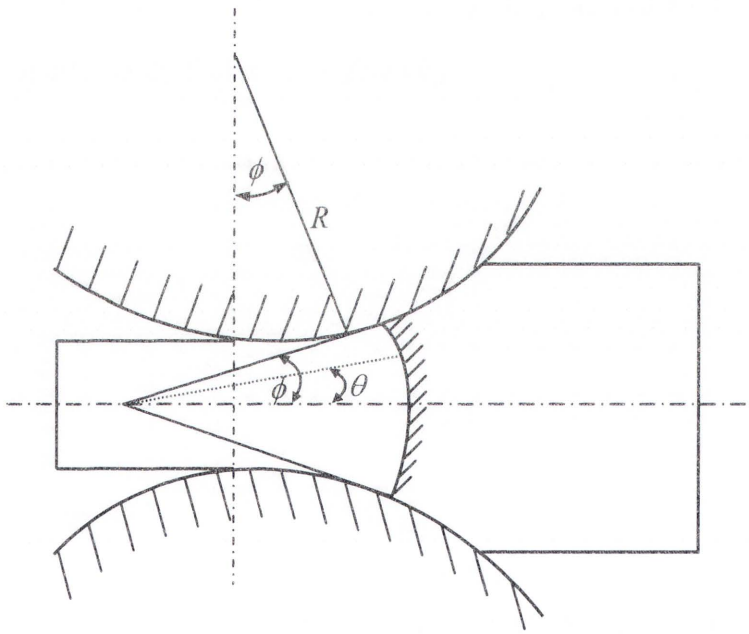

Figure 3-7: Representation of the roll contact angles between cylindrical rolls

3.6.2. Plastic Deformation in the Roll Gap

3.6.2.1. Strain-Hardening

From the equation (3.7), the formulation of the yield stress has been introduced by many researchers (Prakash et al., 1995) for the plane-strain cold rolling. Using the

Eulerian formulation, the strain-rate tensor which is normally used as a measure of deformation is defined by:

$$\dot{\varepsilon}_{ij} = \frac{1}{2}\left(\frac{\partial v_i}{\partial x_j} + \frac{\partial v_j}{\partial x_i} \right) \tag{3.23}$$

Here v_i is the component of the velocity vector with respect to the Cartesian coordinate x_i. For an isotropic rigid-plastic material, the deviatoric part S_{ij} of the stress tensor σ_{ij} is related to $\dot{\varepsilon}_{ij}$ by the relationship (Malvern, 1969)

$$S_{ij} = 2\kappa\dot{\varepsilon}_{ij} \tag{3.24}$$

The hydrostatic part or pressure p has to be determined from the constraint that the rate of volume changes $\dot{\varepsilon}_{kk}$ is zero. For materials yielding according to the von Mises criterion, the proportionality factor κ is given by

$$\kappa = \frac{\sigma_Y}{3\bar{\dot{\varepsilon}}} \tag{3.25}$$

where

$$\bar{\dot{\varepsilon}} = \sqrt{\frac{2}{3}\dot{\varepsilon}_{ij}\dot{\varepsilon}_{ij}}$$

The second invariant of $\dot{\varepsilon}_{ij}$ is called the effective strain rate and σ_Y (the flow stress in tension) is assumed to be independent of $\bar{\dot{\varepsilon}}$ and temperature.

When the loading is proportional, the flow stress of an isotropic strain-hardening material can be expressed in terms of the effective plastic strain $\bar{\varepsilon}$, which later can be obtained by integrating $\bar{\dot{\varepsilon}}$ along the particle path l.

$$\bar{\varepsilon} = \int_0^t \dot{\bar{\varepsilon}} dt \tag{3.26}$$

3.6.2.2. Full Range of Stress-Strain Curve

However, in order to obtain the full range of stress-strain curves for steel alloys, the nonlinear stress-strain behaviour is acknowledged in the American (ASCE, 1991), Australian (AS/NZS 4673, 2001) and South African (SABS, 1997) standards for cold-rolled stainless steel structures which define the stress-strain curve in terms of the Ramberg-Osgood expression (Ramberg and Osgood, 1941).

$$\varepsilon = \frac{\sigma}{E_0} + \varepsilon_p \left(\frac{\sigma}{\sigma_p} \right)^n \tag{3.27}$$

Equation (3.27) was originally developed for aluminium alloys but has proven for other nonlinear metals including stainless steel alloys for cold rolling. It involves the initial Young's modulus (E_0), the proof stress (σ_p) corresponding to the plastic strain ε_p, and a parameter (n) which determines the sharpness of the knee of the stress-strain curve. In the design of aluminium and stainless steel structures, it has become industry practice to use the 0.2% proof stress ($\sigma_{0.2}$) as the equivalent yield stress. For this proof stress, the stress-strain relationship takes the form,

$$\varepsilon = \frac{\sigma}{E_0} + 0.002 \left(\frac{\sigma}{\sigma_{0.2}} \right)^n \tag{3.28}$$

It has also become standard practice to determine the parameter (n) using the 0.01% and 0.2% proof stresses which leads to the following expression,

$$n = \frac{\ln(20)}{\ln(\sigma_{0.2} / \sigma_{0.01})} \tag{3.29}$$

Equation (3.29) ensures that the Ramberg-Osgood approximation matches exactly the measured stress-strain curve at the 0.01% and 0.2% proof stresses. It generally provides

close approximations to measured stress-strain curves for stresses up to the 0.2% proof stress.

In developing a model for the part of the stress-strain curve between the 0.2% proof stress and the ultimate tensile strength (σ_u), it is noted that the stress-strain curve in this range is similar in shape to the initial part of the stress-strain curve up to the 0.2% proof stress. This observation suggests a linear transformation of the stress and strain and the use of the Ramberg-Osgood expression (equation. (3.28)) in the following form,

$$\bar{\varepsilon} = \frac{\bar{\sigma}}{E_{0.2}} + \varepsilon_{u_p}\left(\frac{\bar{\sigma}}{\bar{\sigma}_u}\right)^m \quad \text{for } \sigma > \sigma_{0.2} \tag{3.30}$$

where $\bar{\varepsilon}$ and $\bar{\sigma}$ are the transformed strain and stress, defined as

$$\bar{\varepsilon} = \varepsilon - \varepsilon_{0.2} \tag{3.31}$$

$$\bar{\sigma} = \sigma - \sigma_{0.2} \tag{3.32}$$

The exponent (m) is obtained by trial and error using the stress-strain curves reported by Rasmussen (2003). Recognising that the exponent is dependent on the ultimate tensile strength in relation to the 0.2% proof stress, the following expression was obtained as:

$$m = 1 + 3.5\frac{\sigma_{0.2}}{\sigma_u} \tag{3.33}$$

The full-range stress-strain curve can be written out in full as follows:

$$\varepsilon = \begin{cases} \dfrac{\sigma}{E_0} + 0.002\left(\dfrac{\sigma}{\sigma_{0.2}}\right)^n & \text{for } \sigma \le \sigma_{0.2} \\ \dfrac{\sigma - \sigma_{0.2}}{E_{0.2}} + \varepsilon_u\left(\dfrac{\sigma - \sigma_{0.2}}{\sigma_u - \sigma_{0.2}}\right)^m + \varepsilon_{0.2} & \text{for } \sigma > \sigma_{0.2} \end{cases} \tag{3.34}$$

where n and m are given by equations (3.29) and (3.33), respectively.

In most loaded steel plates or columns, the strains are small when reaching the ultimate load for all practical ranges of length. It is therefore possible to base the design on the Ramberg-Osgood curve and achieve close agreement with experimental strengths.

3.6.2.3. Simplified Stress-Strain Curve

Material forming through flat rolling is one of the typical dynamic plasticity problems. In production, the contact stresses at the interface of roll and work-piece during rolling do significantly influence on productivity, product cost, product quality, and tool life cycle, etc. To properly analyse a process of rolling, correct evaluation of the contact stresses in the roll gap is essential for process design and product development.

Von Karman (1925) considered that the yield stress of the deforming metal would vary with the temperature and the speed of deformation but assumed it to be constant across the roll gap. Orowan (1943) recognised that the yield stress would vary as it deformed due to work-hardening, strain rate variation and temperature changes. It is now known that the magnitude of these effects depends on the history, composition and microstructure of the metal. Swift's stress-strain law (1952) adequately illustrates the versatility of the new formulation of the classical rolling solutions for hot or cold rolling. The exclusion of the derivative $d(2k)/d\phi$ from the reformulated rolling theories allows greater freedom in choosing an appropriate form for the yield stress function. A polynomial curve fit to the static and dynamic yield stress behaviour has been readily incorporated into the computer solution (Freshwater, 1996). The new methods of solution are therefore applicable for both hot and cold rolling where the yield stress is a function of strain, strain-rate, temperature and microstructure.

A great deal of effort has been made to model and measure distributions of the contact stresses. For example, Lenard et al. (1984; 1992) measured distributions of both the normal pressure and the friction stress in various rolling processes such as hot rolling, warm rolling and cold rolling of Al 1100. Until now, distributions of the contact stresses at the interface between the work roll and work-piece were experimentally measured with success. However, theoretical prediction in distribution of the local contact stresses has never been satisfactorily achieved due to the lack of suitable friction model.

First, the flow stress curves are anlaysed by Fields-Backofen equation, which is the common formula for most metal materials (Gronostajski, 2000)

$$\sigma_Y = \sigma_0 \varepsilon^{\gamma_1} \dot{\varepsilon}^{\gamma_2} \tag{3.35}$$

where σ_0 is the base yield stress of the material, γ_1 is the strain hardening exponent, and γ_2 is the strain rate sensitivity exponent. This equation is the most common formula to describe the stress-strain relationship and it can well express the work hardening phenomenon by the strain hardening exponent and the strain rate sensitivity exponent, which is the important parameter to influence the drawability of metal strip. So, the formability of AZ31 magnesium alloy sheet can be well expressed by the parameter in this equation.

The flow stress is given by the following formula that is commonly used:

$$\sigma_Y = \sigma_0 \varepsilon^{\gamma_1} \left(\frac{\dot{\varepsilon}}{\dot{\varepsilon}_{ref}} \right)^{\gamma_2} \tag{3.36}$$

For most metals, the dependence of σ_Y on $\bar{\varepsilon}$ can also be modelled by a power law:

$$\sigma_Y = \sigma_0 \left(1 + B\bar{\varepsilon}\right)^{\gamma_1} \tag{3.37}$$

Here B and γ_1 are material-dependent coefficients determined from the results of experiment. Since the material is assumed to be rigid-plastic, the plastic strains are equal to the total strains and hence the adjective 'plastic' is dropped hereafter when referring to strains.

This is often called Swift's stress-strain law for the yield function. It is adequate to demonstrate the versatility of the new formulations of the classical rolling solutions for hot or cold rolling. The form assumed for the yield stress function $2k(\phi)$ was not limited by the inclusion of the derivative $d(2k)/d\phi$ in the coefficient terms of the

controlling differential equations in the roll gap. Thus a wider range of functions may be used to represent the yield stress characteristics.

3.6.2.4. Effective Stress-Strain Curve

It is important to note that the flow stress is a parameter which specifies the resistance of the material to plastic deformation. It is fundamental to the determination of the force, torque and power required to roll the strip. The flow stress depends on the properties of the material, and also depends on the temperature, heat treatment, strain and strain rate. One model of the flow stress which may be appropriate for cold rolling mill can be defined by the equation:

$$\sigma_Y = \sigma_0 \left(1 + B\varepsilon\right)^{\gamma_1} \dot{\varepsilon}^{\gamma_2} e^{\gamma_3 T} \tag{3.38}$$

where σ_0 is a base value for the flow stress, T is the temperature, ε is the strain, $\dot{\varepsilon}$ is the strain rate, and B, γ_1, γ_2 and γ_3 are constants.

In order to use the dimensionless strain rate, $\dot{\varepsilon}_{ref}$ is given as to be 2000 s^{-1} in this study as the range of strain rate is limited between 1000 and 2000s^{-1}. The temperature influence is neglected because there is little temperature change in the cold rolling.

Also note that the strain rate needs to be expressed by taking the ratio of the roll gap strain rate $\overline{\dot{\varepsilon}}$ to reference strain rate $\dot{\varepsilon}_{ref}$ which was used in determining σ_Y.

$$\dot{\varepsilon} = \left(\frac{\dot{\varepsilon}_{gap}}{\dot{\varepsilon}_{ref}} \right) \tag{3.39}$$

3.7. STRAIN EXPONENT AND STRAIN-RATE SENSITIVITY

Strain rate is defined as the rate at which the strip is strained as it is deformed plastically. In general, the higher the strain rate, the higher the resistance to deformation, and the higher the effective yield stress of the material.

Strain rate effects have the potential to contribute to the chatter phenomenon in two ways. Firstly, as the mill is operating at a high rolling speed, strain rate is higher and the yield stress increases. Secondly, as the work rolls vibrate, there will be variations in the effective strain rate of the material in the roll gap.

For a component of length '*l*',

$$\dot{\varepsilon} = \left(\frac{d\varepsilon}{dt}\right) = \frac{d}{dt}\left(\frac{l - l_0}{l_0}\right)\frac{d}{dt} = \frac{1}{l_0}\frac{dl}{dt} \tag{3.40}$$

The total amount of strain applied to the strip as it moves through the roll gap can also be written as:

$$\varepsilon = \ln\left(\frac{h_e}{h}\right) \tag{3.41}$$

Alternatively, it is stated that the cumulative strain on the strip element passing through a roll gap is expressed as:

$$\varepsilon = \frac{2}{\sqrt{3}}\ln\left(\frac{h_e}{h}\right) \tag{3.42}$$

The difference between the two preceding equations is a constant term introduced to take account for the plane strain condition in the roll gap, that is, the assumption that the width of the strip element does not change.

Various equations have been proposed to model the strain rate. If it can be assumed that the roll gap profile is locally circular with minimum gap h_c and deformed roll radius R_d, then the roll gap at a distance x from the point of minimum actual gap may be represented by:

$$h(x) = h_c + \frac{x^2}{R_d} \tag{3.43}$$

The strain rate at point x with corresponding roll bite angle ϕ to the apparent centre of the deformed roll profile may be expressed by:

$$\dot{\varepsilon} = \frac{1}{h(x)} \frac{dh}{dt} = \frac{1}{h(x)} \frac{dh}{dx} \frac{dx}{dt} \tag{3.44}$$

Also, strain rate may be expressed in terms of the roll bite angle, measure with respect to the apparent centre of the deformed roll radius.

$$\dot{\varepsilon} = \frac{1}{h(\phi)} \frac{dh}{dt} = \frac{1}{h(\phi)} \frac{dh}{d\phi} \frac{d\phi}{dt} \tag{3.45}$$

Taking the derivative of equation (3.4) from the roll gap can be expressed as:

$$\frac{dh}{d\phi} = 2R_d \sin\phi \tag{3.46}$$

And the apparent angular velocity $d\phi / dt$ can be related to the actual angular velocity $d\theta / dt$ as in the following:

$$\frac{d\phi}{dt} = \frac{R_{WR}}{R_d} \frac{d\theta}{dt} = \frac{R_{WR}}{R_d} \frac{2\pi N}{60} \tag{3.47}$$

where N is the peripheral rolling speed of the work roll in unit of *rev/s* and θ is the angle subtended by the actual work roll axis. Therefore, in angular terms, strain rate as a function of the angular location in the roll gap can be written as:

$$\dot{\varepsilon} = \frac{1}{h(\phi)} 2R_d \sin\phi \frac{R_{WR}}{R_d} \frac{2\pi N}{60} \tag{3.48}$$

Strain rate at a given state may be expressed as:

$$\dot{\varepsilon} = \frac{2Lv_R}{R_d h(\phi)} \tag{3.49}$$

Also, due to work hardening in the roll gap, the effective strain rate expressed in terms of strain rate is given by noting that,

$$\dot{\varepsilon} = \frac{4}{\sqrt{3}} \frac{Lv}{R_d h(\phi)} \tag{3.50}$$

Equation (3.50) is equivalent to the form of strain rate presented by Qui et al. (1999) as:

$$\dot{\varepsilon} = \frac{4}{\sqrt{3}} \frac{v_x h_x}{h^2} \tan\phi .$$

3.8. TENSION

To investigate the stress distribution from the entry and exit sides, it is assumed that the entry thickness h_e is constant in a sense that the undesired motions of the work roll and strip do not affect the rolling reduction during the rolling process.

It is possible to assume that the entry speed v_e is constant and the exit speed v_x is the result of the interaction between the work roll and strip. Considering the circumferential speed of the work roll, the exit speed v_x can be written as

$$v_x = R_{WR}\left(\omega_i + \dot{\theta}\right) \tag{3.51}$$

Under the steady-state operating conditions (no-slip happens), which means that the neutral point exists within the certain point of the arc contact; the variations of the circumferential speed $R_{WR}\omega_i$ becomes negligible during rotations. It follows correspondingly that the velocity variation of the rolled strip at an arbitrary or neutral point is given by

$$v_{n,\mathrm{var}} = \frac{h_x R_{WR} \dot{\theta}}{h_n} \tag{3.52}$$

The neutral or delivery thickness h_n needs to be determined within the length of arc of contact when calculating the back and front elongations. The variation $v_{n,\mathrm{var}}$ can then be integrated into two components for the back and front sides at the neutral or delivery point. Therefore, variations of inter-stand distance can be expressed as:

$$\Delta D_b = \int_0^t \left(v_{n\,\mathrm{var}}\right)_b dt = \int_0^t \left(\frac{h_n R_{WR} \dot{\theta}}{h_e} \right)_b dt = \frac{h_n R_{WR} \theta}{h_e} \tag{3.53}$$

$$\Delta D_f = \int_0^t \left(v_{n,\mathrm{var}}\right)_f dt = \int_0^t \left(\frac{h_x R_{WR} \dot{\theta}}{h_n} \right)_f dt = \frac{h_x R_{WR} \theta}{h_n} \tag{3.54}$$

Stresses at both entry and exit sides are in fact the results of inter-stand interaction in a tandem mill configuration. Applying Hooke's law for expressing the back and forth strip tension stresses yields:

$$t_{e,\mathrm{var,i}} = \frac{E}{D_{i-1}} \Delta D_b \tag{3.55}$$

$$t_{x,\mathrm{var,i}} = \frac{E}{D_i} \Delta D_f \tag{3.56}$$

where $(\Delta D)_{b,f}$ is the elongation from back and front sides of the strip.

However, equations (3.55) and (3.56) are only related to torsional vibration due to the angle caused by variation of rolling speed and would require more degrees of freedom to find analytical solution for cold rolling.

3.8.1. Variation of Strip Tension by Arimura and Tlusty

Tlusty (1982) came up with an estimate for the magnitude and phase of rolling force components. He developed a criterion for assessing whether the negative damping effect exceeds the positive damping effect, leading to amplification of the oscillation. Under

Tlusty's assumption of no roll deformation, strip velocity at the entry side can be expressed as:

$$v_e = \left(\frac{v_x}{h_e}\right) h_x = \left(\frac{v_x}{h_e}\right)\left(h_c + 2X\sin(\omega t)\right) \tag{3.57}$$

where X is the amplitude of the work roll, ω is the forcing (operating) frequency and time t is a variable along the roll gap.

Tension is applied on the strip between stands, and it deforms the strip plastically. The deviation of the inter-stand tension is determined by integrating the difference between the variation of the outgoing strip speed at one stand and the variation of the incoming strip speed at the next stand as presented below (Arimura et al., 1970):

$$t_{e,\mathrm{var},i} = \frac{E}{D_{i-1}}\int_0^t \left(v_{e,\mathrm{var},i} - v_{x,\mathrm{var},i-1}\right) dt \tag{3.58}$$

$$t_{x,\mathrm{var},i} = \frac{E}{D_i}\int_0^t \left(v_{e,\mathrm{var},i+1} - v_{x,\mathrm{var},i-1}\right) dt \tag{3.59}$$

Therefore, the strip is subject to a variable amount of elongation ΔD where D is the inter-stand distance.

$$\Delta D(t) = \int_0^t \left(v_{e,\mathrm{var},i} - v_{x,\mathrm{var},i-1}\right) dt = \frac{2Xv_x}{h_e}\int_0^t \sin(\omega t)\, dt = \frac{2Xv_x}{\omega h_e}\left(1-\cos(\omega t)\right) \tag{3.60}$$

Note that

$$\int_0^t \sin(\omega t)\, dt = \left[-\frac{1}{\omega}\cos(\omega t)\right]_0^t = \frac{1}{\omega}\left(1-\cos(\omega t)\right)$$

The variable elongation rises from zero at time t=0, to a maximum value when ωt=π, and then back to zero. Thus, the variable elongation leads to a variation in tension $t_{e,x}$ in the strip between inter-stands, where tension is being expressed as a positive quantity.

$$t_e = t_{avg} + E\frac{\Delta D}{D} = t_{avg} + \frac{2EXv_x}{D\omega h_e}\left(1-\cos\left(\omega t\right)\right) \tag{3.61}$$

Applying Tlusty's simplified rolling force model, the variable component of the rolling with tension variation can be identified. Note that equation (3.61) is for both upper and lower rolls and it should be divided by 2 for one side.

At time ωt=0, cosine term becomes +1, which represents the gap spacing increases. Therefore, tension is increasing as the elongation of the strip on the entry side is increasing, and the rolling force is starting to decrease.

At time $\omega t=\pi/2$, the gap spacing is at its maximum extent. The elongation and tension are rising, and the rolling force is falling significantly.

At time $\omega t=\pi$, the work roll is moving towards each other and the elongation and entry tension reach at maximum value, and the rolling force reaches its minimum.

The phase of this cosine term "leads" the original presumed oscillation by 90 degrees.

3.8.2. Variation of Strip Tension by Yun and Hu

Under conditions by Tlusty's model and many others, when the work roll is oscillating, the mass flow is assumed to constant. The previously performed result based on the linear scheme is also assumed to constant. For dynamic analysis of cold rolling mill, some modifications are necessary. The relationship between the mass flow at the entry and exit sides of the roll gap may be now expressed as:

$$v_e h_e = v_x h_x + \frac{dA}{dt} \tag{3.62}$$

$$A\left(t\right) = A_c + 2\Delta DX\sin\left(\omega t\right) \tag{3.63}$$

$$\frac{dA}{dt} = 2\Delta DX\omega\cos\left(\omega t\right) \tag{3.64}$$

where A represents the cross-sectional area of the roll gap.

The variable speed of the strip at the roll gap entry may now be expressed as:

$$v_e = \frac{1}{h_e}\left(v_x h_x + 2Xv_x \sin(\omega t) + 2\Delta DX\omega\cos(\omega t)\right) \tag{3.65}$$

and the variable elongation can be expressed as

$$\begin{aligned}\Delta D(t) &= \int_0^t \left(v_{e,\mathrm{var},t} - v_{x,\mathrm{var},t-1}\right)dt = \frac{2Xv_x}{h_e}\int_0^t \sin(\omega t)\,dt + \frac{2X\Delta D\omega}{h_e}\int_0^t \cos(\omega t)\,dt \\ &= \frac{2Xv_x}{h_e\omega}\left(1-\cos(\omega t)\right) + \frac{2X\Delta D}{h_e}\sin(\omega t)\end{aligned} \tag{3.66}$$

Therefore, variation of the entry tension can be written as:

$$t_e = t_{avg} + E\frac{\Delta D}{D} = t_{avg} + \frac{2EXv_x}{D\omega h_e}\left(1-\cos(\omega t)\right) + \frac{2EX\Delta D}{Dh_e}\sin(\omega t) \tag{3.67}$$

The variable of tension fluctuation may change the magnitude of rolling force and the roll gap spacing will be changed accordingly. Thus, it will lead vibration response to shift 90 degrees in-phase or out-of-phase with 40-300*MPa* of tension.

It seems to the Author that the vibration responses due to the tension variation have the same phase in response to the roll gap disturbance and operating frequency cannot be treated as an input function for the mill vibration analysis. Nonetheless, the above strip tension stresses define the connections between mill stands which are very useful when studying inter-stand relationships that might give rise to the chatter phenomenon.

3.9. SUMMARY

This chapter has focused on the effects of rolling parameters providing detail explanations how the rolling process works in the roll bite profile. In doing so several key rolling parameters regarding the influence of the roll gap were discussed. Even though rolling chatter has been investigated in various ways, our understanding is still limited because of the complicated nature of the rolling process itself. For instance, elastic flattening of the work roll is not valid when the rolling force caused by the deformation resistance is too high or when the reduction and friction coefficient is very small. Moreover, friction model employed in this study does not precisely take into account hydrodynamic effect in the lubricated roll gap because of its complexity even though there is a large amount of friction model presented to describe the dynamically lubricated contacts. On the other hand, the deformation resistance and tension variation model are quite varied depending on the assumptions made in individual studies.

Among the existing models of the rolling process, some are too simplified to precisely capture the characteristics of the rolling process, while the rest of them are too complicated to allow for an analytical solution. Up to now, only very few are capable of dealing with dynamic behavior in the practical rolling process. Therefore, in Chapter 4, it will be discussed for the improvement of the rolling process model, which should be able to accurately predict the rolling force and be simple enough to have an analytical form.

CHAPTER 4. STEADY-STATE ROLLING FORCE AND DYNAMIC ROLLING FORCE IN THE MODIFIED ROLL GAP MODEL

4.1. INTRODUCTION

This chapter mainly deals with the derivation of the steady-state and dynamic rolling force and its formulation is basically based on the roll gap model resulting from Bland and Ford approach (1948). In cold rolling, there are many factors which are affecting rolling conditions such as the roll radius, friction coefficient, rolling speed, reduction, reduction rate in the roll gap and tension between inter-stands. In the earliest of rolling theories, rolling mill is designed for squeezing and compressing the strip, which is rather thick material such as copper and aluminium with less hard strength. Therefore, utilizing the conventional roll gap model to the state of the art mill technology is rather limited when using very thin strip. Nonetheless, a roll gap model is at the heart of any rolling mill set-up system. The roll gap model basically calculates the rolling force and torque on each stand based on the known strip reduction, friction coefficient, tension yield stress. The prediction of the rolling force must be very accurate so that the roll gap positions and work roll speeds can be set appropriately to achieve the target strip thickness as soon as possible after the strip has threaded through the cold rolling mill.

However, surface conditions are always fluctuating due to the change in friction and the accelerated rolling speed even though mill is accurately set to roll the strip. During the rolling process, rolls are also experiencing the deformation such that the roll gap is changed due to the deformed roll radius. The change in roll radius also allows the coefficient of friction to increase or decrease depending on the rolling speed and the lubrication of oil. Without the accurate control of surface condition in the roll gap, this will cause unstable vibration in the end.

Therefore, this chapter will develop the new method of expressing the mill vibration based on Bland and Ford approach (1948). According to the conventional roll gap model, rolling force and torque are a function of the entry/exit strip thickness, yield

stress, tension and friction coefficient. In fact, rolling force and torque is also dependent upon the rolling speed as the strip deforms plastically with strain and strain rate effect. In Chapter 4, therefore, in order to overcome the limitation of rolling force and torque calculation theory, the effect of the strain and strain rate on work hardening in the roll gap is also presented.

The calculated roll separating force basically contains two parts; frictional and deformational rolling force. If the disturbance in the roll gap occurs, resonant natural frequencies will be shifted due to the change in roll gap profile. Among factors shifting the natural frequency, there will be the variations of the roll gap thickness, the rolling speed, the coefficient of friction, the roll radius and the reduction rate, *i.e.*, the rate of the change in roll gap thickness (with respect to time).

Therefore, this chapter specifically explains the formulation of the dynamic rolling force due to the variations of the roll gap profile; how these variations influence the roll gap profile and what parameters significantly cause unstable vibrations or chatter in a rolling stand of cold rolling mill.

4.2. STEADY-STATE ROLLING FORCE

4.2.1. Normal Pressure at the Entry and Exit Sides

Starting with the classical work of Siebel (1924, 1925) and von Karman (1925), many attempts have been made during the 1920s to obtain an approximate method of calculating roll pressure from the geometrical and physical data of the roll gap profile. Most prominent among them are Orowan (1943) and Bland and Ford (1948) who developed the well known gap model. Their roll gap model assumes that, for the purpose of the calculation, the being rolled gap is considered as consisting of thin vertical segments perpendicular to the direction of rolling, with no shear stress but only normal pressure acting between the neighbouring segments, and the plastic deformation of the segments is assumed to be a homogeneous compression.

The objective of this section is to review the roll gap model used to estimate the steady-state rolling force and torque. Furthermore, it will be described how the roll gap model is closely related to rolling parameters. Its derivation of equation for calculating the

normal pressure distribution curve will be dealt with for identifying the dynamic rolling parameters, which is not a constant during the practical rolling process. The following theories are cited from the literature (Orowan, 1943; Bland and Ford, 1948) and re-edited by Author for convenience.

As shown in Figure 3-1 again, based on the roll gap geometry in terms of surface contact angle (ϕ) rather than the roll gap length ($R_{WR}\sin\phi$), horizontal rolling force is defined as:

$$\frac{df}{d\phi} = 2sR_d\cos\phi\left(\tan\phi \pm \mu\right) = 2sR_d\left(\sin\phi \pm \mu\cos\phi\right) \tag{4.1}$$

where for the exit side, upper sign should be used, while the lower sign is appropriate for the entry side. Equation (4.1) is a variational form of the well-known von Kármán equation (1925).

Note that the above equation is identical with Orowan's homogeneous compression theory. This equation contains two unknown functions, *i.e.*, the horizontal force f and the normal pressure s on the roll surface. To find horizontal force and the normal pressure, it is further assumed that the normal pressure s is approximately equal to the vertical pressure.

Equation (4.1) containing s and f is given by the plasticity condition of approximation since principle stress $p = f/h$. In fact, the state of stress in a strip between the rolls is not uniaxial. However, if there is no lateral spread, there is also another horizontal pressure parallel to the roll axes; ignore this as it vanishes in practically unimportant case of free lateral spread. Both p and q are constant within a vertical plane of the strip if the assumption of homogeneous compression is made. The horizontal pressure p then can be calculated by dividing the horizontal force f by the gap thickness h of the surface contact.

Thus,

$$s = p + \sigma = \frac{f}{h} + \sigma \tag{4.2}$$

Now remove f from equations (4.1) and (4.2), convert the resulting differential equation for s into a convenient form for integration. Using the conditions at entry and exit to determine the integration constants, explicit equations are obtained for s as follows:

$$s = c \times \sigma \times \frac{h}{R_d} \times e^{\pm \mu H} \tag{4.3}$$

where σ is the yield strength. s, c and H are defined by the equation below.

$$s_x = \sigma_x - t_x \tag{4.4}$$

$$c = (\sigma_x - t_x) / \left(\sigma_x \times \frac{h_x}{R_d} \right) = \frac{R_d}{h_x} \left(1 - \frac{t_x}{\sigma_x} \right) \tag{4.5}$$

$$H = 2\sqrt{\frac{R_d}{h_x}} \arctan\left(\sqrt{\frac{R_d}{h_x}} \phi \right) \tag{4.6}$$

Substituting back into equation (4.3) and denoting s on the exit side by s^+, the normal pressure at the exit side can be solved and written as:

$$s^+ = \frac{\sigma h}{h_x} \left(1 - \frac{t_x}{\sigma_x} \right) e^{\mu H} \tag{4.7}$$

Similarly on the entry side, the normal pressure can be expressed as:

$$s^- = \frac{\sigma h}{h_e} \left(1 - \frac{t_e}{\sigma_e} \right) e^{\mu (H_e - H)} \tag{4.8}$$

where t_e and t_x indicate back and front tension expressed as a pressure and s^- denotes s on the entry side. In particular, when no front or back tensions are applied,

$$s^{+} = \frac{\sigma h}{h_x} e^{\mu H} \tag{4.9}$$

and

$$s^{-} = \frac{\sigma h}{h_e} e^{\mu(H_e - H)} \tag{4.10}$$

In order to obtain the pressure distribution, equations (4.7) and (4.8) can be solved in an iterative way. Since the strip thickness decreases and the yield strength increases when the strip travels from the entry to the exit side of the roll gap. However, since the product of the strip thickness and yield stress is not constant along the surface contact in the roll gap when rolls are oscillating, it may not be reasonable to assume that the product of two variables remains as denoted by Yun et al. (1998).

The reason is due to the deformation resistance of the material. When the material is compressed within the roll gap with a certain rolling speed, the strip is deformed plastically due to work-hardening. In most rolling theories, work-hardening is related to the strain exponent only but in fact, it is also affected by the strain rate sensitivity which is affected by the rolling speed. A detailed explanation will be given in Section 4.2.3 to see if the deformation resistance is a function of the strain and strain rate.

4.2.2. The Equation for the Neutral Angle (Point)

When calculating the rolling force or torque, it is of importance to determine the neutral point as it affects the roll gap as one of the most crucial variables. The neutral point contains interesting properties where the normal roll pressure reaches to its maximum and, at this point, the rolling speed is equal to the strip speed. Moreover, it is a critical point where the friction changes its sign with respect to the entry and exit sides. Using the subscript *n* to denote the neutral point, it can be defined as:

$$s_n^{+} = s_n^{-} \tag{4.11}$$

Substituting from equations (4.7) and (4.8),

$$\frac{\sigma_n h_n}{h_x}\left(1-\frac{t_x}{\sigma_x}\right)e^{\mu H_n}=\frac{\sigma_n h_n}{h_e}\left(1-\frac{t_e}{\sigma_e}\right)e^{\mu(H_e-H_n)} \tag{4.12}$$

from which

$$H_n=\frac{H_e}{2}-\frac{1}{2\mu}\ln\left\{\frac{h_e}{h_x}\left(\frac{1-\frac{t_x}{\sigma_x}}{1-\frac{t_e}{\sigma_e}}\right)\right\} \tag{4.13}$$

ln denotes logarithm to base *e*. When no tensions are applied

$$H_n=\frac{H_e}{2}-\frac{1}{2\mu}\ln\left(\frac{h_e}{h_x}\right) \tag{4.14}$$

and from equation (4.6)

$$\phi_n=\sqrt{\frac{h_x}{R_d}}\tan\left(\sqrt{\frac{h_x}{R_d}}\times\frac{H_n}{2}\right) \tag{4.15}$$

The neutral angle ϕ_n is given by combining equations (4.13) and (4.15) when tensions are applied, otherwise by equations (4.14) and (4.15).

Note that this theory had been developed for rolling model with having a high reduction. The strip rolling sample was also based on high conductivity copper with low yield stress. Therefore, the theory has limitations for the very thin cold rolling which cause high yield stress in the roll gap. So the evaluation of the presented theory may not be suitable for certain rolling conditions, for example, less than 0.2*mm* thickness and also less than 0.007 friction coefficient.

4.2.3. Flow Stress

The deformation resistance model for the flow stress, σ_Y, is expressed as:

$$\sigma_Y = \sigma_0 (1+\varepsilon)^{\gamma_1} (\dot{\varepsilon}^*)^{\gamma_2} \tag{4.16}$$

With ε and $\dot{\varepsilon}^*$ being the strain and dimensionless strain rate:

$$\varepsilon = \frac{2}{\sqrt{3}} \ln\left(\frac{h_e}{h(\phi)}\right) \text{ and } \dot{\varepsilon}_{gap} = \frac{4v(\phi)L}{\sqrt{3}h(\phi)R_d}$$

where σ_0 is the base yield strength, ε is the strain, $\dot{\varepsilon}^* = \dot{\varepsilon}_{gap} / \dot{\varepsilon}_{ref}$ is the dimensionless strain rate, $\dot{\varepsilon}_{gap}$ is the strain rate, $\dot{\varepsilon}_{ref}$ is the strain rate reference, γ_1 is the strain hardening exponent and γ_2 is the strain rate sensitivity exponent, which is the important parameter to influence the process of metal sheet. L is the deformed length of arc contact in the roll gap and R_d is the deformed roll radius. Table 4-1 shows many different types of constitutive deformation models for various materials, as reviewed by Alexander et al. (1988), Johnson and Cook (1983), Gronostajski (2000).

Table 4-1: Constitutive models for deformation resistance in metals and alloys

Alexander's empirical model (1988) for copper and aluminium					
$\sigma_Y = \sigma_0 (1+A_1\varepsilon)^{\gamma_1} (1+A_2\dot{\varepsilon}^*)^{\gamma_2}$	$\sigma_0 (MPa)$	A_1	A_2	γ_1	γ_2
	97.75	96.8	1.0	0.2	0.0
Johnson-Cook (JC) Model* (1983) for 1006 steel and 4340 steel					
$\sigma_Y = (A_1 + B_1\varepsilon)^{\gamma_1} (1 + A_2 \log\dot{\varepsilon}^*)(1 - T_n^{m_1})$	$A_1 (MPa)$	$B_1 (MPa)$	A_2	γ_1	m_1
	350	275	0.022	0.36	1.00
$\sigma_Y = (A_2 + B_2\varepsilon)^{\gamma_1} (1 + A_3 \log\dot{\varepsilon}^*)(1 - T_n^{m_2})$	$A_2 (MPa)$	$B_2 (MPa)$	A_3	γ_1	m_2
	792	510	0.014	0.26	1.03
Swift's Model (1952) for mild steel					
$\sigma_Y = \sigma_0 (A_1 + \varepsilon)^{\gamma_1}$	$\sigma_0 (MPa)$	A_1	A_2	γ_1	γ_2
	740	0.01	-	0.23	-
	$\sigma_0 (MPa)$	A_1	A_2	γ_1	γ_2
	811.4	0.002	-	0.24	-
Modified Swift's Model for mild and hard steel (reviewed by Gronostajski, 2000)					
$\sigma_Y = \sigma_0 (A_1 + \varepsilon)^{\gamma_1} (\dot{\varepsilon}^*)^{\gamma_2}$	$\sigma_0 (MPa)$	A_1	A_2	γ_1	γ_2
	600	1.00	-	0.26	0.08

* $T_n = (T - T_r)/(T_m - T_r)$ where T_n is the homologous temperature, T is the current absolute temperature, T_r is the reference temperature and T_m is the melting temperature.

For the determination of deformation resistance model to be used in the cold rolling process, Figure 4-1 presents stress-strain curves for the elastic-plastic and plastic deformations, respectively. Among them are modified Swift's model (1952) used for forming a high-strength steel as indicated by a full-range (elastic and plastic range) stress-strain curve (2003). Strain hardening exponent and strain rate sensitivity have been further investigated to "successfully" evaluate material flows and deformation by Wagoner and Wang (1983).

In Figure 4-2(a) and (b), it is illustrated based on the industry observation that friction coefficient mainly determines the magnitude of friction hill while rolling speed shifts the deformation hill.

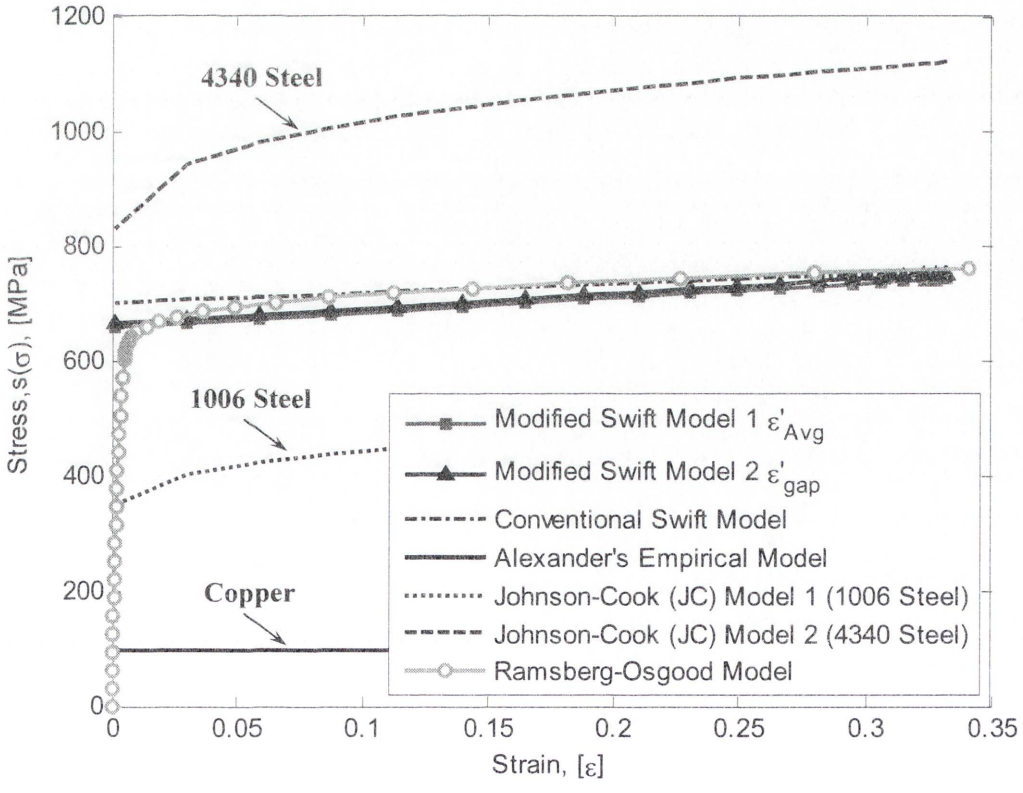

Figure 4-1: Many different types of stress-strain curves used in rolling process [Alexander et al. (1988), Johnson and Cook (1983), Gronostajski (2000)]

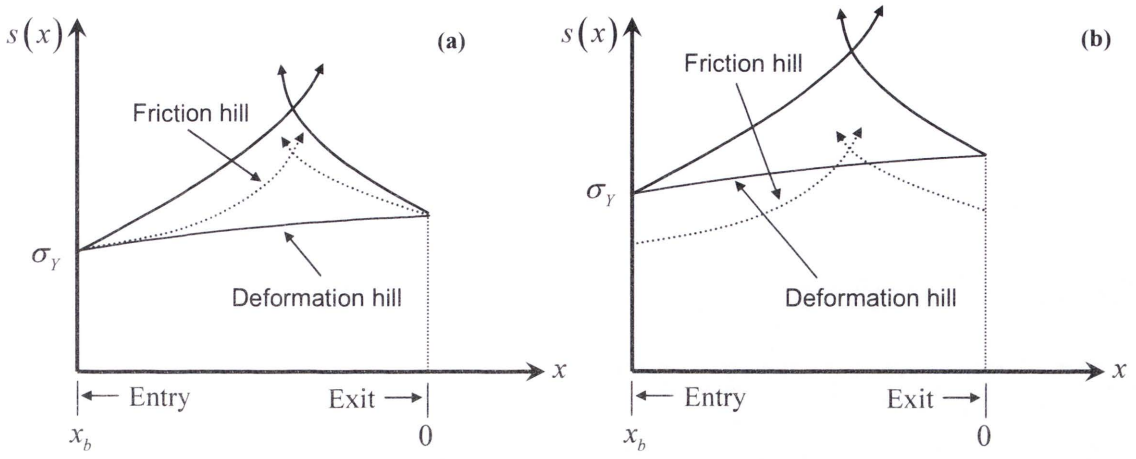

Figure 4-2: Exaggerated curves for illustrating the rolling pressure distribution change in determining (a) friction hill and (b) deformation hill [Roberts (1978)]

In order to identify those trends, as shown in Figure 4-3, four different sets of rolling pressure distributions calculated for the key rolling parameters are presented. Figure 4-3(a) describes the effect of tension applied on the pressure distribution and tensions given on both sides reduce the peak rolling pressure up to 19.3%. Figure 4-3(b) indicates the influence of reduction by keeping the exit thickness constant. More interestingly, friction coefficient and rolling speed have more significant effects on the rolling pressure distribution curve than the others, and peak magnitude rapidly increases as the friction coefficient and roll speed increase at the given conditions. In particular, rolling force is varying with the change in friction coefficient and increases up to 11.4% when the friction coefficient increases to 0.025 from 0.020. In Figure 4-3(d), rolling force also varies with the change in rolling speed and increases up to 1.1% when the rolling speed changes from 1200 to 1300*mpm*, *i.e.*, the change in rolling speed of about 1.67*m/s*. The rate of change of rolling force depending on the increase of rolling speed may differ from the practical experiment set-ups.

On the other hand, the neutral point tends to move towards the entry side for the change in friction coefficient while its position also shifts to the entry side for the change in roll speed, as shown in Figure 4-3(c) and (d), respectively. Note that without the relevant relationship between the friction and roll speed, the position of neutral point cannot properly be traced along the arc of surface contact in the roll gap. Therefore, in this study, it is assumed that a neutral point reasonably maintains its position even though it is moving within the roll bite.

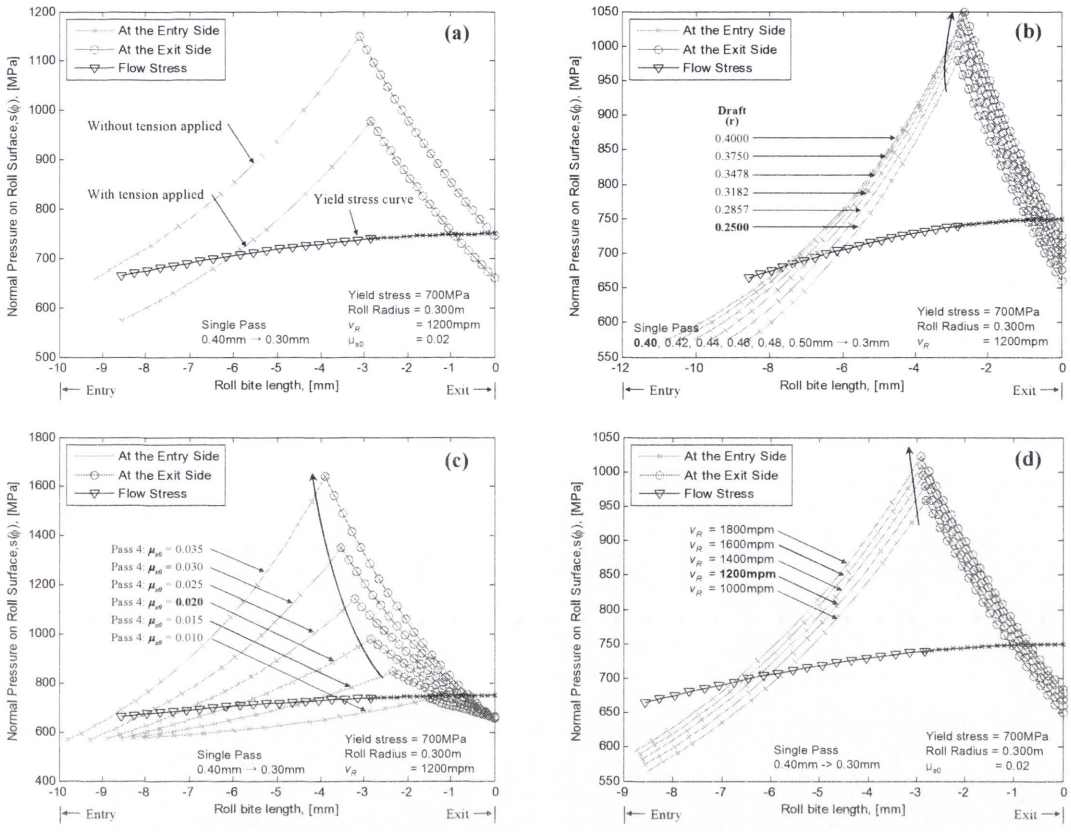

Figure 4-3: The pressure distribution curves based on Bland and Ford theory; (a) with and without tension applied to the strip, (b) reduction change, (c) friction coefficient change and (d) rolling speed change

4.2.4. The Estimation of the Rolling Force

To determine an explicit solution for the steady-state rolling force, the normal pressure distribution curve by Bland and Ford theory (1948), based on Orowan theory (1943), is considered during the steady-state rolling process. By doing so, the rolling force can be calculated by the integration of the pressure distribution under the given roll profile. The roll force per unit width, F_{sp}, is the integral of the vertical pressure, q, along the arc of contact as in the following:

$$F_{sp} = \int_0^{\phi_e} q \times R_d d\phi = R_d \int_0^{\phi_e} q d\phi \tag{4.17}$$

Using approximation that the normal pressure s is equal to the vertical pressure q, rolling force at the steady-state condition can be calculated as:

$$F_R = R_d W \left[\int_{\phi_x}^{\phi_n} s^+ d\phi + \int_{\phi_n}^{\phi_e} s^- d\phi \right] \tag{4.18}$$

where s is the pressure distribution caused by the surface contact between the work roll and strip. s^- and s^+ denotes pressure curve on the entry and exit sides. R_d is the deformed roll radius calculated by Hitchcock theory (1935) and W is the strip width. F_R stands for the resultant rolling force without having any dynamical disturbance and is pointing at the neutral point where the rolling pressure becomes maximum. The horizontal and vertical rolling force can then be defined by the trigonometry as below.

$$F_H = F_R \sin\phi_n \tag{4.19}$$

$$F_V = F_R \cos\phi_n \tag{4.20}$$

Thus the resultant rolling force can be combined using trigonometry again.

$$F_R = \sqrt{F_H^2 + F_V^2} \tag{4.21}$$

Table 4-2: Key rolling parameters for the calculation of the steady-state rolling force

Entry/Exit Thickness, Width, Roll Radius [*mm*], Reduction [*%*], Young's Modulus (*MPa*) and Yield strength (*MPa*), Entry/Exit tension (*MPa*)								
h_e	h_x	W	R_{WR}	R_{BR}	r	E	σ_0	$t_{e,x}$
0.40	0.30	1,224	300	676	25.0	210	700	90

Strain	Work-Hardening Constant		Deformed Roll Radius [*mm*]	Neutral point [*Rad*]	Speed [*m/s*]	Friction	Rolling Force [*MN*]	
ε	γ_1	γ_2	R_d	ϕ_n	V_R	μ_{s0}	F_H	F_V
0.3322	0.26	0.08	733.2	0.0039	20.00	0.02	0.031	8.01

Parameters used for the calculation of pressure distribution curve and rolling force are shown in Table 4-2. By so doing, the rolling force can be calculated by the integration of the pressure distribution under steady state conditions. With the given reduction of 25% flowing out of the roll gap, the steady-state rolling force is estimated around

8.0*MN*. For more details of rolling force calculation procedure, Appendix I is provided with two integration methods evaluated by Simpson's rule and iterative method.

4.2.5. Re-consideration of the Neutral Point (Angle)

A neutral point where the normal pressure is at a maximum is determined by an integral form for pressure distribution curve from entry to exit side of the strip. In this study, neutral point, often referred to neutral angle, is defined by two intersect lines from the integration by Bland and Ford approach (1948). It can be represented by the roll gap parameters such as the reduction, coefficient of friction, deformed roll radius, yield stress and tensions and is usually given as the function below:

$$\phi_n = f\left(\phi, \Delta h, R_d, \sigma_Y, t_{e,x}, \mu_{s0}\right) \tag{4.22}$$

Note that it is assumed that the friction coefficient is constant along the roll gap. Let us have a close look at the movement of the neutral point as shown in Figure 4-4 below. Under the given steady-state condition, the neutral angle given by the change in friction coefficient may move along the deformed arc of contact surface unless the coefficient of friction reduces to less than 0.007 at which it lies beyond boundary limits. The assumption taken is that other rolling conditions remain constant even though a work roll deforms.

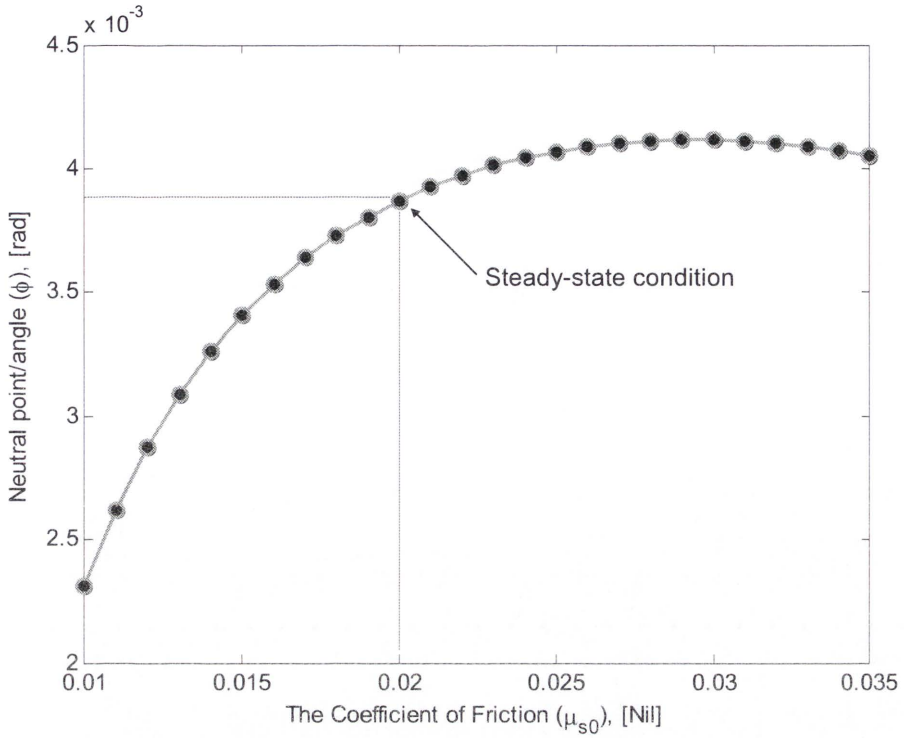

Figure 4-4: Displacements of the neutral point calculated by Bland and Ford theory

4.3. DYNAMIC ROLLING FORCE COMPONENTS

In the roll gap, the resultant rolling force can be described as a function of roll gap parameters in order to represent the variation of force components. The following implicit expression for the resultant component of the dynamic rolling force $F_{dyn,R}^{WR}$ may be written as:

$$F_{dyn,R}^{WR} = f\left(\mu_{s0}, v_R, h_c, \dot{h}_c, \sigma_Y, L, \phi_n\right) \tag{4.23}$$

where μ_{s0} is the coefficient of friction, v_R is the rolling speed, h_c is the roll gap spacing, $\dot{h}_c$ is the reduction rate with respect to time, L is the length from the centerline of the roll to the strip entry plane.

All these variables have close relationships resulting in variations of force components. Considering independent parameters (μ_{s0}, v_R, h_c, $\dot{h}_c$) only, it may be useful for further linearisation. From the relationship with the roll gap parameters, the implicit expression for the variation of the rolling force as a function of the friction coefficient, rolling

speed, strip thickness and the reduction rate in the roll gap can then be expanded using first-order Taylor series expansion.

$$F_{dyn,R}^{WR} = \left(\frac{\partial F_R}{\partial \mu_{s0}}\right) d\mu_{s0} + \left(\frac{\partial F_R}{\partial h_c}\right) dh_c + \left(\frac{\partial F_R}{\partial v_R}\right) dv_R + \left(\frac{\partial F_R}{\partial \dot{h}_c}\right) d\dot{h}_c \tag{4.24}$$

During the cold rolling process, the friction coefficient variation in the first term of the RHS in the above equation (4.24) is largely due to the rolling speed variation and it is coupled implicitly in terms of vibration analysis. In order to identify the coupling in explicit form in the direction of two translational motions, equation (4.24) needs to be rewritten as:

$$F_{dyn,R}^{WR} = K_{ij}^{\text{var}}\left(x_{WR}, y_{WR}\right) + C_{ij}^{\text{var}}\left(\dot{x}_{WR}, \dot{y}_{WR}\right) \tag{4.25}$$

where K and C indicate stiffness and damping coefficients in the dynamic roll gap, superscript 'var' represents components resulting from variations of the friction coefficient, strip thickness, rolling speed and reduction rate, and subscript 'ij' refers to x- and y-directional components, respectively.

4.3.1. Dynamic Rolling Force Components Resulting from Negative Gradient Friction Coefficient with Rolling Speed

The frictional sliding force results from the inter-relationship between the friction coefficient and rolling speed. The first term in the RHS of equation (4.24), however, is unknown as the lubricant characteristics under the deformation condition, the roll and strip surface topology is not readily available. Instead, Yuen et al. (1998, 1999, 2003) correlated the variation of the friction coefficient with the rolling speed based on mill data. This was performed by estimating the friction coefficient from the measured rolling force. Yuen et al. (1998) also presented the friction formulae according to the rolling speed and roll wear with different grades of steel.

Based on the above, this thesis introduces a negative gradient of friction coefficient with rolling speed to represent the lubrication condition due to rolling speed, which can also be expressed in terms of the relative velocity between the work roll and strip speed at

the exit of the roll bite (assuming the forward slip remains unchanged). A linearised equation to describe friction in the roll bite is given for the effect of negative gradient friction in the mill vibration model as shown in Figure 4-5.

Firstly, the coefficient of friction can be linearised to an initial condition value and gradient α_s in mixed-film lubrication region (Qiu et al., 1999) from Stribeck Curve.

$$\mu_{sl} = \mu_{s0} - \alpha_s \left(v_S - v_{WR}\right) \tag{4.26}$$

where μ_{sl} is the sliding friction, μ_{s0} is the coefficient of friction at the steady-state condition, α_s is the gradient of friction with unit $[\frac{1}{m/s}]$, v_S is the strip velocity at the exit and v_{WR} is the work roll velocity.

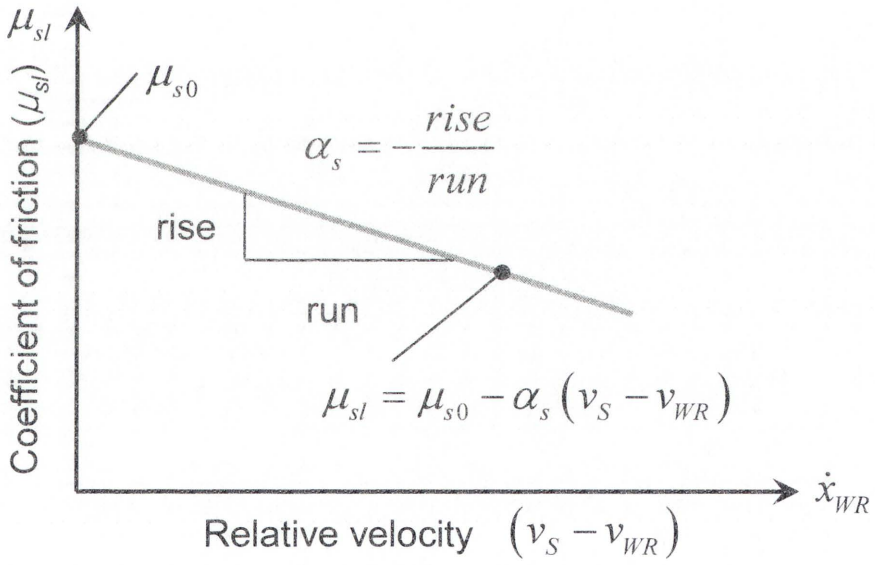

Figure 4-5: Variation of the friction coefficient with relative velocity

Secondly, if the strip is moving at the same speed as the work roll, the relative velocity of the strip is thus zero. However, the cumulative velocity of the strip is continuously affected by the oscillation resulting from the forward slip. In order to represent the variation of the friction coefficient with rolling speed, it is assumed that the forward slip and gradient of friction is constant. Therefore, the variation of the friction coefficient due to vibrations can be given by:

$$\mu_{s0,\mathrm{var}} = \alpha_s \dot{x}_{WR} \tag{4.27}$$

Also, note that the relative velocity between the work roll and strip can further be defined using forward slip concept.

$$\left(\dot{x}_S - \dot{x}_{WR}\right) = S_f \dot{x}_{WR} \tag{4.28}$$

where S_f is the forward slip.

Note that the sign is changed. Thus frictional component of dynamic rolling force given by the first term of RHS in equation (4.24) can be re-written as:

$$F_{dyn,R1}^{WR} = \left(\frac{\partial F_R}{\partial \mu_{s0}}\right)\left(\frac{\partial \mu_{s0}}{\partial v_R}\right) dv_R = C_{\mathrm{var}\,0}\alpha_s \dot{x}_{WR} \tag{4.29}$$

where $\partial F_R / \partial \mu_{s0}$ is the variation of rolling force to the change in friction coefficient which can be obtained from the modified roll gap model and is denoted by $C_{\mathrm{var}\,0}$. $\partial \mu_{s0} / \partial v_R$ represents the gradient of friction coefficient α_s and $\dot{x}_{WR}$ is the velocity of the work-roll, respectively.

4.3.2. Dynamic Rolling Force Components Resulting from the Reduction, Reduction Rate and Rolling Speed Change

From second to fourth terms in equation (4.24), the resultant component of the dynamic rolling force can also be linearized. In order to determine the component of coupled terms with associated variables, rearranging the above equation using chain rule at the neutral point yields:

$$F_{dyn,R2-R4}^{WR} = \left(\frac{\partial F_R}{\partial \phi}\frac{\partial \phi}{\partial h_c}\right) dh_c + \left(\frac{\partial F_R}{\partial \phi}\frac{\partial \phi}{\partial v_R}\right) dv_R + \left(\frac{\partial F_R}{\partial \phi}\frac{\partial \phi}{\partial \dot{h}_c}\right) d\dot{h}_c \tag{4.30}$$

where the partial derivatives $\partial F_R / \partial \phi$ in each component term may be obtained from the integration of the area of the pressure distribution at the neutral angle.

However, expanding equations at the neutral point can be incorrect since the rolling force is located at the centre of the deformed roll according to Hitchcock roll deformation (1935).

Thus, three terms in the RHS of equation (4.24) can be expanded as the dynamic components of rolling force at the exit side of the work roll due to the reduction, reduction rate and rolling speed change.

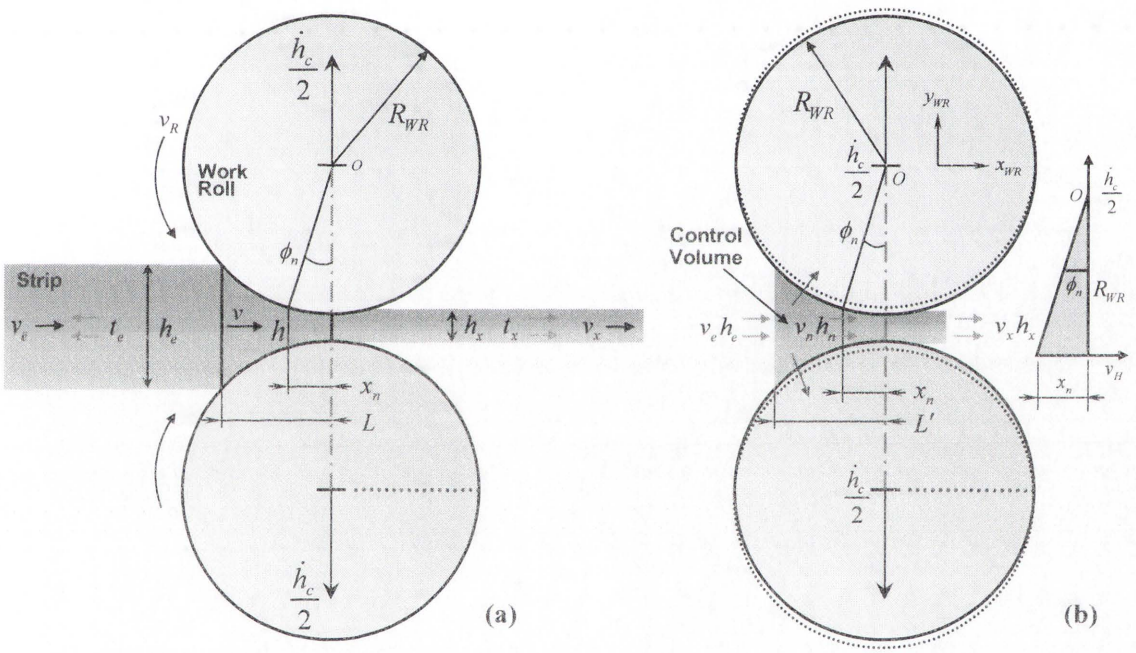

Figure 4-6: The roll bite geometry: (a) when rolls are in steady-state conditions and (b) when rolls are oscillating along the roll contact surface

$$F_{dyn,R2-R4}^{WR} = \left(\frac{\partial F_R}{\partial h_c}\right)\Delta h_c + \left(\frac{\partial F_R}{\partial v_R}\right)\Delta v_R + \left(\frac{\partial F_R}{\partial \dot{h}_c}\right)\Delta \dot{h}_c \tag{4.31}$$

Providing that the roll vibration is coupled with the horizontal and vertical motion, the variations of the above dynamic rolling force still remain uncoupled due to the absence of the coupled force components.

Referring to Figure 4-6, under the steady-state condition, strip thickness along the arbitrary roll gap profile is determined by trigonometry.

$$h = h_c + 2R_{WR}\left(1-\cos\phi\right) \tag{4.32}$$

where $h_{c0} = h_c$ at exit side when the roll gap experiences with elastic recovery.

On the other hand, under the dynamic disturbance, variations of the strip thickness between the two work rolls Δh_c are simply calculated from the relationship $2\left(\Delta y_{WR}\right)$. However, according to industry observations, it is reported that the mill stand behaves as a spring although it is very large and stiff. In order to represent the roll gap opening and elastic elongation of the mill stand in an appropriate manner, the strip thickness between the two work rolls h_c is often achieved by using gauge-meter principle known as Automatic Gauge Control (AGC). Thus variation of strip thickness on the exit side can then be defined as:

$$\Delta h_c = \Delta S_0 - \frac{Q\Delta h_c}{M_m} \tag{4.33}$$

where Δh_c is variation of the roll gap spacing, governing the exit strip thickness. ΔS_0 is variation of the dynamic roll displacement where its magnitude is equivalent to the vertical motion of the work roll y_{WR}. Q is the rolling force variation per the change in exit strip thickness based on the strip plastic deformation. M_m is the elastic mill modulus ($4.0MN/mm$). The rate of change of the roll gap spacing and dynamic roll displacement can be calculated from equation (4.33) as $\left(\Delta y_{WR} / \Delta h_c\right) = 1 + \left(Q / M_m\right)$. Therefore a dynamic rolling force component given by the second term of RHS in equation (4.24) can be rewritten by:

$$F_{dyn,R2}^{WR} = \left(\frac{\partial F_R}{\partial h_c}\right)\left(\frac{\partial h_c}{\partial y_{WR}}\right) y_{WR} \tag{4.34}$$

Another condition at the exit plane may be used to determine an expression for the roll bite length x_n at the neutral point (Bland and Ford, 1948). Note that rolling speed v_R is same as the strip speed at the neutral point where roll pressure is a maximum. Consider a small disturbance at the neutral point, *i.e.*, a very small change of rolling speed compared to that of strip velocity, *i.e.*, $\Delta v_R \approx \Delta \dot{x}_{WR} / \cos\phi_n$. Note that the vertical component of peripheral rolling speed becomes zero at the exit side. Thus, a dynamic rolling force component given by the third term of RHS in equation (4.24) may be expressed as:

$$F_{dyn,R3}^{WR} = \left(\frac{\partial F_R}{\partial v_R} \right) \frac{\dot{x}_{WR}}{\cos\phi_n} \tag{4.35}$$

From the geometry in Figure 4-7, if the velocity triangle is uniform along the roll bite during the rolling process, a neutral point along the roll surface contact may be used to determine the relationship in terms of a velocity triangle.

$$\tan\phi_n = \frac{x_n}{R_{WR}} = \frac{\Delta \dot{h}_c}{2\Delta v_H} \tag{4.36}$$

where ϕ_n is the neutral angle or point, x_n is the roll bite length from the exit side to the neutral angle. R_{WR} is the undeformed roll radius from the centre of origin and the horizontal component of work roll velocity Δv_H is $\Delta v_R \cos\phi_n$. Thus, the reduction rate can be defined as:

$$\Delta \dot{h}_c = 2\Delta v_R \sin\phi_n \tag{4.37}$$

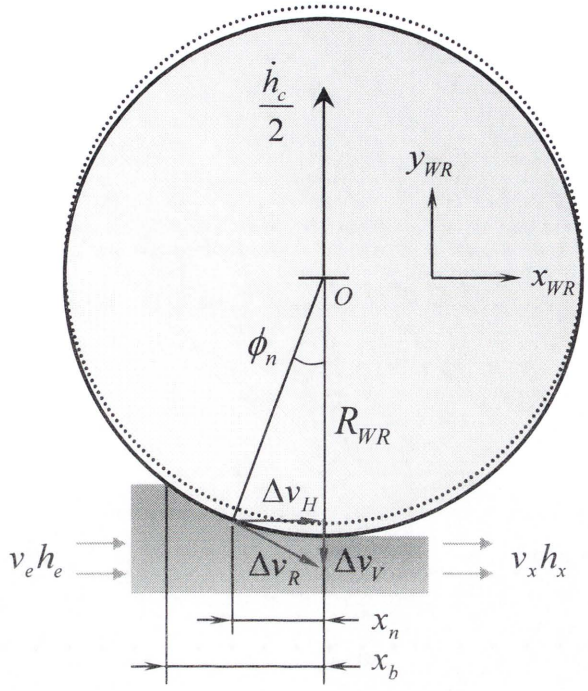

Figure 4-7: The roll velocity triangle at the neutral point

Note that the reduction rate $\Delta\dot{h}_c = 2\Delta\dot{y}_{WR}$ as proposed by Yun et al., (1998). This means the rate of change in reduction with respect to time, $\Delta\dot{h}_c$, is equal to two times $\Delta\dot{y}_{WR}$. Therefore, throughout this paper, the dynamic roll velocity is adopted as below.

$$\Delta\dot{y}_{WR} = \frac{\Delta\dot{h}_c}{2} \tag{4.38}$$

It follows that the velocity of the work roll from equation (4.38) can be defined as:

$$\Delta\dot{y}_{WR} = \Delta v_R \sin\phi_n \tag{4.39}$$

Lastly, a dynamic rolling force component given by the fourth term of RHS in equation (4.24) can be rewritten as:

$$F_{dyn,R4}^{WR} = \left(\frac{\partial F_R}{\partial \dot{y}_{WR}}\right)\dot{y}_{WR} \tag{4.40}$$

In order to prove the validity of the equation (4.36) from the geometry of the roll gap, Simple check can be performed using time derivative of $x_n = R\tan\phi_n$,

$$\frac{dx_n}{dt} = \frac{dR}{dt}\tan\phi_n + R\frac{d(\tan\phi_n)}{dt}\dot{\phi}_n = \dot{R}\tan\phi_n + \frac{R\dot{\phi}_n}{\cos^2\phi_n}$$

where $\cos^2\phi_2 \approx 1$ with very small angle.

Rearranging,

$$\dot{R}\tan\phi_n = \dot{x}_n - R\dot{\phi}_n \text{ or } \tan\phi_n = \frac{\dot{x}_n - R\dot{\phi}_n}{\dot{R}}$$

If $\dot{R} \approx \frac{\dot{h}_c}{2}$ and $\dot{\phi}_n \approx 0$ as torsional vibration is not considered here, then we still have equation (4.36).

Based on the fact that the above expansion holds true with the negligible error, rearranging relations from equations (3.34), (3.35) and (4.40) yields as:

$$F_{dyn,R2-R4}^{WR} = \left(\frac{\partial F_R}{\partial h_c}\right)\left(\frac{\partial h_c}{\partial y_{WR}}\right)y_{WR} + \left(\frac{\partial F_R}{\partial v_R}\right)\frac{\dot{x}_{WR}}{\cos\phi_n} + \left(\frac{\partial F_R}{\partial \dot{y}_{WR}}\right)\dot{y}_{WR} \tag{4.41}$$

During the rolling process, the variation of the coupled dynamic rolling force as a function of each variable may be rewritten as:

$$F_{dyn,R2-R4}^{WR} = K_{\text{var}1}y_{WR} + C_{\text{var}1}\dot{x}_{WR} + C_{\text{var}2}\dot{y}_{WR} \tag{4.42}$$

where $K_{\text{var}1}$ is the stiffness component of the dynamic rolling force due to the variation of the vertical displacements $(\partial F_R / \partial y_{WR})$, $C_{\text{var}1}$ is the damping component of the dynamic rolling force due to the variation of the horizontal velocity $(\partial F_R / \partial v_H)$ and

$C_{\text{var}2}$ is the damping component of the dynamic rolling force due to the variation of the dynamic roll gap $\left(\partial F_R / \partial \dot{y}_{WR}\right)$.

4.3.3. Dynamically Coupled Vibration Model (Explicit Formula)

In previous section, dynamically coupled rolling force components in terms of vibrational displacement and velocity are determined for characterising the dynamic mill vibration model. All components of the dynamic rolling force can be re-arranged as follows:

$$\begin{aligned} F_{dyn,R}^{WR} &= F_{dyn,R1}^{WR} + F_{dyn,R2}^{WR} + F_{dyn,R3}^{WR} + F_{dyn,R4}^{WR} \\ &= \alpha_s C_{\text{var}0}\dot{x}_{WR} + K_{\text{var}1} y_{WR} + C_{\text{var}1}\dot{x}_{WR} + C_{\text{var}2}\dot{y}_{WR} \end{aligned} \tag{4.43}$$

Note that so far the estimated rolling force is the resultant force which can be resolved into the horizontal and vertical components. The cross-coupled components of the linearised spring and damper are as follows. The horizontal component of stiffness is zero as we only consider the vertical compression of strip and ignore the spread of strip width.

$$K_{xx}^{\text{var}1}=0 \text{ and } K_{yx}^{\text{var}1}=0 \tag{4.44}$$

The vertical components of stiffness have a significant influence as the strip is highly compressed with rolling force and also experiences a change of yield strength, as reviewed by Gronostajski (2000).

$$K_{xy}^{\text{var}1} = K_{\text{var}1}\sin\phi_n \text{ and } K_{yy}^{\text{var}1} = K_{\text{var}1}\cos\phi_n \tag{4.45}$$

The damping components due to relative motion between the work roll and strip during the rolling process can be linearised as:

$$C_{xx}^{\text{var}1} = C_{\text{var}0}\sin\phi_n,\ C_{xy}^{\text{var}1} = 0,\ C_{yx}^{\text{var}1} = C_{\text{var}0}\cos\phi_n \text{ and } C_{yy}^{\text{var}1} = 0 \tag{4.46}$$

The damping components caused by variations of rolling speed are decomposed as:

$$C_{xx}^{\text{var}2} = C_{\text{var}1}\tan\phi_n,\ C_{xy}^{\text{var}2} = 0,\ C_{yx}^{\text{var}2} = C_{\text{var}1} \text{ and } C_{yy}^{\text{var}2} = 0 \tag{4.47}$$

Lastly, the damping components due to the reduction rate in the roll gap are as in the following.

$$C_{xx}^{\text{var}3}=0,\ C_{xy}^{\text{var}3} = C_{\text{var}2}\sin\phi_n,\ C_{yx}^{\text{var}3} = 0,\ C_{yy}^{\text{var}3} = C_{\text{var}2}\cos\phi_n \tag{4.48}$$

At the neutral angle, the horizontal and vertical components of the dynamic rolling force are determined as:

$$\begin{aligned} F_{dyn,x}^{WR} &= F_{dyn,R}^{WR}\sin\phi_n = \left(\alpha_s C_{\text{var}0}\dot{x}_{WR} + K_{\text{var}1}y_{WR} + C_{\text{var}1}\dot{x}_{WR} + C_{\text{var}2}\dot{y}_{WR}\right)\sin\phi_n \\ &= C_{xx}^{\text{var}1}\dot{x}_{WR} + K_{xy}^{\text{var}1}y_{WR} + C_{xx}^{\text{var}2}\dot{x}_{WR} + C_{xy}^{\text{var}3}\dot{y}_{WR} \end{aligned} \tag{4.49}$$

$$\begin{aligned} F_{dyn,y}^{WR} &= F_{dyn,R}^{WR}\cos\phi_n = \left(\alpha_s C_{\text{var}0}\dot{x}_{WR} + K_{\text{var}1}y_{WR} + C_{\text{var}1}\dot{x}_{WR} + C_{\text{var}2}\dot{y}_{WR}\right)\cos\phi_n \\ &= C_{yx}^{\text{var}1}\dot{x}_{WR} + K_{yy}^{\text{var}1}y_{WR} + C_{yx}^{\text{var}2}\dot{x}_{WR} + C_{yy}^{\text{var}3}\dot{y}_{WR} \end{aligned} \tag{4.50}$$

The linearisation of the dynamic rolling force as springs and dampers is given in Figure 4-8. For clarity, cross-coupling terms of springs and dampers are not illustrated in here.

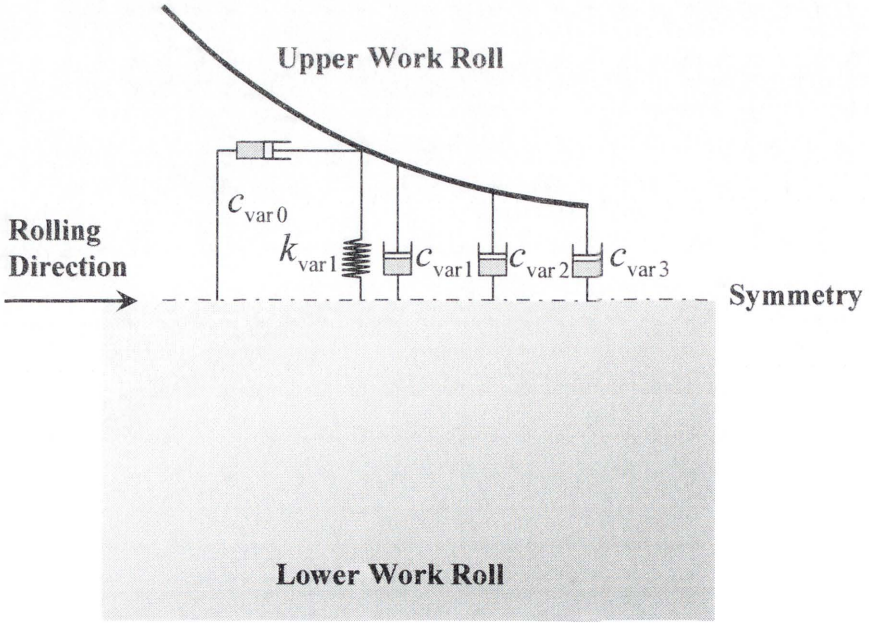

Figure 4-8: Linearisation of dynamic spring and damper in the roll gap

4.3.4. Discussion

In Section 4.3.3, a linearised mill vibration model is established for mass elements assuming small variations about a steady-state operating point of the same order as normal vibration. In Section 3, rolling force components changing dynamic characteristics of the cold rolling mill have been linearised by taking into account small variations of reduction, reduction rate, friction coefficient and rolling speed. For the purpose of vibration analysis of a cold rolling mill the presented model is coupled to motion of adjacent mass element and closely associated with system conditions including rolling parameters in Table 4-2. In order to identify how these force variations in the roll gap affect the mill system, simulation codes are developed. As shown in Figure 4-9, dynamic variations of stiffness and damping coefficients in the roll gap are calculated through the change of rolling speed at friction coefficient in the range of 0.010-0.035; Figure 4-9(a) presents variations of rolling force depending on the small change in friction coefficient from 0.010 to 0.035. The magnitude of $\partial F_R / \partial \mu_{s0}$ presents small differences in low speed range regardless of friction coefficient change. Its variations in high speed range are more significant suggesting the system may easily fall into unstable vibration. For the given friction gradient, the first term acts like a negative damping. Figure 4-9(b) shows variations of rolling force depending on small change in rolling speed from 10m/s to 35m/s. $\partial F_R / \partial v_R$ varies with a high difference in high friction range with respect to the rolling speed and affects system stability as positive damping (Tamiya et al. 1980; Tlusty et al. 1982). However, in higher rolling speed range, positive damping effect resulted from the rolling speed reduces considerably. Figure 4-9(c) indicates variation of rolling force depending on the strip thickness change. $\partial F_R / \partial y_{WR}$ initially varies with a significant magnitude and settles at a high rolling speed around $35 m/s$, which explains why it does not significantly change stiffness coefficients in the roll gap even though the rolling speed increases over $35 m/s$. Finally, Figure 4-9(d) displays variations of rolling force depending on the reduction rate change (Yun et al. 1998; Hu et al. 2006) and has a significant effect on the roll gap compared to Figure 4-9(b). In Figure 4-9(d), positive damping effect decreases with the increasing rolling speed while negative damping effect increases with the increasing rolling speed in Figure 4-9(a).

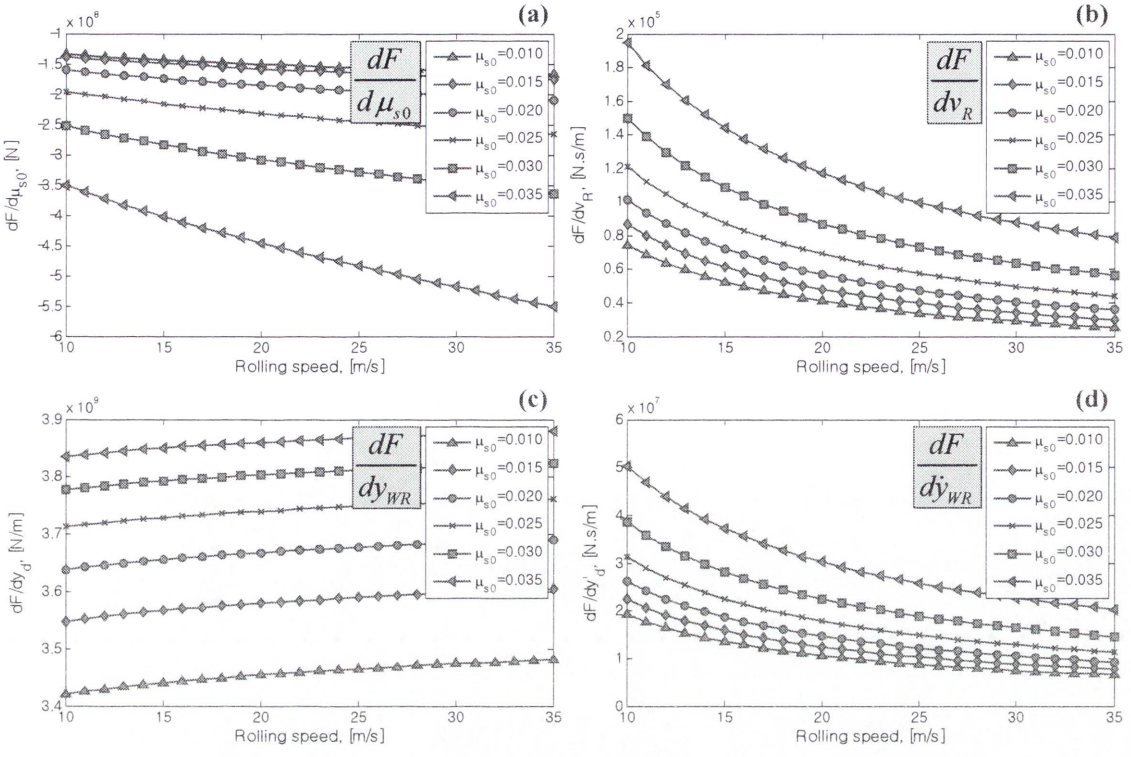

Figure 4-9: Force variations in the roll gap depending on the change in the key rolling parameters (a) friction coefficient, (b) rolling speed, (c) reduction and (d) reduction rate

However, it should be noted that, in the range of friction coefficient over 0.030, variations of rolling force do not fit with the linear scheme any more as system characteristics also change with the state (position) of the bearing and roller. As a result of simulation, it is identified that rolling force variations have an interacting relationship in the roll gap which may affect system stability. Determination of stability regime through the change of friction coefficient and rolling speed will be methodically discussed in Chapter 6 of this thesis.

As afore mentioned in previous section, these force variations act like springs and dampers in the dynamic roll gap, and thus shift natural frequency range and change the system characteristics in the cold rolling stand. Of course, there are many system parameters that may alter dynamic characteristics of the cold rolling system. However, this study is focused on system characteristics that can be altered by the change of reduction, reduction rate, friction coefficient and rolling speed while the change of other parameters remains constant.

4.4. FRICTION FORCE

According to the friction definition in physics (Tipler, 2004), friction is the resistance of moment at the interface between two bodies, or two elements, or two particles or two things. Material moment in rolling is always in a single direction or in the rolling direction. If friction resists the material moving, the friction direction has to be opposite to the material moment direction, or rolling direction, for the whole deforming region. Thus, the friction force is resisting force against the rolling force. The roll gap has friction forces due to the surface contact at two sides, *i.e.*, bottom surface between the work roll and strip and top surface between the work roll and backup roll. For the upper part only, all the force components at surface contact are given in Figure 4-10. The backup roll and work roll have *6mm* offsets with surface contact. Owing to the offset between two rolls, contact angle of two rolls is tilted with the oblique. Neglecting the roll deformation of two rolls, the tilted angle can be calculated as:

$$\beta = \tan^{-1}\left(\frac{Offset}{\approx\left(R_{BR}+R_{WR}\right)}\right) \tag{4.46}$$

When the work roll is oscillating with the small change of rolling force, the neutral point moves inward or outward in the roll gap and surface contact angle of two rolls changes, accordingly.

Therefore, due to the change of the surface contact region, friction force is affected by oscillation of rolls. Specifically, friction direction in the work roll is given in Figure 4-11. Once the work roll driven by motor is rotating in a counter-clock-wise direction, a friction component in the bottom surface of the work roll resists the rolling and another in the top surface of the work roll is against the backup roll rotation. On the other hand, the backup roll at the surface contact with the work roll will be accelerated by the friction force and its rotation is purely initiated by the friction force against the roll contact.

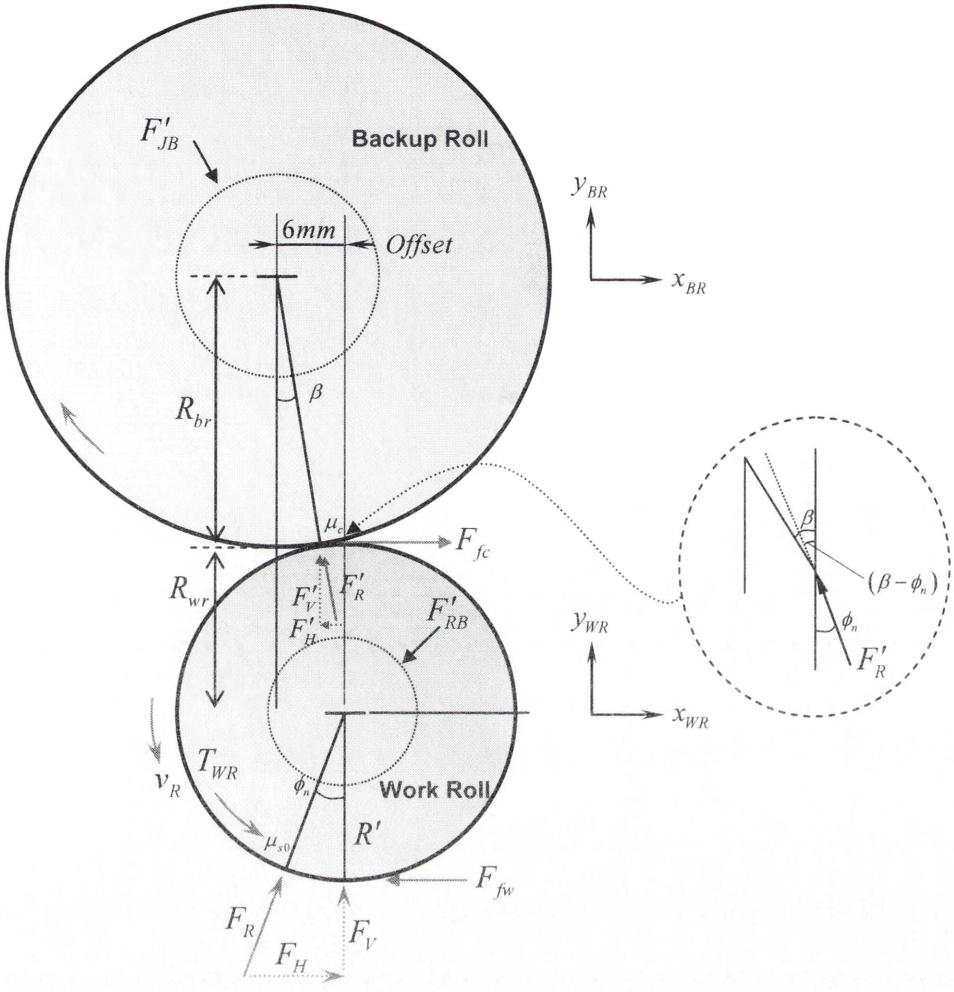

Figure 4-10: Roll stack model based on the force components in the surface contact (a upper backup and work roll)

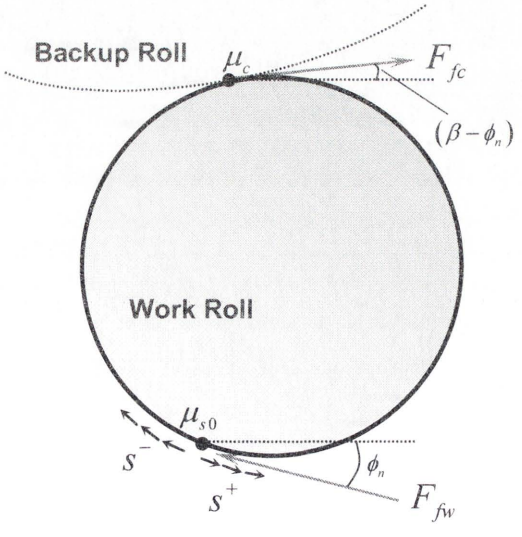

Figure 4-11: Friction force components at the work roll surface

At a certain steady-state condition, friction is uniform along the contact of arc length as lubrication of oil is continuously supplied onto the roll bite. Thus, frictional force on the roll surface, therefore, can be defined by:

$$F_{fw} = \mu_{s0}\sqrt{F_H^2 + F_V^2} \tag{4.47}$$

For the frictional force in the vertical direction, its magnitude is less than 1 per cent compared to the horizontal force as the resultant rolling force acting on the neutral point is almost in the vertical direction. As shown in Figure 4-11, as frictional force changes sign at the neutral point, the horizontal friction force in the roll gap becomes:

$$F_{fw,x} = \mu_{s0}F_V = \mu_{s0}R'W\left[\int_{\phi_n}^{\phi_i} s^- d\phi + \int_{\phi_x}^{\phi_n} s^+ d\phi\right] \tag{4.48}$$

On the other hand, the other frictional force from the surface contact between the backup roll and work roll, F_{fc}, is simply written as $\mu_c F_R'$. Note that the direction of two frictional forces is opposite to each other and friction coefficient in the metal-to-metal contact is assumed to be 0.1. Therefore, considering the offset and force direction between two rolls, horizontal friction force between the backup roll and work roll becomes:

$$F_{fc,x} = \mu_c F_V' \cos(\beta - \phi_n) \tag{4.49}$$

CHAPTER 5. MILL VIBRATION MODEL WITH A 6DOF SYSTEM

5.1. INTRODUCTION

This chapter mainly deals with linearisation scheme used for developing a proposed mill vibration model with assumptions and simplifications. In the determination of linearised stiffness and damping coefficient in the support bearings and surface contact, it is considered a cold rolling mill at the 4^{th} stand is operating at a steady-state condition at the friction coefficient of 0.02 and rolling speed of $20m/s$. With the given rolling force from the roll gap model presented in Chapter 4, the journal bearing analysis has been performed in order to find the bearing forces and equilibrium states in the lubrication film and the separate analysis for the tapered roller bearing also has been carried out for the purpose of identifying bearing characteristics. Then, coefficients of stiffness and damping are calculated at these steady-state conditions. Surface contact between the backup roll and work roll, on the other hand, has been linearised by utilising Hertz contact mechanism. It should be noted that current study is only valid for small change in rolling parameters as all the calculated coefficients are changing with the roller's position as well as lubrication conditions in the roll gap. Nonetheless, it seems to Author with confidence for standard mill vibration analysis that this approach is still appropriate to identify characteristics of the cold rolling mill. In Chapter 8, in order to overcome limitation introduced in this study, a new concept for a fully transient model will be taken into consideration as all the stiffness and damping coefficients resulting from those support bearings and dynamic roll gap are varying with state, which significantly varies with the displacement and velocity of the backup roll and work roll.

5.1.1. Design of Cold Rolling Mill for a Rolling-Stand

In Figure 5-1, the complete assemblies of a rolling stand in cold rolling mill are presented in order to provide the fundamental understanding of how the system looks like and works at the given condition. Note that some of minor details are not drawn here for the purpose of the general overview. In this thesis, the overall system can be

condensed to Figure 5.2 as the main concern is to identify the coupled dynamics in a cold rolling mill. Figures 5.3 to 5.5 show the individual displays of half-stand cold rolling mill in terms of viewpoints.

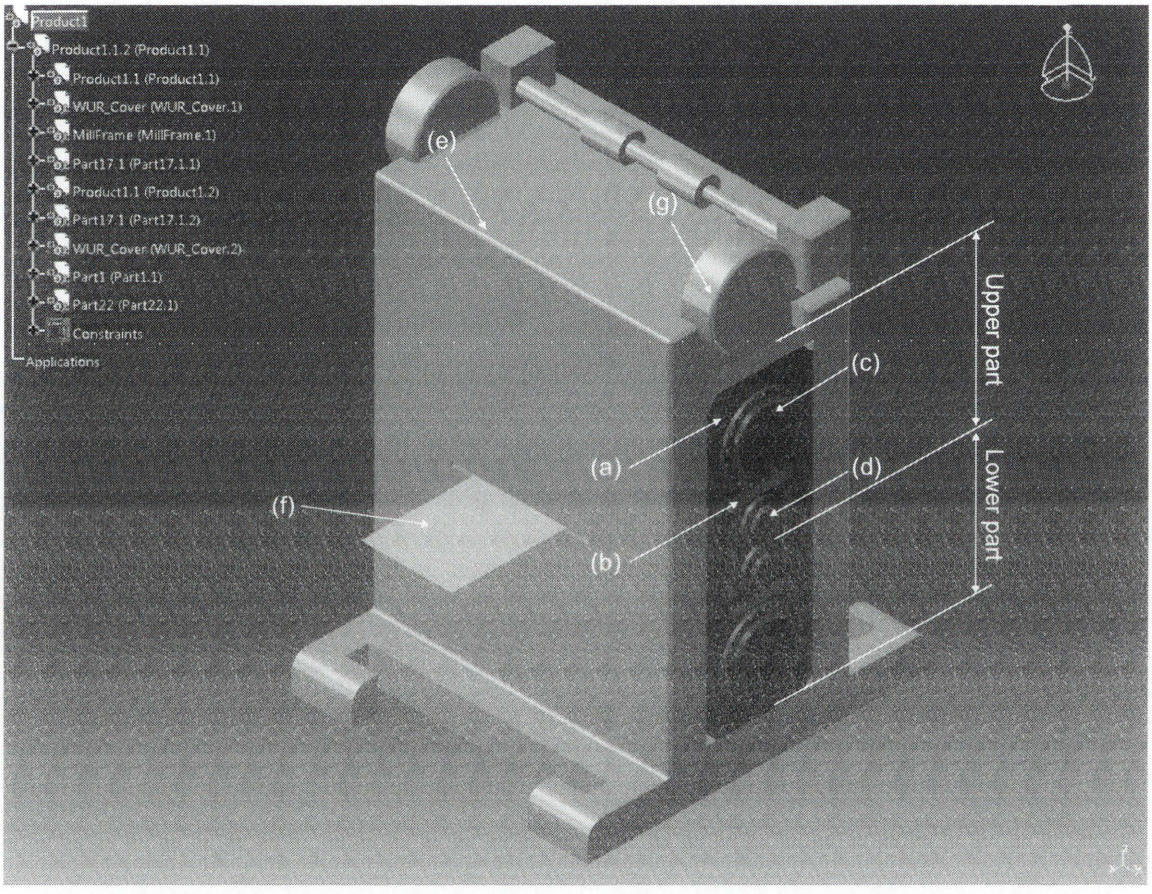

Figure 5-1: Assembly of a rolling stand in cold rolling mill: (a) backup roll bearing housing chock, (b) work roll bearing housing chock, (c) backup roll, (d) work roll, (e) mill Stand, (f) strip and (g) hydraulic cylinder

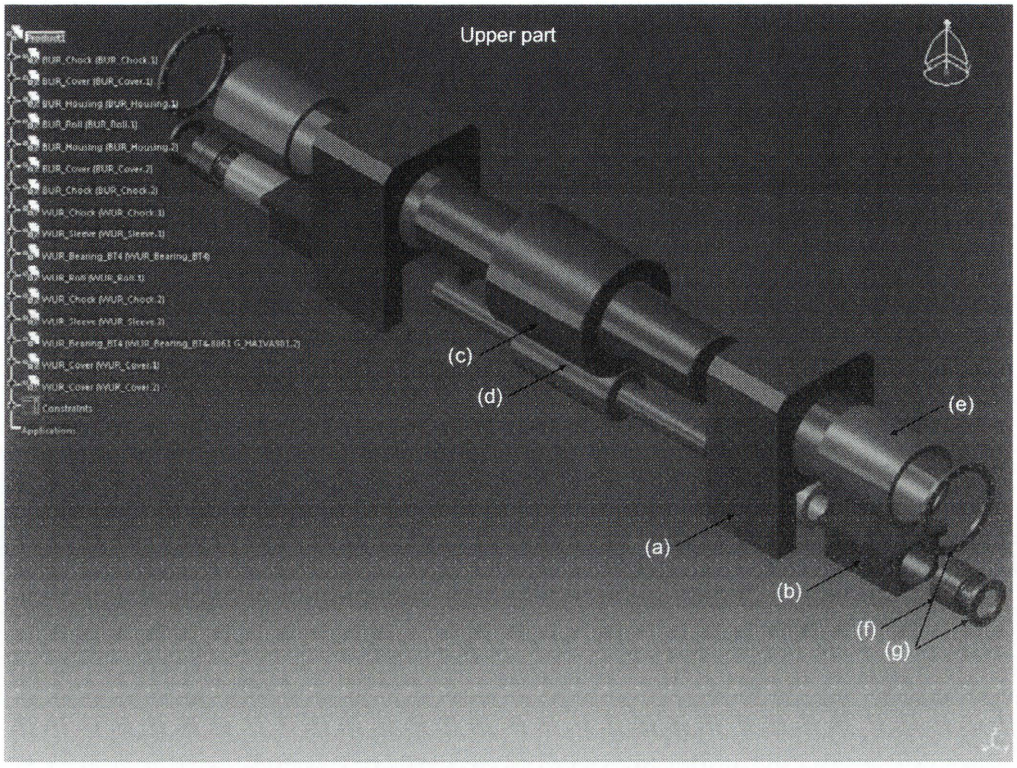

Figure 5-2: Assembly of the upper part of a rolling stand: (a) backup roll bearing housing chock, (b) work roll bearing housing chock, (c) backup roll, (d) work roll, (e) journal bearing, (f) tapered roller bearing, (g) gasket (cover)

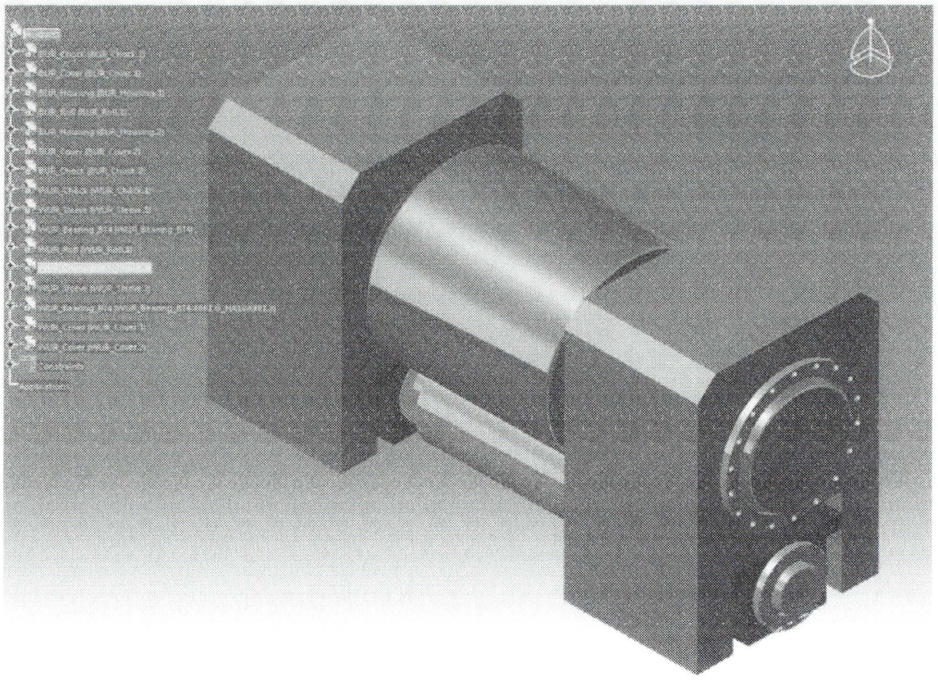

Figure 5-3: Perspective view of the upper rolling stand in cold rolling mill

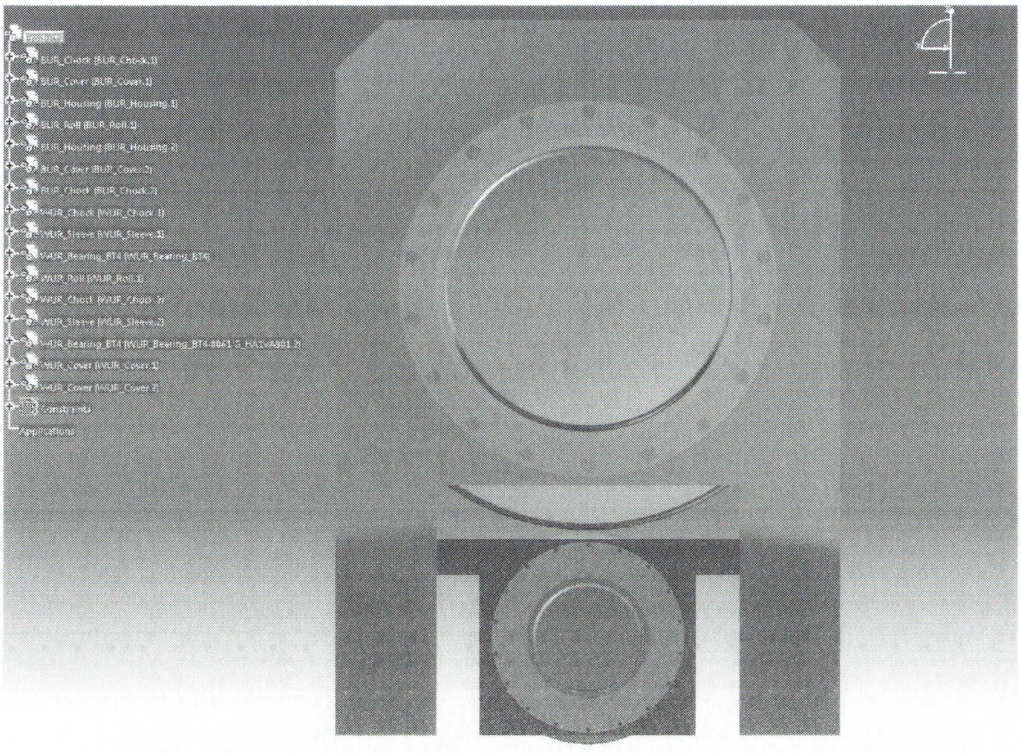

Figure 5-4: Side view of the upper rolling stand in cold rolling mill

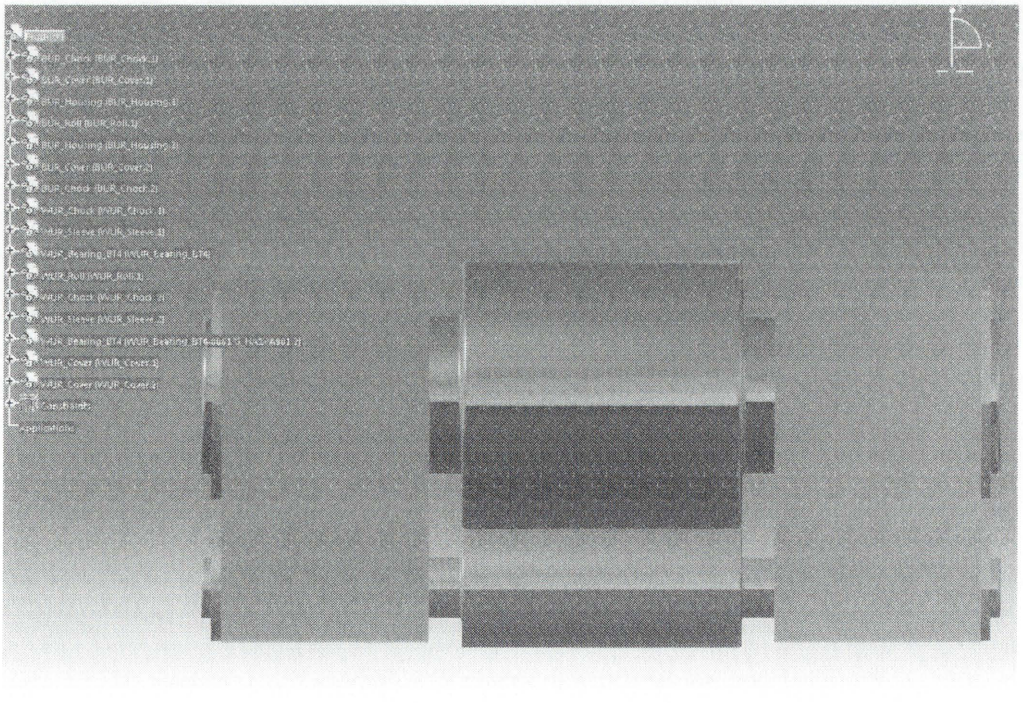

Figure 5-5: Front view of the upper rolling stand in cold rolling mill

5.2. VIBRATION MODEL OF A ROLLING STAND IN COLD ROLLING MILL

In order to develop a mathematical model describing the coupled mill vibrations, the dynamic mill vibration model presented in this study includes x- and y-translational displacements of the bearing housing chock, backup roll (BR) and work roll (WR). All force components of each mass element have highly nonlinear characteristics. In order to linearise these force components as stiffness and damping coefficients, the following assumptions and simplifications are made.

5.2.1. Assumptions and Simplifications

The assumptions made in the classical theories of rolling presented by Orowan (1943), Bland and Ford (1948) are considered to hold true. For the dynamic analysis in rolling process, further considerations are given as follows:

(1) It is considered that the bearing housing chock, backup roll and work roll oscillate with bi-directional (x and y direction) degrees of freedom. The strip continuously passes through the roll gap, and thus the change in rolling speed and friction coefficient may cause severe noise and vibrations in the translational motions.

(2) The upper and lower parts of a mill stand are assumed to be symmetrical with respect to the roll gap. The dynamic conditions of both parts of the individual stand are considered to be exactly identical (in fact, there exist some differences between structural features of upper and lower rolls). Consequently, the upper part of the rolling stand is only analysed.

(3) Work roll (WR) and backup roll (BR) are supported by tapered roller bearings and journal bearings, respectively. Variations of displacement and velocity of rolls alter the dynamic force component and thus change natural frequency range.

(4) Surface contact between the backup roll and work roll can be linearised by using Hertzian Contact theory, and the collective effects resulted from the bearings are represented by the linearized stiffness and damping coefficient, as shown in Figure 5-6.

(5) It is also assumed that the collective frictional force and rolling force acting in the roll bite are applied at the neutral point. Thus, by the relationship of $F_{fw}=\mu_{s0}N$, the frictional force F_{fw} is considered to be proportional to the force N that is normal to the strip surface.

5.2.2. Mill Vibration Model

Force components for the upper part of a mill stand are shown in Figure 5-6. To derive the equation of motions, it is important to separate the forces into the *x*- and *y*-directional components in the dynamic mill vibration model. Then the equations of motions can be constructed by using force components only. Notations for symbols used are given in Table 5-1.

$$m_{BH}\ddot{x}_{BH} = -F'_{JBH} + F_{HCH} \tag{5.1}$$

$$m_{BH}\ddot{y}_{BH} = F'_{JBV} - F_{HCV} + F_{HCf} \tag{5.2}$$

$$m_{BR}\ddot{x}_{BR} = F'_{JBH} - F'_{H} - F_{fc}\cos(\beta - \phi_n) \tag{5.3}$$

$$m_{BR}\ddot{y}_{BR} = -F'_{JBV} + F'_{V} - F_{fc}\sin(\beta - \phi_n) \tag{5.4}$$

$$m_{WR}\ddot{x}_{WR} = F_{H} + F'_{H} - F'_{RBH} - F_{fw}\cos\phi_n + F_{fc}\cos(\beta - \phi_n) + F^{WR}_{dyn,x} \tag{5.5}$$

$$m_{WR}\ddot{y}_{WR} = F_{V} - F'_{V} - F'_{RBV} + F_{fw}\sin\phi_n + F_{fc}\sin(\beta - \phi_n) + F^{WR}_{dyn,y} \tag{5.6}$$

Table 5-1: Notations of symbols for a given free-body-diagram

m_{BH} , m_{BR} , m_{WR}	Lumped mass of the bearing housing chock, BR and WR [*kg*]
F_{HCH}	Reaction force from the mill frame [*N*]
F_{HCV}	Screw-down forces on top [*N*]
F'_{JBH} , F'_{JBV} , F'_{RBH} , F'_{RBV}	Bearing forces resulted from support bearings [*N*]
F_H , F_V	Horizontal and vertical rolling force in the roll gap [*N*]
F'_H , F'_V	Surface contact force components between BR and WR [*N*]
F_R , F'_R	Resultant rolling force [*N*]
F_{HCf}	Frictional force in the sliding surface of the housing chock [*N*]
F_{fc} , F_{fw}	Frictional forces in the BR and WR, respectively [*N*]
$F^{WR}_{dyn,x}$, $F^{WR}_{dyn,y}$	Dynamic rolling force [*N*]
ϕ_n	Neutral point/angle in the roll gap [*Radian*]
β	Contact angle transferred between two rolls [*Radian*]
v_R	Rolling speed [*m/s*]
x_{BH} , y_{BH} , x_{BR} , y_{BR} , x_{WR} , y_{WR}	Coordinates of the cold rolling mill system [*m*]
JB , *RB*	Refer to the journal bearing and tapered roller bearing, respectively

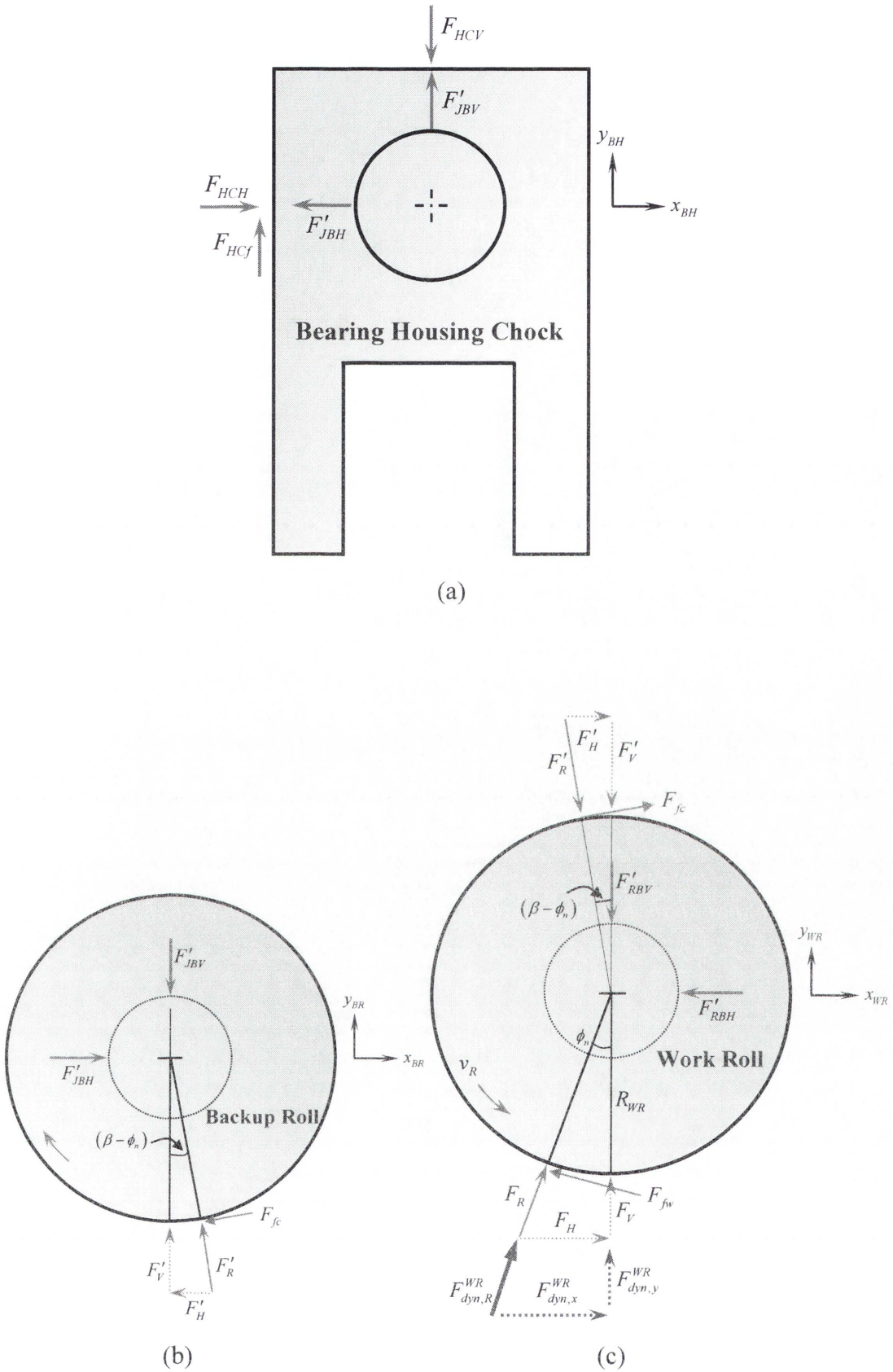

Figure 5-6: Free-body-diagrams of lumped mass components; (a) bearing housing chock, (b) backup roll and (c) work roll

Force components in equations (5.1)-(5.6) have non-linear characteristics and may be determined experimentally. In order to identify the vibrational features in the cold rolling mill, it is necessary to linearise these force components by assuming small variations of the same order as normal vibration about a steady-state operating point. Consequently, all force components (except friction force and dynamic force components) will be expressed in terms of stiffness and damping coefficients, respectively. Weights of mass elements are not considered and origin of the coordinates is assumed to be at the centre of each mass.

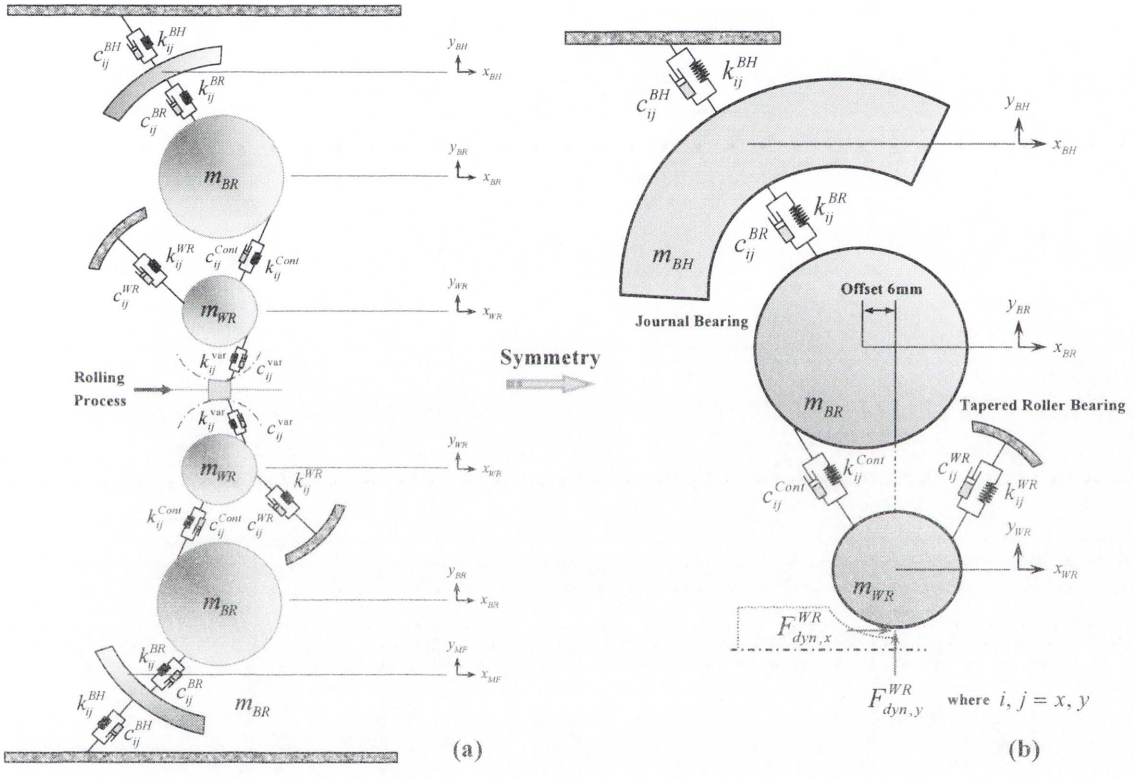

Figure 5-7: An extended schematic of dynamically coupled cold rolling mill (6DOF)

First, a mass-spring-damper system with 12 degrees of freedom is shown in Figure 5-7(a). The mass of system consists of the horizontal and vertical motion, respectively. By symmetry, the present study will focus on the motion of the upper part of a mill stand which is the essential part to understand the physical phenomena in a rolling stand system. Thus, as shown in Figure 5-7(b), this model can be reduced to a six DOF mass-spring-damper system due to the symmetry in relation to the roll gap. The simplified system consists of three masses, corresponding to the bearing housing chock, backup roll and work roll. Each mass also contains spring and damper elements with the two

translational degrees of freedom. The vibration model of the rolling mill stand can then be modelled as a linear lumped parameter system.

From the given free-body-diagram (Figure 5-6) and schematic (Figure 5-7), the equations of motion governing the vibrations of the mass element can be obtained by applying Newton's second law of motion:

$$\begin{aligned} m_{BH}\ddot{x}_{BH} = &-k_{xx}^{BH}x_{BH} - k_{xx}^{BR}\left(x_{BH}-x_{BR}\right) - k_{xy}^{BR}\left(y_{BH}-y_{BR}\right) \\ &- c_{xx}^{BH}\dot{x}_{BH} - c_{xx}^{BR}\left(\dot{x}_{BH}-\dot{x}_{BR}\right) - c_{xy}^{BR}\left(\dot{y}_{BH}-\dot{y}_{BR}\right) \end{aligned} \tag{5.7}$$

$$\begin{aligned} m_{BH}\ddot{y}_{BH} = &-k_{yy}^{BH}y_{BH} - k_{yx}^{BR}\left(x_{BH}-x_{BR}\right) - k_{yy}^{BR}\left(y_{BH}-y_{BR}\right) \\ &- c_{yy}^{BH}\dot{y}_{BH} - c_{yx}^{BR}\left(\dot{x}_{BH}-\dot{x}_{BR}\right) - c_{yy}^{BR}\left(\dot{y}_{BH}-\dot{y}_{BR}\right) + F_{HCf} \end{aligned} \tag{5.8}$$

$$\begin{aligned} m_{BR}\ddot{x}_{BR} = &-k_{xx}^{BR}\left(x_{BR}-x_{BH}\right) - k_{xy}^{BR}\left(y_{BR}-y_{BH}\right) - k_{xx}^{Cont}\left(x_{BR}-x_{WR}\right) - k_{xy}^{Cont}\left(y_{BR}-y_{WR}\right) \\ &- c_{xx}^{BR}\left(\dot{x}_{BR}-\dot{x}_{BH}\right) - c_{xy}^{BR}\left(\dot{y}_{BR}-\dot{y}_{BH}\right) - c_{xx}^{Cont}\left(\dot{x}_{BR}-\dot{x}_{WR}\right) - c_{xy}^{Cont}\left(\dot{y}_{BR}-\dot{y}_{WR}\right) \\ &- F_{fc}\cos\left(\beta-\phi_n\right) \end{aligned} \tag{5.9}$$

$$\begin{aligned} m_{BR}\ddot{y}_{BR} = &-k_{yx}^{BR}\left(x_{BR}-x_{BH}\right) - k_{yy}^{BR}\left(y_{BR}-y_{BH}\right) - k_{yx}^{Cont}\left(x_{BR}-x_{WR}\right) - k_{yy}^{Cont}\left(y_{BR}-y_{WR}\right) \\ &- c_{yx}^{BR}\left(\dot{x}_{BR}-\dot{x}_{BH}\right) - c_{yy}^{BR}\left(\dot{y}_{BR}-\dot{y}_{BH}\right) - c_{yx}^{Cont}\left(\dot{x}_{BR}-\dot{x}_{WR}\right) - c_{yy}^{Cont}\left(\dot{y}_{BR}-\dot{y}_{WR}\right) \\ &- F_{fc}\sin\left(\beta-\phi_n\right) \end{aligned} \tag{5.10}$$

$$\begin{aligned} m_{WR}\ddot{x}_{WR} = &-k_{xx}^{WR}x_{WR} - k_{xy}^{WR}y_{WR} - k_{xx}^{Cont}\left(x_{WR}-x_{BR}\right) - k_{xy}^{Cont}\left(y_{WR}-y_{BR}\right) \\ &- c_{xx}^{WR}\dot{x}_{WR} - c_{xy}^{WR}\dot{y}_{WR} - c_{xx}^{Cont}\left(\dot{x}_{WR}-\dot{x}_{BR}\right) - c_{xy}^{Cont}\left(\dot{y}_{WR}-\dot{y}_{BR}\right) \\ &- F_{fw}\cos\phi_n + F_{fc}\cos\left(\beta-\phi_n\right) + F_{dyn,x}^{WR} \end{aligned} \tag{5.11}$$

$$\begin{aligned} m_{WR}\ddot{y}_{WR} = &-k_{yx}^{WR}x_{WR} - k_{yy}^{WR}y_{WR} - k_{yx}^{Cont}\left(x_{WR}-x_{BR}\right) - k_{yy}^{Cont}\left(y_{WR}-y_{BR}\right) \\ &- c_{yx}^{WR}\dot{x}_{WR} - c_{yy}^{WR}\dot{y}_{WR} - c_{yx}^{Cont}\left(\dot{x}_{WR}-\dot{x}_{BR}\right) - c_{yy}^{Cont}\left(\dot{y}_{WR}-\dot{y}_{BR}\right) \\ &+ F_{fw}\sin\phi_n + F_{fc}\sin\left(\beta-\phi_n\right) + F_{dyn,y}^{WR} \end{aligned} \tag{5.12}$$

where k_{ij}^{n} and c_{ij}^{n} represent the stiffness and damping coefficient of the system resulted from the bearing housing, backup roll and work roll; superscript n denotes *BH*, *BR*, *WR* and *Cont*, and subscript i and j each indicates x or y, respectively. $F_{dyn,x}^{WR}$ and $F_{dyn,y}^{WR}$ are the dynamic rolling forces caused by the roll gap being investigated.

Note that the force components in the screw-down on top, surface contact, journal bearing (Rezvani and Hahn, 1993) and tapered roller bearing (Lim, 1990), respectively,

have been linearised as the stiffness and damping coefficients under the steady-state rolling conditions. The force components acting on the surface contact are also linearised using Hertzian contact theory (Roark, 2002).

Equations (5.7) to (5.12) can then be rewritten as:

$$[M]\ddot{X}+[C]\dot{X}+[K]X=F_{tot} \tag{5.13}$$

where [M], [C] and [K] can be expanded from equations (5.7) to (5.12) and F_{tot} is the frictional and dynamic rolling force components. The linearisation of stiffness and damping coefficients will be discussed in next section 5.3.

Throughout this study, friction is uniform along the contact of arc length as long as lubrication of oil is continuously supplied onto the roll bite. Frictional force changes sign at the neutral point, as shown in Figure 4-11. On the one hand, the direction of frictional force is tangential to the rolling speed. One frictional force on the roll surface between the strip and work roll, therefore, can be defined by the assumption (5) in Section 5.2.1. On the other hand, the other frictional force on the surface contact between the backup roll and work roll, F_{fc}, is simply written as $\mu_c N'$ where μ_c is the friction coefficient in the metal-to-metal contact and N' is the normal force between two rolls. Note that the direction of two frictional forces is opposite to each other.

5.3. LINEARISATION OF FORCE COMPONENTS

5.3.1. Linearisation Scheme

A common way of dealing with a nonlinear system equation is to linearise it about a certain operating point resulting in small but insignificant errors. This section mainly presents the linearisation scheme for the afore-mentioned force components.

5.3.2. Bearing Housing Chock

Bearing housing chock are assumed to be very stiff, meaning, that one or more strongly damped mode is present. Stiffness coefficients for the vertical vibration analysis are listed by Kimura et al. (2003). Besides, these values can be approximated from the ratio of transferred force variation to vibrational displacement. Here, under the given rolling force variation of $150kN$ at the steady-state condition, it is assumed that variations of displacements of bearing housing chock are less than $0.5\mu m$.

5.3.3. Cross-Coupling Effect in the Journal Bearing

Bearings include one of the most essential components in the cold roll mill. Their influence on the rotor dynamic performance and stability of the machine (cold rolling mill system) cannot be ignored. Many of the problems we face with machinery today can be attributed to the design and application of the bearings. An understanding of how bearings work and some knowledge of the basic principles that highlight their operation is therefore essential for making the in-detail design that best matches the operation requirements in question.

Bearings support the applied load and weight of the rotating shaft by developing a hydrodynamic pressure in the fluid film formed by the shaft and the bearing surface. The pressure profile in the oil film is characteristic of the journal bearings. This gives rise to an attitude angle formed by the line of centers (line connecting the center of the shaft and the center of the bearing) and the load vector. This characteristic is indicative of the presence of cross-coupling in the bearing. The load, which in this case is due primarily to the rolling force, is acting directly upward on the journal bearing. Integration of the pressure profile results in a net force that balances the rotor. This force generated in the film is accompanied by a shaft displacement with a component

that is along the load direction (direct) and a displacement that is orthogonal to the load direction and is shifted in the direction of rotation (cross). This cross-coupling effect influences stability of all rotating machinery where a fluid is rotating with the shaft in a small annulus.

This phenomenon is unique to rotating machinery and is not present in other non-rotating structures or mechanisms. It is this cross-coupled stiffness force that promotes self-excited, sub-synchronous vibrations and instability in rotating machinery. In fluid film bearings this is referred to as oil whirl where the shaft will whirl at a frequency that is equal to a fraction of the running speed frequency. This sub-synchronous component tracks the running speed until it locks on a natural frequency where its amplitude will increase rapidly and results in oil whip. The frequency of the sub-synchronous vibrations in the oil whirl region is dependent on the *L/D* ratio of the bearing. The higher that ratio is, the closer the sub-synchronous oil whirl is to half running speed.

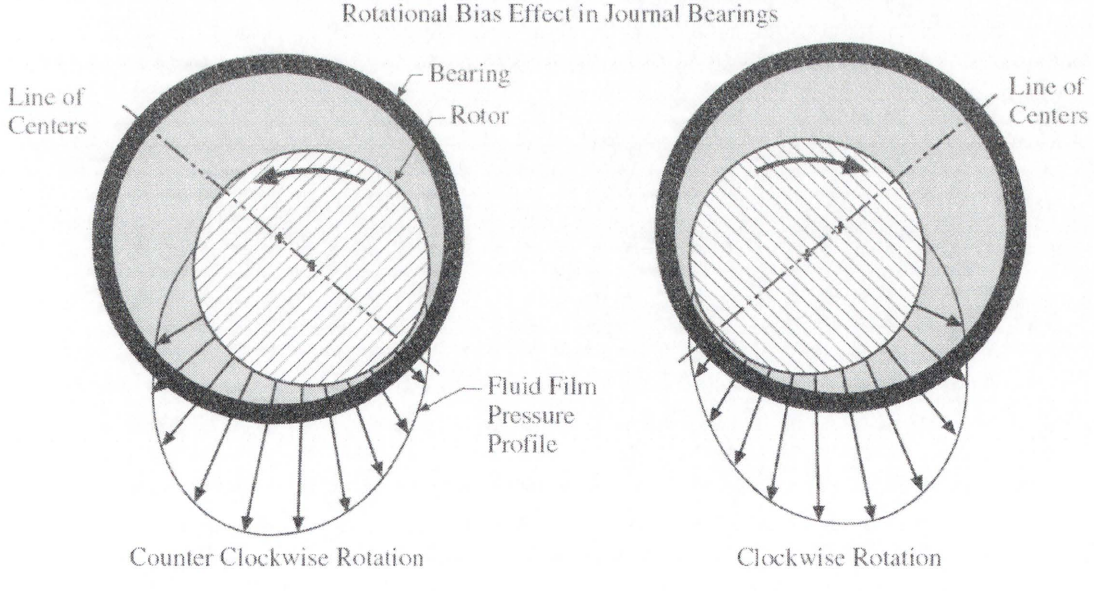

Figure 5-8: Rotational Bias Caused by Cross-Coupled Stiffness Coefficients

It is also worth noting that the cross-coupling in the journal bearing tends to always move or push the shaft to the opposite side of the fluid film. Therefore, this cross-coupling effect ($k_{xy}y$ and $k_{yx}x$) is always biased by the direction of rotation as shown in Figure 5-8. The term rotational bias is often used to describe this phenomenon

(Khonsari and Chang, 1993). All these terms are often used to describe this destabilizing force (generated from the cross-coupled stiffness), which acts in the same manner as direct damping but in the opposite direction to direct damping, thus the term negative damping. Positive damping dissipates energy and in this manner it reduces vibrations and whirl amplitude, while the negative damping adds energy to the dynamic system and therefore increases vibrations and amplitude of motion.

5.3.3.1. Oil Film Force Calculation in a BR

Approximations of oil film forces of the dynamically loaded bearing are presented in Reference (Adiletta et al., 1995; Rezvani and Hahn, 1993) as well as many other studies (Holmes, 1960; Khonsari and Chang, 1993; Wang and Khonsari, 2006). In this study, long bearing solutions (modified short bearing approach) by Rezvani and Hahn (1993) are adopted to calculate oil film bearing forces in the BR.

$$\{F'_{JBH} \quad F'_{JBV}\} = f\left(x_{rel}, y_{rel}, \dot{x}_{rel}, \dot{y}_{rel}, R_{bb}, L_{bb}, \eta, C_{bb}, \omega_{bb}\right) \tag{5.14}$$

where F'_{JBH} and F'_{JBV} is the pressurised oil film forces in the horizontal and vertical direction, subscript '*rel*' indicates relative motion of the bearing housing chock and roll and '*bb*' represents backup roll bearing (Refer to Table 5-2). Therefore, stiffness and damping coefficients with cross-coupled terms are calculated in the following:

$$[K_{BR}] = \begin{bmatrix} \dfrac{\partial F'_{JBH}}{\partial x_{rel}} & \dfrac{\partial F'_{JBH}}{\partial y_{rel}} \\ \dfrac{\partial F'_{JBV}}{\partial x_{rel}} & \dfrac{\partial F'_{JBV}}{\partial y_{rel}} \end{bmatrix} = \begin{bmatrix} k_{xx}^{BR} & k_{xy}^{BR} \\ k_{yx}^{BR} & k_{yy}^{BR} \end{bmatrix} \tag{5.15}$$

$$[C_{BR}] = \begin{bmatrix} \dfrac{\partial F'_{JBH}}{\partial \dot{x}_{rel}} & \dfrac{\partial F'_{JBH}}{\partial \dot{y}_{rel}} \\ \dfrac{\partial F'_{JBV}}{\partial \dot{x}_{rel}} & \dfrac{\partial F'_{JBV}}{\partial \dot{y}_{rel}} \end{bmatrix} = \begin{bmatrix} c_{xx}^{BR} & c_{xy}^{BR} \\ c_{yx}^{BR} & c_{yy}^{BR} \end{bmatrix} \tag{5.16}$$

The journal bearing model introduced in this study is intensively investigated and validated with a different model (Shigley and Mischke, 1986; Adiletta et al., 1995). For more detail information with respect to its validation and characteristic result, refer to Appendix II.

Table 5-2: Journal bearing parameters used for calculations

Bearing radius [*mm*]	Bearing length [*mm*]	Bearing clearance [*μm*]	Viscosity [*Pa·s*]	Eccentricity	Rotational Speed [*RPM*]
R_{bb}	L_{bb}	C_{bb}	η	ε_{bb}	ω_{bb}
400	800	400	0.04	0.872	29.6 (CW)

5.3.4. Mean Bearing Forces of the Tapered Roller Bearing in a WR

Roller bearing or rolling element bearing is much more efficient in delivering or supporting the work roll than the journal bearing as the force applied onto the rotor is distributed effectively rather than pressurising the oil-film in the journal. Thus, many industries are installing the tapered roller bearings for alleviating the huge magnitude of force exerted on the rollers (Timken bearing catalogue, 2001).

In Reference (Harris et al., 2007; Gargiulo, 1980; Lim, 1990), a comprehensive bearing stiffness matrix is proposed which clearly demonstrates a coupling between the translational motions by using the mean bearing displacement vector. A symmetrical bearing stiffness matrix for a WR is defined as:

$$[K_{WR}] = \begin{bmatrix} \dfrac{\partial F'_{RBH}}{\partial \delta_{xm}} & \dfrac{\partial F'_{RBH}}{\partial \delta_{ym}} \\ \dfrac{\partial F'_{RBV}}{\partial \delta_{xm}} & \dfrac{\partial F'_{RBV}}{\partial \delta_{ym}} \end{bmatrix} = \begin{bmatrix} k_{xx}^{WR} & k_{xy}^{WR} \\ k_{yx}^{WR} & k_{yy}^{WR} \end{bmatrix} \tag{5.17}$$

where F'_{RBH} and F'_{RBV} is the mean bearing forces in the horizontal and vertical direction, δ_{im} indicates the mean bearing displacements, subscript 'i' represents x or y. Therefore, tapered roller bearing stiffness coefficients are given explicitly as:

$$k_{xx}^{WR} = nK_n \cos^2 \alpha_0 \sum_j^z \delta_{Rj}^{n-1} \cos^2 \psi_j \tag{5.18}$$

$$k_{xy}^{WR} = k_{yx}^{WR} = \frac{n}{2} K_n \cos^2 \alpha_0 \sum_j^z \delta_{Rj}^{n-1} \sin 2\psi_j \tag{5.19}$$

$$k_{yy}^{WR} = nK_n \cos^2 \alpha_0 \sum_j^z \delta_{Rj}^{n-1} \sin^2 \psi_j \tag{5.20}$$

where subscript '*j*' indicates the *j*th rolling element, the cross-coupling is identical and these bearing stiffness coefficients are only dependent on the translational displacements unless the rotational displacements are significant. Here we assume no damping in the WR as it is negligible compared to that of the journal bearing and roll gap. Also, note that other rotational stiffness coefficients are ignored.

Table 5-3: Tapered roller bearing parameters used for calculations

Bearing radius [*mm*]	Bearing length [*mm*]	Bearing clearance [μm]	Number of rolling element	Exponent	Load deflection constant [*MN/m*]	Rolling element angle [*deg*]	Rotational speed [*RPM*]
R_{wb}	L_{wb}	C_{wb}	Z	n	K_n	α_0	ω_{wb}
150	150	50	50	10/9	300	15	133.33 (CCW)

The tapered rolling bearing model used in this study, unfortunately, does not sufficiently provide detail information about bearing force approximations as it is assembled into two-row or four-row configurations. Nonetheless, bearing stiffness coefficients obtained from this model still are in series combinations in terms of vibrations if any thrust force in the direction of the work roll length does not significantly affect the roller's positions but cancels out each other due to the opposite arrays of roller elements in the tapered roller bearing. For more detail information with respect to its validation and characteristic result, refer to Appendix III.

5.3.5. Load-Displacement Relations between a BR and WR

Surface contact relationship between the BR and WR has been intensively investigated in many studies (e.g., Chefnuex et al., 1984; Robert and Qi, 1994; Lin et al., 2003). However, systems so far are only free to oscillate in the vertical direction only and horizontal coupling is consistently ignored. Therefore, the deformation between the backup and work roll contact is described in two translational directions using linear elasticity by Hertz contact theory. The relative displacement Δ_{ij} between the centers of two rolls of the same material due to a compressive load per unit length f from the roll gap model is well known and given by Roark and Young(2002) as:

$$\Delta_{ij} = \frac{2f_{ij}(1-\nu^2)}{\pi E}\left[\frac{2}{3} + \ln\left(\frac{0.78125E(D_{BR}+D_{WR})}{f_{ij}(1-\nu^2)}\right)\right] \tag{5.21}$$

where Δ_{ij} is relative motion along the axis of loading of two points, v is Poisson's ratio, E is modulus of elasticity. It is assumed here that the roll (BR and WR) length L is large as compared with D_i where i = subscript WR and BR such that Hertzian contact theory is applicable. Subscript 'ij' refer to xx- and yy-directional degrees of freedom, respectively. Taking the derivative form of the relative displacement with respect to applied load yields:

$$\frac{d\Delta_{ij}}{df_{ij}} = \frac{2(1-\nu^2)}{\pi E}\left[\frac{-1}{3} + \ln\left(\frac{0.78125E(D_{BR}+D_{WR})}{f_{ij}(1-\nu^2)}\right)\right] \tag{5.22}$$

It is noted here that the load f in equation (5.22) is to be substituted by the resultant rolling force F_{ij} in the derivation that follows. The effective stiffness coefficient due to surface contact between the upper backup roll and work roll can be defined as follows:

$$k_{ij}^{C} = \frac{dF_{ij}}{d\Delta_{ij}} = \frac{\pi E}{2(1-\nu^2)\left[\frac{-1}{3} + \ln\left(\frac{0.78125E(D_{BR}+D_{WR})}{F_{ij}(1-\nu^2)}\right)\right]} \tag{5.23}$$

In order to obtain the useful coupling between the BR and WR, consider the spring and damper system illustrated in Figure 5-9. ϕ_n is called neutral point/angle where the work roll speed and strip speed are same, θ is the subtended angle at the surface contact between rolls, and φ is the rotational angle ($\pi/2$-θ). The stiffness matrix for this system may be written by using linear transformation below. Note that with φ=0, stiffness matrix becomes U_2 again. For damping matrix, it applies to the same rule. However the damping in the surface contact is very small and thus ignored with minor errors. This can be further explained from the fact that the elastic deformation is modelled under the steady-state condition, and surface is in metal-to-metal contact such that damping is insignificant.

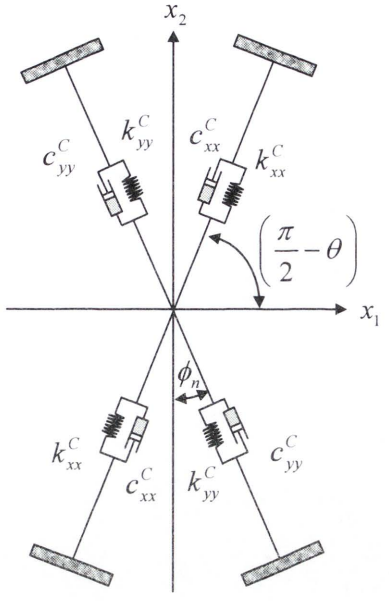

$$U_1 = \begin{bmatrix} \cos\left(\frac{\pi}{2}-\theta\right) & -\sin\left(\frac{\pi}{2}-\theta\right) \\ \sin\left(\frac{\pi}{2}-\theta\right) & \cos\left(\frac{\pi}{2}-\theta\right) \end{bmatrix} \qquad U_2 = \begin{bmatrix} k_{xx}^C & 0 \\ 0 & k_{yy}^C \end{bmatrix}$$

$$U_3 = \begin{bmatrix} \cos\left(\frac{\pi}{2}-\theta\right) & \sin\left(\frac{\pi}{2}-\theta\right) \\ -\sin\left(\frac{\pi}{2}-\theta\right) & \cos\left(\frac{\pi}{2}-\theta\right) \end{bmatrix}$$

$$k_{ij}^{Cont}(\varphi) = U_1 U_2 U_3 = \begin{bmatrix} k_{xx}^{Cont} & k_{xy}^{Cont} \\ k_{xx}^{Cont} & k_{yy}^{Cont} \end{bmatrix}$$

$$= \begin{bmatrix} k_{xx}^C \cos^2\varphi + k_{yy}^C \sin^2\varphi & k_{xx}^C \sin\varphi\cos\varphi - k_{yy}^C \sin\varphi\cos\varphi \\ k_{xx}^C \sin\varphi\cos\varphi - k_{yy}^C \sin\varphi\cos\varphi & k_{xx}^C \sin^2\varphi + k_{yy}^C \cos^2\varphi \end{bmatrix}$$

where $\theta = (\beta - \phi_n)$, $\varphi = \left(\frac{\pi}{2} - \theta\right)$

Figure 5-9: Mode coupling between the contact surface of BR and WR

Table 5-4 shows the stiffness and damping coefficients resulted from the steady-state rolling. Damping coefficients in the BR are significant in the cold rolling mill while those in the bearing housing chock and WR are ignored.

Table 5-4: Stiffness and damping coefficients calculated for a cold rolling mill analysis

Stiffness [*MN/mm*] damping [*MN·s/mm*] coefficients for the bearing housing chock							
k_{xx}^{BH}	k_{xy}^{BH}	k_{yx}^{BH}	k_{yy}^{BH}	c_{xx}^{BH}	c_{xy}^{BH}	c_{yx}^{BH}	c_{yy}^{BH}
31.00	0.0	0.0	32.30	0.0	0.0	0.0	0.0
Stiffness [*MN/mm*] and damping [*MN·s/mm*] coefficients of contact surface between BR and WR							
k_{xx}^{Cont}	k_{xy}^{Cont}	k_{yx}^{Cont}	k_{yy}^{Cont}	c_{xx}^{Cont}	c_{xy}^{Cont}	c_{yx}^{Cont}	c_{yy}^{Cont}
21.78	-0.029	-0.029	34.33	0.0	0.0	0.0	0.0
Stiffness [*MN/mm*] and damping [*MN·s/mm*] coefficients of a upper BR							
k_{xx}^{BR}	k_{xy}^{BR}	k_{yx}^{BR}	k_{yy}^{BR}	c_{xx}^{BR}	c_{xy}^{BR}	c_{yx}^{BR}	c_{yy}^{BR}
29.32	7.63	88.87	158.21	0.89	1.31	2.03	6.79
Stiffness [*MN/mm*] and damping [*MN·s/mm*] coefficients of a upper WR							
k_{xx}^{WR}	k_{xy}^{WR}	k_{yx}^{WR}	k_{yy}^{WR}	c_{xx}^{WR}	c_{xy}^{WR}	c_{yx}^{WR}	c_{yy}^{WR}
3.07	-0.12	-0.12	3.38	0.0	0.0	0.0	0.0

5.4. CALCULATIONS OF ROLLING FORCE IN STANDS

In chapter 4, dynamic force components have been derived in order to identify the coupling effect in the dynamic roll gap and also have been linearised as stiffness and damping coefficients in terms of vibrations. Furthermore, in previous Section 5.3, under the steady-state condition, force components of bearing supports and surface contact are linearised as stiffness and damping coefficients, respectively. These linearisation schemes are valid only when the support bearings are rotating in a steady-state operation. This is due to the state and speed dependency of the bearing supports. If the steady-state condition is guaranteed in the bearing supports even though small disturbance occurs in the roll gap, free and forced vibration analysis can further be performed to determine the relationship between the rolling speed and friction coefficient through investigations of eigenvalues and eigenvectors from the linearised matrix form. For more detailed analysis and results will be given in Chapter 6.

5.4.1. Rolling Force Calculation Schedule

For the calculation of rolling force in a consecutive stand, the homogeneous rolling process model given by equation (4.18) is required. The developed roll gap model is dependent on the rolling speed and friction coefficient if other parameters do not change under the steady-state condition. Table 5-5 shows the rolling force calculation results for the individual stand. The magnitude of rolling force is varied quite a lot depending on the reduction per cent, tension, friction coefficient, work roll radius, rolling speed. Noticeably, the roll radius is deformed more than two times compared to the undeformed roll radius at Pass 5. As a consequence, the estimated rolling force increases due to the elongated contact length between the work roll and strip.

It is worth it a while that the contact length in the deformed roll gap decreases depending on the reduction and tension. As denoted by equation (3.5), the Hitchcock (1935) roll deformation affects to the magnitude of rolling force in the case of thinner and harder strip rolling. Of course, it should be mentioned that the roll deformation fails to converge at the rolling case such as the strip thickness less than $0.1mm$ and friction coefficient less than 0.07.

Moreover, in order to provide more understanding of how the rolling force is calculated, Figure 5-10 demonstrates a good example of iterative calculation for the Pass 4 and iteration has been set to 20 steps so as to estimate accurately rolling force, contact length in the roll gap and deformed roll radius. It is evident that all three parameters are converging quickly within 7 iterations and slow down when approaching the convergence points.

Table 5-5: Rolling force calculation for each stand in a tandem cold rolling mill

Stand	Pass 1	Pass 2	Pass 3	Pass 4	Pass 5
Entry Thickness h_e, (mm)	1.35	0.90	0.60	0.40	0.30
Exit Thickness h_x, (mm)	0.90	0.60	0.40	0.30	0.24
Reduction $(\%)$	33.33	33.33	33.33	25.00	20.00
Back Tension t_e, (MPa)	100	120	120	90 (44kN)	90 (44kN)
Front Tension t_x, (MPa)	100	120	120	90	90
Undeformed Work Roll Radius R_{WR}, (mm)	300	300	290	300	300
Friction Coefficient μ_{s0}	0.025	0.023	0.022	0.020	0.018
Rolling Speed v_R, (m/s)	6.67	10.0	15.0	20.0	23.67
Deformed Work Roll Radius R_d, (mm)	0.400	0.459	0.513	0.733	0.947
Rolling Force (MN)	9.49	8.83	8.52	8.01	7.18

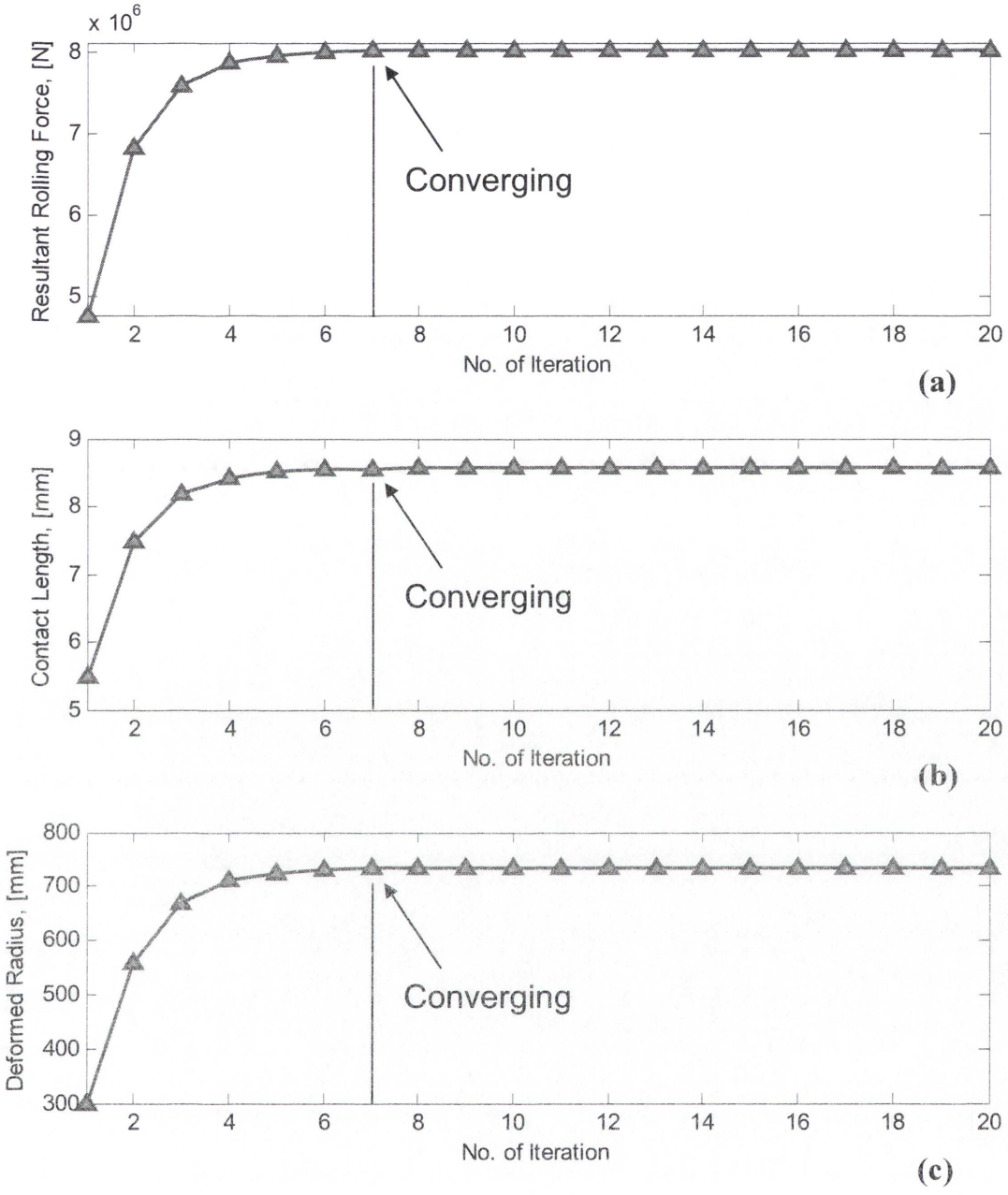

Figure 5-10: Iterative rolling force calculations: (a) resultant rolling force, (b) deformed contact length, (c) deformed roll radius

CHAPTER 6. STABILITY ANALYSIS OF A ROLLING STAND IN COLD ROLLING MILL

6.1. INTRODUCTION

This chapter specifically focuses on stability analysis of a coupled mill vibration model resulting from the force variations in the dynamic roll gap, surface contact and support bearings studied in Chapters 4 and 5. For the determination of system stability regime, all the stiffness and damping coefficients have been linearised from the journal bearing analysis of the backup roll as well as from the tapered roller bearing analysis of the work roll. This linearisation scheme however can result in cumulative error in estimating the accurate bearing forces when the bearing is rotating in a steady-state condition and even whirling at the unstable vibration mode. The main reason for this error is that bearing forces are varying with the positions and relative motions of support bearings during the rolling process. In this chapter, therefore, we ignore the bearing faults/defects resulting from the bearing wear and lack of lubrication, and only consider the steady-state rotating condition such that the stiffness and damping coefficients of bearings can be used in stability analysis.

In order to build a fundamental understanding of a rolling stand in a cold rolling mill, tension variations between stands will not be considered because the coefficients of stiffness and damping are calculated under the steady-state rolling condition. Most significantly, tension variation models, so far presented by Tlusty et al., (1982) and Yun et al., (1998) are assumed harmonic and tension stresses are determined by the sinusoidal function rather than rolling states. Due to the inability to linearise tension variations during the rolling process, the stability criterion will be presented in this chapter without considering effects of the front and back tension variations.

6.2. MODEL COMPARISON

6.2.1. Damping Coefficient in the Dynamic Roll Gap

As presented by Tlusty et al. (1982) and Kimura et al. (2003), the effects of the damping coefficient in the roll gap due to the rolling speed are best explored in a rolling stand of

cold rolling mill. Recalling the damping formula of a variable force component depending on the rolling speed yields (Tlusty et al. 1982; Kimura et al. (2003):

$$C^1_{Tlusty} = (\sigma_x - t_x)_{\text{var}} \frac{WR_{WR} X \omega \cos(\omega t)}{v_x} \tag{6.1}$$

$$C^1_{Kimura} \approx \frac{k_f WR_{WR}}{2v_R} \tag{6.2}$$

In order to identify the negative damping effect in the roll gap, Tlusty et al., (1982) also presented the formula as follows:

$$C^2_{Tlusty} = (\sigma_x - t_x)_{\text{var}} \frac{2WXv_x E\sqrt{R_{WR}(h_e - h_x)}\cos(\omega t)}{Lh_e\omega} \tag{6.3}$$

A cosine term in equation (6.3) precedes the sine term of the harmonic vibration and harmonic force "leads" the vertical vibration by 90°. They suggested that such a force variation represents negative damping and may cause self-excited vibration.

These damping coefficients are well employed in a dynamic roll gap analysis in order to identify the positive or negative damping effect from the characteristic equation of the chatter model. For the second order differential equations of motion in the dynamic roll gap, therefore, the damping force component can be approximated as:

$$(C_{Gap} - C_{\text{var}})\dot{X} > 0 \tag{6.4}$$

where $\dot{X}$ are the velocities of the mass elements, C_{Gap} is the positive damping in the bearing support (resulted from the mill structure) and the dynamic roll gap, and C_{var} are negative damping in the roll gap as indicated by Tlusty et al., (1982) and Kimura et al., (2003), respectively.

This concept is first introduced by Tlusty et al., (1982) although the model is very limited to certain rolling conditions. In order to better understand the damping model

presented in equations (6.1) and (6.2), it is necessary to evaluate the force variations with respect to various rolling conditions. In comparison to the current damping coefficient presented in equations (4.44) and (4.45) of Chapter 4, however, it is almost impossible to validate the estimated damping coefficient as the used rolling parameters and the resistance deformation of the material differ from other models. Nonetheless, the calculation results provide a similar trend of the damping coefficient in the roll gap. As an example, the estimated damping coefficient using equation (6.1) varies with the amplitude and frequency used, and the value cannot be evaluated without knowing the amplitude of work roll. The value for equation (6.2) is estimated around 6.8 *MNs/m*. The rough approximation of the material damping coefficients depending on the rolling speed is due to simplifications of the roll gap model. According to the calculation of damping coefficient by Zhao et al., (2008), it is confirmed that the damping coefficient decreases with the increasing rolling speed in a nonlinear fashion as demonstrated in Figure 6-1.

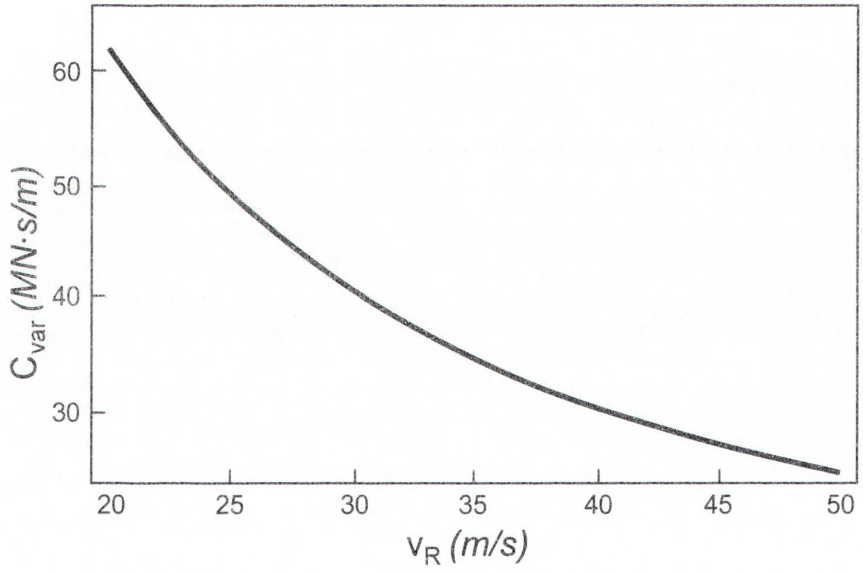

Figure 6-1: Variations of damping coefficient depending on the rolling speed (Zhao et al., 2008)

In Figure 4-9(b), it is also shown that rolling force variations with respect to the small change in the rolling speed decrease with the increasing rolling speed, indicating that force variations in the dynamic roll gap result in positive damping effects. In other words, the calculation result demonstrates that C_{var} is very sensitive to the change of rolling speed and proportional to the inverse of the rolling speed.

In addition to the effect of rolling speed, As reported by Tlusty et al. (1982), they concluded that variations of inter-stand tension also affect the rolling force and result in an increase of a negative damping effect. According to the investigation of Yun et al., (1998), on the other hand, it is understood that negative damping effect resulting from the back tension variations affects the rolling force variation and has a significant influence on the overall magnitude of the strip thickness variation. However, it is not clear how the force variation is combined for the purpose of the calculation of damping coefficient.

6.2.2. Stiffness Coefficient in the Dynamic Roll Gap

As indicated by Tlusty et al., (1982) again, the force variations due to the change in the roll gap spacing represent the stiffness coefficient. Therefore, these variations are added to the roll gap as a form of elastic force and increase the natural frequency of the coupled rolling mill system. The calculated force variations act as a spring rather than a damper in the dynamic roll gap and do not have an effect on the unstable conditions due to the positive effect. Recalling the stiffness formula of a variable force component depending on the roll gap spacing yields:

$$K_{Tlusty} = \left(\sigma_x - t_x\right)_{\text{var}} W \sqrt{\frac{R_d}{h_e - h_x}} \tag{6.5}$$

$$K_{Kimura} = \left(\frac{\partial F_V}{\partial h_c}\right) \tag{6.6}$$

These two stiffness coefficients are also employed in a dynamic roll gap analysis in order to identify the natural frequency range resulted from the characteristic equation of the chatter model. The value for equation (6.5) is equal to 68.1 *MN/mm* and the value of 44.16 *MN/mm* is calculated from equation (6.6). This is a good example for comparison in terms of the linearisation as a spring and damper for the vibration analysis and has been evaluated in Figure 4-9(c). In the second order differential equations of motion in the dynamic roll gap, the spring force component can be defined as:

$$\left(K_{Gap} - K_{\text{var}}\right) X > 0 \tag{6.7}$$

where X are the displacements of the mass elements, K_{Gap} is the stiffness coefficient in the bearing support (resulted from the mill structure) and K_{var} is the stiffness coefficient in the deformed strip by Tlusty et al., (1982) and Kimura et al., (2003), respectively. It should be mentioned that the resulting value of K_{var} generally becomes positive when rearranging it from the RHS of the differential equation.

6.3. SYSTEM MATRIX

Rewriting equations (5.7) – (5.12) and substituting the dynamic force components of equations (4.43) and (4.44) in matrix form of the first-order

$$\dot{X} = \mathrm{A}X \tag{6.8}$$

where $X = \left(x_{BH}, y_{BH}, x_{BR}, y_{BR}, x_{WR}, y_{WR}, \dot{x}_{BH}, \dot{y}_{BH}, \dot{x}_{BR}, \dot{y}_{BR}, \dot{x}_{WR}, \dot{y}_{WR}\right)^T$.

The system matrix is given by

$$\mathrm{A} = \begin{bmatrix} 0_6 & \mathrm{I}_{D6} \\ -M^{-1}\mathrm{K} & -M^{-1}\mathrm{C} \end{bmatrix} \tag{6.9}$$

where 0_6 is a 6×6 zero matrix and I_{D6} is a 6×6 identity matrix.

Therefore, system mass, stiffness and damping matrix including the dynamic force components can be defined as:

$$[M] = \begin{bmatrix} m_{BH} & 0 & 0 & 0 & 0 & 0 \\ 0 & m_{BH} & 0 & 0 & 0 & 0 \\ 0 & 0 & m_{BR} & 0 & 0 & 0 \\ 0 & 0 & 0 & m_{BR} & 0 & 0 \\ 0 & 0 & 0 & 0 & m_{WR} & 0 \\ 0 & 0 & 0 & 0 & 0 & m_{WR} \end{bmatrix},$$

$$[K]=\begin{bmatrix} \left(k_{xx}^{BH}+k_{xx}^{BR}\right) & \left(k_{xy}^{BR}\right) & -k_{xx}^{BR} & -k_{xy}^{BR} & 0 & 0 \\ \left(k_{yx}^{BR}\right) & \left(k_{yy}^{BH}+k_{yy}^{BR}\right) & -k_{yx}^{BR} & -k_{yx}^{BR} & 0 & 0 \\ -k_{xx}^{BR} & -k_{xy}^{BR} & \left(k_{xx}^{BR}+k_{xx}^{Cont}\right) & \left(k_{xy}^{BR}+k_{xy}^{Cont}\right) & -k_{xx}^{Cont} & -k_{xy}^{Cont} \\ -k_{yx}^{BR} & -k_{yx}^{BR} & \left(k_{yx}^{BR}+k_{yx}^{Cont}\right) & \left(k_{yy}^{BR}+k_{yy}^{Cont}\right) & -k_{yx}^{Cont} & -k_{yy}^{Cont} \\ 0 & 0 & -k_{xx}^{Cont} & -k_{xy}^{Cont} & \left(k_{xx}^{WR}+k_{xx}^{Cont}\right) & \left(k_{xy}^{WR}+k_{xy}^{Cont}-K_{xy}^{\text{var1}}\right) \\ 0 & 0 & -k_{yx}^{Cont} & -k_{yy}^{Cont} & \left(k_{yx}^{WR}+k_{yx}^{Cont}\right) & \left(k_{yy}^{WR}+k_{yy}^{Cont}-K_{yy}^{\text{var1}}\right) \end{bmatrix} \text{ and}$$

$$[C]=\begin{bmatrix} \left(c_{xx}^{BH}+c_{xx}^{BR}\right) & \left(c_{xy}^{BR}\right) & -c_{xx}^{BR} & -c_{xy}^{BR} & 0 & 0 \\ \left(c_{yx}^{BR}\right) & \left(c_{yy}^{BH}+c_{yy}^{BR}\right) & -c_{yx}^{BR} & -c_{yx}^{BR} & 0 & 0 \\ -c_{xx}^{BR} & -c_{xy}^{BR} & \left(c_{xx}^{BR}+c_{xx}^{Cont}\right) & \left(c_{xy}^{BR}+c_{xy}^{Cont}\right) & -c_{xx}^{Cont} & -c_{xy}^{Cont} \\ -c_{yx}^{BR} & -c_{yx}^{BR} & \left(c_{yx}^{BR}+c_{yx}^{Cont}\right) & \left(c_{yy}^{BR}+c_{yy}^{Cont}\right) & -c_{yx}^{Cont} & -c_{yy}^{Cont} \\ 0 & 0 & -c_{xx}^{Cont} & -c_{xy}^{Cont} & \left(c_{xx}^{WR}+c_{xx}^{Cont}-C_{xx}^{\text{var1}}-C_{xx}^{\text{var2}}\right) & \left(c_{xy}^{WR}+c_{xy}^{Cont}-C_{xy}^{\text{var3}}\right) \\ 0 & 0 & -c_{yx}^{Cont} & -c_{yy}^{Cont} & \left(c_{yx}^{WR}+c_{yx}^{Cont}-C_{yx}^{\text{var1}}-C_{yx}^{\text{var2}}\right) & \left(c_{yy}^{WR}+c_{yy}^{Cont}-C_{yy}^{\text{var3}}\right) \end{bmatrix}$$

The system matrix A is used to study the vibrational mode and stability analysis. With linearised stiffness and damping coefficients, the system matrix includes the effect of the friction coefficient and rolling speed variation at a given friction sloped gradient. The stability analysis yields two eigenvalues that are complex conjugate pairs representing the system frequencies of x- and y-directional vibration and two eigenvalues that are real frequency pairs representing the rigid body modes of the system.

6.3.1. Mode Shapes

In Figure 5-7, the reference and the displaced configuration of the plain roll stack model are given. Each roll is considered as a rigid body and has two degrees of freedom (horizontal and vertical translational motions). The motion of rolls is described in an inertial coordinate system. The relative coordinates between the rolls are included to describe the plain motion of the rolls. Since the rolls are constrained to move in the x- and y-directions, only two coordinates are required to specify positions of one roll. The differential equations of the motion in terms of the generalised coordinates have been derived based on the linear theorem; the spring and damper characteristic curves of a rolling stand in the horizontal and vertical direction are calculated by the dynamic roll gap model. The model equations can be expressed in a compact form for free vibration analysis as following:

$$[\mathrm{M}]\ddot{X}+[\mathrm{C}]\dot{X}+[\mathrm{K}]X=0 \tag{6.10}$$

where [M] is the mass matrix, [C] is the damping matrix and [K] is the stiffness matrix.

The numerical linearisation of the proposed model delivers statements about the natural frequencies and the corresponding modes. Table 6-1 shows mode analysis results at the friction coefficient of 0.02, rolling speed of 28*m/s* with friction gradient of 0.026*s/m*. It shows six modes as result of the calculations with the corresponding frequencies under the steady-state condition. This is a basis for explanation of possible external-, parametric-, and self-excited vibration characteristics and for specific qualitative predictions of the occurrence of chatter or undesirable vibrations. Such dynamic effects may be related to the uneven/irregular strip surface.

Table 6-1: Unstable vibrational mode for the free vibration analysis at the friction coefficient of 0.02 and rolling speed of 28.0*m/s* with the friction gradient of 0.026*s/m*

Mode Shapes		Frequencies (*Hz*)											
		f_1		f_2		f_3		f_4		f_5		f_6	
		Damped		**7.92**		**119.22**		**131.75**		**274.97**		**342.95**	
Damping Ratio (ζ)		100%		91.75%		1.30%		11.29%		-0.0123%		21.59%	
Amplitude & Phase(*deg*)		Amp	Phase	Amp	Phase	Amp	Phase	Amp	Phase	Amp	Phase	Amp	Phase
m_{BH}	x_{BH}	0.207	0.0	0.089	178.2	0.881	2.3	0.017	186.0	0.226	178.8	0.002	257.4
	y_{BH}	**1.000**	**0.0**	0.049	288.6	0.392	33.4	**1.000**	**0.0**	0.116	233.0	0.199	145.5
m_{BR}	x_{BR}	0.138	-180.0	**1.000**	**0.0**	0.882	-0.5	0.017	153.4	0.227	180.5	0.0	206.3
	y_{BR}	0.667	-180.0	0.300	109.6	0.399	34.7	0.999	-0.4	0.114	232.6	0.198	145.9
m_{WR}	x_{WR}	$8.3e^{-7}$	-180.0	0.876	0.1	**1.000**	**0.0**	0.014	161.7	**1.000**	**0.0**	0.007	99.6
	y_{WR}	$6.4e^{-6}$	-180.0	0.255	109.7	0.444	32.9	0.993	-13.1	0.275	52.6	**1.000**	**0.0**

Note that the force components in the bearing housing chock, journal bearing and tapered roller bearing, respectively, have been linearised as the stiffness and damping coefficients under the steady-state rolling conditions. The force components acting on the surface contact are also linearised using Hertzian contact theory. Table 4-2 shows the key rolling parameters used for the rolling force calculation (Also refer to Table 5-2 and 5-3 for the bearing analysis, and Table 5-4 for the results of stiffness and damping coefficients).

For the modes of mass elements, the first mode indicates the overdamped frequency as there are no complex conjugate eigenvalues, and thus natural frequencies cannot be calculated. In the second mode, rolls have same phase in relation to the roll gap. BR moves in phase with the WR in the x- and y-directions while the bearing housing chock has the opposite phase with rolls. In the third mode, it can be considered all mass elements are in phase in relation to the roll gap as phase difference is very small in this mode. When ignoring vibrations of the bearing housing chock, it can be regarded the second, third, fourth modes are the mass center motion showing two rolls are in-phase motions except the last two modes. Among those illustrated modes, the fifth and sixth modes are distinct where both rolls are opposing each other or motion is out of phase.

Comparing to the information given by Johnson and Qi (1994), Chen et al. (2002) and Lin et al. (2003), this is in good agreement with the numerical results obtained from the four DOF model. The second mode falls to the vibration mode corresponding to a natural frequency around 8.0 Hz. The third and fourth modes are not significant and indicate more or less the third-octave mode. The eigen-mode implies that all components are vibrating in a separating or squeezing manner, respectively where all the mass elements have the negligible off-phase motion in the y-direction. Particularly, the fifth mode is within the range of third-octave mode chatter (Chen et al., 2002) where both rolls are out-of-phase motion. The sixth mode lies in the range of the fifth-octave mode chatter (Lin et al., 2003; Hu and Ehmann, 2001) showing out-of-phase motion. In fifth and sixth modes, two rolls are opposite motion in the y-direction and the bearing housing chock is in-phase motions with BR in the y-direction.

If one of these modes is excited during the rolling process, the eigen-mode suggests that WR vibrates in a separating or squeezing manner with much larger amplitude than that of BR or any other components.

More interestingly, at the given condition, the fifth mode would significantly produce gauge variations due to the negative damping effect. Also, it is shown from mode analysis that relative motion between rolls and roll gap surfaces can also be a source of chatter, resulting in high amplitude compared to other motions. Table 6-2 shows a summary of the model features used in the calculation of dynamic roll gap model.

Table 6-2: Summing-up of the dynamic model

Properties	Bearing force components (Journal bearing and tapered roller bearing) Linear surface contact between rolls (Hertzian Contact), Non-linear roll gap including negative gradient of friction coefficient (Negative damping effect), Two dimensional motions (Bearing supports and roll gap model), Elastic rolls (Hitchcock roll deformation), Elastic boundary conditions, Rolling force (Ford and Bland approach).
Assumptions	Neutral point/angle is not moving, Constant negative damping factor α_s $[s/m]$.
Realisation	MATLAB.
Results	Mode shapes, Natural frequencies.

6.3.2. Stability Threshold Curve (STC)

The stability of the cold rolling mill can be determined by investigating the real part eigenvalues of the characteristic equation which are obtained from the equations governing the mill vibrations. The system will be stable if all the eigenvalues of the characteristic equations have negative real parts. In this study, the bearing faults/defects

resulted from the bearing wear and lack of lubrication are ignored. Considering small disturbance in the roll gap only at the steady-state rolling condition, linearised bearing coefficients can be used in stability analysis.

Matthews and Yuen (2006) reported that both high and low friction conditions can lead to increased rolling force, resulting in strip thickness variation, poor shape in the cold rolled production and skidding (or sliding) when the work roll speed is higher than the strip speed. It is also generally understood that the rolling speed of the cold rolling mill needs to be reduced to relieve the problems associated with sliding.

In order to explain dynamic characteristics of the cold rolling mill, a simulation model is devised from the given roll profile. Stability threshold curves (STC) have been determined through the change in the key rolling parameters to identify the stable and unstable rolling conditions. In this approach the real part of eigenvalues of the system matrix is utilised to judge stability regime, it is considered stable if the real part of eigenvalues is negative or unstable if positive. Here, controlling parameters are the friction coefficient and rolling speed at a given friction gradient (α_s). Table 6-3 shows the complex conjugate pairs and corresponding frequencies for four different values of the friction gradient.

Table 6-3: Results for various gradients of the friction (v_{CR} =22.73*m/s*, μ_{s0} =0.02)

α_s = 0.024 [*s/m*]		α_s = 0.025 [*s/m*]		α_s = **0.026** [*s/m*]		α_s = 0.027 [*s/m*]		Damped Freq (*Hz*) at α_s = **0.026**
*Re**	*Im**	*Re**	*Im**	*Re**	*Im**	*Re**	*Im**	
−39554	±0.0i	−39554	±0.0i	−39554	±0.0i	−39554	±0.0i	Damped (100%)
−37.7	±15.8i	−37.7	±15.8i	−37.7	±15.8i	−37.7	±15.8i	6.51 (92.3%)
−10.0	±749.1i	−10.0	±749.1i	−9.97	±749.1i	−9.90	±749.1i	119.23 (1.33%)
−111.1	±828.1i	−111.1	±828.1i	−111.1	±828.2i	−111.2	±828.2i	132.99 (13.3%)
−0.088	±1726.0i	−0.044	±1726.0i	**±0.0000**	±1725.9i	+0.044	±1725.9i	**274.69 (0.00%)**
−552.1	±2059.5i	−552.1	±2059.6i	−552.1	±2059.6i	−552.1	±2059.7i	339.38 (25.9%)

* *Re* and *Im* are the real and imaginary part of complex conjugate pairs, respectively. Minor error included due to the complexity of finding the exact zero of the real part in this calculation.

For different gradients of friction gradient, one eigenvalue will respond with underdamped (or periodic) oscillations in those modes to any disturbance to equilibrium and the other will exhibit self-excited oscillations. For instance, for a zero or negative gradient, the system has six stable roots and will respond with damped oscillations. For a positive gradient, the system has a pure imaginary complex conjugate pairs and stable or unstable root in the vicinity of the curve. Thus its response will be in stable, marginally stable or unstable motions, respectively.

In order to clearly divide the stable and unstable regime, one case is chosen for the friction gradient $0.026s/m$. Each symbol (diamond, circle, rectangle and triangle) stands for the critical operating condition at STC as shown in Figure 6-2. The marginal stability regime is highly dependent on the friction gradient, shifting the stability threshold curve to the left side as the friction gradient increases up to $0.027s/m$ from $0.026s/m$ whilst it is likely to move toward the right-hand side resulting in more stable regime when it steadily decreases to $0.024s/m$, which shows that the negative damping effect due to the effect of sliding or slip is less considerable. In the vicinity of the stable rolling threshold, moreover, the system behaviour is significantly affected by the change of the rolling speed and friction coefficient, respectively. In the range of friction coefficient of 0.010 – 0.016, stability is more likely to be significantly affected by the rolling speed change. Within this range, the likelihood of instability occurs when the friction coefficient decreases. On the other hand, in the range of around 0.016 – 0.03, instability is likely to arise from the increase of the friction coefficient.

Also, stability of the system is greatly affected by the change of the rolling speed, becoming unstable as the rolling speed increases. Under the given condition with the gradient of friction of $0.026s/m$, the critical rolling speed (critical operating point, C.O.P) has been calculated as $22.73m/s$. In other words, the proposed system is likely to be in unstable motion when the rolling speed is faster than $+2.73m/s$ at the assumed steady-state condition.

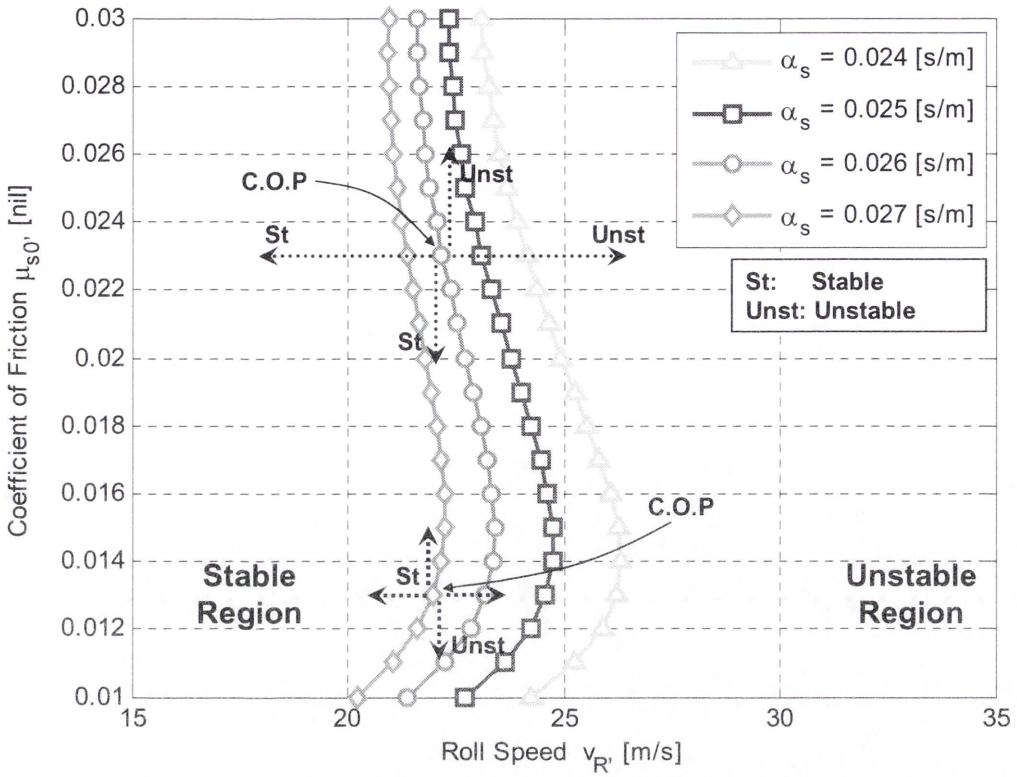

Figure 6-2: Stability threshold curves depending on the rolling speed and friction coefficient change at α_s =0.024 to 0.027, respectively

The obtained results agree well with those observed in production, even though the gradient of friction slope is assumed to be a constant. A similar case study of calculating the close relationship between the friction coefficient and rolling speed has been performed by Kimura et al. (2003). Yuen et. al (Yuen et al., 1998; Qiu et al., 1999; Yuen, 1999; Yuen and Matthews, 2003; Yuen, 2003) conducted the important characteristics of friction coefficient and rolling speed, taking into consideration in order to appropriately calculate the start-up condition. The objective of set-up for a rolling schedule is to determine and preset the mill control actuators at the start of rolling process.

On closer examination of the correlation of the friction with rolling speed, they found that although there are significant scatters in the data (because of the wide variations in mill conditions); the trend exhibited for each individual stand follows that of the average variation closely. However, the variation of friction coefficient results from the deduction in the measured mill data. In other words, in order to avoid skidding and

other problems, they simply presented the scattering data of the trend due to the variations in mill condition; not through the change in dynamic conditions but through the steady-state mill conditions.

Note that it is assumed that the neutral point/angle does not move around the roll contact angle and the stiffness and damping coefficients of the system model used are chosen from the results of transient bearing analysis when oscillations are stabilised. Therefore, it may not be accurate for the full-transient analysis as the coefficients for the bearings are varying with the acceleration and deceleration of the cold rolling mill.

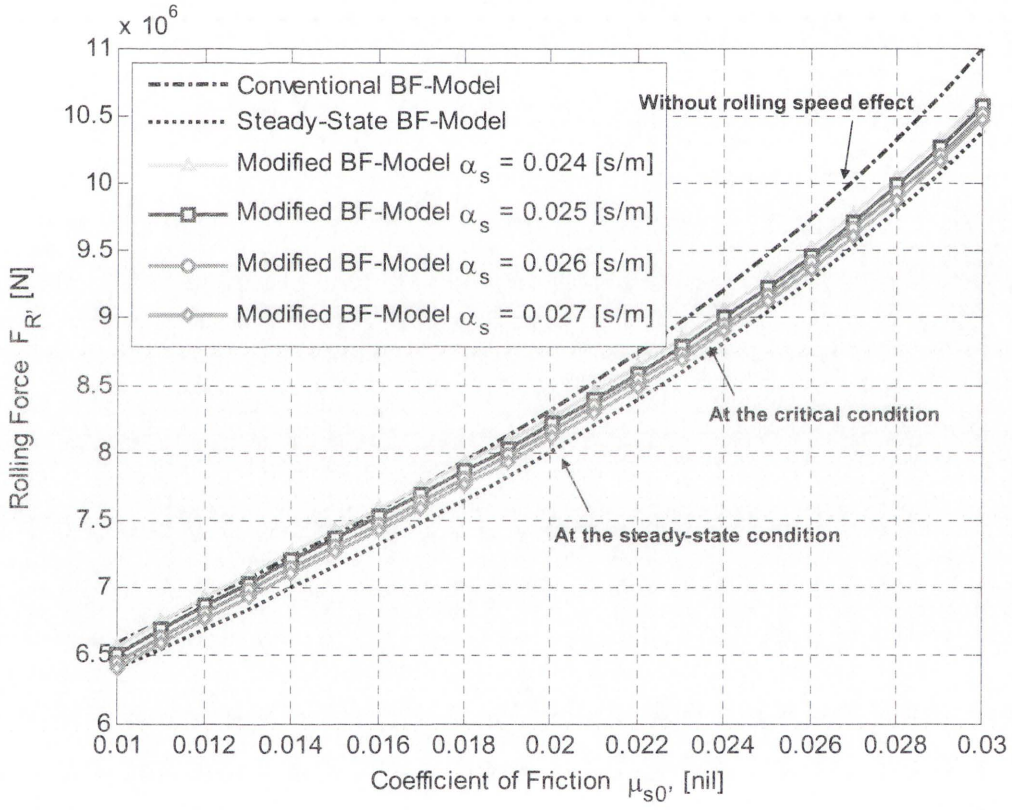

Figure 6-3: Resultant rolling force variations recalculated from the critical rolling conditions of stability threshold curve (STC)

6.3.3. Other Aspects of Stability Threshold Curve (STC)

In order to identify different aspects of stability threshold curve (STC) with respect to other rolling parameters, it should be mentioned that stability threshold curves (STCs) determined through this study are valid only when the steady-state conditions are maintained. Therefore it is considered that equilibrium positions of the model are not affected by the change in other rolling parameters such as the strip width and thickness, roll radius, strain and strain rate exponent.

Based on the aforementioned definition, different stability threshold curves have been established in the same manner as demonstrated in Figure 6-2. In particular, each stability threshold curve is compared with the reference result (a circle symbol with the friction gradient of $0.026s/m$) determined in Figure 6-2.

6.3.3.1. Influence of Strip Width

In order to investigate the effect of the strip width on mill stability, a reference curve (strip width $1.224m$) determined in Figure 6-2 is chosen. In comparison to this curve, Figure 6-4 demonstrates that stability threshold curve is significantly affected by the change of the strip width as the rolling force is proportional to the strip width as indicated in equation (4.18). Specifically, the system is likely to be stabilised with the increase of friction coefficient at the strip width of $1.5m$ while it appears to be unstable with the increase of friction coefficient (over the range of 0.016) when the strip width is set to $1.0m$. Notably, in the range of strip width from 1.224 to $1.5m$, it shows that stability is significantly influenced by the change of the strip width in the lower range of friction coefficient (0.01 to 0.016) while it tends to move toward the right hand side in the higher range of friction coefficient (0.017 to 0.03). Overall, it can be concluded that the system is more likely to stable as the strip width decreases in the lower friction coefficient range. Also, it appears to the Author that maximum allowable rolling speed increases if the strip width decreases to $1.0m$ while in the higher friction coefficient range instability more rapidly arises with the increase of friction coefficient.

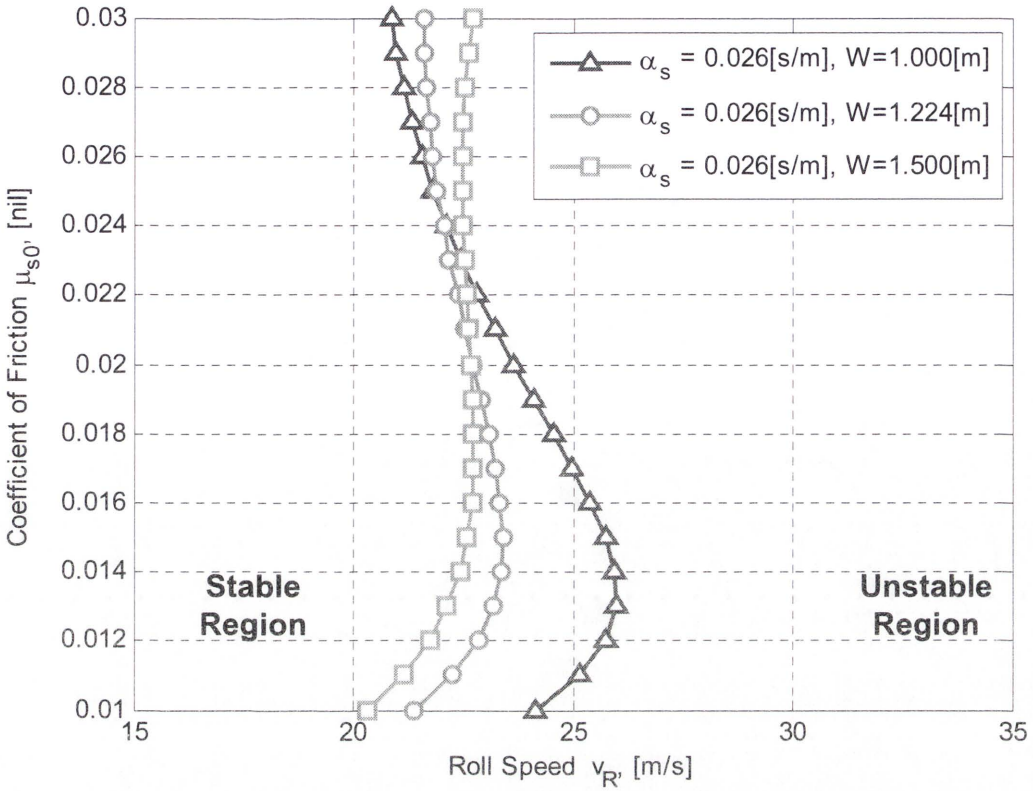

Figure 6-4: Stability threshold curves depending on the rolling speed and friction coefficient change at α_s =0.026*s/m* and W =1.000 to 1.500 *m*, respectively

6.3.3.2. Influence of Roll Diameter

Before discussing the influence of roll diameter on stability threshold curve, it may be necessary to mention that the mill system's stability is more highly dependent on the roll roughness rather than the size of the roll diameter. Nonetheless, it is a good example of how the dimension of roll diameter contributes to the system stability in a way that the magnitude of the resulting force in the roll gap will be changed due to the change in the deformed contact length of the lubricated surface. Figure 6-5 demonstrates the influence of the size of the roll diameter on the mill stability although its effects are not significant. For the smaller roll radius (0.28*m*), the resulting rolling force reduces owing to the relationship of the proportion of the rolling force and roll radius in equation (4.18). Therefore, it can be concluded that with the smaller resulting rolling force stability threshold curve (STC) moves towards the right, indicating increased stability. For the bigger roll radius (0.32*m*), the resulting rolling force arises such that STC shifts

to the left hand side compared to STC of the roll radius $0.3m$, representing more unstable regions.

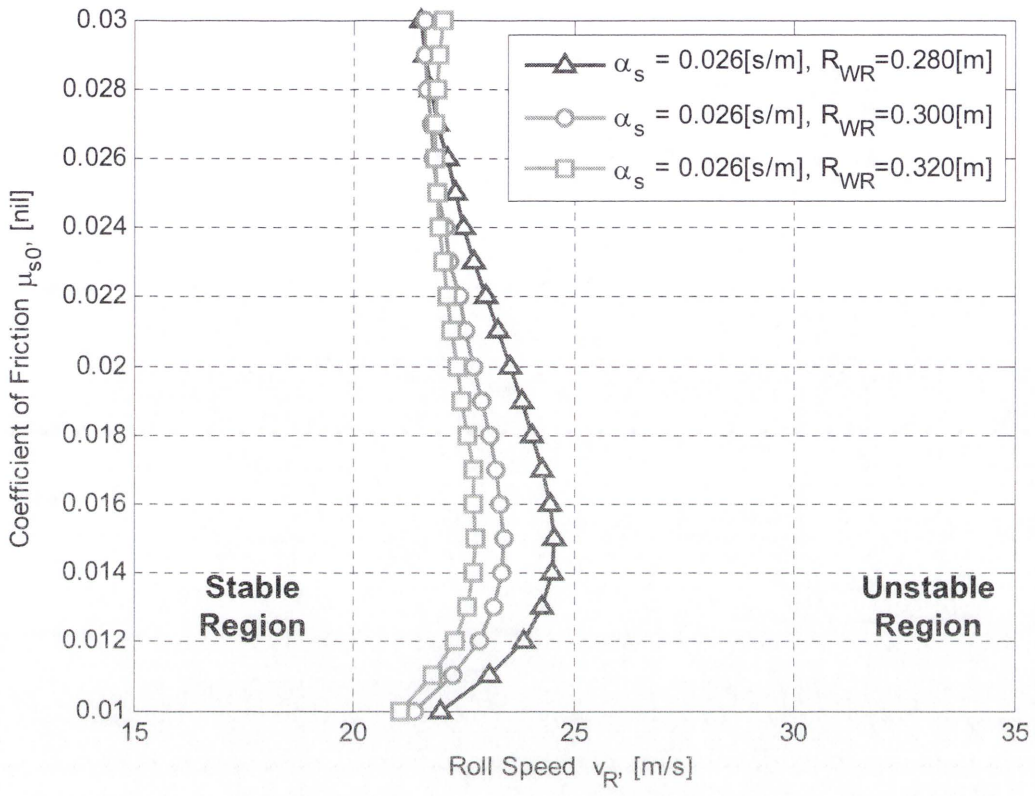

Figure 6-5: Stability threshold curves depending on the rolling speed and friction coefficient change at α_s =0.026s/m and R_{WR} =0.28 to 0.32 m, respectively

6.3.3.3. Influence of Strip Thickness

In Chapter 3, the strip reduction, indicating the difference of the entry and exit thickness in the given roll profile, contributes to the contact length of the deformed roll surface. Of course, the deformed roll radius estimated by Hitchcock (1935) roll flattening results in the deformed roll contact length as defined by equation (3.3). Thus, the elongated contact length results in high rolling force in the deformed roll gap as demonstrated by Figure 4-3(b). In order to identify the sensitivity of variations of the exit thickness, stability threshold curve (STC) has further been determined by changing of the exit thickness of the roll gap.

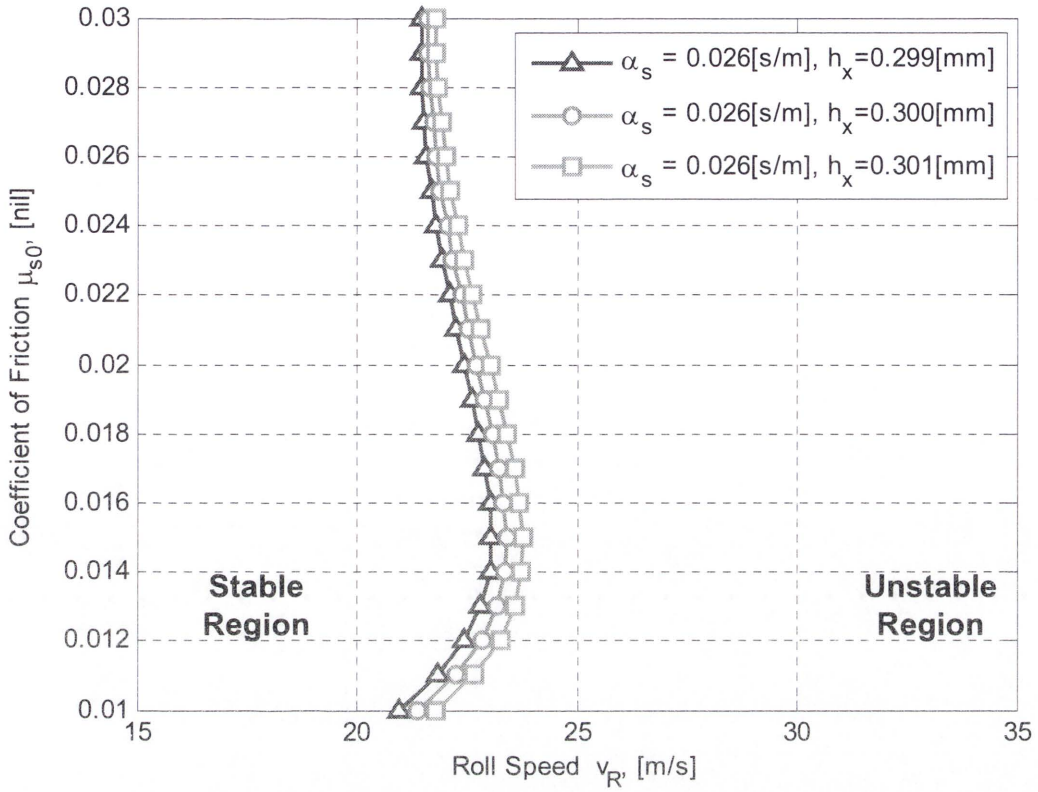

Figure 6-6: Stability threshold curves depending on the rolling speed and friction coefficient change at α_s=0.026*s/m* and h_x=0.299*mm* to 0.301*mm*, respectively

As demonstrated in Figure 6-6, stability threshold curve moves towards the left hand side as the reduction in the roll gap increases while it is likely to shift to the right hand side as the reduction reduces. For instance, the one curve denoted by the exit thickness of 0.301*mm* indicates the high reduction (0.101*mm*) by the subtraction of the entry and exit thickness and the other represented by the exit thickness of 0.299*mm* shows the low reduction (0.099*mm*).

6.3.3.4. Influence of Strain Exponent

Exponents (γ_1 and γ_2) in equation (4.16) significantly affect to the estimation of rolling force resulting from the presented roll gap model in the steady-state conditions and are usually determined from the experiment of the being rolled materials. As represented in equation (3.38), the flow stress (yield strength) is affected by three different exponents such as the strain, strain rate and temperature. In this study, the effects of the temperature in the deformation resistance model are ignored as the temperature in the

cold rolling is generally maintained at the room temperature compared to the hot rolling process. Nonetheless, it is considered that the strain exponent in the deformation resistance model may slightly be varied by the dynamic rolling process. From the simulation, the change in strain exponent negligibly affects the system stability in comparison to the reduction change. As shown in the magnified scale of Figure 6-7, the system stability is negligibly affected by the increase or decrease of the strain exponent, representing the more unstable if the value of γ_1=0.28, the more stable if γ_1=0.24.

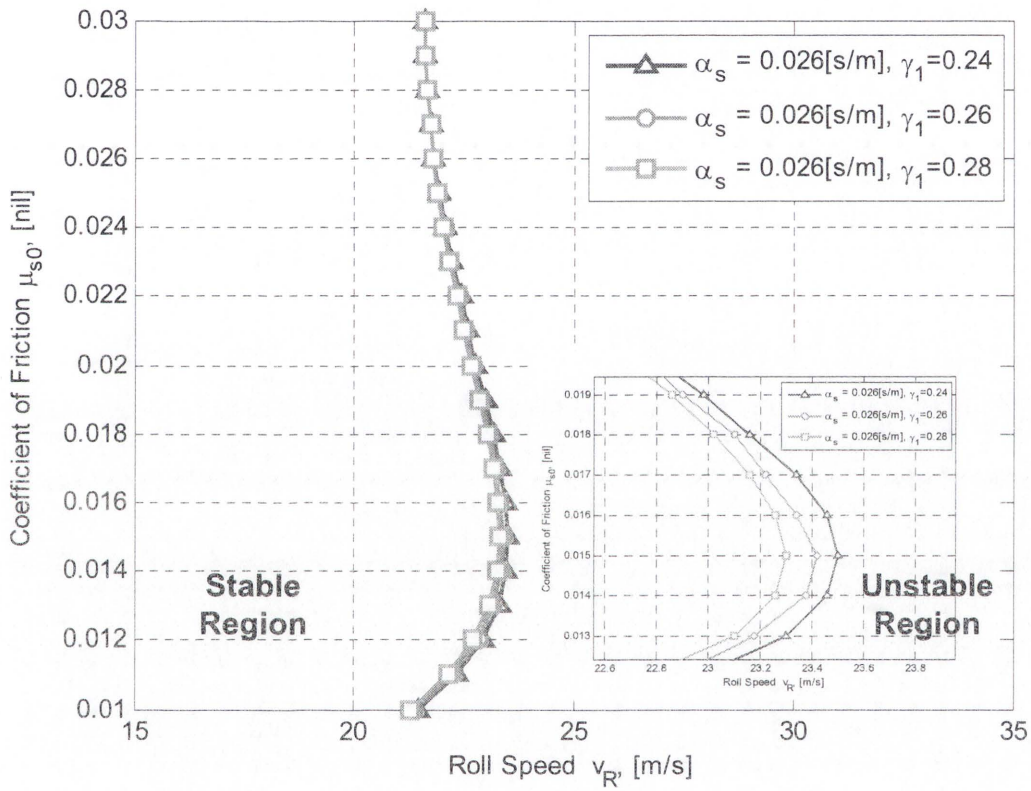

Figure 6-7: Stability threshold curves depending on the rolling speed and friction coefficient change at α_s=0.026*s/m* and γ_1=0.24 to 0.28, respectively

6.3.3.5. Influence of Strain-Rate Exponent

The exponent γ_2 in equation (4.16) also affect to the estimation of rolling force and is highly dependent on the rolling speed of the strip being rolled. Based on the stability analysis, it is identified that the change in strain-rate exponent more significantly affects the system stability than the strain exponent. As shown in Figure 6-8, instability arises from the decrease of the strain-rate exponent as the rolling force would increase with the

decreasing strain-rate sensitivity. Thus, the stability threshold curve shifts to the left hand side at γ_2=0.078 while it tends to move towards the right hand side at γ_2=0.082.

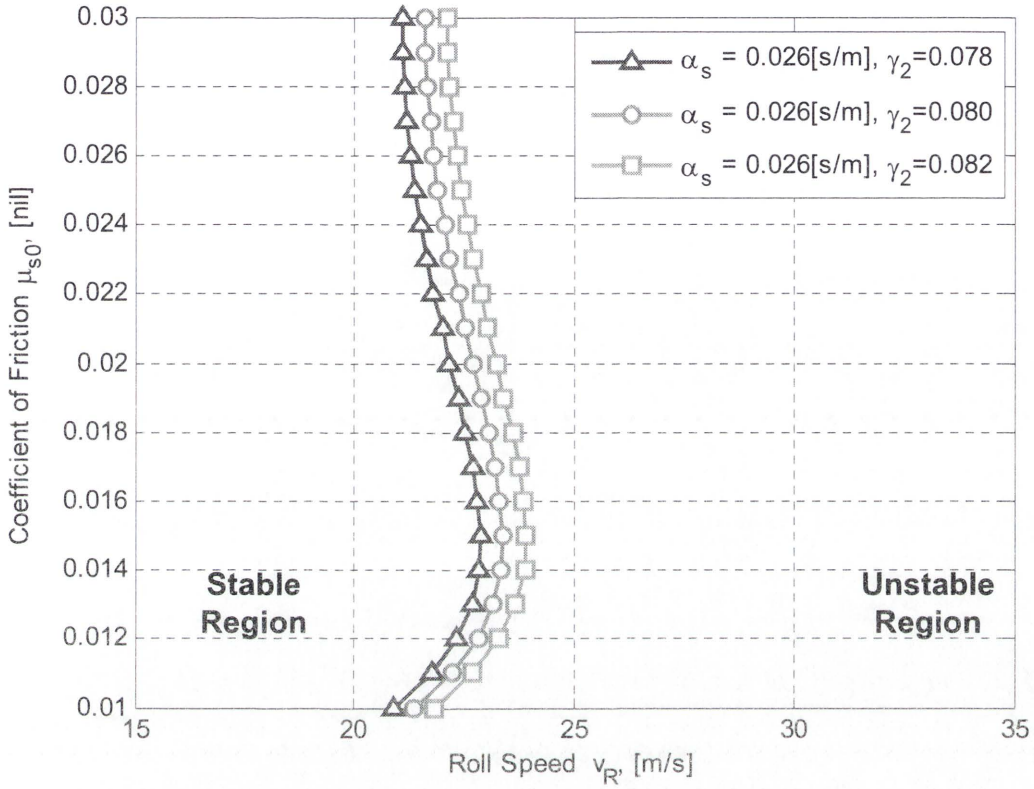

Figure 6-8: Stability threshold curves depending on the rolling speed and friction coefficient change at α_s=0.026*s/m* and γ_2=0.078 to 0.082, respectively

6.3.3.6. Influence of Offset in Two Rolls (BR and WR)

As illustrated in Figure 5-7, schematic of a dynamically coupled rolling stand has an offset distance of 6*mm* with rolls (BR and WR). In order to identify the influence of the offset on the mill system, the stability analysis is carried out with the changing offset distance between rolls. In Figure 6-9, it is likely that stability is maintained in the offset of 6 and 7*mm* while instability arises in an early stage when the offset is set to 5 and 10*mm*, respectively. Specifically, in the lower friction coefficient range, stability threshold curve (STC) is shifted to the left hand side compared to curve denoted by the 6*mm* offset. It can be concluded that the force variation in contact surface between rolls changes the system characteristics as offset distance is larger or smaller.

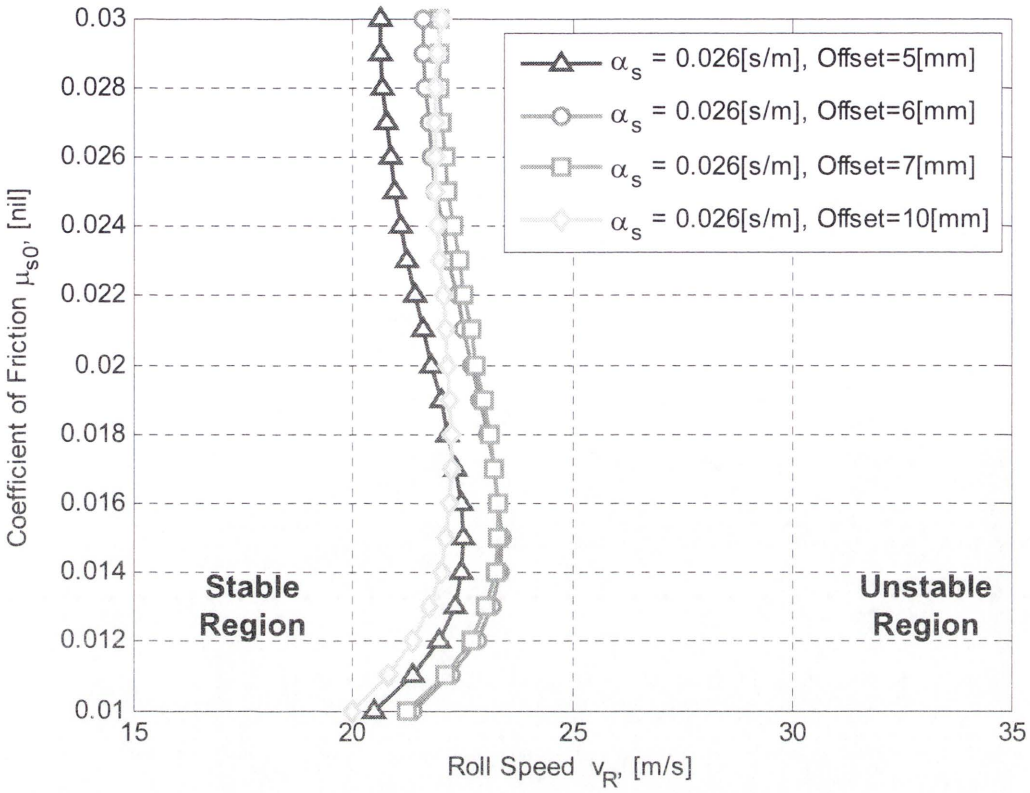

Figure 6-9: Stability threshold curves depending on the rolling speed and friction coefficient change at α_s =0.026*s/m* and offset from 5 to 10*mm*, respectively

6.3.3.7. Influence of Journal Bearing Viscosity in a BR

Oil-film thickness in the bearing supports is significantly affected by the bearing parameters as demonstrated in equation (5.14). For instance, apart from the bearing positions and rotational speed, bearing forces are determined by the bearing viscosity, length and clearance. First, the viscosity of the lubricant is strongly pressure dependent. The viscosity-pressure relation is governed by the Barus equation (Barus, 1893):

$$\eta = \eta_0 e^{\alpha P} \tag{6.11}$$

where η_0 is the viscosity at ambient pressure and temperature $[Pa.s]$, α is the pressure coefficient of viscosity $[Pa^{-1}]$, $P_{\max}$ is the oil-film pressure at a maximum $[Pa]$. Unfortunately, the viscosity may not be estimated from equation (6.11) as pressure coefficient of viscosity (α) is not readily available.

On the other hand, the dynamic viscosity (η) in the journal bearing can approximately be estimated as in the following:

$$\eta = \rho\upsilon \tag{6.12}$$

where η is the dynamic viscosity, ρ is the density of the fluid and υ is the kinematic viscosity.

According to bearing manufacturing industry such as Timken PTY LTD, a generally accepted minimum viscosity of the oil at the operating temperature for journal bearings is 13cSt (Centi-Stokes), although some designs allow for an oil as thin as 7 or 8cSt at the operating temperature. The optimum viscosity at operating temperature is 22 to 35cSt, for moderate-speed bearings if no shock loading occurs. The optimum viscosity may be as high as 95cSt for low-speed, heavily loaded or shock-loaded journal bearings. Note here 1cSt is equal to $1mm^2/s$ and kinematic viscosity and fluid density used in this study for calculating the dynamic viscosity are 50cSt and $800kg/m^3$, respectively. Also note that the bearing viscosity is dependent on the temperature and decreases with the increasing temperature.

As demonstrated in Figure 6-10, the viscosity in the journal bearing considerably affects the system stability; the mill system stability reduces as the dynamic viscosity increases. In order to identify the direct influence of the viscosity, oil-film force in the journal bearing may need to be reconsidered. The oil-film force is proportional to the dynamic viscosity and increases with the increasing viscosity. Moreover, it can be conjectured from the stability analysis that the friction gradient needs to be reduced to maintain stability when the dynamic viscosity builds up with other effects.

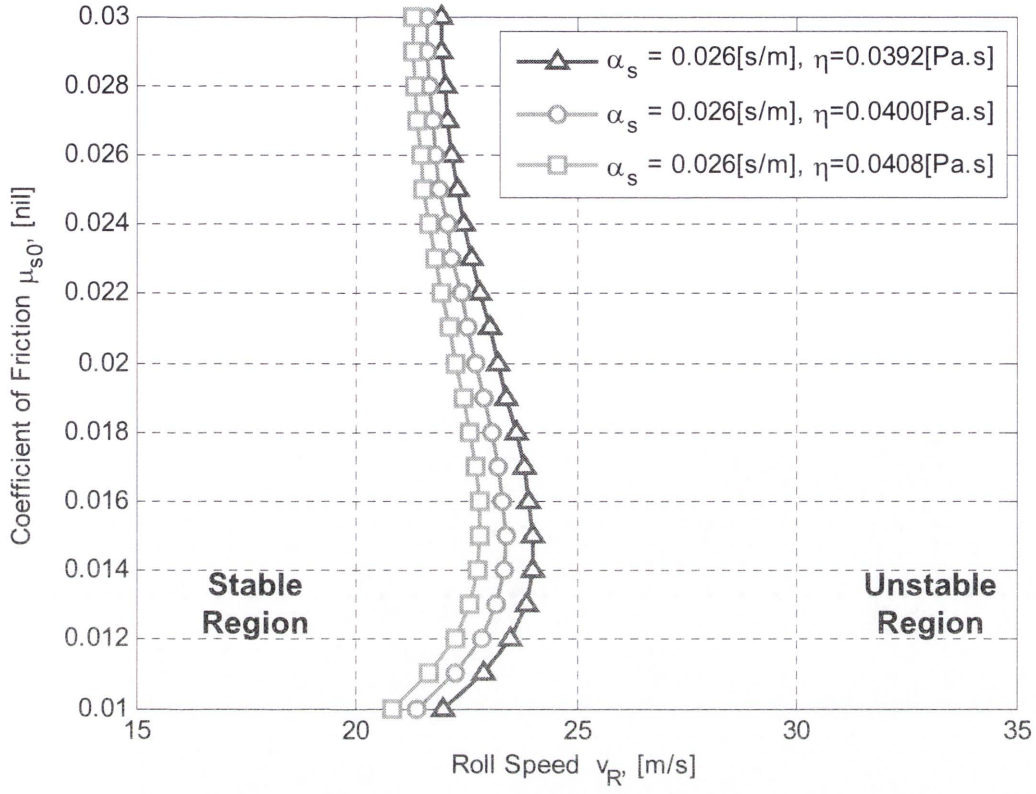

Figure 6-10: Stability threshold curves depending on the rolling speed and friction coefficient change at α_s=0.026s/m and η=0.0392 to 0.0408$Pa.s$, respectively

Specifically, Figure 6-11 displays variations of the bearing force component and eccentricity. With the increasing bearing viscosity in the backup roll, the bearing force increases accordingly. Under the given conditions, it is found that the eccentricity of the journal bearing is not affected by the viscosity change. Figure 6-12 and 6-13 demonstrate the linearised coefficients of stiffness and damping for the range of viscosity used. These coefficients are also increasing with the increasing viscosity, indicating the support easily becomes very stiff and the effect of the cross-coupling terms are considerable, although the viscosity variation is not noteworthy

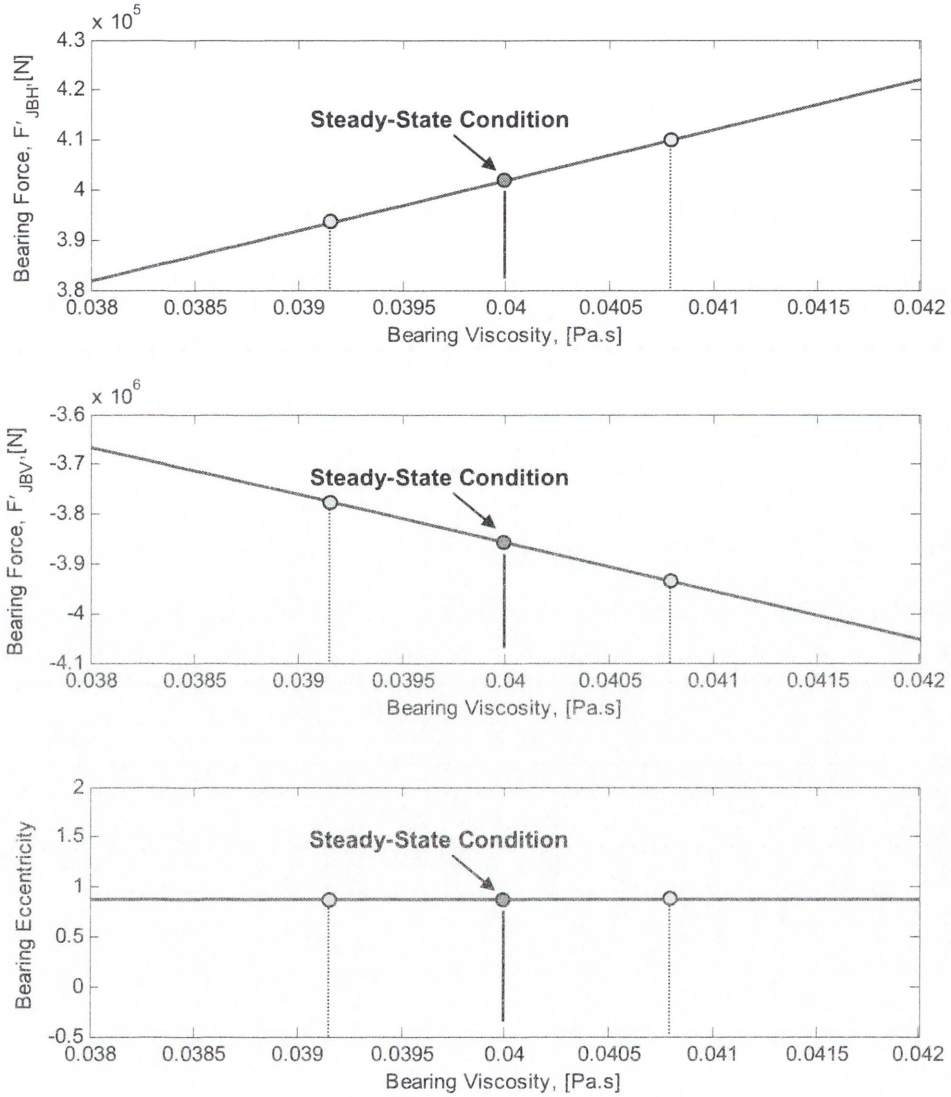

Figure 6-11: Oil-film force and eccentricity variations due to the change in the bearing viscosity

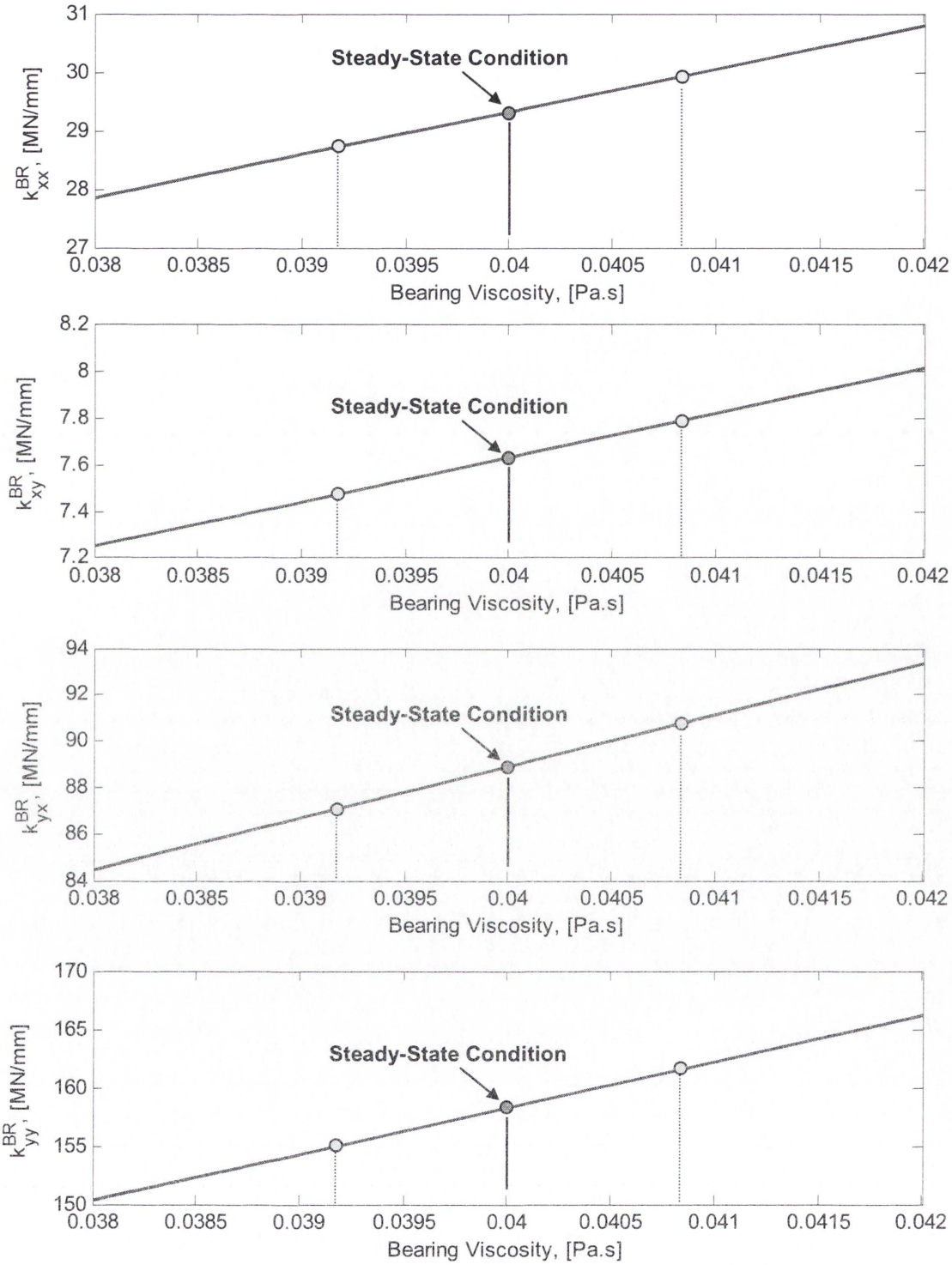

Figure 6-12: Variations of bearing stiffness coefficients due to the change in the bearing viscosity

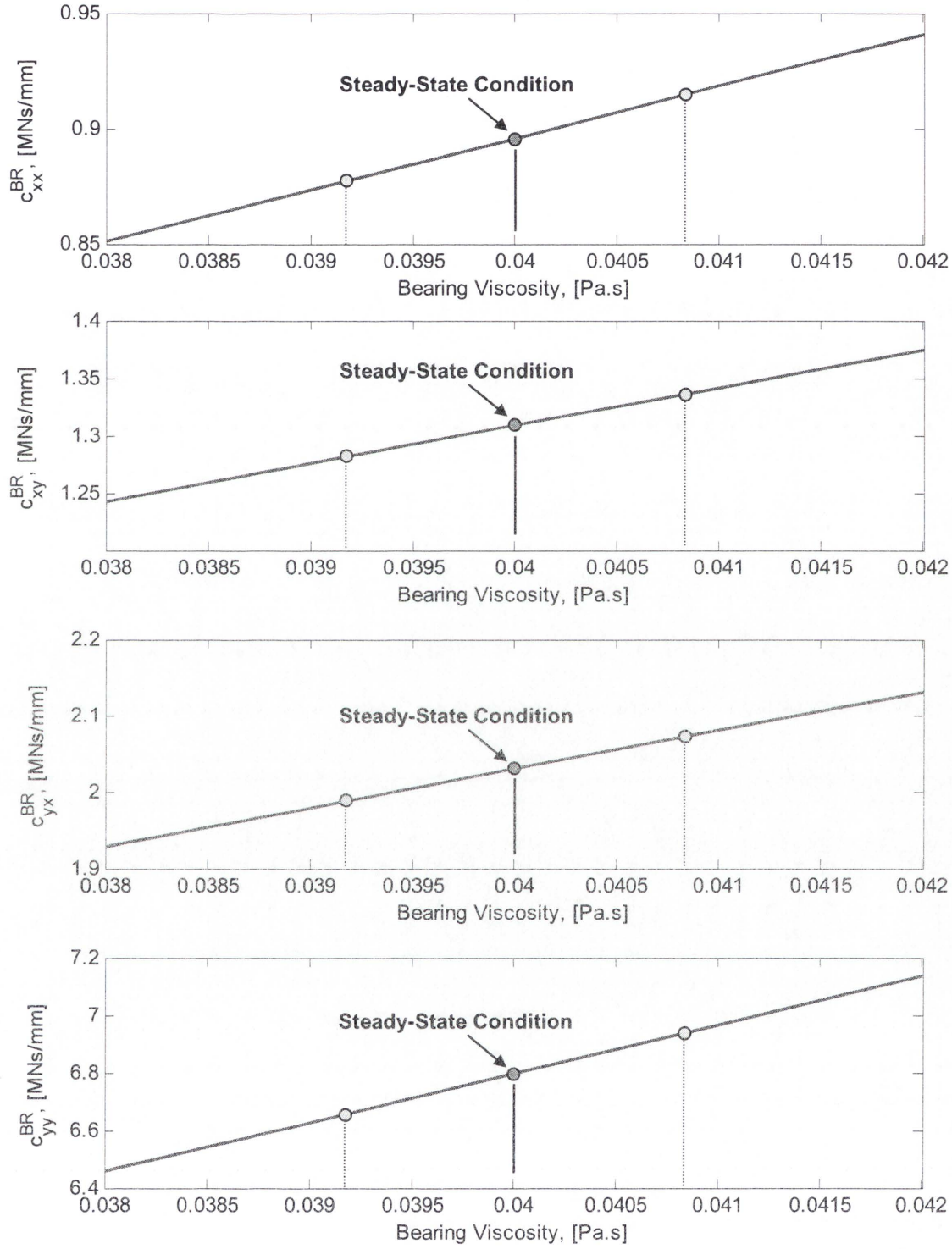

Figure 6-13: Variations of bearing damping coefficients due to the change in the bearing viscosity

6.3.3.8. Influence of Journal Bearing Length in a BR

In a similar way, oil-film thickness in the bearing supports is also notably affected by the bearing length. As demonstrated in Figure 6-14, the length of the journal bearing affects the system stability; the mill system reduces stability as the length increases. The oil-film force is proportional to the bearing length and increases with the increasing bearing length. This may be one reason why the mill system moves into the unstable regime. Approach taken here is the long bearing solution, which the ratio of the bearing length and diameter ($L_{bb} / D_{bb} = 1$) is maintained at 1, for calculating the oil-film force in the journal bearing.

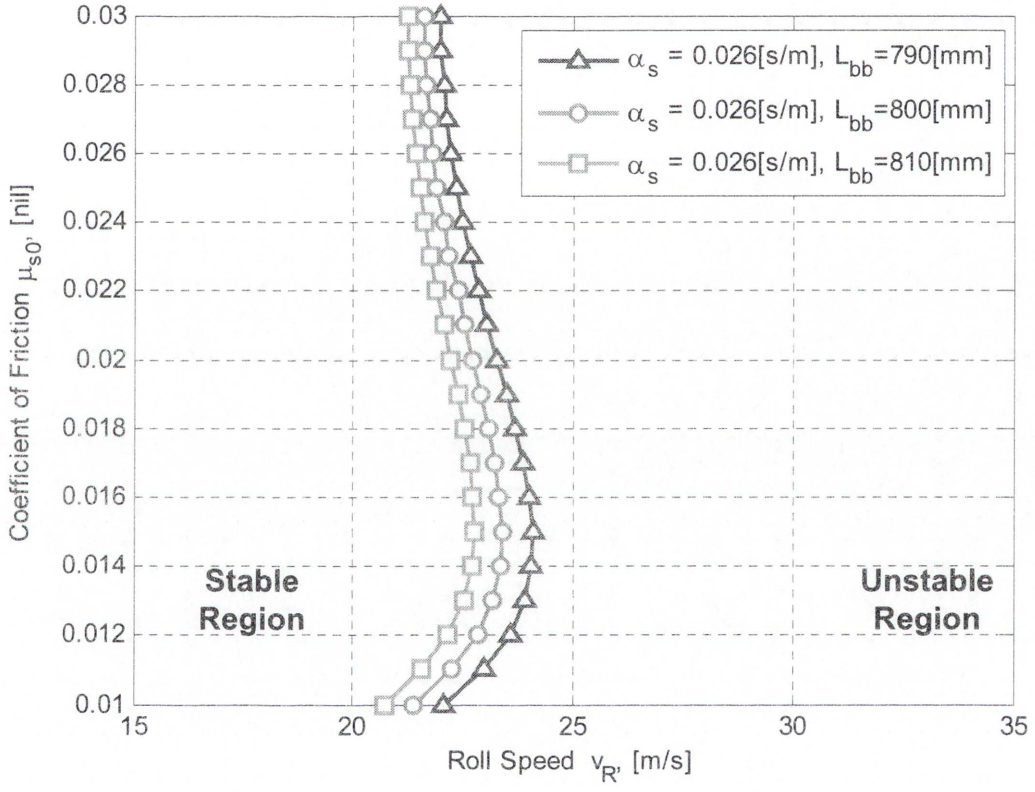

Figure 6-14: Stability threshold curves depending on the rolling speed and friction coefficient change at α_s =0.026*s/m* and L_{bb}=790 to 810*mm*, respectively

Figure 6-16 and Figure 6-17 show the linearised coefficients of stiffness and damping for the range of bearing length used. These coefficients are also increasing with the increasing bearing length indicating the support easily becomes very stiff and the effect of the cross-coupling terms are considerable although its variation is not significant.

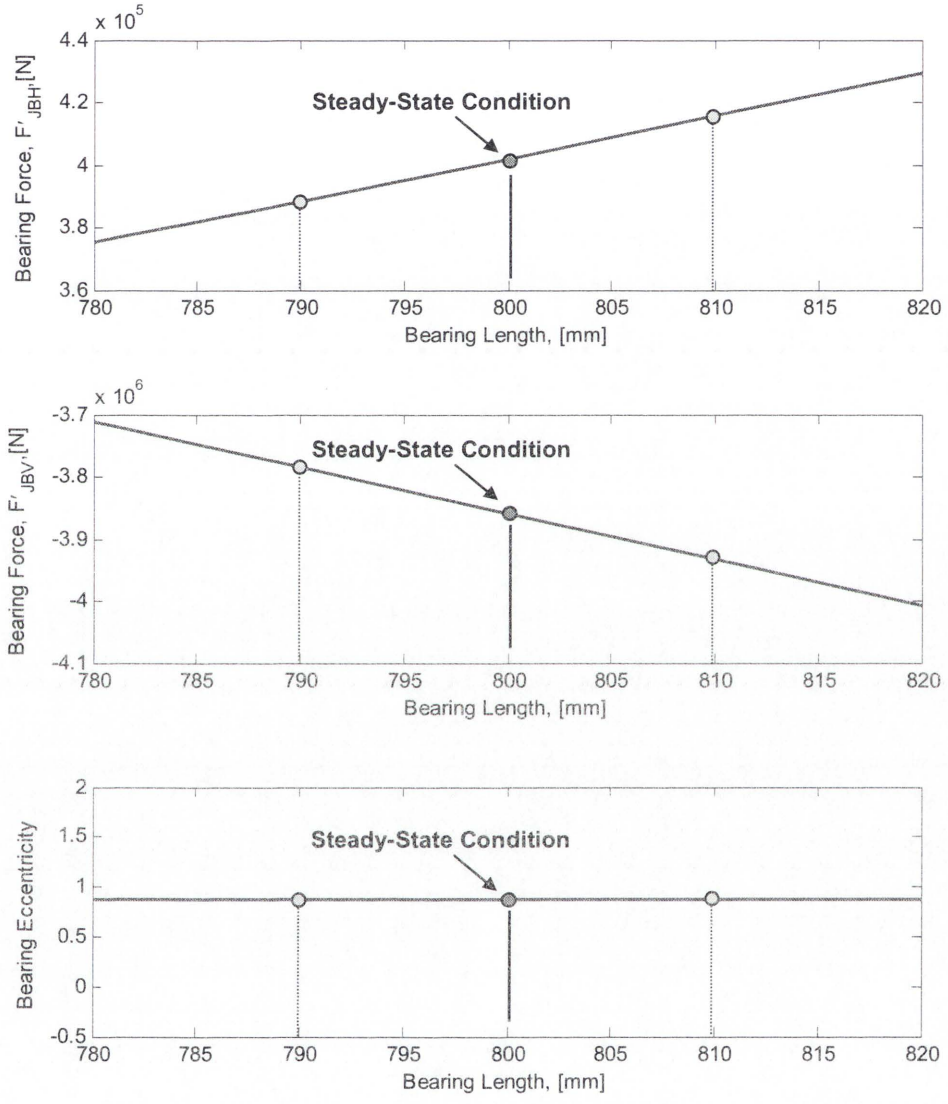

Figure 6-15: Oil-film force and eccentricity variations due to the change in the bearing length

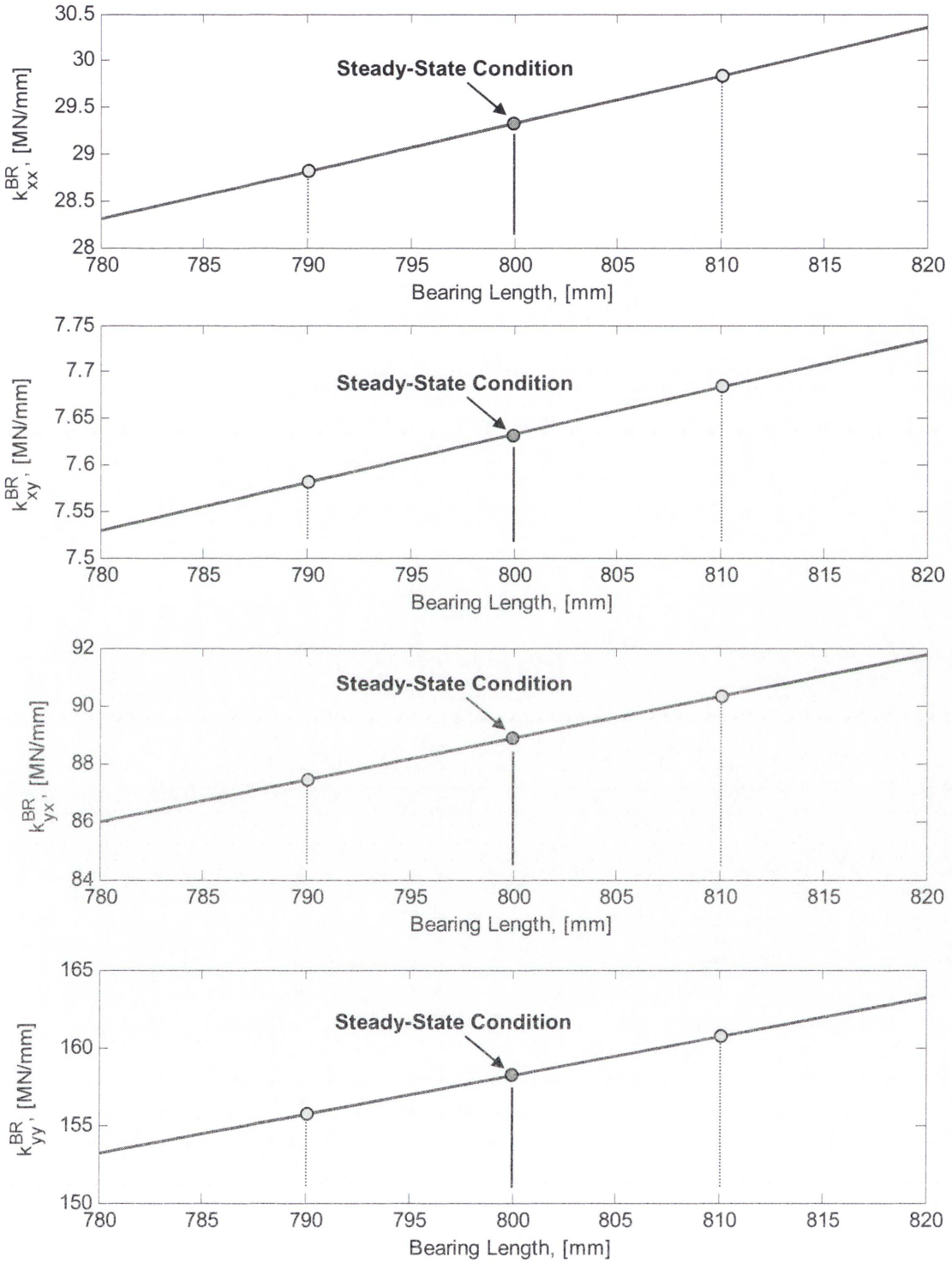

Figure 6-16: Variations of bearing stiffness coefficients due to the change in the bearing length

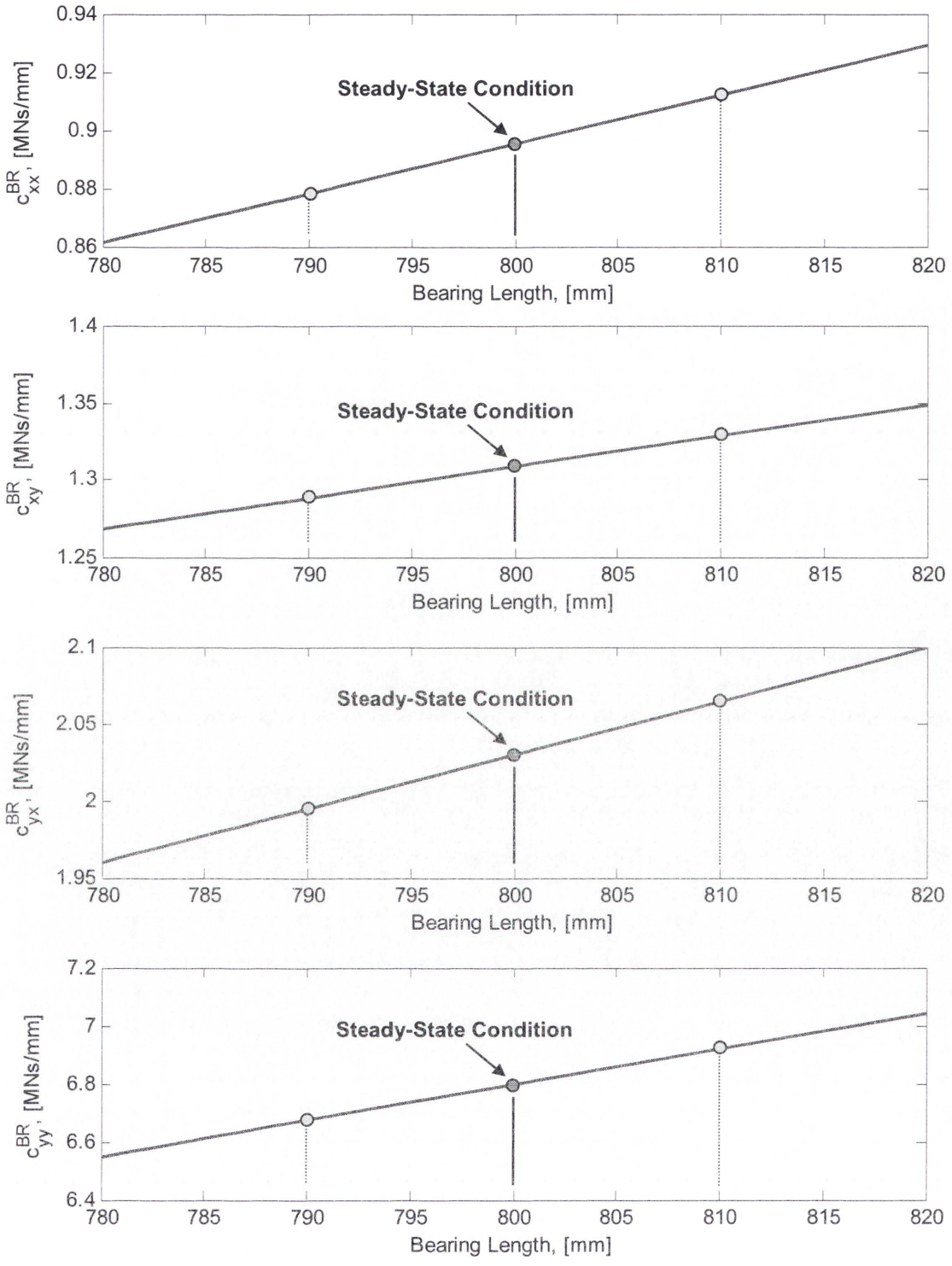

Figure 6-17: Variations of bearing damping coefficients due to the change in the bearing length

6.3.3.9. Influence of Journal Bearing Clearance in a BR

Oil-film thickness in the bearing supports is also significantly affected by the bearing clearance change. As shown in Figure 6-18, the clearance level of the journal bearing more significantly affects the system stability than any other parameter; the mill system easily becomes stable as the bearing clearance increases. Unlike Section 6.3.3.7, the oil-film force is inversely proportional to the bearing clearance level and decreases with the increasing bearing clearance. This may be one reason why the mill system develops into the stable regime.

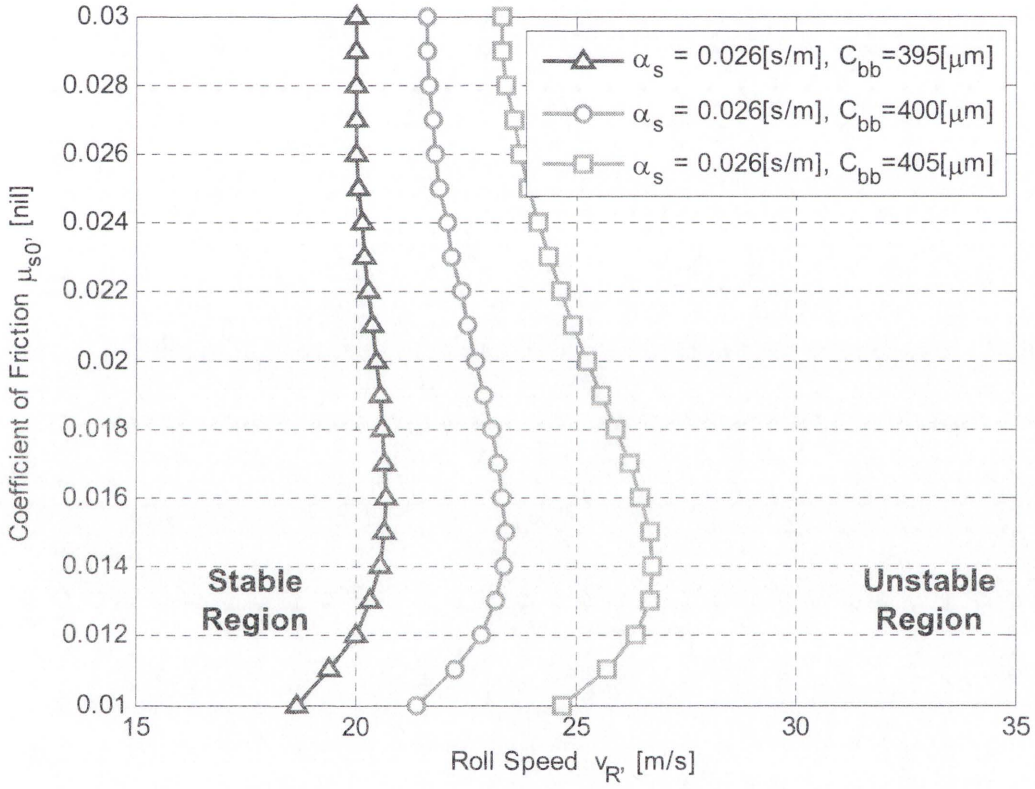

Figure 6-18: Stability threshold curves depending on the rolling speed and friction coefficient change at α_s=0.026s/m and C_{bb}=395 to 405μm, respectively

In particular, Figure 6-19 presents variations of the bearing force component and eccentricity. With the increasing bearing clearance in the backup roll, the bearing force increases in the horizontal direction and decreases in the vertical direction, respectively. In addition, the eccentricity of the journal bearing is significantly affected by the clearance change, representing the stable condition with the falling clearance. Figures 6-20 and 6-21 demonstrate the linearised coefficients of stiffness and damping for the

range of clearance used. These coefficients also decrease with the increasing bearing clearance indicating the support easily becomes flexible and the effect of the cross-coupling terms is insignificant.

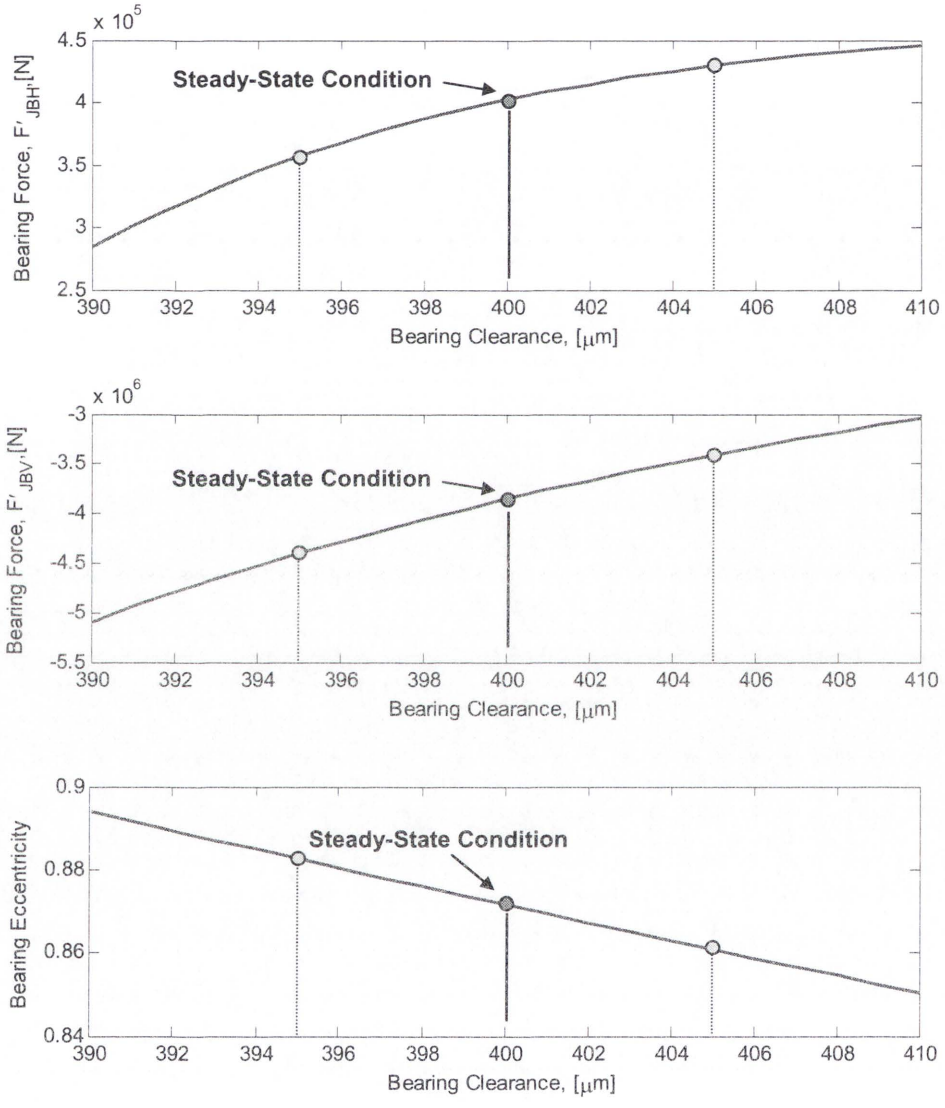

Figure 6-19: Oil-film force and eccentricity variations due to the change in the bearing clearance

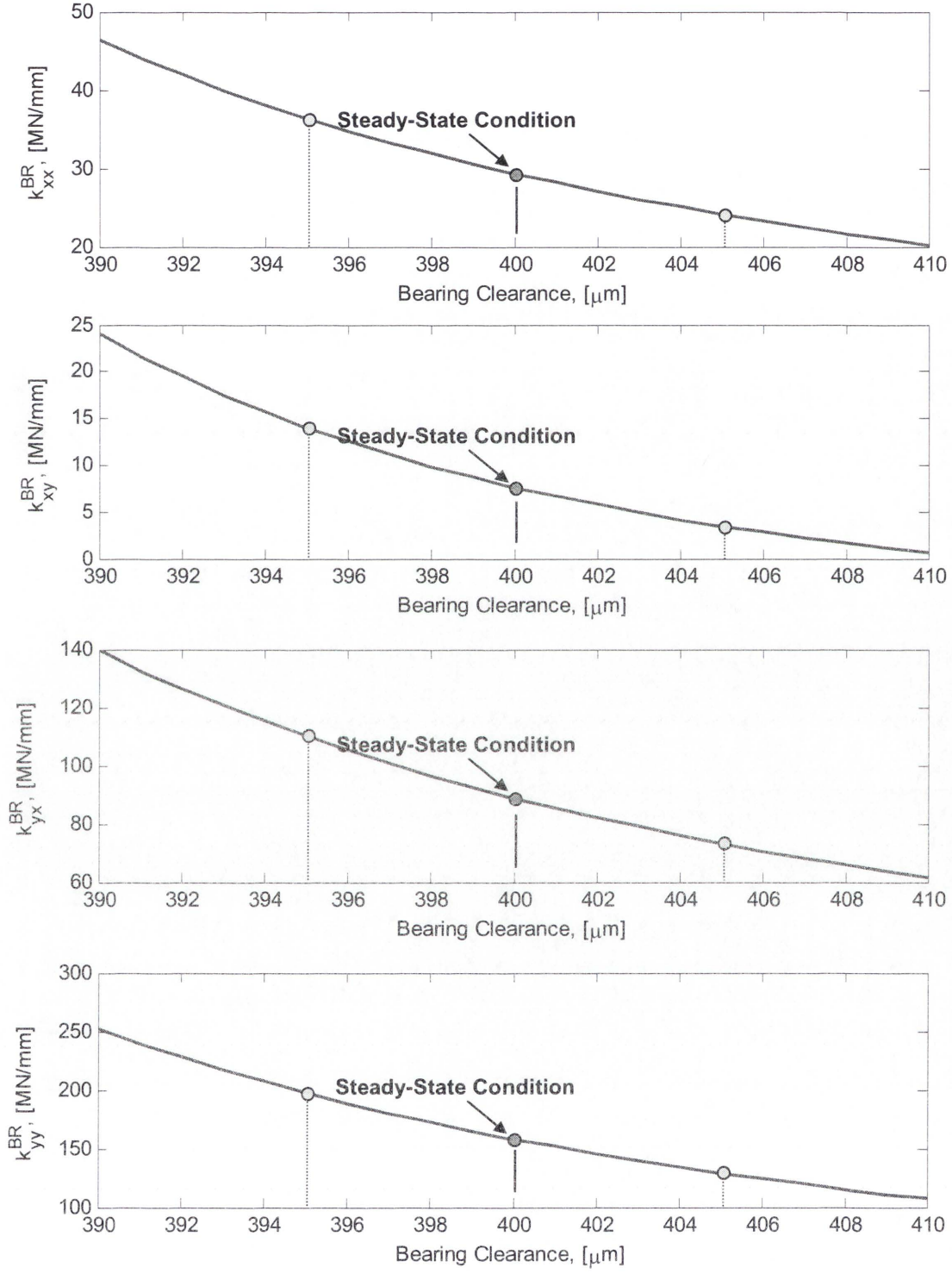

Figure 6-20: Variations of bearing stiffness coefficients due to the change in the bearing clearance

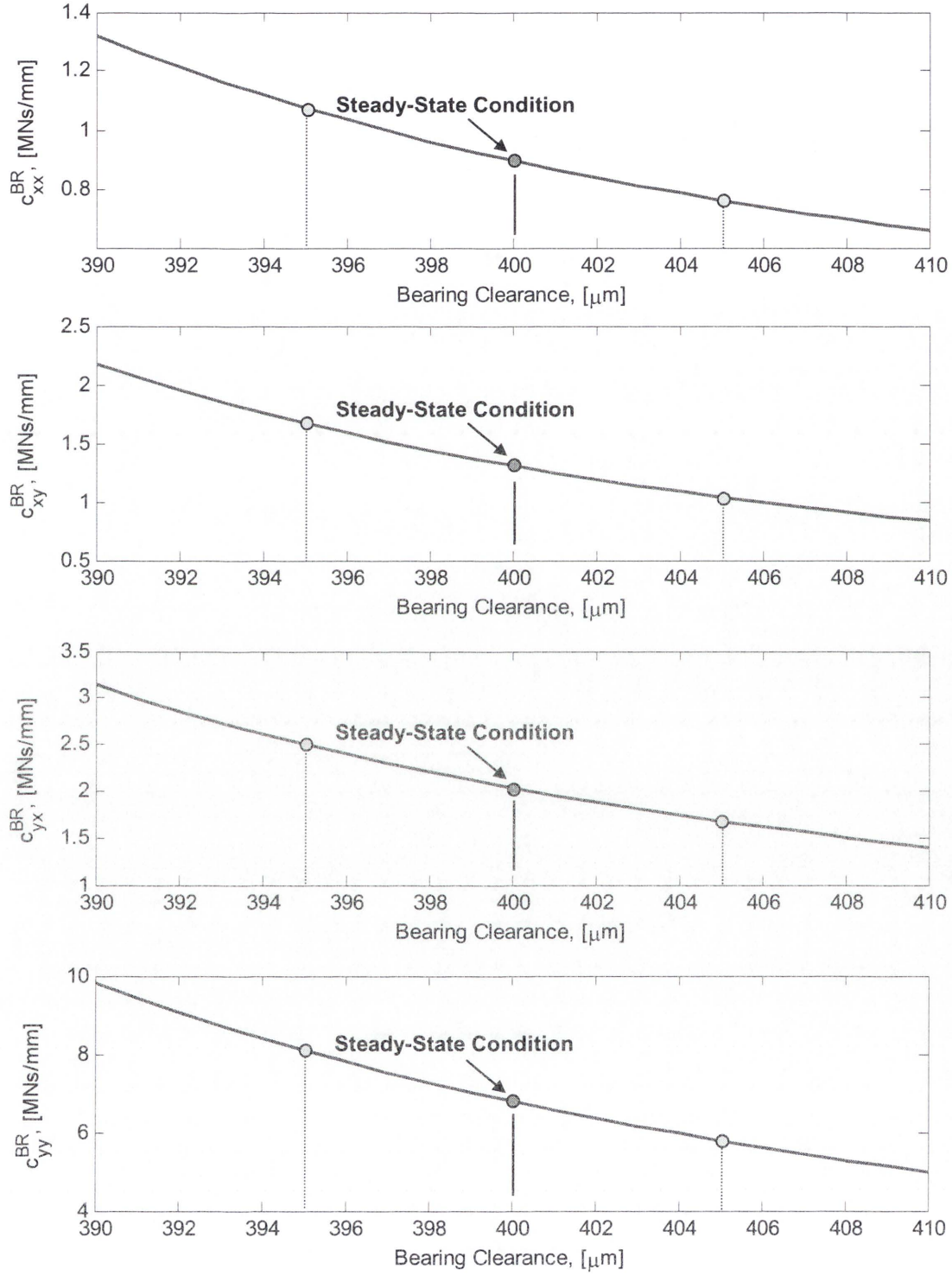

Figure 6-21: Variations of bearing damping coefficients due to the change in the bearing clearance

6.4. SUMMARY

This chapter investigates the impact of various nonlinearities on performance of a rolling stand in cold rolling. This is achieved by proposing a 6DOF coupled vibration model incorporating the dynamic roll gap model, support bearings and contact surface mechanism. For the oil-film force components and equilibriums of support bearings, it is linearised as stiffness and damping coefficients. Then, stability analysis is carried out to identify natural frequencies and mode shapes and performed by investigating real part eigenvalues to determine stable and unstable rolling conditions.

Based on the reference curve of the stability threshold curves (STC) in Figure 6-2, the determination of STC is extended to parametric studies; changing the strip width, roll radius, strip thickness, strain and strain-rate exponent and roll offset. Furthermore, in order to identify the influence of the support journal bearing on the rolling mill stability, STC is determined through the change in bearing parameters such as the dynamic viscosity, bearing length and clearance. Based on the obtained stability threshold curves, a detailed summary in this chapter can be made as in the following:

- STC is highly dependent on the friction gradient. Mill chatter arises as friction gradient increases, representing that relative motions between the work roll and strip are significant due to the increased forward slip.
- STC is also affected by the change in key rolling parameters. It is shown that instability gradually arises as the strip thickness is wider, the roll radius increases, the reduction increases, strain exponent increases, strain-rate exponent decreases, offset remains, oil-film viscosity increases, the bearing length increases, or the bearing clearance decreases.

CHAPTER 7. TRANSIENT ANALYSIS BASED ON LINEARISATION OF FORCE COMPONENTS

7.1. INTRODUCTION

This chapter is an extensive version of Chapter 6 and mainly deals with transient responses from the linearised mill vibration model. Based on the dynamic roll gap disturbance in the proposed model, including dynamic characteristics of the support bearings and surface contact mechanism, simulations are performed in order to identify the dynamic characteristics of a 6 D.O.F rolling mill system and validate stability threshold curves presented in previous Chapter 6. In numerical calculations of the presented model, all the assumptions and simplifications used in stability analysis are adopted in accordance with the predetermined results; among them is the neutral point is fixed at the steady-state conditions rather than shifting in the roll gap. As a result of transient analyses demonstrating the chatter phenomenon (cause and effect), different aspects of responses are obtained indicating that instability is indeed originated from the relative motion between the work roll and strip as well as the inter-relationship between the friction coefficient and rolling speed.

7.2. ANALYSIS METHOD

Regarding the transient analysis procedure presented in equation (6.9), the steady-state rolling force is calculated under the specified rolling conditions. The dynamic analysis of the bearing supports is performed in order to find the equilibrium positions and identify the stiffness and damping coefficients of the journal bearing and tapered roller bearing, respectively. Also, assuming that two rolls (BR and WR) are in surface contact, stiffness coefficients caused by the line contact of rolls are obtained. Damping coefficients, however, are ignored as BR and WR are only in the surface contact. System matrix is then constructed by using the linearised methodology of the coupled force terms resulted from the very tiny disturbance in the roll gap. Mode shapes and natural frequencies are then obtained from the previous calculations (Chapter 6). Figure 7-1 gives a brief algorithm of the proposed simulation model.

The proposed system model has non-linear characteristics so that more accurate numerical integration method is required. In this study, 4th order Runge-Kutta method is preferably utilised for the entire simulation process and time step is set to $1\mu s$. Applying the equilibrium positions resulted from the journal bearing analysis (Rezvani and Hahn, 1993) and the tapered roller bearing analysis (Lim, 1989), simulations have been performed to identify the transient characteristics of a rolling stand in cold rolling under study. Specifically, a friction coefficient of 0.02 and critical rolling speed of $22.73m/s$, which represents a critical operating condition at the friction gradient of $0.026s/m$ from the calculated stability threshold curve, were chosen in order to demonstrate the rolling instability depending on the change in the friction coefficient and rolling speed.

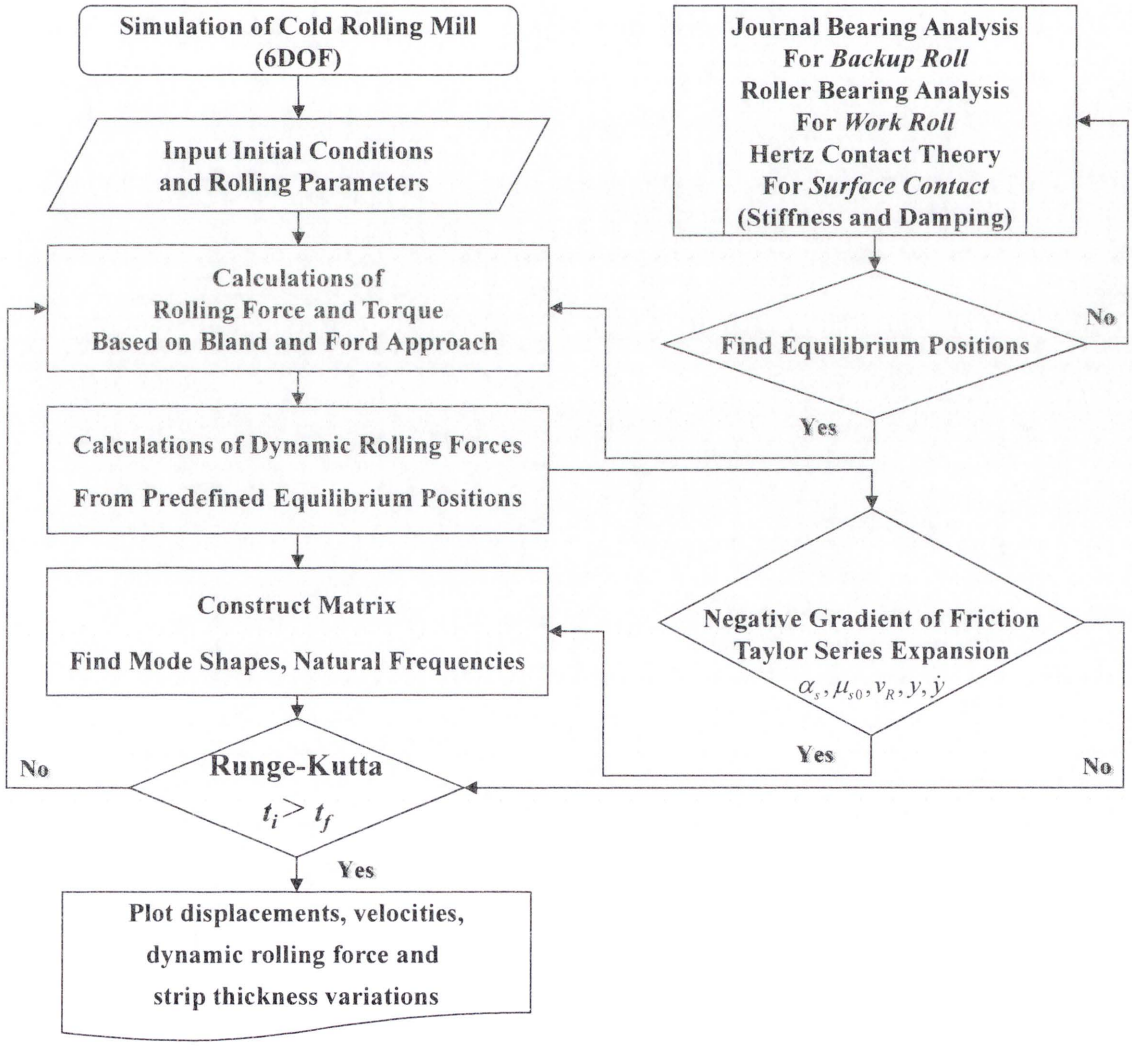

Figure 7-1: Flow chart for numerical simulations in a cold rolling mill

7.3. TRANSIENT CHARACTERISTICS IN THE DYNAMIC ROLL GAP

As afore mentioned, the proposed mill vibration model takes into account the dynamic variations of the rolling force components resulting from the roll gap model. Stability is maintained until the loss of kinetic relationship between the WR and strip occurs in the roll gap where the neutral plane will shift within the arc of roll contact. If this relationship is broken and thus system becomes unstable, the neutral plane will be relocated inward or outward the arc of roll contact, which leads to the chatter or shudder phenomenon.

The transient simulation provides the translational displacements, velocities and accelerations of all mass elements. Figure 7-2 demonstrates the steady-state mill vibration without relative motion in the roll gap and the horizontal and vertical displacements of each mass are shown on the plot. All mass elements are stationary with a zero friction gradient until the start of the relative vibration, *i.e.* sliding between the work roll and strip.

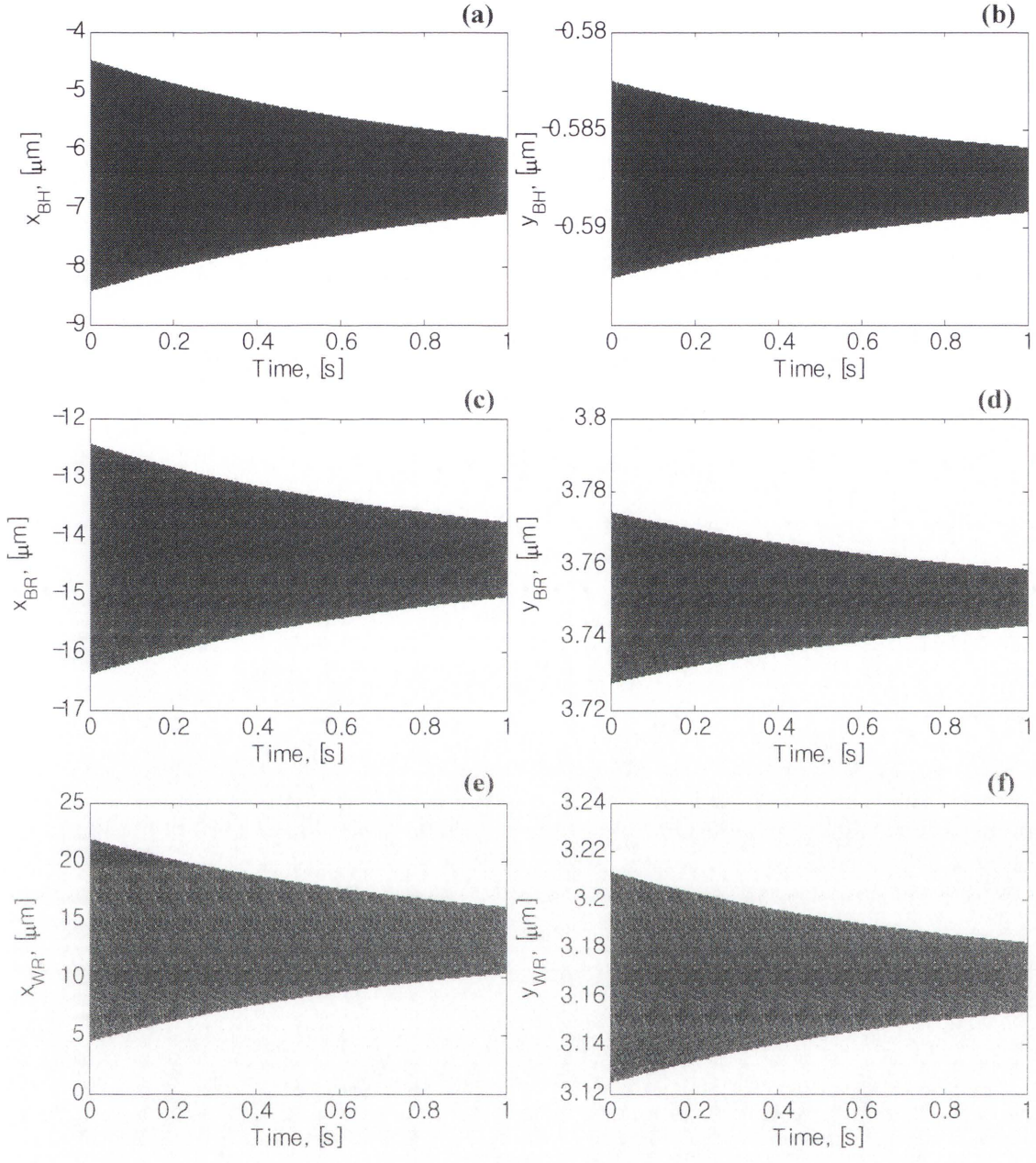

Figure 7-2: Transient oscillations at friction coefficient 0.02 and rolling speed 20.0m/s with a zero friction gradient α_s =0.0*s/m*; (a), (c) and (e): *x*-coordinates, (b), (d) and (f): *y*-coordinates of the bearing housing chock, backup roll and work roll

As the model presents with a high degree of coupling if any mass element becomes unstable other masses will be unstable. Thus, from now on, it will be focused on the vibration of rolls only. With a constant friction gradient of 0.026*s/m*, friction coefficient of 0.02 and rolling speed of 20.0m/s, the translational displacements of rolls of the mill system are presented in Figure 7-3. These displacements are related to the surface

sliding between the work roll and strip and correlates with the expected vibration in the adjacent mill stand. However, under the given conditions, vibrations are damped over time as force components caused by relative motion between the strip and work roll effectively dissipate energy through the rolling process.

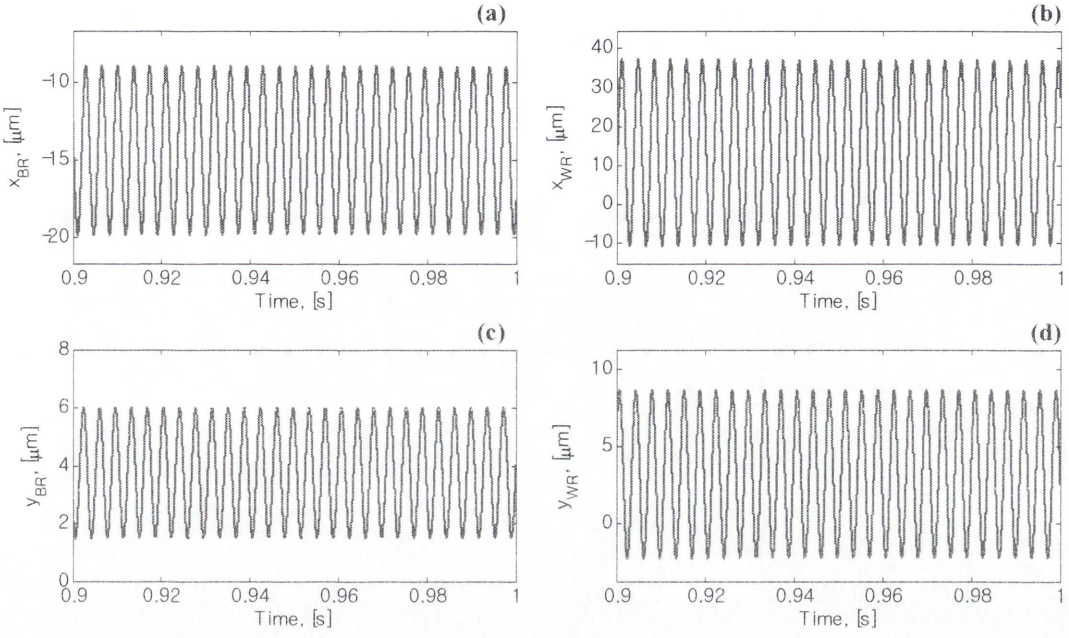

Figure 7-3: Transient oscillations at friction coefficient of 0.020 and rolling speed of 20.0*m/s* with the friction gradient of 0.026*s/m*; (a) x_{BR}, (b) x_{WR}, (c) y_{BR} and (d) y_{WR}

In order to demonstrate the unstable vibration through the change in the friction gradient, friction coefficient and rolling speed, Figure 7-4(a)–(f) present transient responses of the work roll according to the change in friction gradient, friction coefficient and rolling speed. As illustrated, it is shown that tendency of instability by the friction gradient, friction coefficient and rolling speed follows the stability threshold curve (STC) determined in Chapter 6 as the proposed model is significantly affected by the change in these parameters.

Specifically, Figure 7-4(a) and (b) demonstrates unstable vibrations with the increase in the friction gradient at critical rolling conditions. Figure 7-4(c) and (d) reveal chatter with the decrease in the friction coefficient. Figure 7-4(e) and (f) also show the transient response from the chosen point in the STC using a friction coefficient of 0.02 and rolling speed of 28.0*m/s*, which represents unstable conditions. In comparison to stable

response, the amplitude grows bigger resulting in self-excited vibration as indicated by the STC (hollow circle symbol ○) in Figure 6-2 (Chapter 6). This plot best describes the global translational vibration of the third-octave mode oscillating at the frequency of 274.97 *Hz*. Moreover, a vibrational mode with high frequency of 7.92 and 342.95 *Hz* for the relative motion between the backup roll and work roll decays with time. Other frequencies calculated in Section 4 may also be one of chatter sources possible at high rolling speed. Nonetheless, these are damped over time as long as the system is not excited by its resonant frequency. Therefore it is considered that those frequencies in this study are not directly related to a main cause of unstable vibrations, especially for negative damping caused by relative motion between the work roll and strip. However, it is evident that vibrational response will be divergent if force components are excited with harmonics at or near the obtained natural frequency range.

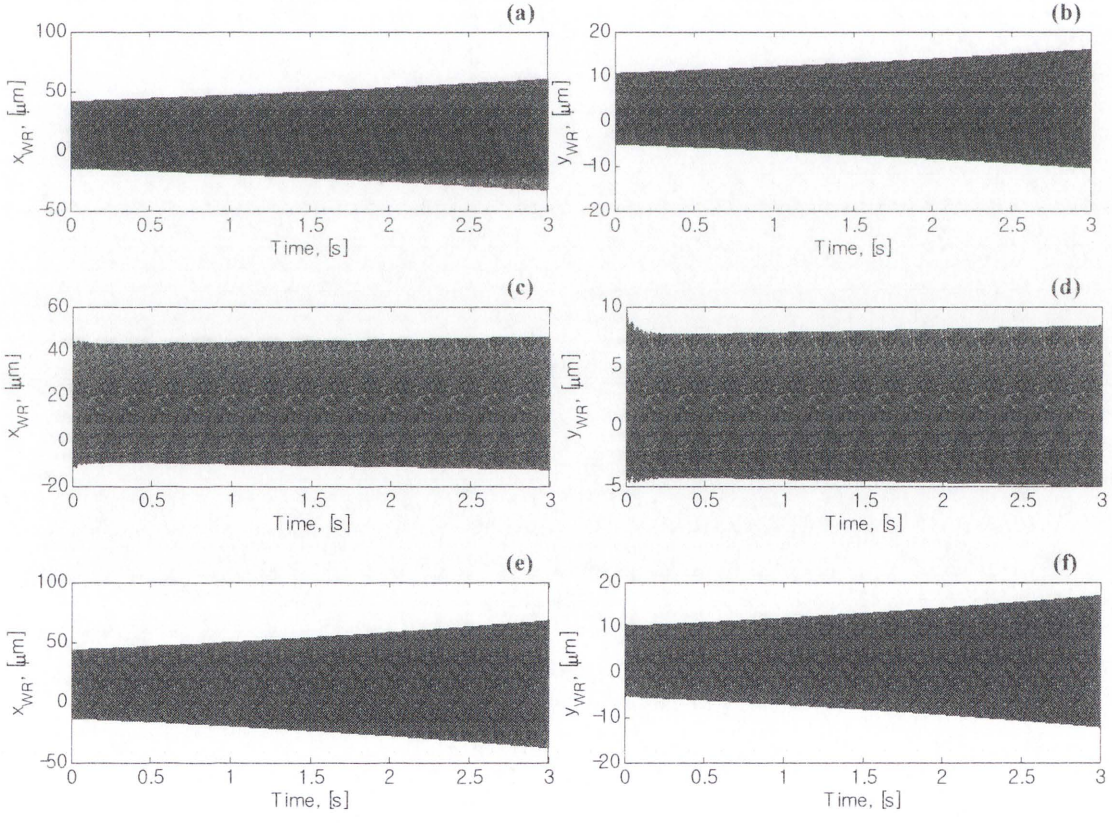

Figure 7-4: Unstable vibrations of the work roll (x_{WR} and y_{WR}): (a) and (b) – α_s =0.030*s/m*, μ_{s0} =0.02 and v_{CR} =22.73*m/s*; (c) and (d) – α_s =0.026*s/m*, μ_{s0} =0.01 and v_{CR} =22.73*m/s*; (e) and (f) – α_s =0.026*s/m*, μ_{s0} =0.02 and v_{CR} =28.00*m/s*

Subsequent investigation enables study of the phase relationships between the motion of mass elements and various rolling force components. Hu et al. (2006) has stated that rolling chatter is generated by the vertical force variation caused by tension change. A 90° lead of force over displacement will encourage large amplitudes; such a condition should be avoided to prevent chatter from the initiation. In the present study, simulation results can be used to show the underlying relationship as demonstrated by Table 6-1. It can be seen from Figures 7-5(a) and (b), in which time scale is magnified, that the bearing housing chock and backup roll oscillate in the opposite phase with respect to the work roll in x- and y- coordinates, representing the third-octave mode of vibration in the six degrees of freedom system. Moreover, rolling force variations play a critical role in influencing the displacement of mass elements, and their relationships are too complicated to be described simply due to its interaction in the dynamic roll gap.

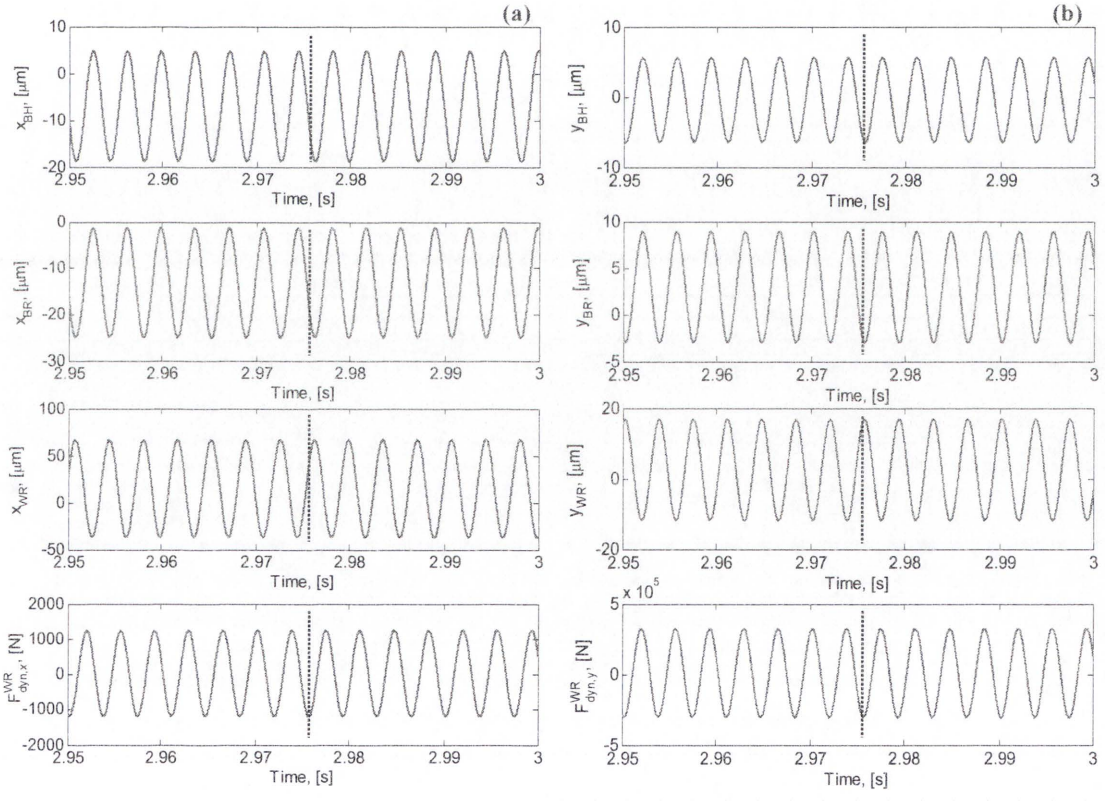

Figure 7-5: (a) and (b): Phase difference of mass elements and dynamic forces in x- and y-directions, respectively. Enlarged scale of Figures 7-4(e) and (f)

Nonetheless, it is identified from simulation results in case of unstable vibrations that rolling force variations have an opposite phase in relation to the work roll vibration. From the simulation results, it can be concluded that self-excited vibration in cold roll mills is not only resulted from tension variation at entry roll gap but also from negative damping in the roll gap. Comprehensive transient study including negative damping effect as well as tension variation would be required for investigating the nature of third- and fifth-octave-mode chatter intensively. Concerning the mill vibration model including the tension, it will be discussed in Chapter 8 of this thesis.

Based on the response of the transient analysis at friction gradient of 0.026*s/m*, friction coefficient of 0.02 and rolling speed of 28m/s, FFT (Fast Fourier Transform) has been performed to find the natural frequency components of a signal dormant in a time domain signal. Figure 7-6(a) and (b) illustrate frequency components of the bearing housing chock, backup roll and work roll, where instability mainly occurs. Most frequency range can be identified except the frequencies of 7.92 and 342.95 *Hz* as the frequency contains high damping as indicated by Table 6-1. Note that frequency range varies with the changes of friction coefficient and rolling speed.

Finally, based on the stability threshold curve presented in Chapter 6, it is shown that a sudden change in the friction coefficient and rolling speed causes mill system to vibrate with high amplitude at a given friction gradient. Of course, vibrational modes are affected by other key rolling parameters such as the work hardening, tension, bearing faults and roll bending effect. However these influences are beyond the scope of this research. From the transient simulation result, the likelihood of instability increases with the increase of the rolling speed and friction coefficient in the relatively high friction range, while the chance of severe vibrational fluctuation in the relatively low friction range arises from the decrease of friction coefficient and the increase of rolling speed, respectively. Most likely, this is the main reason why many industries try to guarantee the sufficient lubrication of oil, and eliminate the chatter for third-octave-mode and shudder for fifth-octave-mode.

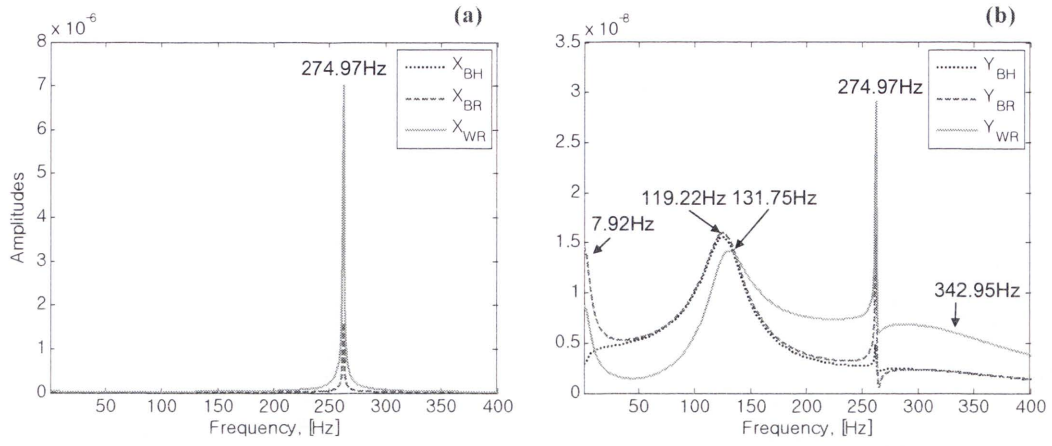

Figure 7-6: (a) and (b): FFT frequency spectrum defined from vibration responses in transient analysis

7.4. SUMMARY

A six DOF coupled mill vibration model, including translational motions in two directions, is developed to study the chatter mechanism in a single cold rolling mill. Under the given conditions, stability analysis for the friction gradient is performed for determining stability threshold curve or critical operating points. From the key rolling parameters, the obtained result shows the friction coefficient and rolling speed have a significant effect on the system stability in cold rolling mill. Therefore, based on the determined stability threshold curve, a steady-state operating point with the friction 0.02 and roll speed $20.0m/s$ is chosen to demonstrate the transient characteristics of the proposed vibration model. It is found from simulations that in the lower rolling speed range, the friction coefficient in the roll gap can be reduced to maintain a stable rolling process; whereas in the high rolling speed range, the friction coefficient has to be increased in order to maintain stability. Within lower rolling speed range, the mill stability is more sensitive to the change of friction coefficient; in higher rolling speed range, it is more sensitive to the change of the rolling speed. In light of the simulation results, it is found that self-excited vibration at the rolling stand may occur due to the negative damping effect when the friction coefficient is not properly guaranteed or the rolling speed increases beyond the stability threshold.

CHAPTER 8. FULLY TRANSIENT STUDIES OF A ROLLING STAND IN COLD ROLLING MILL

8.1. INTRODUCTION

This chapter mainly studies fully transient analysis for a proposed mill vibration model. Based on the nonlinearities of the dynamic roll gap, support bearings, and surface contact between rolls, simulations are performed in order to identify the dynamic characteristics of a 6 D.O.F rolling mill system and validate stability threshold curves presented in previous Chapter 6.

In a rotating machine with support bearings, forces generated in the thin oil-film fluctuate depending on the rotational speed if the other conditions are considered constant. In this respect, bearing supports, under such conditions, can be linearised as stiffness and damping coefficients with respect to the small change in equilibrium positions. However, oil-film forces that rely on position are also dependent on the state, clearance, length and viscosity. In other words, bearing force components are highly dependent on the bearing state in a specific configuration. In order to clearly reveal the source of chatter, therefore, simulation codes of a 6DOF coupled vibration model are required to be modified as a function of the bearing displacements and velocities. In this way, it is anticipated that system characteristics can be more clearly identified with the nonlinear support bearings, surface contact between rolls, and roll gap between the work roll and strip. Unfortunately, it is inevitable that some discrepancies will result as the presented system is based on the linearised stiffness and damping matrix in a real-time rolling process. Even so, the obtained responses are still applicable to predict chatter phenomenon where the relative motion between the work roll and strip and relationship between the friction coefficient and rolling speed are of significance.

In order to investigate the effect of strip tension on the dynamic roll gap, the system model introduces tension variation models presented by Tlusty et al. (1982) and Yun et al. (1998). The reason for introducing tension variation models in this chapter is due to the fact that their tension models are assumed to be a function of harmonic oscillation ($\sin(\omega t)$) and thus have an inability to linearise variations of the tension stress as

stiffness or damping coefficients. In Section 3.8 of Chapter 3, tension variations by Tlusty et al. (1982) and Yun et al. (1998) are established for the identification of the influence of these models. Moreover, based on the fact that the in-flux of the incoming strip to the control volume must be equal to the out-flux of the outgoing strip from the control volume, a new tension variation model is introduced to predict the chatter phenomenon. Thus, tension in the strip is no longer constant.

So as to identify the chatter phenomenon, this chapter is focused on presentation of nonlinear mill vibration models. Firstly, dynamic behaviours of the journal bearing and tapered roller bearing are thoroughly investigated by the linearisation of the stiffness and damping coefficients at each state and time. As a result of transient analyses, it is found that the journal bearing coefficients in the backup roll are heavily dependent on oil-film thickness change. It is also found from the tapered roller bearing coefficients in the work roll that coefficients are alternating with dynamic rolling force exerted in the roll gap. Secondly, system responses are also plotted to investigate frequency fluctuations due to state-dependency on system's natural frequency, and compared to see if both frequencies approach and make the system unstable. Thirdly, chatter responses of the backup roll and work roll have been obtained depending on the change in the friction coefficient, rolling speed and friction gradient. Furthermore, oil-film force variations and roll motions in clearance are also scrutinised to identify chatter in rolling. Finally, fully-transient analyses have been performed in order to identify the state-dependent characteristics of strip tension variation; how unstable vibration/chatter occurs, what natural frequency impacts on in rolling process.

8.2. TENSION VARIATION MODEL IN THE DYNAMIC ROLL GAP

In Chapter 3, the effect of tension variations at entry on mill vibration is discussed in detail and its feasible influences are explained through studying the work by Tlusty et al. (1982) and Yun et al. (1998). Although tension variation models are suitable for reproducing the rolling force caused by the deformation resistance of the strip, these influences have not been properly investigated for determining stability in a rolling stand of cold rolling. As a matter of fact, conditions when the work roll is oscillating cannot be considered harmonic as the roll gap profile changes with nonlinear

characteristics and becomes more complicated than those presented in Chapter 3 (Section 3.8).

Due to rolls either approaching one another or moving away from one another in the vertical direction, the rate of mass flow within the roll gap profile changes. As a result of oscillation of rolls, the strip velocity changes along the roll gap and also changes the length of arc contact (surface area). In order to model the mass flow due to this fluctuation in terms of the rate of change in the roll gap spacing (work roll velocity), the conventional approach of modelling this situation is unsuitable. Therefore, considering the control volume for mass conservation, that is, the in-flux of the incoming strip to the control volume must equal to the out-flux of the outgoing strip from the control volume, as shown in Figure 4-6, which represents the mass flow of the being rolled strip at any arbitrary distance from the center of the rolls, may be written as:

$$v_e h_e = v_x h_x + \frac{dA}{dt} \tag{8.1}$$

Noting that,

$$A(t) = A_c + 2\Delta L y_{WR} \tag{8.2}$$

where A represents the cross-sectional area along the roll gap and ΔL is the length of arc contact. Its derivative with respect to time yields as:

$$\frac{dA}{dt} = 2\Delta L \dot{y}_{WR} \tag{8.3}$$

The variable speed of the strip at the roll gap entry now may be expressed as:

$$v_e = \frac{1}{h_e}\left(v_x h_x + 2\Delta L \dot{y}_{WR}\right) = \frac{v_x}{h_e}\left[h_x + \frac{\left(2\Delta L \dot{y}_{WR}\right)}{v_x}\right] \tag{8.4}$$

All terms in RHS except the second term are constant at steady-state condition and thus the variable elongation can be expressed as:

$$\Delta D(t) = \int_0^t \left(v_{e,\mathrm{var},i} - v_{x,\mathrm{var},i-1} \right) dt = \frac{2\Delta L}{h_e} \int_0^t \dot{y}_{WR} dt = \frac{2\Delta L y_{WR}}{h_e} \tag{8.5}$$

Therefore, the entry tension can be written as:

$$t_e = t_{e,avg} + E\frac{\Delta D}{D} = t_{e,avg} + \frac{2E\Delta L}{Dh_e} y_{WR} \tag{8.6}$$

Recalling equations (3.61) and (3.67) proposed by Tlusty and Yun, it is concluded that tension at the entry roll gap varies with the work roll amplitude in the vertical direction and is determined by the operating frequency which may exist in the system. Of course, it is clear that tension stress will be exacerbated if the work roll displacement fluctuates to system frequency ranges or oscillates with time delay from adjacent mill stand.

Equation (8.6) provides a good example for more direct effect caused by tension variation as long as the work roll and strip are oscillating together, in a way of approaching or moving away from one another. Note that tension variations are highly dependent on oscillations of the work roll, unlike tension models by Tlusty and Yun that include any system operational or natural frequency. Thus it may be necessary to compare tension variations in equation (8.6) with that of equations (3.61) and (3.67).

This may also be a good comparison for validating the current tension model as equation (8.6) is purely dependent on variation of the inter-stand distance and vertical vibration of the work roll. Therefore, it would be indicative that the current tension model is capable of predicting the system response with the work roll vertical vibration.

Moreover, apart from the horizontal vibration of the mill stand, the dynamic oscillation of the work roll at the steady-state conditions can be linearised as:

$$dy_i = \left(\frac{\partial y_i}{\partial h_c} \right) dh_c + \left(\frac{\partial y_i}{\partial \dot{h}_c} \right) d\dot{h}_c + \left(\frac{\partial y_i}{\partial t_e} \right) dt_e + \left(\frac{\partial y_i}{\partial v_R} \right) dv_R \tag{8.7}$$

In a similar way, Hu and Ehmann (2000) defined a set of essential independent rolling variables for input and dependent rolling variables for output. In Chapter 4, the coupled vibration model depending on direct or indirect interactions is presented except the tension variation in the third term of RHS in equation (8.7). Inclusion of tension variation in the entry roll gap suggests that the dynamic model be solved in every time step due to its state dependency. Note that equations (3.61) and (6.67) cannot be linearised as spring and damper due to the existence of sinusoidal function. Therefore, fully transient simulations are required for the validation of each tension variation model through the calculation of dynamic rolling force components in the roll gap.

Figure 8-1 illustrates the calculation process of the force variation according to the tension variation model. To be specific, individual tension variation models are applied into the dynamic roll gap model and thus the resulting rolling force varies with the tension variation. Once the tension significantly varies with either of the natural frequency range of the system or affects the system as negative damping, the proposed mill vibration model will be unstable.

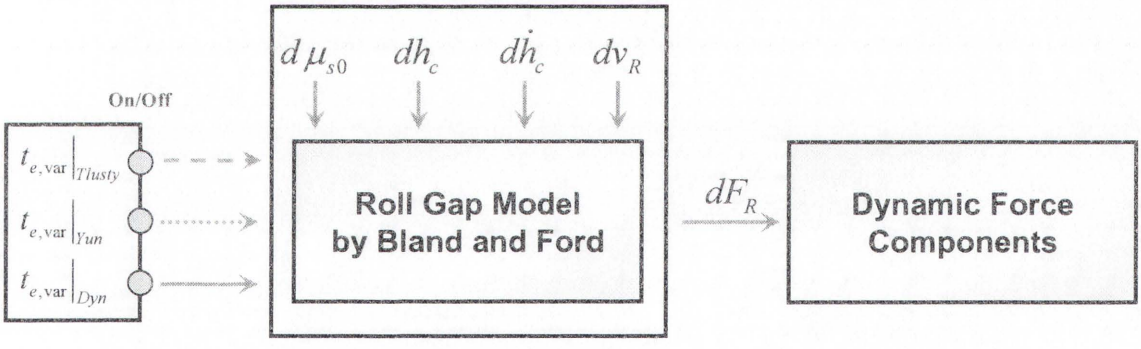

Figure 8-1: Effect of tension variations by Tlusty, Yun and the current model on mill stability (Numerical flow of force variations depending on each tension model)

Recalling equations (3.61) and (3.67) again, both tension variation models include cosine term and cause phase to shift. Compared to those models, Yun's tension variation model adds additional effect (sinusoidal function) due to the change in the cross-sectional area during rolling process. In order to observe the difference between two tension variation models, transient simulation is performed at a steady-state condition and results are shown in Figure 8-2(a). In comparison to tension variation model by Tlusty (1982), Yun's tension variation model is almost identical to Tlusty's model

indicating the variation of 250MPa and insignificantly adds up the magnitude of tension due to the existence of area change. On the other hand, in Figure 8-2(b), the current tension variation model demonstrates the small variation compared to those in Figure 8-2(a). For the verification of tension models, inter-stand distance is set to $4.0m$.

It should be mentioned that the two tension models demonstrated in Figure 8-2(a) are based on the assumption that the amplitude in equations (3.61) and (3.67) is constant; that is, the strip from adjacent mill stand is continuously fed into the current stand. For these models, tension variation will generate instability when the tension frequency equals a system natural frequency.

Figure 8-3(a) displays variations of the strip velocity in the dynamic roll gap by Tlusty's tension model. The exit velocity can possibly be further turbulent even though variations of the entry velocity are not significant. Figure 8-3(b) also shows those of the strip velocity by the current tension model. For the calculation of tension variation in the roll gap, the forcing frequency used is around 8.3 *Hz* indicating the damped vibration mode. In Sections 8.5 and 8.6, a detailed explanation will be presented for reducing vibrations caused by tension variation models.

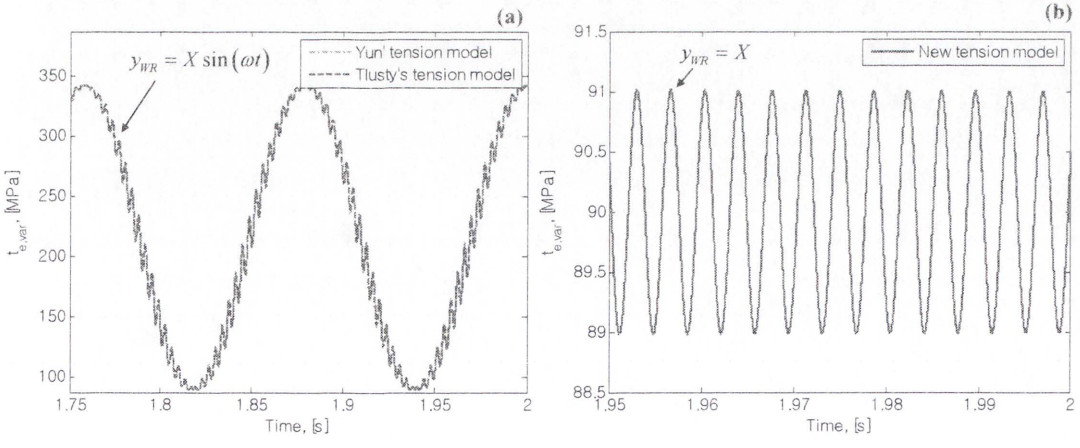

Figure 8-2: Comparison of tension variation results by (a) Yun and Tlusty, (b) current tension model

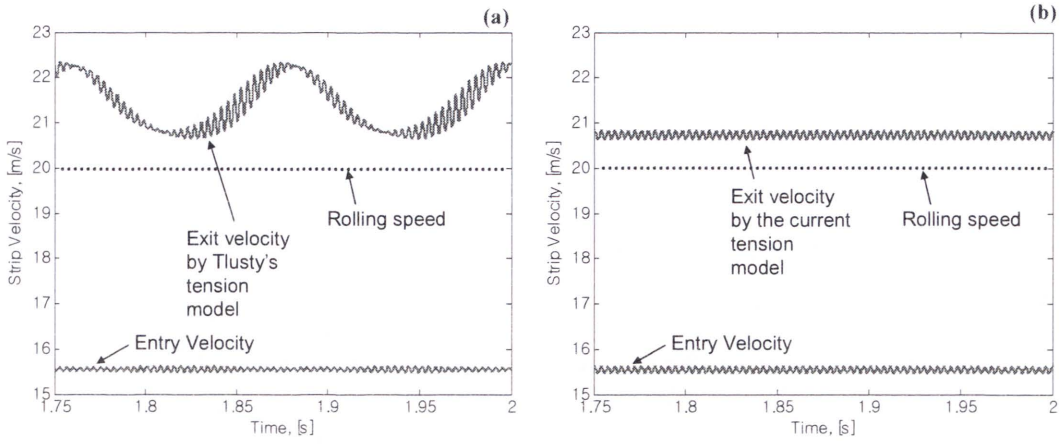

Figure 8-3: Variations of entry and exit velocity of the strip by (a) Tlusty, (b) current tension model

8.3. ANALYSIS METHOD OF FULLY TRANSIENT MODELS

In order to investigate the dynamic coupling effect of the proposed system, transient analyses need to be performed to study if the time-variant oscillations are stable. Figure 8-4 gives a brief algorithm of the proposed simulation model. From the calculated stability threshold curve, a friction coefficient of 0.02 and roll speed 20.00*m/s* were chosen to demonstrate the rolling instability according to the change of friction coefficient and rolling speed. Applying the initial conditions for the roll from the results of the journal bearing analysis (Rezvani and Hahn, 1993) and the tapered roller bearing analysis (Lim, 1990), several simulations for the coupled roll vibrations have been performed to check the transient characteristics of a rolling stand under study.

Regarding the analysis procedure, rolling force/torque is first calculated by the specified rolling condition. Next, bearing analyses are initiated in order to identify the dynamic characteristics of the journal bearing and tapered roller bearing and find the equilibrium positions of the bearings. Also, assuming that two rolls (BR and WR) are in contact, contact stiffness coefficients caused by the line contact are obtained. Based on the coefficients of bearings under steady-state conditions, linearised stability analysis can be performed with changing the coefficient of friction and rolling speed (see Chapter 5). Mode shapes and natural frequencies are then obtained from the previous calculations.

In the meanwhile, dynamic characteristics of the coupled mill vibration model are thoroughly investigated by applying the tension variation models to the dynamic roll

gap. Increasing tension reduces the resulting rolling force, as defined in equations (4.7) and (4.8). However, if force variations have a phase difference with tension variations, *i.e.*, tension variation generates more than 90 degrees of phase difference with respect to force variation; it is generally considered that the mill system becomes unstable. Tension variation at the entry roll gap changes deformation resistance of the strip to affect the resultant rolling force and thus varying the entry thickness of strip due to the work roll oscillation. In the dynamic roll gap, disturbances are assumed to be less than 0.1% of the rolling parameters such as the rolling speed, coefficient of friction, reduction, and reduction rate with respect time. As such, force components with tension variations are linearised as spring and damper in the dynamic roll gap.

A further modification is required to identify dynamic characteristics of support bearings and contact surface between rolls. This is due to the fact that positions (displacement and velocity) of bearings change as the rolling speed accelerates or decelerates. Rolling force will vary with the applied tension and thus shifting natural frequency ranges.

The proposed system model is highly non-linear so that more exact/complicated numerical integration method is required. In this study, 4^{th} order Runge-Kutta method is preferably utilised for the entire simulation process and time step is set to $1\mu s$. In simulation programming, it is devised that all the displacements/velocity, tension, natural frequency, dynamic rolling force variations are to be recorded for the purpose of the identification of chatter characteristics.

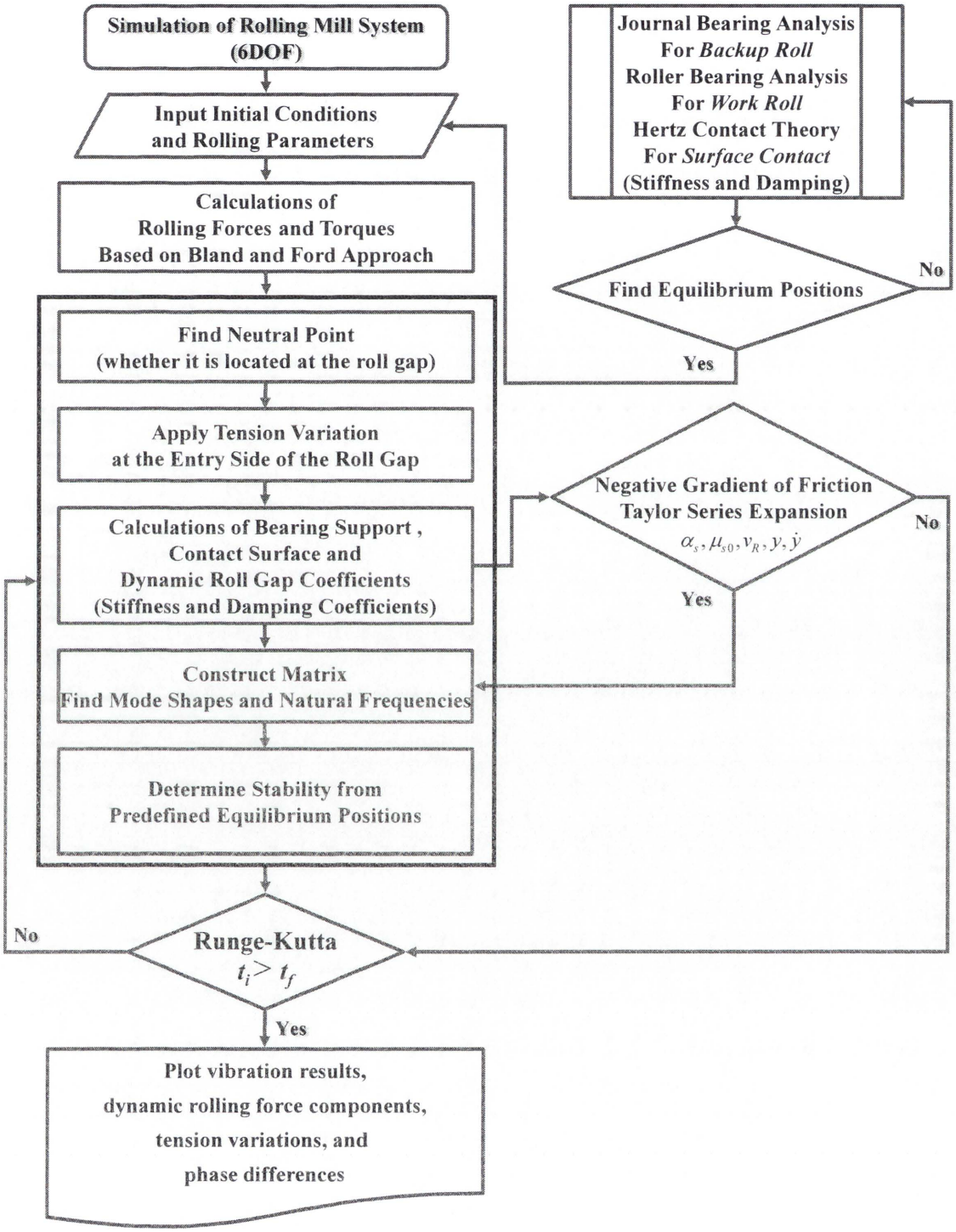

Figure 8-4: Flow chart for fully transient numerical simulations in a rolling stand in cold rolling mill system

8.4. TRANSIENT CHARACTERISTICS UNDER THE STEADY-STATE CONDITIONS

8.4.1. Variations of Stiffness and Damping Coefficients in the Journal Bearing

For the journal bearing of the backup roll, all the bearing stiffness and damping coefficients are calculated by Rezvani and Hahn (1993) approach which assumes laminar and isothermal lubrication in long journal bearing and also introduces the x- and y- coordinates system. The components of the fluid film force that appear in equations are obtained with dimensionless pressure and modified Sommerfeld number through integration along the lubricated arc of bearing. For simplicity, it is assumed that the roller (BR) is rotating under the steady-state condition (friction coefficient of 0.02, roll speed of $20.00m/s$, friction gradient of $0.02s/m$) which is given in Chapter 4. In order to obtain the linearised coefficients in the journal bearing at every time step, very small disturbance ($\pm x$ or y, $\pm \dot{x}$ or $\dot{y}$) is applied within the simulation process. This is due to the identification of system modes and natural frequencies which may affect the system stability. The calculated bearing coefficients are the result of the oil-film force difference divided by the relative displacement and velocity at each time step. Furthermore, so as to reduce the error resulted from the linearised coefficients; the time step is set to very small with $1e^{-6}s$. Simulation time span also needs to be long enough to study the vibrational response. As shown in Figure 8-5, stiffness coefficients of the journal bearing are given as a time-history fluctuation. Figure 8-5(b) also shows time-variations of the damping coefficients. Under the given conditions, all the bearing coefficients are settling down with relatively small fluctuations after small disturbance in the dynamic roll gap. Note that the roller (BR) in the journal bearing is experiencing the significant pressure variations due to the oil-film thickness change. Also note that in this study, the bearing faults are deliberately ignored as rolling mill seemingly is running with a low speed.

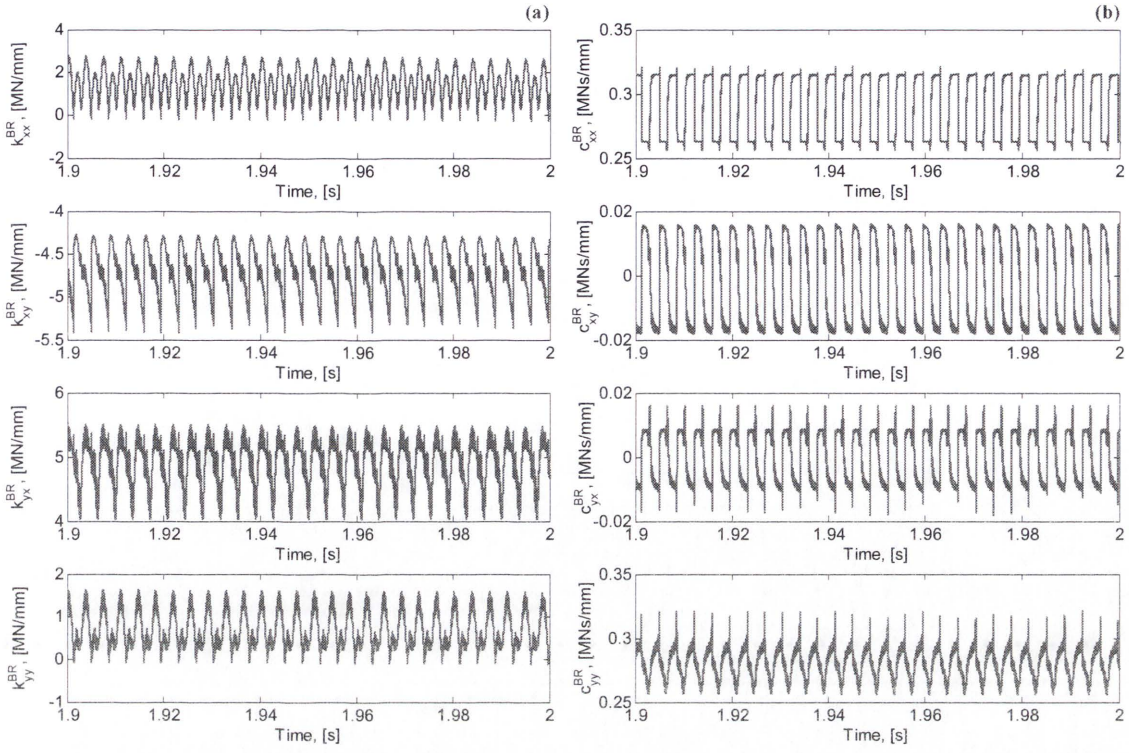

Figure 8-5: Dynamic characteristics of the journal bearing in the backup roll: (a) variations of stiffness coefficients (b) variations of damping coefficients

8.4.2. Variations of Stiffness Coefficients in the Tapered Roller Bearing

For the tapered roller bearing of the work roll, all the bearing stiffness coefficients are calculated using Lim's approach (1990). His approximation of the tapered roller bearing coefficients defines a symmetric bearing matrix form by assuming the average bearing displacement vectors. For simplicity, it is also assumed that the rotor (roller) is rotating under the steady-state condition. These calculated bearing coefficients are the direct result (Direct Method I) of the explicit expressions for the tapered roller bearing. As shown in Figure 8-6, stiffness coefficients of the tapered roller bearing are given as a time-history and varying with small oscillations. Under the given conditions, all the bearing coefficients including cross-coupling terms are alternating with minor fluctuations compared to those of the journal bearing. Also, ensure that damping coefficients in the work roll bearing are ignored as damping effect is negligible in the metal to metal contact and more significant in the dynamic roll gap.

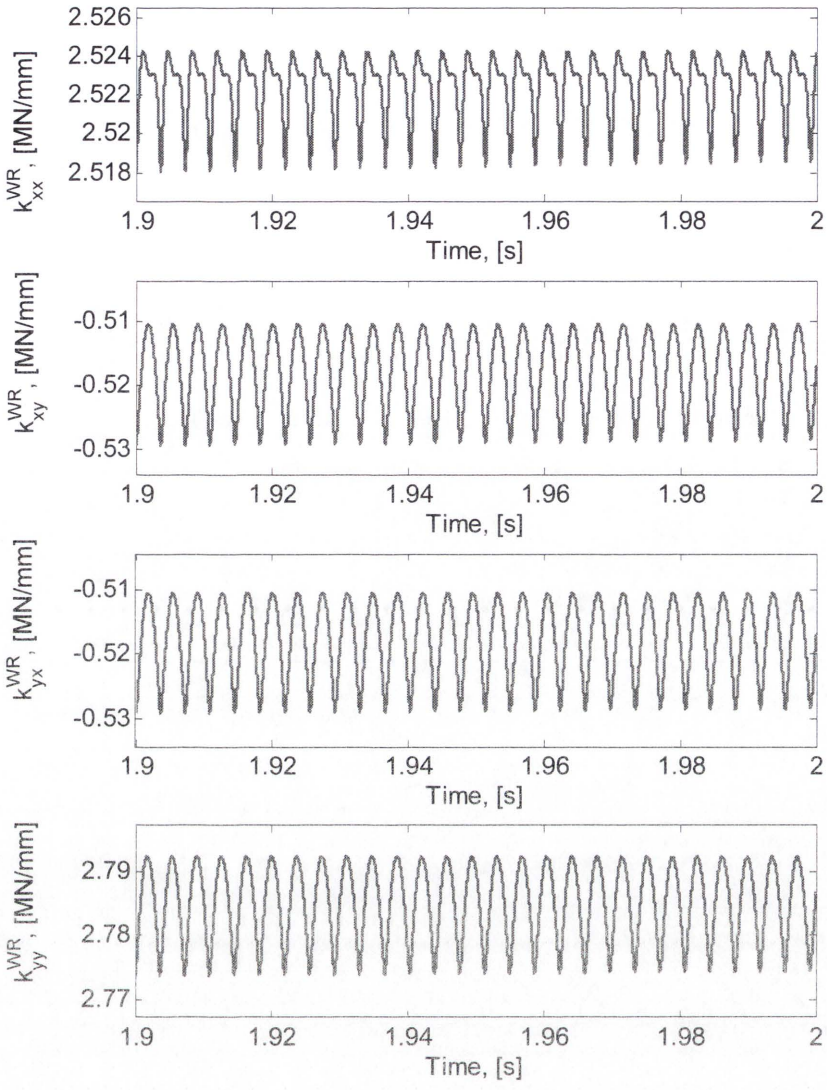

Figure 8-6: Variations of stiffness coefficients in the work roll tapered roller bearing

8.4.3. Variations of Stiffness Coefficients in the Surface Contact between the Backup Roll and Work Roll

Figure 8-7 shows variations of stiffness coefficients in the surface contact between the backup roll and work roll. Diagonal components are very stiff compared to those presented in Figures 8-5(a) and 8-6. Therefore, it can be concluded that the system characteristics are dominated by the surface contact between two rolls. In light of this result, it is also considered that this would be the main reason why cold rolling research consistently ignored support bearings and simplified as one lumped mass. As illustrated in Figure 5-9, cross-coupling stiffness coefficients are resulted from mode coupling using linear transformation matrix and are insignificant. If the rotational angle is zero

those coefficients become zero, which means there is no force transfer in the horizontal and vertical directions.

Here, damping coefficients in the surface contact are ignored as damping effect is negligible in the metal to metal contact. It should be noted that surface contact mechanism using Hertzian contact theory is not an exact solution as the dynamics of circular contact between two rolls is not readily known. Hertzian contact theory, nonetheless, provides a good estimation explaining the metal-to-metal contact mechanism (elastic deformation) in cold rolling even though it yields an approximated result.

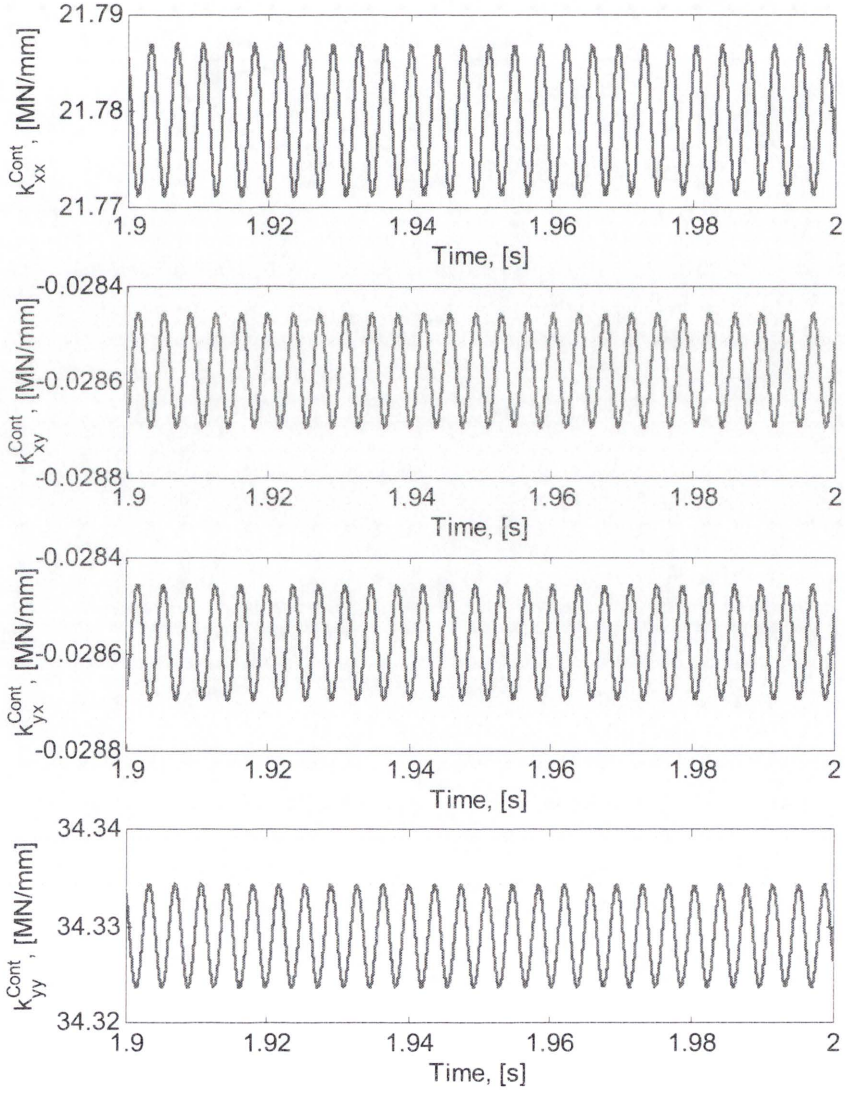

Figure 8-7: Variations of stiffness coefficients in the surface contact between rolls

8.4.4. Variations of Stiffness and Damping Coefficients in the Dynamic Roll Gap

Figure 8-8 shows variations of stiffness and damping coefficients in the dynamic roll gap. In Chapter 4, rolling force variations - due to the friction coefficient, rolling speed, reduction and reduction rate with respect to time - have been linearised as spring and damper. These stiffness and damping coefficients are varying in time-history simulation as the tension variations are applied into the dynamic roll gap in every time step. Figure 8-8(a) demonstrates the variations of stiffness coefficients in the dynamic roll gap. These variations are calculated from the strip deformation when the strip thickness experiences small oscillations. Noticeably, there are no stiffness variations in the horizontal direction as it is assumed no spread of strip width. Note that a cross-coupling is resulted from the resultant rolling force. Figure 8-8(b) represents the negative damping effect in the dynamic roll gap resulted from friction gradient between the work roll and strip. The value is negatively increasing when sliding effect becomes significant and rolling speed increases. Due to the negative damping effect, the system is considerably influenced by these force variations in terms of stability. Figure 8-8(c) reveals the positive damping effect in the dynamic roll gap due to the rolling speed. As illustrated in Figure 6-1, positive damping effect decreases with the increasing rolling speed as the force variations are proportional to the inverse of the rolling speed. However, positive damping does not approach to zero below and maintains its sign with the acceleration of rolling speed. Figure 8-8(d) also displays positive damping effect in the dynamic roll gap. Positive damping, due to the reduction rate with respect to time, maintains system stability providing enough damping force in the dynamic roll gap.

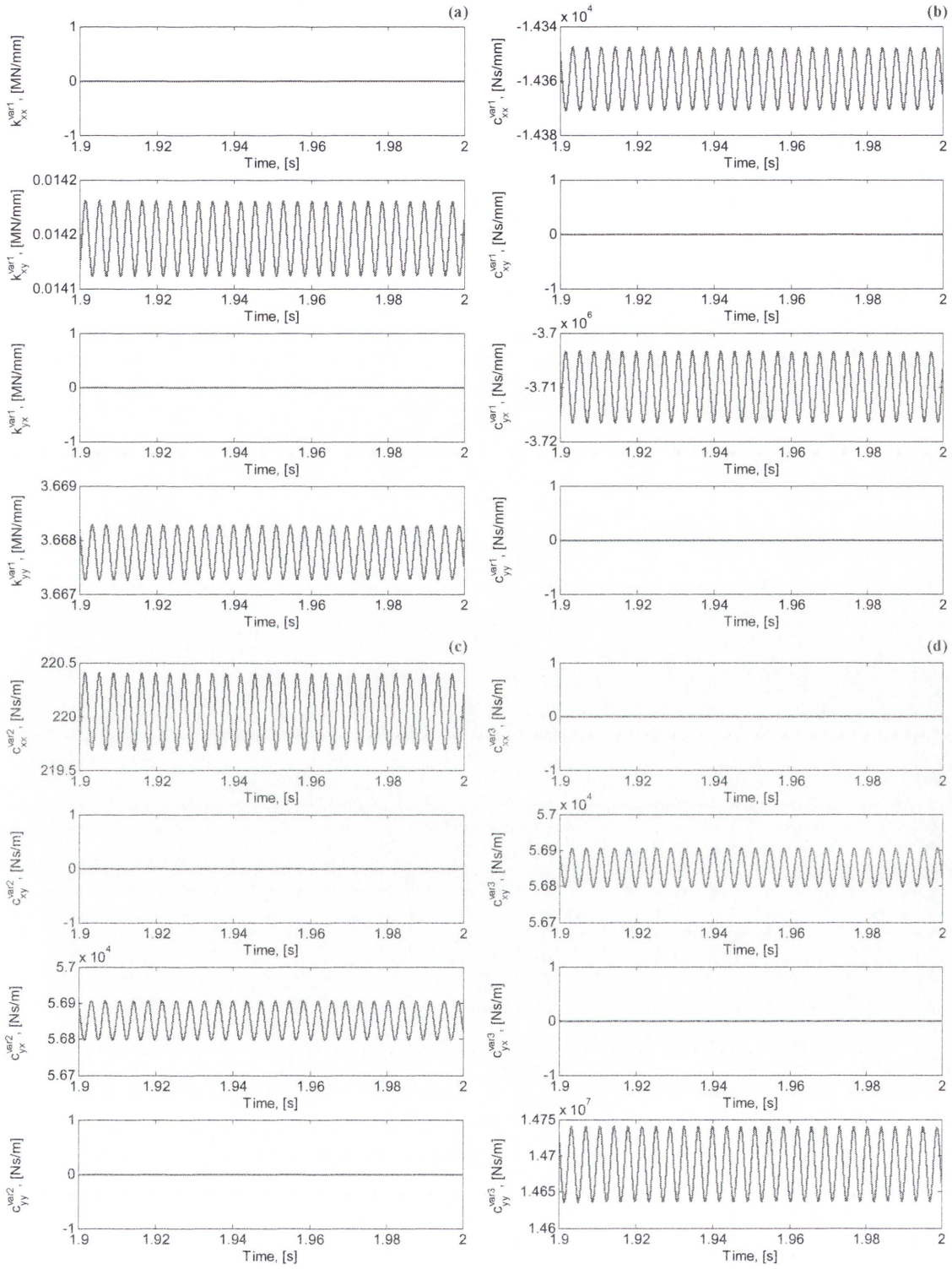

Figure 8-8: Dynamic characteristics in the roll gap: (a) variations of stiffness coefficients, (b) variations of negative damping coefficients, (c) variations of positive damping coefficients and (d) variations of positive damping coefficients

8.4.5. Frequency Variations

As afore-shown in Figures 8-5 to 8-8, dynamic responses of mass elements, *i.e.*, the support bearings, surface contact of rolls and the roll gap, are identified and vibrations are stabilised within $2s$ at the steady-state conditions. Force variations of the journal bearing in the backup roll are heavily fluctuating due to the film-pressure deviation in EHL region (Elasto-Hydrodynamic Lubrication). This indicates that the journal bearing of the backup roll is more likely to initiate the unstable vibration – in this case, bearing whirling or chatter – if the force variations or sliding effects becomes considerable. Therefore, the journal bearing needs more careful management to prevent the onset of chatter in advance. In Figure 8-9, frequencies for mass elements are given in time series under the steady-state conditions (friction coefficient 0.02, rolling speed $20.00m/s$). Each figure represents the system frequency variations in the bearing housing chock, backup roll and work roll regardless of order. In time-history rolling process, the system natural frequencies are mainly varying depending on the change in the tension stress applied. Of course, the support bearings, contact surface and dynamic roll gap also affect variations of the system natural frequency. Comparing to Table 6-3 presented in Chapter 6, the first mode is damped indicating no oscillation at this mode. In the second mode, frequency varies in the range of 3-4 *Hz* representing 53.9% of difference in frequency and the third mode shows no significant change in frequency variations. Around 2% and 3% of frequency variations are identified in the fourth and sixth mode, respectively. Among them is the fifth mode one of the crucial sources of chatter in mill system representing 274.55 *Hz*. In this vibration mode, oscillations of the coupled mill vibration model rapidly arise within few seconds and produce the unstable vibration or chatter.

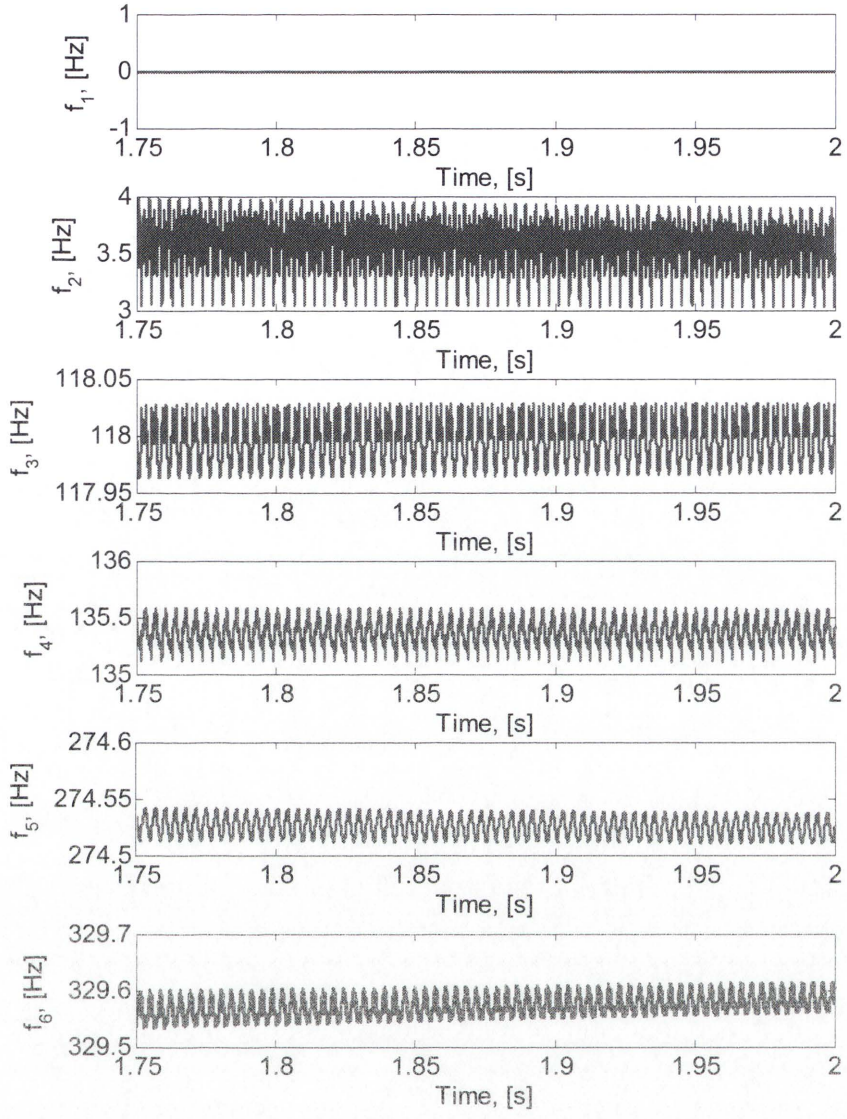

Figure 8-9: Frequency variations at friction coefficient of 0.02 and rolling speed of 20.00m/s

8.4.6. Rolling Force Variations in the Dynamic Roll Gap

As demonstrated in Figure 8-10, dynamic rolling force variations are calculated from equations (4.44) and (4.45) and phase differences are negligible when considering the magnitude of neutral point. This is attributed to insignificant effect of the roll gap variation on the dynamic component of the rolling force. The horizontal force variations are about $400N$ and vertical force variations $100kN$. Noticeably, the variations of vertical force component are much higher than those of horizontal force component.

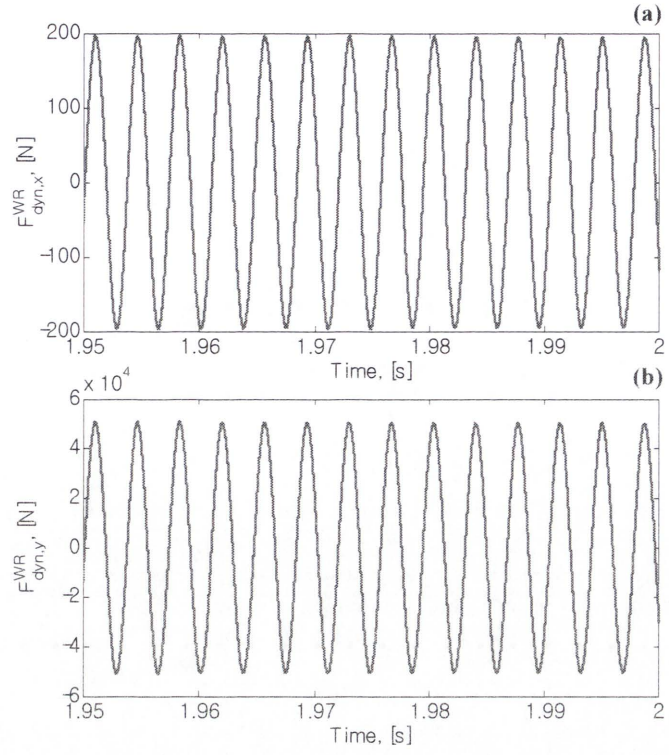

Figure 8-10: Dynamic rolling force variations at friction coefficient of 0.02 and rolling speed of 20.00m/s

8.4.7. Phase Difference between Mass Elements

Figure 8-11 provides the phase relationship of mass elements including the bearing housing chock, backup roll and work roll. At a given steady-state condition, the vertical vibration leads the horizontal one with a phase of 40 degrees as the response at rest is mainly dominated by the frequency of 274.5 *Hz*. As exhibited in Section 6.3.1, the bearing housing chock and backup roll have an opposite phase with the work roll in terms of the horizontal vibration while in the vertical direction, the work roll has an opposite phase with the rest of mass elements. In addition, it is shown that the magnitude of the horizontal vibration is at least two times bigger than the vertical vibration. Responses are due to the existence of friction gradient which may affect the system stability in a negative way although its value is small.

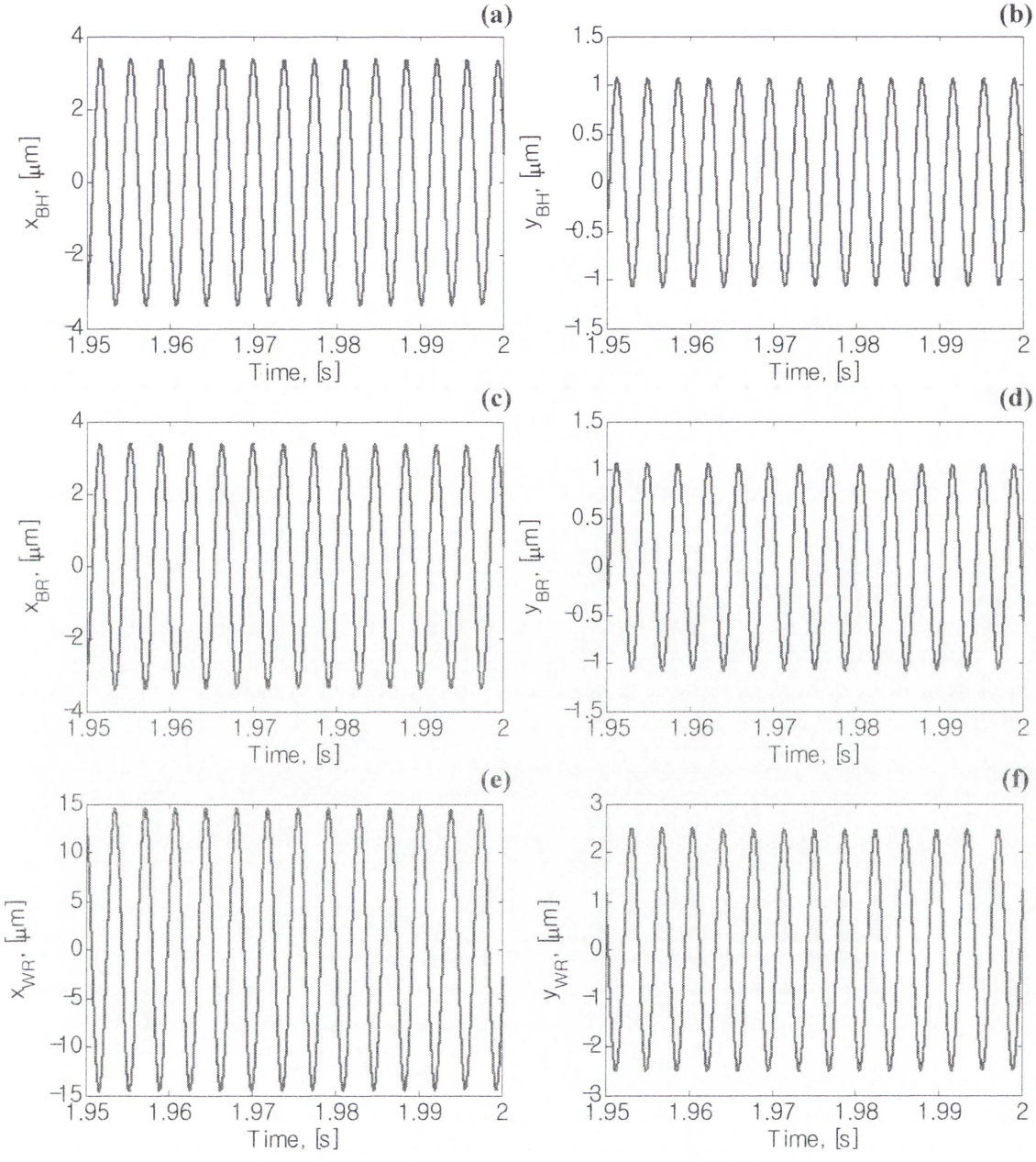

Figure 8-11: Phase difference between mass elements at friction coefficient of 0.02 and rolling speed of 20.00m/s by the current tension model

Figure 8-12 displays the phase-plane motions of mass elements in steady state conditions. At the initiation of rolling process, the motions would start from the origin, which represents the steady-state conditions, and grow into a limit cycle after the transient responses settle down.

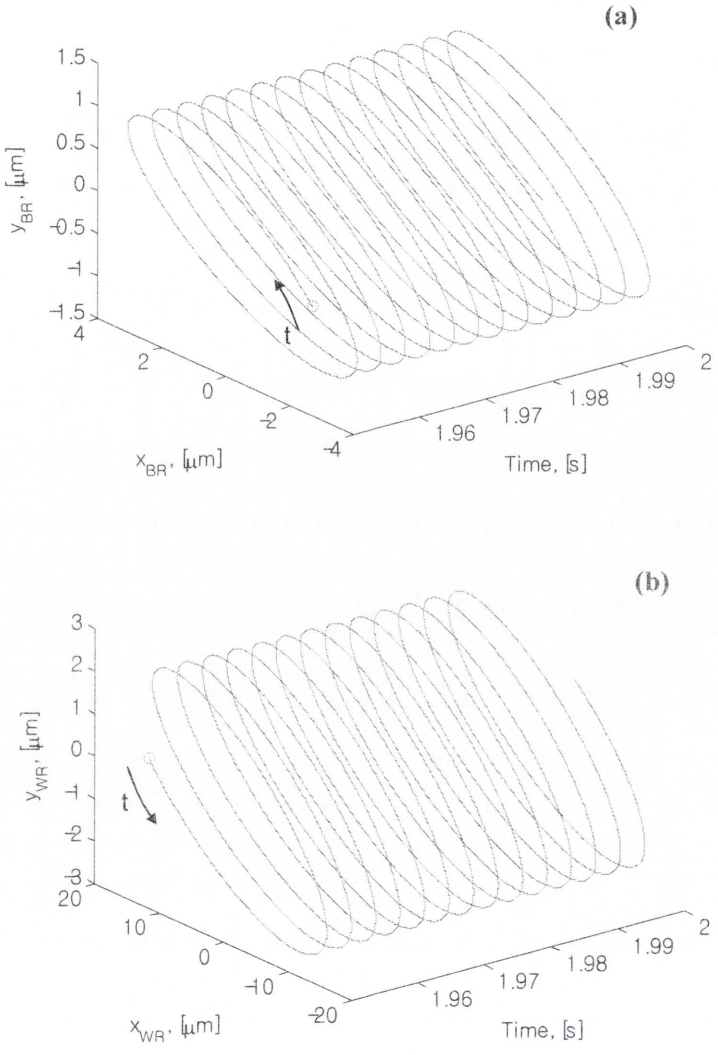

(a) Transient oscillations of the backup roll (b) Transient oscillations of the work roll

Figure 8-12: Phase-plane motions of mass elements by the current tension model

Figure 8-13 demonstrates the transient oscillation of the neutral point. The angle formed between the roll movements in x- and y- directions is caused by the different magnitudes of the dynamic rolling forces in the associated directions. It is also of interest to point out that, under the same conditions, the system would turn to unstable if the friction gradient increases providing more negative damping effects.

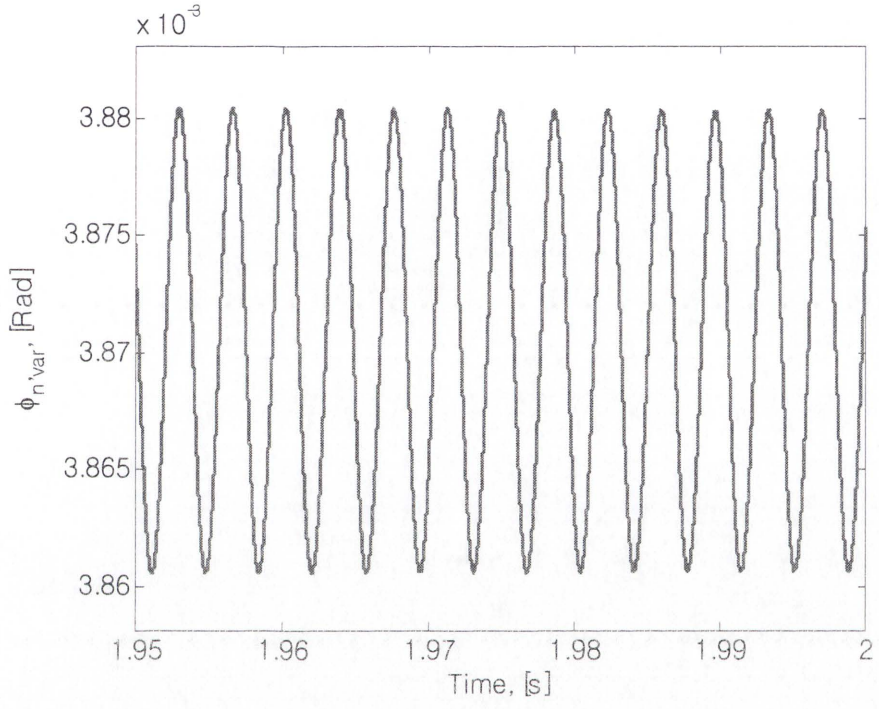

Figure 8-13: Displacements of the neutral point by the current tension model

Figure 8-14 represents the phase relationship with the vertical roll displacement and tension variation at the steady-state conditions. The vertical displacement of the work roll is displaying the in-phase motions with the tension variation. It can be considered that once the rolling parameters change or tension is applied with the time delay at the entry roll gap, the dynamic response can become unstable.

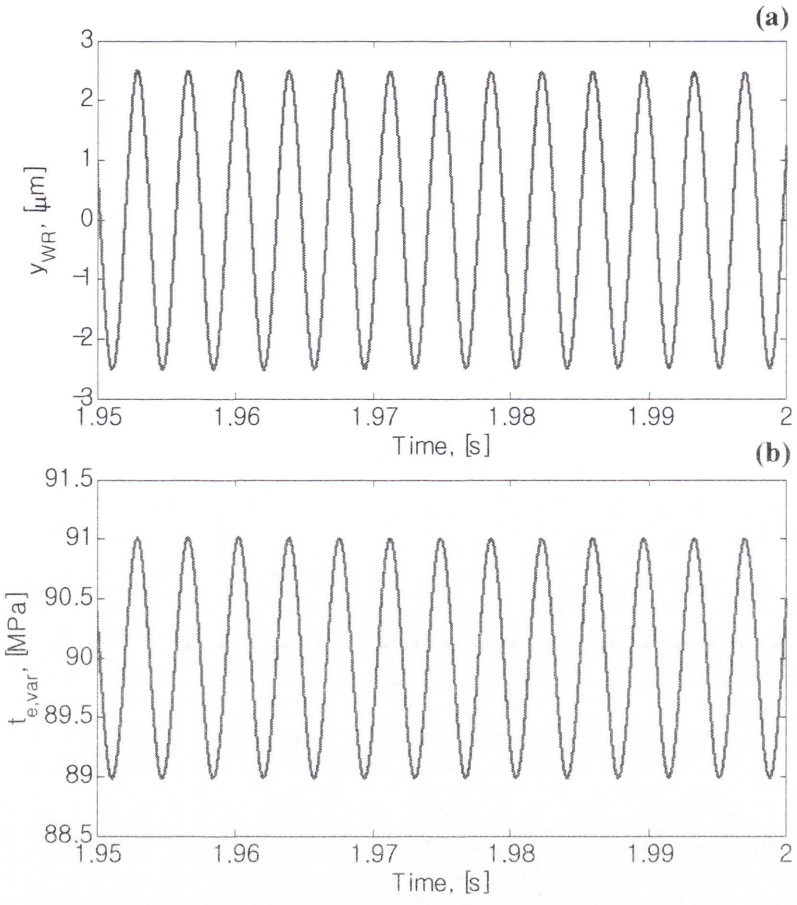

Figure 8-14: Phase difference between the vertical work roll displacement and tension variation by the current tension model

8.5. TRANSIENT RESPONSES IN TENSION VARIATION MODELS BY TLUSTY AND YUN

In comparison of the current tension variation model with the model presented by Tlusty and Yun, it should be mentioned that the current tension model is distinct in terms of coupled vibrations as it is defined by a function of the vertical displacement of the work roll. As denoted in Section 3.8, the tension variation model by Tlusty and Yun is assumed to be harmonic. Thus, the inclusion of sinusoidal function makes the tension variations impossible to linearise as stiffness coefficient. Here, tension is only related to the oscillation in the vertical direction only, as defined by equation (8.7).

For this reason, it is almost impossible to compare these tension variation models. Nonetheless, it may be possible to approximate the tension variation, assuming that the amplitude (X) of the work roll is fed into the roll gap with no fluctuation and frequency

(ω) of the strip is fluctuating around 8.25 Hz when entering the dynamic roll gap. This modification is more plausible to identify the tension effect at entry roll gap otherwise the cumulative tension fluctuations due to the amplitude of the work roll make the system impossible to estimate the force variations.

Figure 8-15 represents variations of stiffness and damping coefficients in the journal bearing. From the fully transient simulation results, variations of stiffness coefficient are almost identical as shown in Figure 8-15(a) and (b) while Figure 8-15(c) and (d) are indistinguishable. Figure 8-16 also shows the identical variations of stiffness coefficients in the work roll bearing. This is resulted from negligible variation in the tension variation models applied (see Figure 8-2).

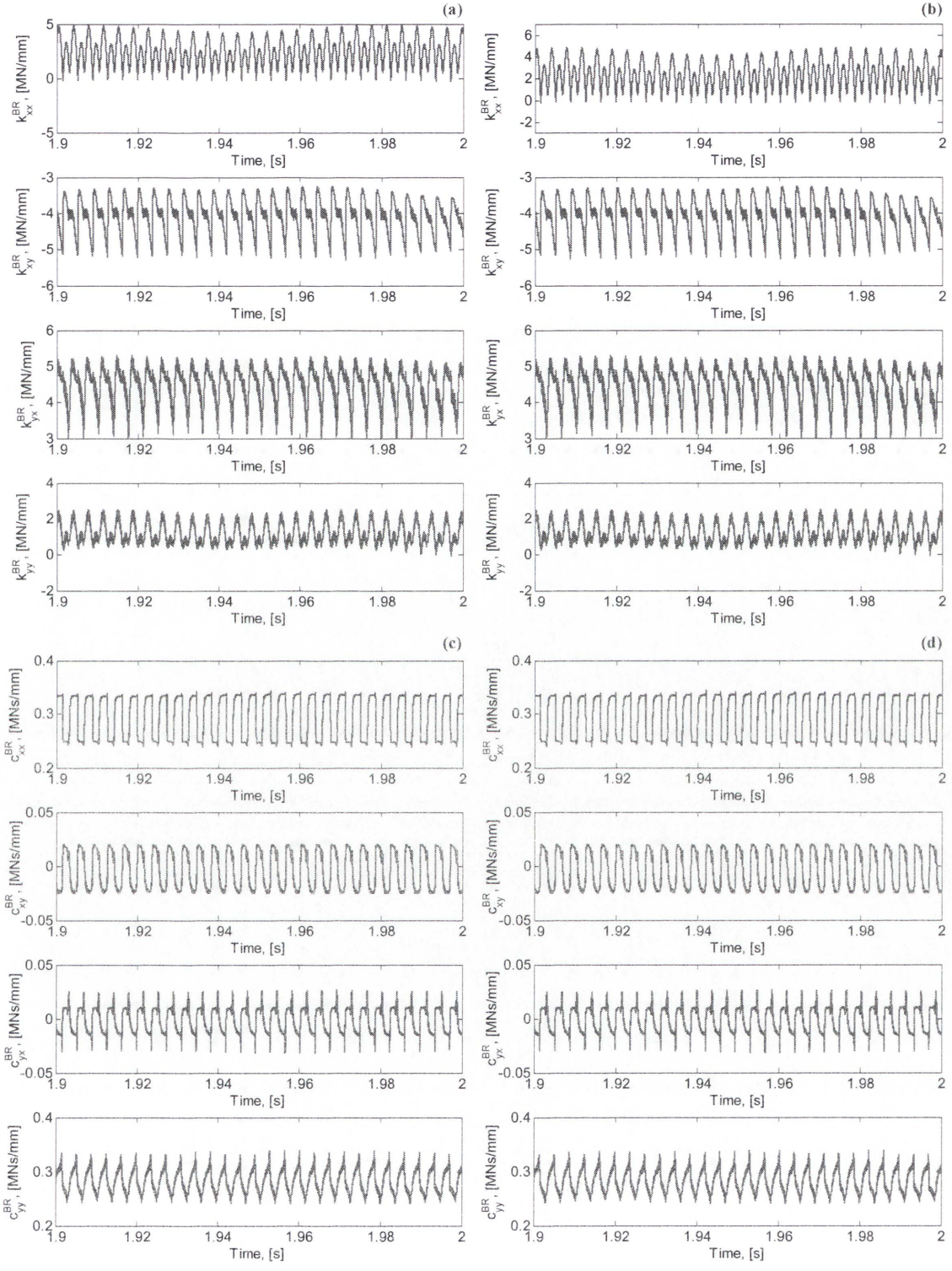

Figure 8-15: Dynamic characteristics of the journal bearing in the backup roll: variations of stiffness coefficients by (a) Tlusty and (b) Yun, variations of damping coefficients by (c) Tlusty and (d) Yun

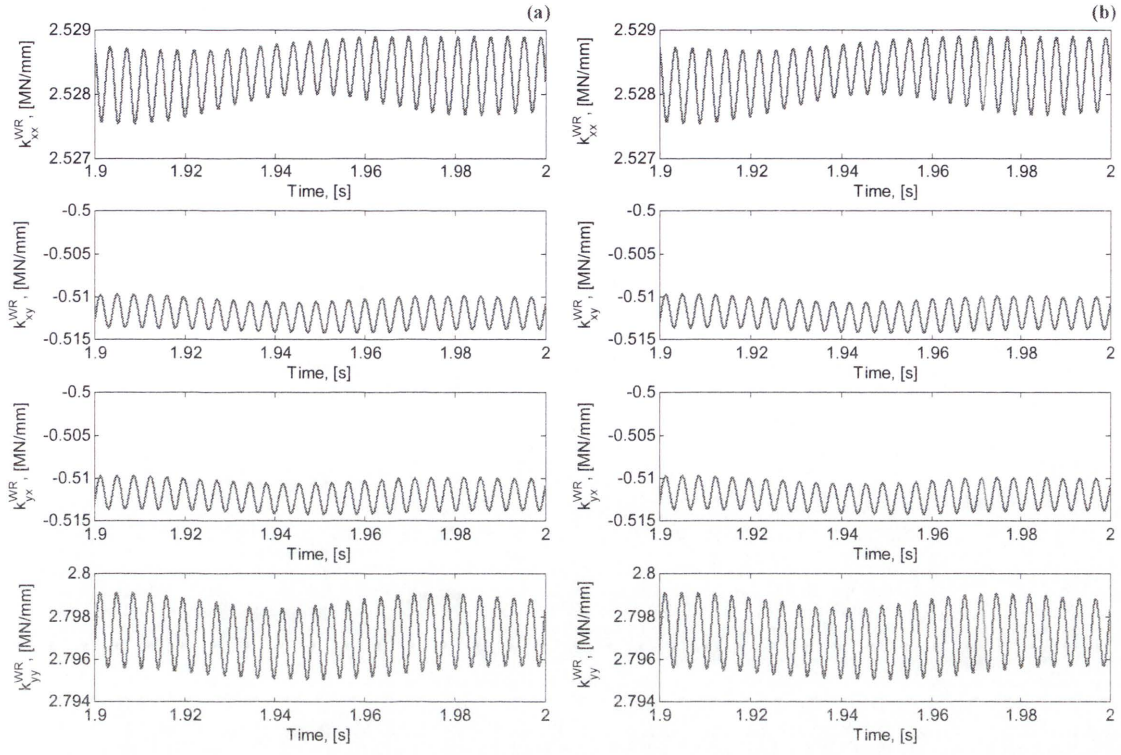

Figure 8-16: Variations of stiffness coefficients in the work roll tapered roller bearing, (a) Tlusty and (b) Yun

Therefore, it can be concluded that the transient responses by Tlusty and Yun would be identical as long as the other input parameters are maintained. In comparison to Figure 8-11 by the current tension variation model, it is likely that the amplitude of vibration is highly fluctuating as shown in Figure 8-17. However, these oscillations settle down as time goes by and the system maintains stability. Figure 8-18 also shows the phase-plane motions of the backup roll and work roll obtained by Tlusty's tension model. Figure 8-19 demonstrates the displacements of the neutral point and its oscillations are much turbulent comparing to Figure 8-13. Therefore, mill stability would be more susceptible to Tlusty's tension model and although variations of dynamic rolling force are much smaller than those by the current tension model (see Figures 8-10 and 8-20). The result is mainly due to the inclusion of sinusoidal function in Tlusty's tension model.

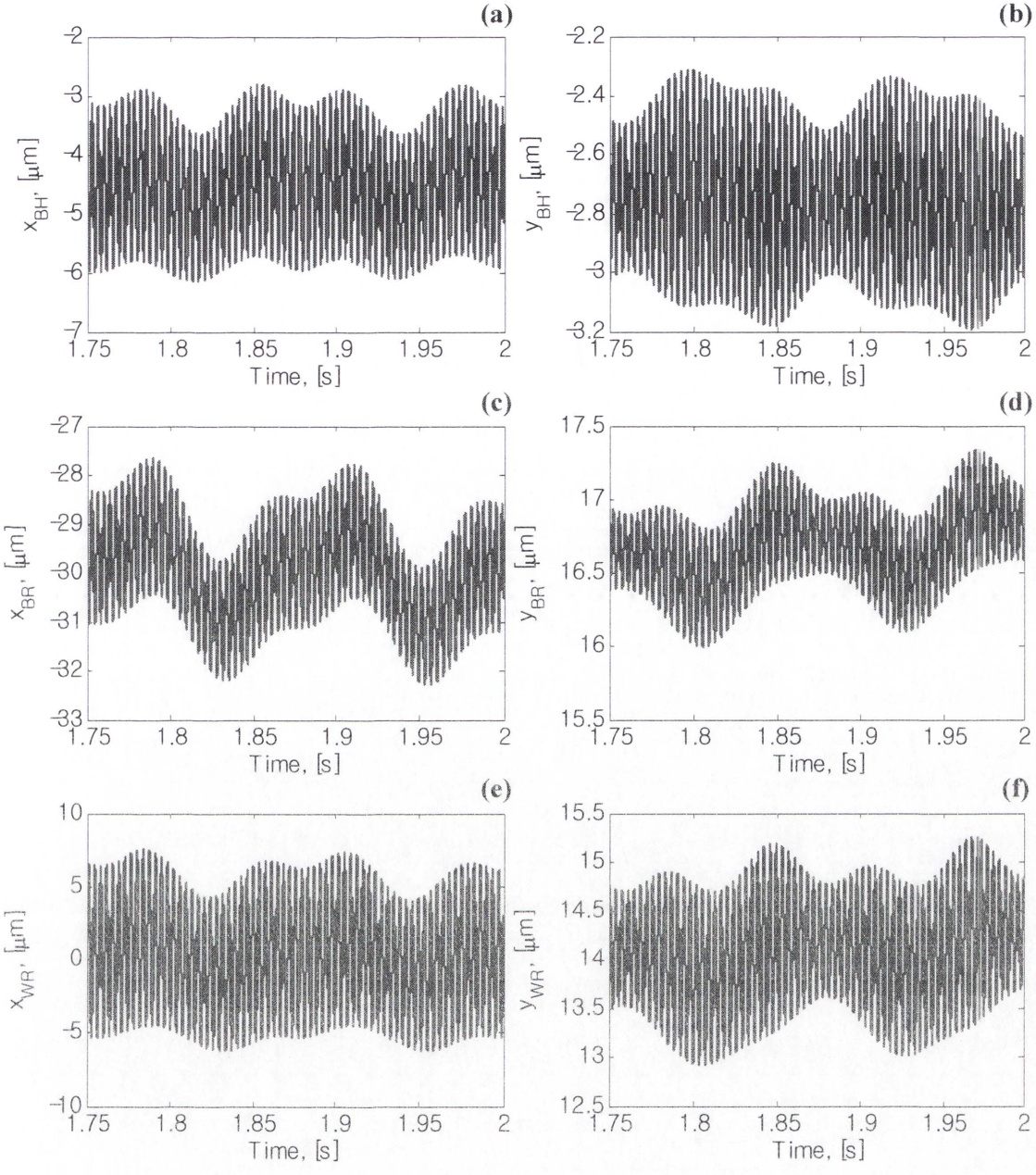

Figure 8-17: Transient oscillations of mass elements and force variations by Tlusty's tension model

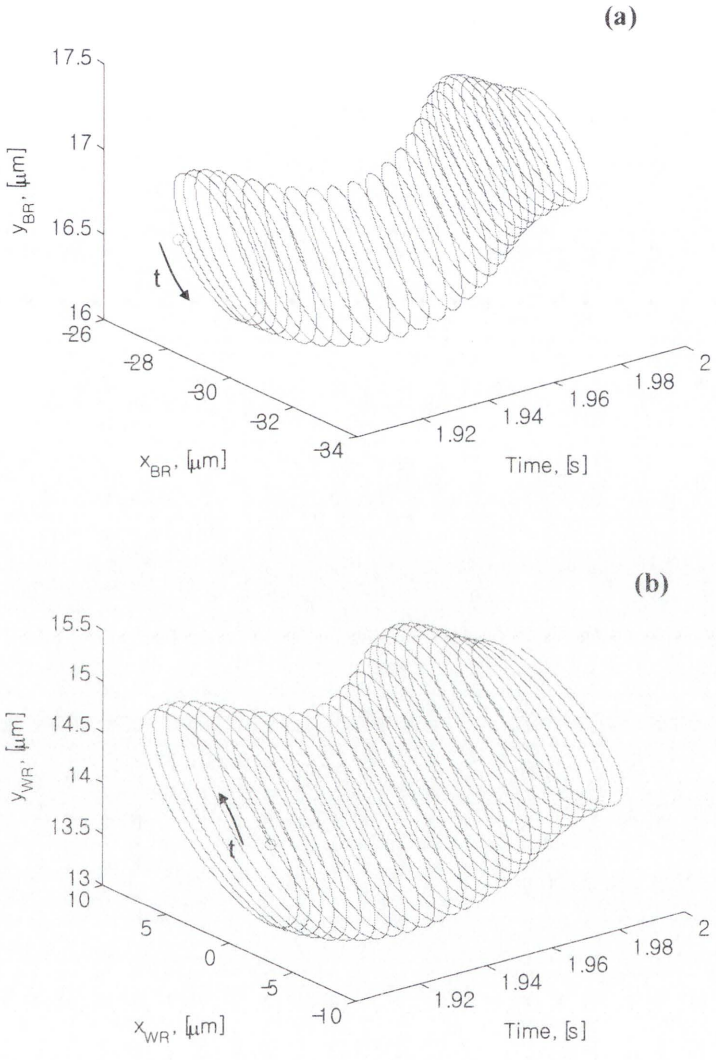

(a) Transient oscillations of the backup roll (b) Transient oscillations of the work roll

Figure 8-18: Phase-plane motions of mass elements by Tlusty' tension model

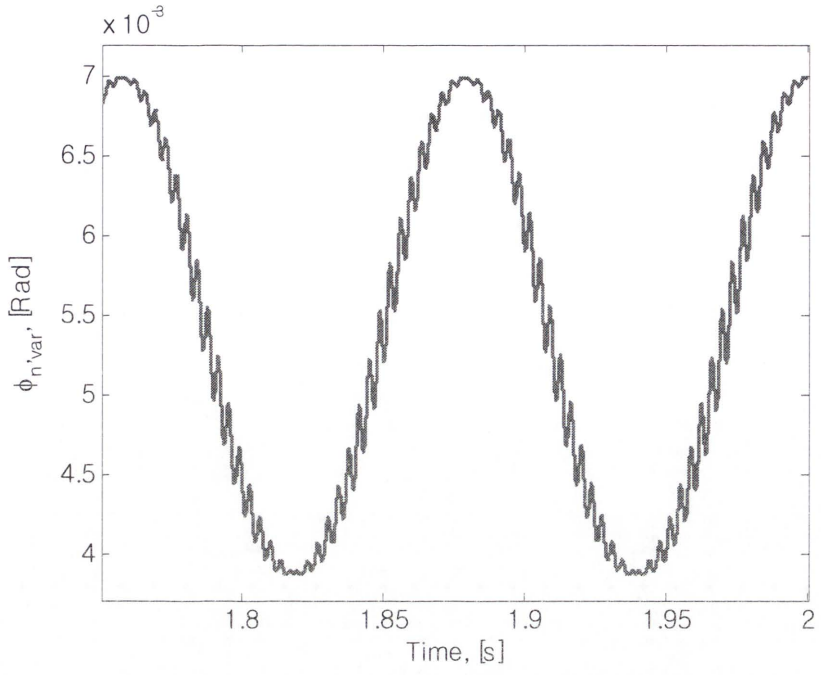

Figure 8-19: Displacements of the neutral point by Tlusty's tension model

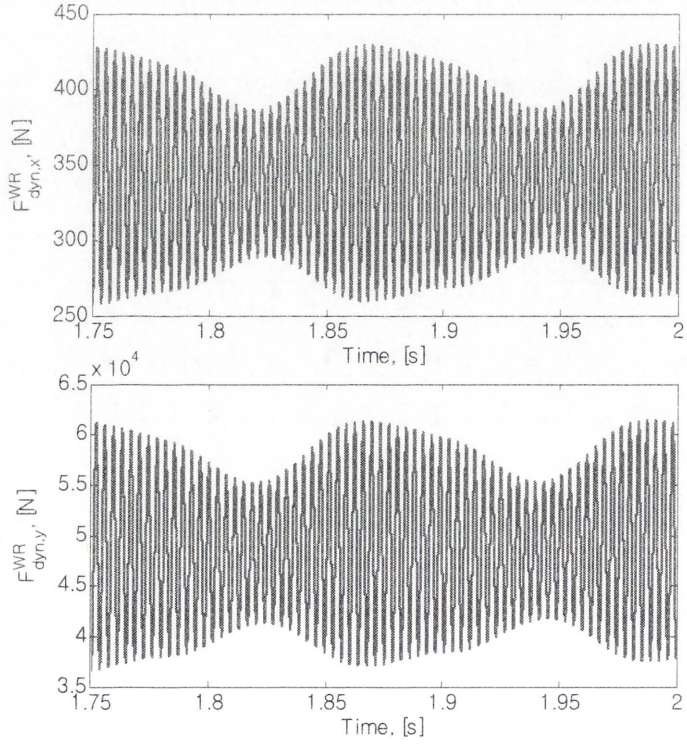

Figure 8-20: Dynamic rolling force variations by Tlusty's tension model

8.6. CHATTER OCCURRENCE

In Chapter 6 of this thesis, the contributors to rolling forces required for keeping stability of a rolling stand in cold rolling are studied. Formulation of the dynamic roll gap for a steady-state rolling was performed (Chapter 4), modeling and control methodology (Chapter 5) of a coupled dynamics were investigated for a 6DOF mill vibration system. Stability and linear transient studies (Chapters 6 and 7) were performed to determine the stability threshold curve under a variety of rolling operating conditions. Fundamentally, mill stability has been determined through the change in friction coefficient and rolling speed at an assumed friction gradient. In the following sections of this chapter fully-transient simulations have been performed to identify the chatter occurrence in terms of rolling parameters in a similar manner. This means linear stability does not compensate for the compliance of springs and dampers due to the state dependency of support bearings and surface contact between rolls.

8.6.1. Simulation Results in Case of Rolling Speed of $28m/s$

In Section 6.3.2 of Chapter 6, several different stability threshold curves (STC) were obtained for the different friction gradients through the change in rolling speed and friction coefficient. As demonstrated in Figure 6-2, it is shown that mill stability is most significantly affected by the rolling speed, representing self-excited vibration occurring due to the negative damping effect of the friction gradient as the rolling speed increases.

In a fully-transient simulation result in Figure 8-21, it is shown that transient oscillations demonstrate instability even though the friction gradient is reduced to by $0.006s/m$. When applying the current tension model, chatter rises with the increasing rolling speed due to the decreased damping in the dynamic roll gap (see Figure 4-9(a)). Note that the rolling speed is related to the forward slip but not described in here. In x-directional vibration, amplitudes of mass elements gradually grow up with the rolling process and reaches to over $100\mu m$ in 2 seconds while variations of horizontal rolling force grow up to 2000N. On the other hand, in y-direction vibration, amplitudes become unstable reaching up to $20\mu m$ and variations of vertical rolling force are also increasing. Also, in Figure 8-22, it is identified from Tlusty's tension variation model that chatter occurs due to the negative damping effect in the dynamic roll gap, regardless of the magnitude of tension applied.

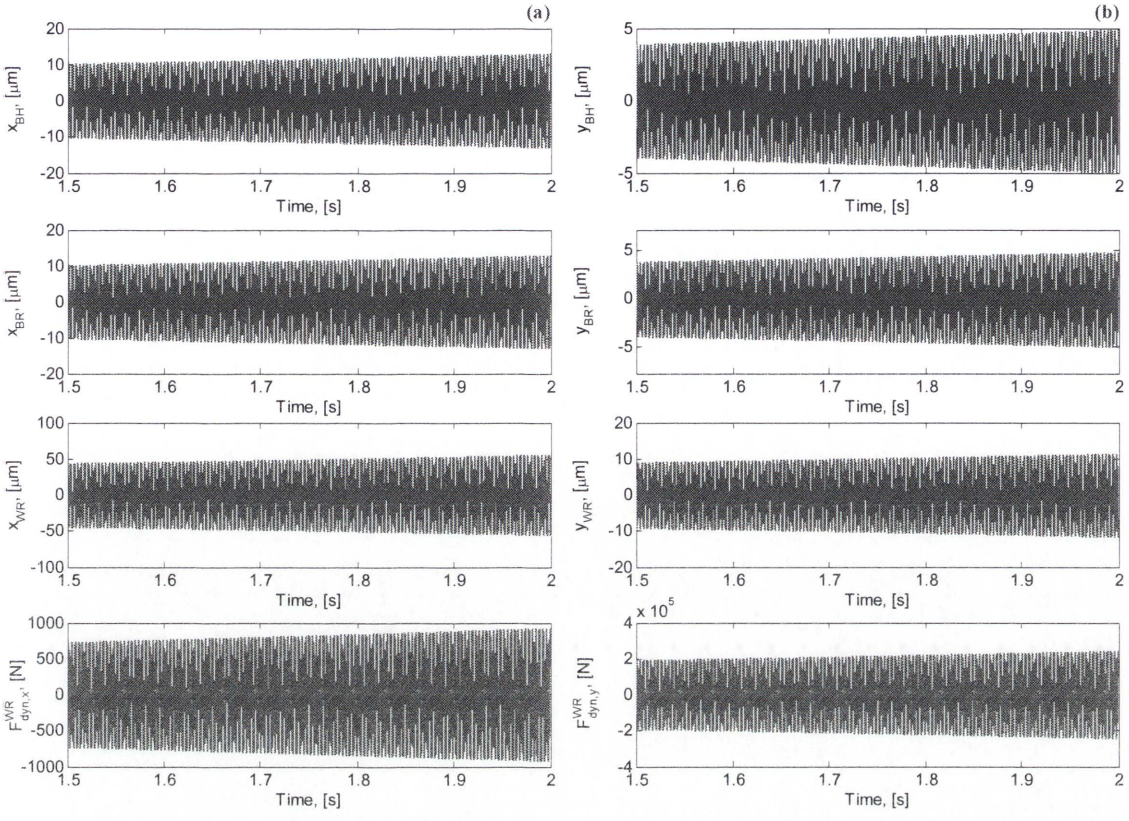

Figure 8-21: Transient oscillations by the current tension model at the friction coefficient of 0.02, rolling speed of 28.0*m/s*, the friction gradient of 0.020*s/m* and inter-stand distance of 4.0*m*

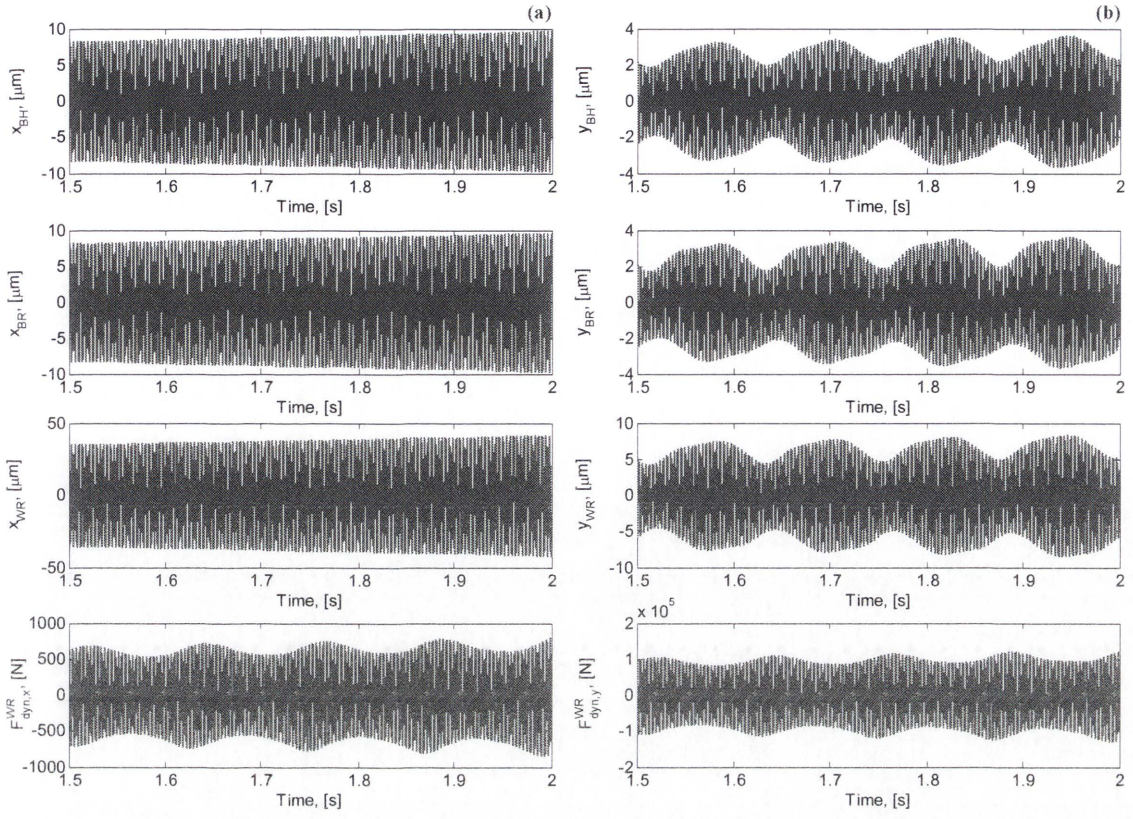

Figure 8-22: Transient oscillations by Tlusty's tension model at the friction coefficient of 0.02, rolling speed of 28.0*m/s*, the friction gradient of 0.020*s/m* and inter-stand distance of 4.0*m*

8.6.2. Simulation Results in Case of Friction Gradient of 0.026*s/m*

As described in Section 4.3.1, dynamic rolling force results from the inter-relationship between the friction coefficient and rolling speed. However, its lubricated condition is not readily known and easy to represent as the relative motion between the work roll and strip. In order to express friction in the roll bite, therefore, a linearised equation in equation (4.27) is given for studying the effect of negative gradient of friction. Friction gradient have a similar characteristic with forward slip which slowly but surely increases with the increasing rolling speed. It can be explained using the forward slip concept in equation (4.28) by similarity. In Section 3.5.2, analytical and experimental methods further are examined for the calculation of forward slip.

Analytical calculation of the forward slip requires more careful attention and needs to determine the strip velocity at the entry and exit sides. The calculation of the strip velocity at both sides entails 'positioning' of the neutral point and deformed roll radius, and is then calculated from the mass flow equation (3.1) if the strip thickness at the

neutral point is determined. In Section 6.3.2, the critical operating conditions are identified from the stability analysis of the linearised model. In fully-transient simulations, it is shown that system responses (Figures 8-23 and 8-24) are severely amplified with the given conditions (friction coefficient of 0.02, rolling speed of 22.73*m/s* and friction gradient of 0.026*s/m*). Table 8-1 shows the calculated natural frequency and damping ratio of the system, and represents negligible difference between the linear and transient model.

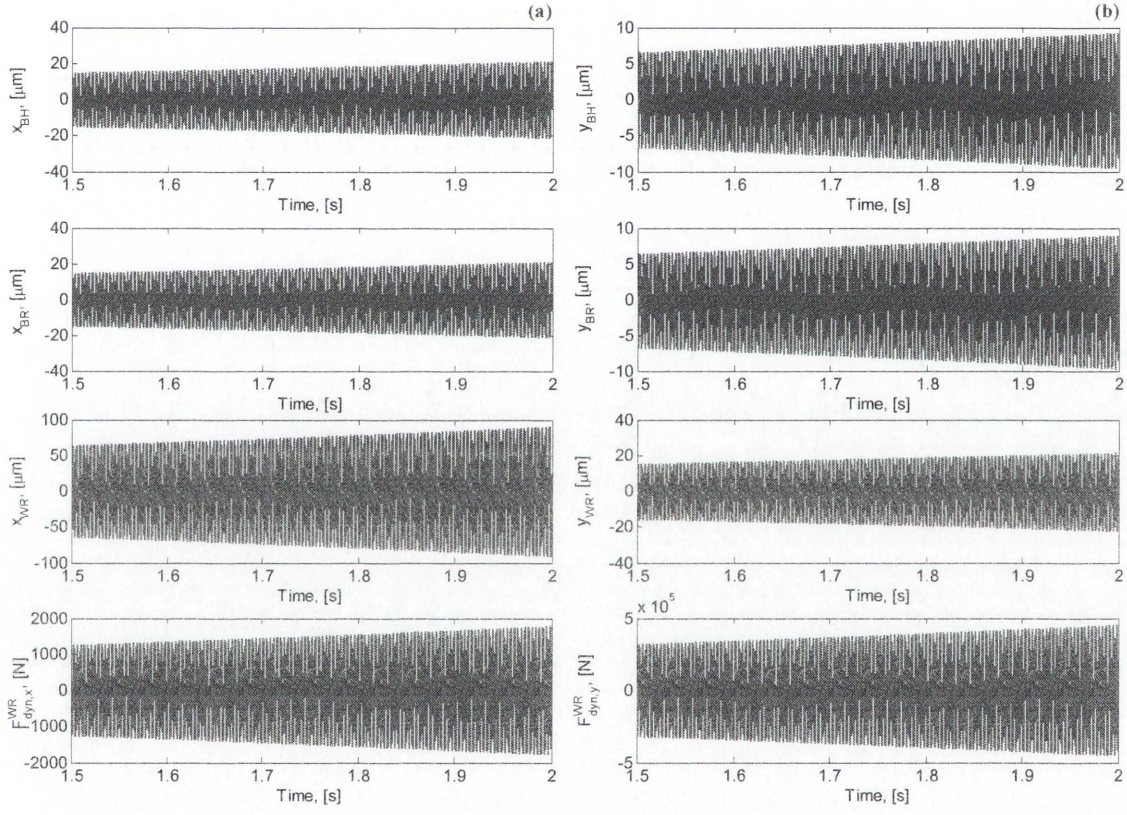

Figure 8-23: Transient oscillations by the current tension model at the friction coefficient of 0.02, rolling speed of 22.73*m/s*, the friction gradient of 0.026*s/m* and inter-stand distance of 4.0*m*

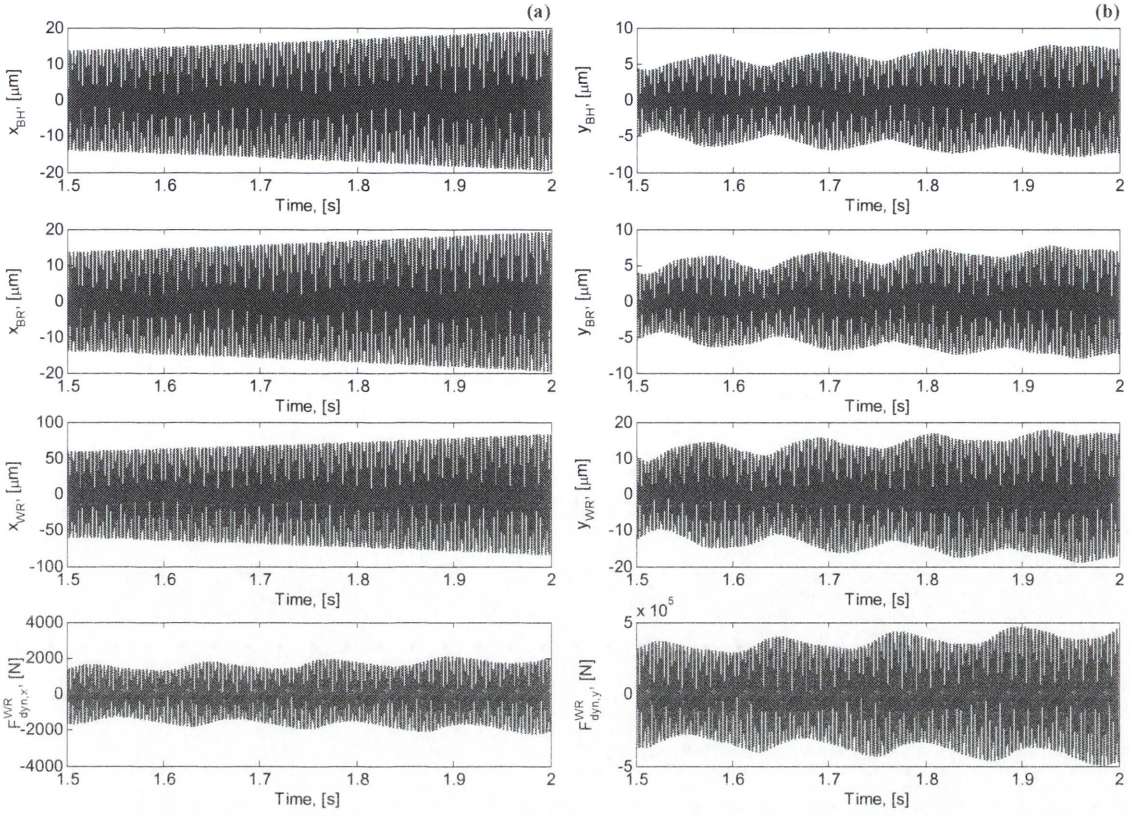

Figure 8-24: Transient oscillations by Tlusty's tension model at the friction coefficient of 0.02, rolling speed of 22.73*m/s*, the friction gradient of 0.026*s/m* and inter-stand distance of 4.0*m*

Table 8-1: Comparison of linear and transient results at friction gradient of 0.026*s/m*

System state			Natural frequencies and damping ratio					
Linearised Model	Constant tension	Natural frequencies (*Hz*)	**0.0**	**7.92**	**119.22**	**131.75**	**274.97**	**342.95**
		Damping Ratio (ζ)	100%	91.75%	1.30%	11.29%	-0.012%	21.59%
Fully-transient Model	Current tension variation model	Natural frequencies (*Hz*)	0.0	0.0	116.98	133.21	272.12	338.23
		Damping Ratio (ζ)	100%	100%	2.43%	15.04%	-0.038%	25.67%
	Tlusty's tension variation model	Natural frequencies (*Hz*)	0.0	9.36	117.79	132.03	272.62	341.27
		Damping Ratio (ζ)	100%	98.96%	2.59%	13.08%	-0.033%	21.59%

8.6.3. Simulation Results in Case of Inter-Stand Distance of 3.0*m*

In Sections 3.8.1 and 3.8.2, it is shown that the variable elongation leads to a variation in tension between inter-stands. Equations (3.61) and (3.67) reveal tension variation models presented by Tlusty and Yun. Apart from the variation in sinusoidal function, those tension models include six independent parameters such as Young's modulus, amplitude, inter-stand distance, entry thickness, strip exit speed and elongation. As reported by Tlusty et al. (1982), tension fluctuation would increase as Young's modulus, amplitude, elongation and strip exit speed increases. Here, Young's modulus is generally unchanged and amplitude of the work roll is assumed to be constant.

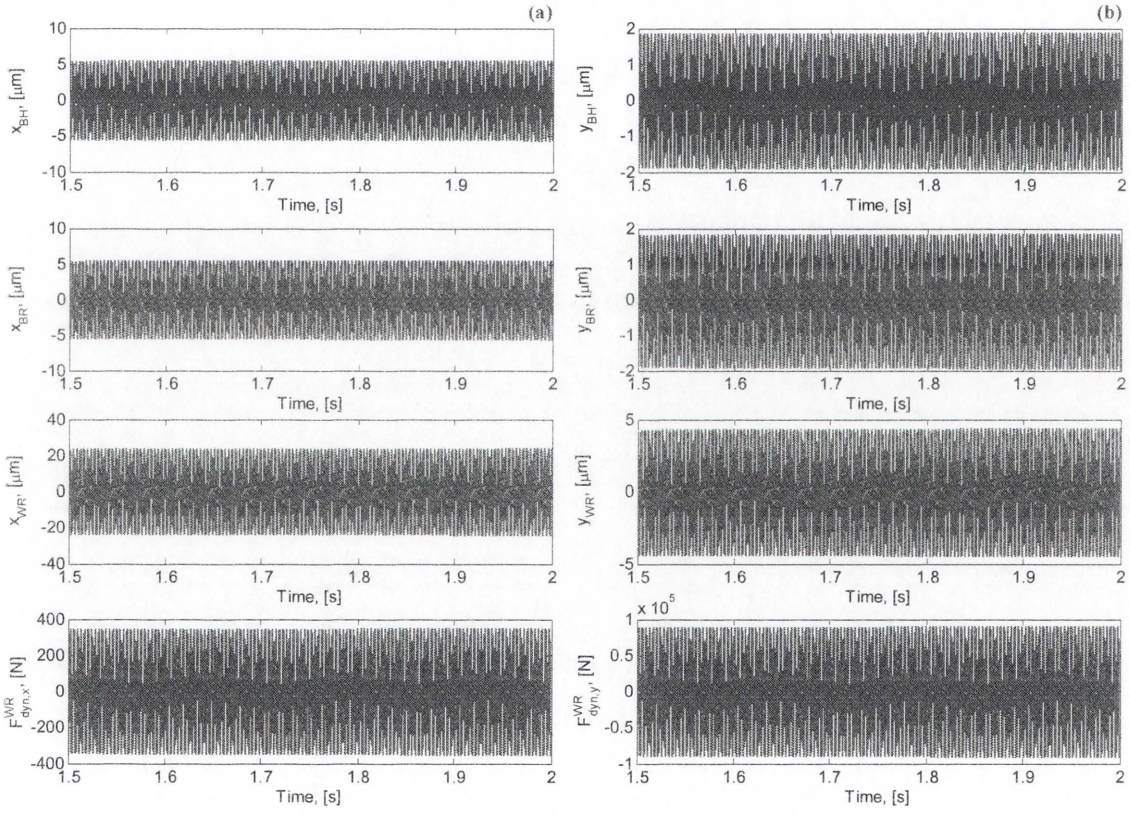

Figure 8-25: Transient oscillations by the current tension model at the friction coefficient of 0.02, rolling speed of 22.73*m/s*, the friction gradient of 0.020*s/m* and inter-stand distance of 3.0*m*

Thus, it may be conjectured from the above equation that the rest of two parameters are the plausible source of chatter. At first, the amount of elongation between inter-stands mainly causes oscillations and its value highly relies on the reduction, representing the amount of compression (*i.e.*, subtraction of the entry and exit thickness). In light of this, if possible, the reduction should be reduced to maintain tension fluctuation and thus the stability. This is also demonstrated in Section 6.3.3.3 and Figure 6-6 which indicate that the smaller the reduction becomes, the better the stability.

Once again, from equations (3.61) and (3.67), inter-stand distance should be increased to stabilise the mill operation otherwise the magnitude of tension variation grows due to the inverse proportionality with inter-stand distance. However, as reported by Tamiya et al. (1980), replacing mill configuration will result in too much cost and it may be a better way to find out an appropriate lubrication condition in the support bearings and roll gap. Chatter occurrence due to the decreased inter-stand distance is shown in Figures 8-25 and 8-26.

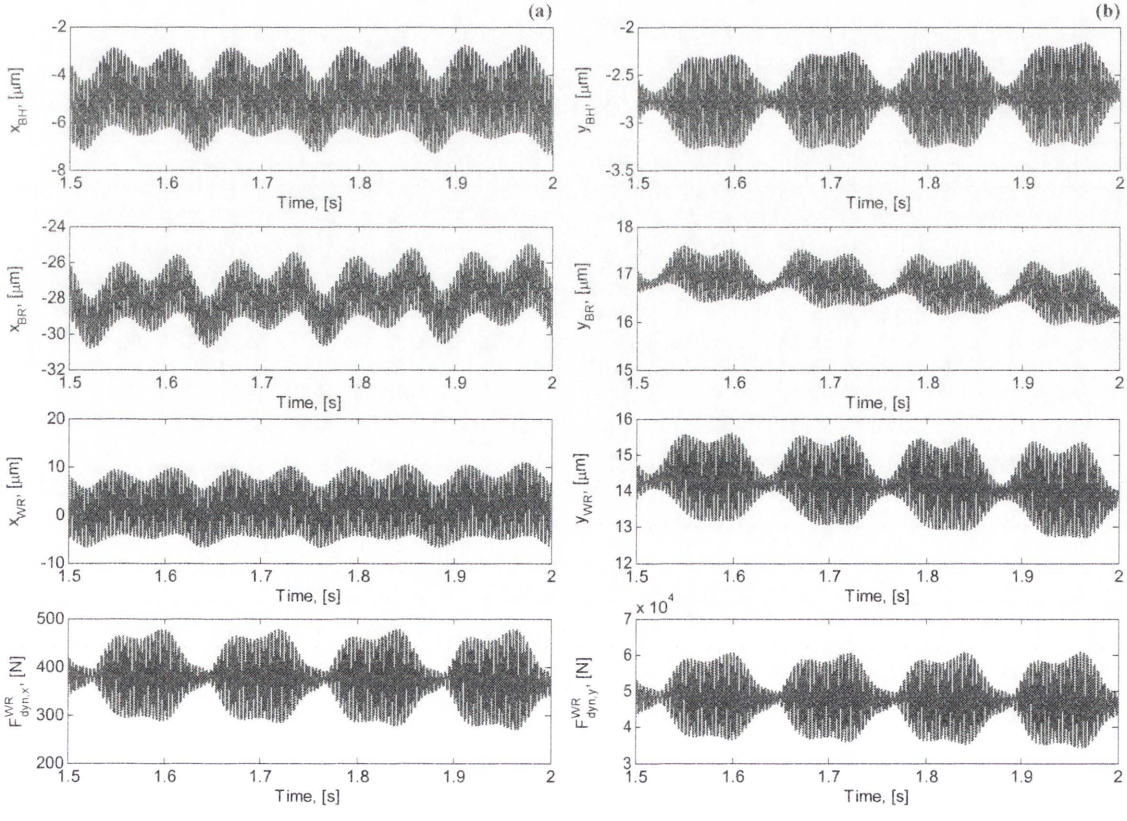

Figure 8-26: Transient oscillations by Tlusty's tension model at the friction coefficient of 0.02, rolling speed of 22.73m/s, the friction gradient of 0.020s/m and inter-stand distance of 3.0m

For identifying more distinct effects from the inter-stand distance, Figure 8-27(a) shows the tension variation resulted from the change in inter-stand distance. The amplitude of tension variation reduces less than $2.0MPa$ when inter-stand distance increased to $5.0m$ while the variation slightly increase up to $3.0MPa$ when distance is set to $3.0m$. Furthermore, the effect becomes more noticeable when applied tension variations by Tlusty's model. Tension variation is shown in Figure 8-27(b) and increases with the decreasing inter-stand distance. As demonstrated in Figures 8-27(a) and (b), it can be concluded that tension variation by Tlusty's model would be more vulnerable or susceptible to mill chatter even though the resulting rolling force reduces due to the increased tension.

There remains one question for the tension variation as two figures are still independent and cannot be comparable to each other due to its difference of high variation. Therefore, it can be concluded that tension variation by Tlusty's model is oversimplified or the incoming strip speed variation frequency may be higher than that of Tlusty's and Yun's tension model. This will be discussed in the next section.

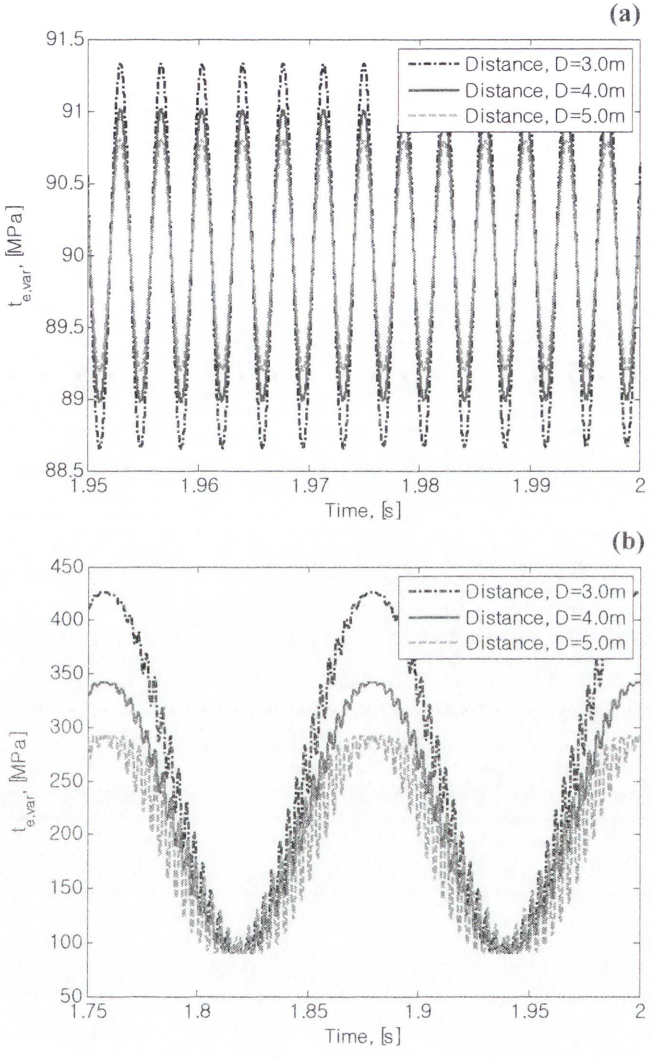

Figure 8-27: Effect of inter-stand distance on (a) the current tension variation and (b) Tlusty's tension variation

8.6.4. Simulation Results in Case of Time-Delay

In order to identify how the strip thickness variation from one stand affects the next stand, inter-stand relationship by Arimura et al. (1970) is given in Section 2.3. It is presented that the interactions between stands play an important role in increasing the possibility of self-excited vibration and also change the phase relationship as the strip at exit of (i-1)th stand is fed into the entry of (i)th stand with the certain amount of time-delay. In equation (2.8), the time delay is expressed as the ratio of the inter-stand distance to the strip velocity. As such, the tension variation equation is required to change its form including the time-delay and the elongation of the strip between stands can be expressed as:

$$\Delta D(t)\big|_{Tlusty} = \frac{2Xv_x}{\omega h_e}\left(1-\cos\left(\omega t-\Delta_i\right)\right) \tag{8.8}$$

$$\Delta D(t)\big|_{Yun} = \frac{2Xv_x}{h_e\omega}\left(1-\cos\left(\omega t-\Delta_i\right)\right)+\frac{2X\Delta D}{h_e}\sin\left(\omega t-\Delta_i\right) \tag{8.9}$$

where ΔD and Δ_i are the elongation and time-delay between stands.

As demonstrated by Tlusty et al. (1982), simulation results indicate in Figure 8-28 that the coupled mill vibration model gradually loses stability when the time-delay is applied to the roll gap with phase difference more than 90 degrees. Simulation results also identified the critical vibration is significantly affected by the frequency of the incoming strip and the work roll oscillation reduces as the incoming strip frequency increases. However, it is noted that the frequency range which makes the system resonant should be avoided, as shown in Figure 8-29.

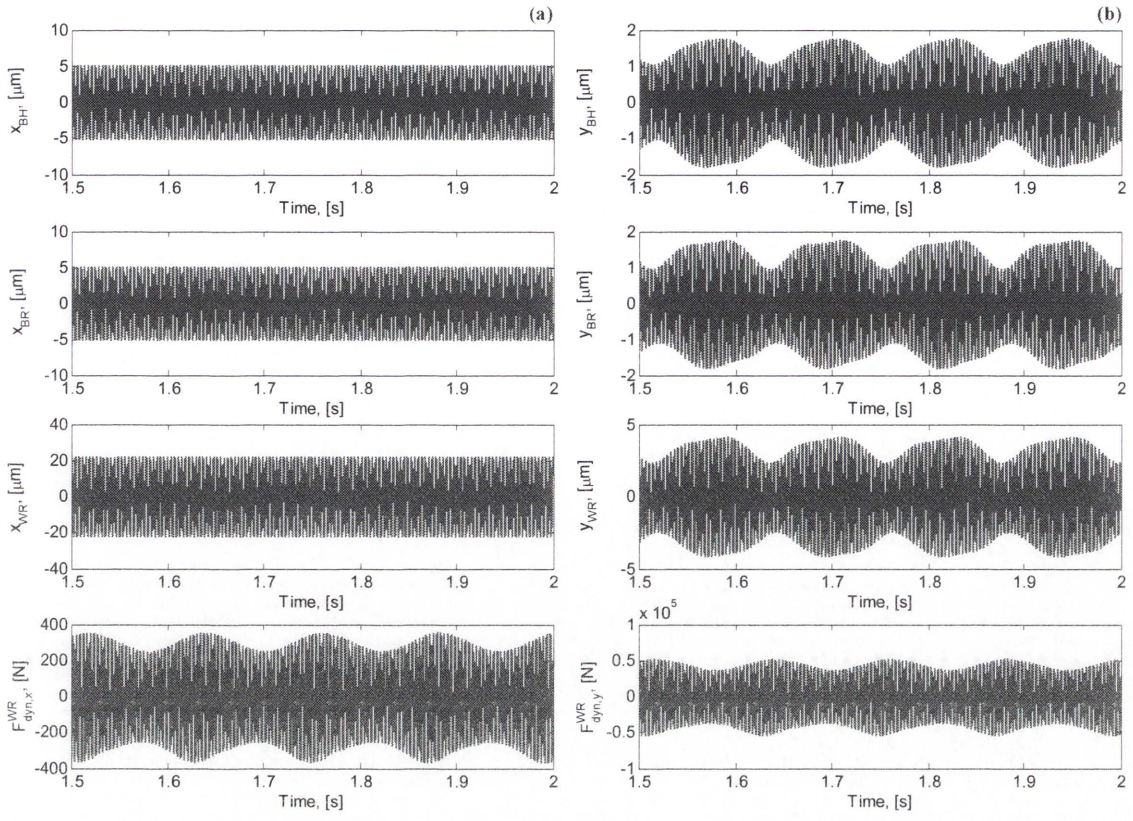

Figure 8-28: Transient oscillations by Tlusty's tension model with the time-delay of 90°

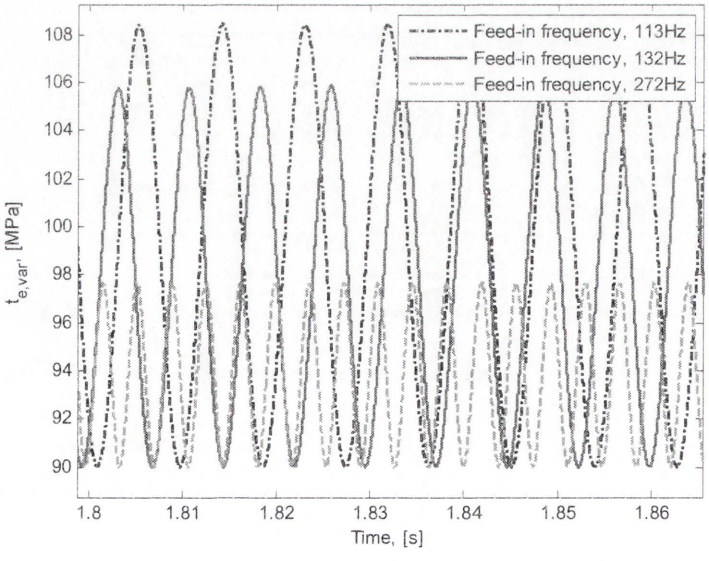

Figure 8-29: Tension variations with the resonant frequencies by Tlusty's tension model

8.7. SUMMARY

This chapter has sought to present a fully-transient method for reducing cumulative error and investigates the impact of various nonlinearities in estimating the dynamic mill characteristics during the rolling process. A nonlinear 6DOF mill vibration model has been developed for identifying the onset of chatter and used to investigate the transient response to rolling parameters. Transient response in a rolling stand requires a combined roll gap model with tension variations and detailed structural models. The modified mill vibration model (6DOF) takes into account the dynamic variations of the force component resulting from the roll gap, support bearings and contact surface. In addition, three different types of tension variation models are applied into the dynamic roll gap for examining the effects of tension on force variations of a rolling stand in cold rolling. This provides a broad spectrum of excitation frequencies in a rolling stand for excitation under sliding motions. Four transient conditions were studied changing mill operating conditions. These are (1) rolling speed, (2) friction gradient, (3) inter-stand distance and (4) tension variation by time delay at entry side.

In a similar way compared to Chapter 6, again it has been demonstrated in these simulations that instability is initially developed in the journal bearing and the chatter responses are initiated from the dynamic roll gap as a results of negative damping effect. Specifically, mill chatter is prevalent in results (1) for increasing rolling speed up to $28m/s$, (2) for increasing friction gradient up to $0.026s/m$, (3) for reducing distance between stands and (4) for time delay more than 90 degrees at entry side.

- For the high rolling speed rolling, typical unstable response indicates the onset of chatter initiated by the reduced damping which is also a result of the increasing rolling speed.
- The friction gradient linearised from the relative motion between the work roll and strip in the roll gap, greatly affects the damping force for which it acts as a negative damping.
- Inter-stand distance contributes to the magnitude of tension variation and should be long enough for maintaining stability as tension stresses are the reverse proportionality to inter-stand distance.

- The time-delay happens during the rolling process when the strip thickness variation at the exit side of one stand differs from that at the entry side of the next stand. Due to this time-delay between stands, tension is applied to the roll gap with the phase difference and rolling force is affected by tension variation. In this way, it has been shown that self-excited vibration may arise within a few seconds.

CHAPTER 9. CONCLUSION, CONTRIBUTIONS AND FUTURE WORK

9.1. SUMMARY OF THESIS

The multi-body dynamics and its components of a rolling stand in cold rolling have been investigated in this thesis, including studies into dynamic characterisation of the support bearings, the surface contact between two rolls and the roll gap with the inclusion of multiple nonlinearities. It is considered that the bearing housing chock, backup roll and work roll oscillate with bi-directional (x and y directions) degrees of freedom. Initially extensive literature research identified major components of a cold rolling stand in addition to methods available for modelling and the extent to which modelling and analysis have been performed. The majority of this thesis has been devoted to the modelling, simulation and analysis of these components and a rolling stand as a complete system.

To study a dynamic rolling stand mechanism based on the given rolling profile, effects of rolling parameters on mill characteristics were investigated incorporating the deformation resistance model as a function of strain and strain-rate exponent, as well as tension variation model (Chapter 3). Under the steady-state condition (friction coefficient of 0.02 and rolling speed of $20m/s$), pressure distribution curves have been calculated from the dynamic roll gap model and the unique point, at which the pressure reaches a maximum, or neutral point was accordingly identified. Dynamic rolling force components were formulated considering the small disturbance of the roll gap (Chapter 4). These force variations have been further linearised as stiffness and damping coefficients and the significant influence of force variations was identified from the change in rolling parameters such as the friction coefficient, rolling speed, reduction and reduction rate. In order to simplify the mill system at 4^{th} stand, the upper and lower parts of a rolling stand were assumed to be symmetrical with respect to the centre plane of the roll gap. Introducing support bearing models (journal bearing for a backup roll and tapered roller bearing for a work roll), the bearing force components have been linearised as stiffness and damping coefficients, respectively. In order to express the surface contact mechanism between the backup roll and work roll, the deformation

between two rolls was described using linear elasticity by Hertzian contact theory. Then, incorporating the dynamic roll gap model with the mechanical model, a coupled mill vibration model has been formulated (Chapter 5). For the determination of system stability, the linearised stiffness and damping coefficients, predetermined at the steady-state condition, have been compared with other models in order to provide the validity of the proposed system. A highly coupled mill vibration model (6DOF) is rearranged in matrix form of the first order and the system matrix is used for the calculation of natural frequencies and the corresponding modes. With the change of friction coefficient and rolling speed at assumed friction gradients, stability threshold curves (STC) have been determined through the examination of corresponding rolling forces. In order to identify different aspects of stability threshold curve (STC), the effects of other rolling parameters on a rolling stand were studied (Chapter 6). Linear transient simulations have been carried out to validate the determined STCs and its responses were studied with the change of rolling parameters and through investigation of the phase difference. The resonant frequency components are further identified from the response existing in the obtained signal using Fast Fourier Transform (FFT) (Chapter 7).

Finally, to relax the assumptions and simplification made in the linear model, a fully-transient model was developed incorporating the tension variation at the entry side with the dynamic roll gap. In comparison to the linearised model using free vibration analysis transient responses demonstrated reasonable compatibility even though the friction gradient was required to be reduced for maintaining stability in a rolling stand. When applied the tension variation at the entry side of the roll gap, the dynamic characteristics of the support bearings, the surface contact between two rolls and the dynamic roll gap were significantly influenced and shown to be critical to mill stability. With these tension variations, transient simulations were performed to identify the chatter occurrence in terms of rolling parameters in a similar manner in Chapter 6 and 7. Consideration of reducing inter-stand distance and time delay in the entry tension variation model was further shown to generate mill instability, apart from the friction gradient, friction coefficient and rolling speed.

9.2. SUMMARY OF FINDINGS AND CONTRIBUTIONS

The objectives of this project identified in the introduction are repeated here along with the primary findings and contributions that have resulted from this investigation:

1. Model the dynamic roll gap of a rolling stand by using the deformation resistance model as a function of the reduction and rolling speed.

The major components of a rolling stand in cold rolling have been modelled in Section 4.2 for the steady-state roll gap model, Section 4.3 for the dynamic rolling force components and Chapter 8 for the fully-transient model of each identified rolling state including tension variations at the entry side of the roll gap.

i) Deformation resistance models have been developed and validated for more precisely estimating rolling force, introducing strain and strain-rate effect at the steady-state condition.

ii) Pressure distribution curves have been calculated through the change of tension, draft, friction coefficient and rolling speed. The significant effects were identified demonstrating that pressure peak arises and neutral point shifts as rolling parameters change.

iii) Rolling force components were formulated in order to identify the dynamic characteristics resulting from the small disturbance in the dynamic roll gap. These force components have been linearised as the stiffness and damping coefficients introducing the negative gradient of friction coefficient.

iv) It was found that the negative damping effect is significantly caused by friction variation with the rolling speed and its force variations negatively increase with the increasing rolling speed.

v) It was identified that the rolling speed itself positively affects the dynamic roll gap and its force variations decrease with the increasing rolling speed.

vi) It was also shown that the strip thickness variation positively affects the dynamic roll gap. The force variations directly influence the natural frequency range of the system model since these variations act like a spring which increases with the increasing rolling speed.

2. Model the main components of a rolling stand and integrate them into a coupled mill vibration model for predicting the linear and transient characteristics during the rolling process.

The major components of a rolling stand in cold rolling have been modelled in Chapter 5, incorporating two different bearing solutions (the journal bearing for the

backup roll and the tapered roller bearing for the work roll) and surface contact mechanism between two rolls. Based on the associated dynamics of these components, the coupled mill vibration model has been developed considering relative motions between mass elements. Each mass element has two degrees of freedom including two dimensional motions in the horizontal and vertical directions. The dynamic conditions of both parts of the individual stand are assumed to be symmetrical with respect to the roll gap and considered to be exactly identical.

i) For an upper part of a rolling stand, the mill vibration model was developed using force components only. The model provides the dynamic characteristics of cold rolling in a nonlinear fashion.

ii) In order to determine stability threshold representing the critical operating conditions, these force components have been linearised as stiffness and damping coefficients and used for free vibration analysis.

iii) The journal bearing solutions have been adopted to explain lubrication condition about how the oil-film thickness varies and the tapered roller bearing theory (rather simplified) was also utilised to represent a coupling between the translational motions.

iv) Surface contact mechanism between the backup roll and work roll has been intensively investigated to explain the relative motion in the horizontal and vertical directions. The force components have been linearised as a spring, and thus the effective stiffness coefficients are obtained by utilising mode coupling theory.

v) Considering the steady-state rolling conditions, all force components have been linearised, producing the stiffness and damping coefficients, in a way that these are determined from different operating conditions and highly dependent on the rolling parameters such as the friction coefficient, rolling speed, reduction and reduction rate with respect to time.

3. Develop numerical solutions of the linearised model for mill stability to investigate dynamic coupling between multiple nonlinearities for accurate assessment of stability characteristics.

Numerical studies were carried out in Chapter 6 for determining stability through the examination of eigenvalues and studies with detailed identification of the system model in Chapter 7. At assumed friction gradients, mill vibrational modes and

natural frequencies have been identified through free vibration analysis, specifically for unstable conditions. In order to clearly separate the stable and unstable regime, stability threshold curves (STC) have been determined through the change in friction coefficient and rolling speed with different rolling conditions. The major results are as follows:

i) Mill stability is highly dependent on friction gradients which is assumed in the steady-state conditions and becomes unstable as it increases.

ii) The system is likely to be stabilised with the increase of friction coefficient as the strip width increases while it appears to be unstable with the increase of friction coefficient when the strip width is set to $1.0m$.

iii) The system becomes unstable as the size of the roll increases. In fact, it is more influenced by the roughness of the roll than the size of the roll.

iv) Stability threshold curve (STC) moves towards the left hand (unstable region) as the reduction in the roll gap increases while it is likely to shift to the right hand (stable region) as the reduction reduces.

v) It is shown that stability is more likely affected by strain-rate exponent rather than strain exponent demonstrating the rolling speed dependent.

vi) The roll offset also affects the mill stability. However, it is found it would be better to maintain at $6mm$.

vii) For the journal bearing parameters, mill stability is maintained as the dynamic viscosity slightly decreases, the bearing length slightly decreases and the bearing clearance slightly increases.

viii) Linear transient studies produce results that match the stability threshold curves presented in Chapter 6.

4. Develop a fully-transient model including nonlinearities in the support bearings, the surface contact between rolls and the dynamic roll gap in addition to different tension variation models at the entry side.

Fully-transient studies were performed in Chapter 8 for determining the system stability and demonstrating limitations of the linearised model. Dynamic characteristics of the coupled mill vibration model have been identified depending on the rolling speed, friction gradient, inter-stand distance and time-delay, specifically for unstable conditions. The major outcomes are as follows:

i) Comparison of the fully-transient model with a 6DOF model from Chapter 6 shows higher vibration amplitude in comparison to that with no tension variation.

ii) Force vibrations from the harmonic tension at the entry side introduce uncertainty in rolling force estimation, a significant issue in Chapter 8, and can introduce negative damping effect due to the significant relative motion between the work roll and strip during the rolling process.

iii) The current tension variation model presented exhibits instability caused by the work roll displacement in the vertical direction.

iv) In a similar way, more reliable responses are obtained from the fully-transient model that chatter indeed arises from the increasing rolling speed and friction gradient. Instability occurs as inter-stand distance becomes longer and the strip is fed into the roll gap with time-delay of more than 90 degrees of phase difference.

9.3. LIMITATIONS TO RESEARCH

Four limitations of this thesis are highlighted, particularly as there is only limited capacity to verify results of this work.

1. The most significant limitation to this research has been the capability to undertake any form of validation to many models introduced in this thesis. While popular and established methods have been used to evaluate a range of issues such as rolling force, support bearing or surface contact mechanism model, the accuracy of such models is limited. Validation of part or all of these models will increase the certainty that can be placed on the quality of results. To the extent that these models could be verified this was performed, with the roll gap model compared to typical data suggested in BSL (BlueScope Steel LTD), while free vibration analysis of a rolling stand suggests that these are representative of a typical tandem cold rolling mill. With results containing rigid body modes, first-octave mode between 2-10Hz, third-octave mode between 110-300Hz and fifth-octave mode between 300-1000Hz among typical rolling mill vibration frequencies, are indicating that the presented model is reasonable for simulations.

2. Generally simulations have been performed with available data, such that the values of parameters used in these simulations are typical to what will be expected in a tandem cold rolling mill, however a lack of accurate and reliable data limits confidence in results. Consider negative damping effects caused by nonlinearities of friction variation, it is highly dependent on design parameters such as rolling speed and forward slip and the friction coefficient eventually decreases in the dynamic roll gap. Thus while the simulations in this thesis provide indication of how these nonlinearities will affect the chatter response, more accurate information is required to provide more than demonstrative simulations on current work.
3. Friction coefficient for the dynamic roll gap and surface contact between rolls are assumed to be constant. The linear friction gradient of rolling speed dependent friction coefficients for the dynamic roll gap in particular will contribute further to an understanding of nonlinearities in tandem cold rolling mill.
4. Tension variation applied at the entry side of the dynamic roll gap greatly affects the system characteristics, leading or lagging the phase of the incoming strip. However, the feed-in frequency of the incoming strip is not readily known and reconstructing inter-stand distance costs too much. In the meanwhile even though there are many trials installing 'Touch Roll' between stands to reduce tension variations, many industries are still experiencing chatter phenomenon. For the more detailed tension variation model, it is required to explain precise tension variations from Pay-off reel to Pick(Take)-up reel. Nonetheless, simulation results in this thesis demonstrate the negative damping effect, caused by the significant relative motion between the work roll and strip as well as the tension variation between stands, is one of the plausible sources of chatter phenomenon.

9.4. FURTHER RESEARCH

Approach for further research into cold rolling mill transients and control include:

1. The limitations to this research in terms of validation and use of actual rolling parameters (tension and forward slip in the strip) provides a significant

opportunity for experimental research, particularly as at the time of writing this thesis the author found difficulties in performing experiments pertaining to validation of transient responses of cold rolling mill at an academic level. One aspect that should be considered is the use of experimentally determined friction coefficient and friction gradient, particularly as these have been shown to alter the behavior of rolling mill responses significantly.

2. Tension variation models, presented by Tlusty et al. (1982) and Yun et al (1998) so far, are significantly oversimplified introducing harmonic oscillation in formula even though the current tension variation model utilise the work roll amplitude in the vertical direction. Furthermore, time delay effect in control of tension at entry side has been demonstrated here to hold promise in continued improvement to the mill system.
3. One of the main drawbacks of reducing chatter in the rolling mill industry has been the limitations in vibration response during the initiation of significant forward slip.
4. Further investigation into methods for reducing chatter phenomenon will also provide an interesting addition to research. Minimising negative damping effects through the method suggested here or by alternate means will increase productivity and quality in rolling process. Very high rolling force and friction condition in the dynamic roll gap are the impediment to rapid and reliable rolling process. Modification of lubrication condition and tension regulation such as aiding rolling process using 'Touch Roll', can also reduce the influence of recognisable negative damping on mill stability.

9.5. CONCLUSION

The principal aims of this thesis were twofold: study of linear stability of a rolling stand in cold rolling and the investigation into the dynamic characterisation of transient mechanisms. These have been achieved through the development of extensive mathematical models for the support bearings, surface contact mechanism and dynamic roll gap.

The evaluation of a rolling stand in cold rolling as a heavily damped dynamic system brings to the forefront issues in chatter phenomenon, where precise estimation of

bearing forces and consideration of dynamic roll gap model and influences of tension variation are likely to significantly impact the capability to achieve high quality strip thickness. The inclusion of multiple nonlinearities is all shown to impact the mill chatter, with significant contribution from the negative damping effect in the dynamic roll gap.

The coupled mill vibration model is by far the most complete chatter model since it does not only include negative damping effects in a rolling stand, but also considers the tension variation at the entry side of the roll gap. In a linearised model, stability analysis is significantly affected by the negative damping effect caused by the relative motion between the work roll and strip in a rolling stand. As a result, stability threshold curves have been determined through the change of the rolling parameters. For the fully transient model, different tension models are introduced in the dynamic roll gap such that parametric studies are performed to identify the transient characteristics of the coupled mill vibration model, coupled with the support bearings, surface contact mechanism and the dynamic roll gap model. The influence of various process parameters on stability is also investigated by changing the rolling speed, friction gradient, operating frequency, inter-stand distance and time delay. Regardless of the tension model presented, the negative damping has the most significant influence in mill chatter resulted from the increased rolling speed. The inter-stand interactions through tension variations and the strip thickness variation in a rolling stand are much more significant than that of tension variations alone. It is also identified that the time delay effect significantly increases the tendency of chatter and thus reduces the stability of the rolling process.

APPENDIX

APPENDIX A: ROLLING FORCE CALCULATIONS

An example is given for the calculation of roll force and torque at a 4th stand where front and back tensions are applied. The principal formulae are

$$s^{+} = \frac{\sigma h}{h_x}\left(1-\frac{t_x}{\sigma_x}\right)e^{\mu H}$$

$$s^{-} = \frac{\sigma h}{h_e}\left(1-\frac{t_e}{\sigma_e}\right)e^{\mu(H_e-H)}$$

$$F_R = R_d W\left[\int_0^{\phi_n} s^{+}d\phi + \int_{\phi_n}^{\phi_e} s^{-}d\phi\right]$$

$$T_R = R_{WR}R_d\left[\int_0^{\phi_e} s\phi\, d\phi + \frac{t_e h_e - t_x h_x}{2R_d}\right]$$

Initial thickness of strip $h_f = 1.000mm = 0.0010m$

Entry thickness of strip $h_e = 0.40mm = 0.0004m$

Exit thickness of strip $h_x = 0.30mm = 0.0003m$

Mean width of strip $W = 1224mm = 1.224m$

The total roll force = $1.224m \times 6.533MN/m = 8.009MN$

The mean torque per roll = $1.224m \times 21.998kN = 26.925kNm$

Back tension = $t_x = 23.06kN/(0.0004\times1.224m^2) \Rightarrow 90.0MPa$ *(Assumed)*

Front tension = $t_e = 32.94kN/(0.0003\times1.224m^2) => 90.0MPa$ *(Assumed)*

Undeformed roll radius = $R_{WR} = 300mm = 0.30m$

A-1. Hitchcock Constant

Elastic constant of the rolls = $c = 2.20695\times10^{-5}m^2/MN$

$$c = 16\frac{(1-\nu^2)}{\pi E} = 16\frac{(1-0.3^2)}{\pi\times210\times10^9} = 2.20695\times10^{-5}m^2/MN$$

For the BSL = $c = 2.20695\times10^{-11}m/N = 2.20695\times10^{-5}m^2/MN$

A-2. Roll Flattening

The strip passing between a pair of rolls is compressed by the hydraulic pressure on top backup roll, but the reaction is transferred to the bearings and housing chock, which are capable of only limited yield strength because of their large dimensions. If an attempt is made to compress thin hard material further, the reaction becomes so large that the rolls deform elastically and the radius of curvature of the arc of contact is increased. The extent of this flattening depends on the magnitude of the reaction force and the elastic constants of the rolls. Attempts to determine R_d, the deformed radius of curvature, have failed as the arc of contact did not remain circular and give a proper solution. Even though there is a limit in estimating the deformed roll radius, it can be confidently considered that for a thin cold rolling with the limited roll deformation is still valid.

$$\frac{R_d}{R_{WR}} = \left(1 + \frac{cF_R}{W\Delta h}\right) = \left(1 + \frac{cF_{sp}}{\Delta h}\right)$$

where R_d is the deformed radius, R_{wr} the undeformed radius.

$$c = 16\frac{\left(1-\nu^2\right)}{\pi E}$$

v is poisson's ratio 0.3 for mild steel, E is Young's Modulus $210GPa$, F_{sp} is the specific rolling force based on the deformed radius R_d, W is the width of the strip and Δh is the reduction. To calculate a value for R_d successive approximations are necessary.

The yield stress curves are shown in Figure 4-1 (Chapter 4). The coefficient of friction used in this calculation is 0.02. The deformed roll radius is calculated by Hitchcock's formula from the calculated rolling force per unit with, F_{sp}

$$R_d = R_{WR}\left(1 + \frac{cF_{sp}}{\Delta h}\right) = 0.30\left(1 + \frac{2.20695\times10^{-5}\,m^2/MN \times 6.544MN/m}{(0.0004-0.0003)m}\right) = 0.30(1+1.444)$$

$$= 0.7332m$$

Based on the numerical integration by Simpson's rule (Approximated Value)

$$R_d = R_{WR}\left(1+\frac{cF_{sp}}{\Delta h}\right) = 0.30\left(1+\frac{2.20695\times10^{-5}\,m^2/MN\times 6.5643MN/m}{(0.0004-0.0003)m}\right) = 0.30(1+1.4487)$$

$$= 0.7346m$$

A-3. Roll Contact Angle at Entry

The angle of contact can be calculated as:

$$\phi_e = \sqrt{\frac{h_e - h_x}{R_d}} = \sqrt{\frac{0.0001}{0.7346}} = 0.0117 \ radians$$

A-4. Neutral Point

For the neutral angle, calculation process is as follows:

$$\sqrt{\frac{R_d}{h_x}},\ H_e,\ k_x,\ k_e,\ \ln\left\{\frac{h_e}{h_x}\left(\frac{1-\frac{t_x}{\sigma_x}}{1-\frac{t_e}{\sigma_e}}\right)\right\},\ H_n \text{ and finally } \phi_n$$

$$\sqrt{\frac{R_d}{h_x}} = \sqrt{\frac{0.7332}{0.0003}} = 49.437 \text{ (Real)} \qquad \sqrt{\frac{R_d}{h_x}} = \sqrt{\frac{0.7346}{0.0003}} = 49.484 \text{ (Approx.)}$$

$$H_e = 2\sqrt{\frac{R_d}{h_x}}\arctan\left(\sqrt{\frac{R_d}{h_x}}\phi_e\right) = 2\times 49.484\times\arctan(49.484\times 0.0117) \qquad \underline{\text{at } R_d=0.7346m}$$

$$= 2\times 49.484\times 0.52481 = 51.939$$

The percentage reduction at exit

$$\frac{0.001-0.0003}{0.001}\times 100 = 70.0\%$$

Yield stress at exit = σ_x = yield stress at 70.0 per cent reduction = 749.88*MPa*.

The percentage reduction at entry

$$\frac{0.001-0.0004}{0.001}\times 100 = 60\%$$

Yield stress at entry = σ_e = yield stress at 60 per cent reduction = 664.85*MPa*.

A-5. When Both Tensions are Applied

$$\ln\left\{\frac{h_e}{h_x}\left(\frac{1-\frac{t_x}{\sigma_x}}{1-\frac{t_e}{\sigma_e}}\right)\right\} = \ln\left\{\frac{0.0004}{0.0003}\left(\frac{1-\frac{90}{749.88}}{1-\frac{90}{664.85}}\right)\right\} = \ln\left\{1.333\left(\frac{0.87998}{0.86463}\right)\right\}$$

$$= \ln(1.357) = 0.3053$$

$$H_n = \frac{H_e}{2} - \frac{1}{2\mu}\ln\left\{\frac{h_e}{h_x}\left(\frac{1-\frac{t_x}{\sigma_x}}{1-\frac{t_e}{\sigma_e}}\right)\right\} = \frac{51.939}{2} - \frac{0.3053}{2\times 0.02} = 25.97 - 7.6325 = 18.337$$

$$\phi_n = \sqrt{\frac{h_x}{R_d}}\tan\sqrt{\frac{h_x}{R_d}}\times\frac{H_n}{2} = 0.020209\times\tan\left(0.020209\times\frac{18.337}{2}\right)$$

$$= 0.020209\times 0.18744 = \underline{0.003788} \text{ radians}$$

Small truncation error results in the change of neutral point.

A-6. When Both Tensions are Zero (with different R_d)

$$H_n = \frac{H_e}{2} - \frac{1}{2\mu}\ln\left\{\frac{h_e}{h_x}\left(\frac{1-\frac{t_x}{\sigma_x}}{1-\frac{t_e}{\sigma_e}}\right)\right\} = \frac{51.939}{2} - \frac{0.28768}{2\times 0.02} = 25.97 - 7.192 = 18.778$$

$$\phi_n = \sqrt{\frac{h_x}{R_d}}\tan\left(\sqrt{\frac{h_x}{R_d}}\times\frac{H_n}{2}\right) = 0.020209\tan\left(0.020209\times\frac{18.778}{2}\right)$$

$$= 0.020209\times 0.19205 = \underline{0.003881} \text{ radians}$$

A-7. Rolling force and torque calculation

The integral in equations below are evaluated by Simpson's rule. To do this it is necessary to calculate the values of s and $s\phi$ at points equally spaced between the neutral point and exit and the neutral point and entry. In this example three points have been taken in the first interval and four in the second. The points are the values of ϕ in Table A-1.

$$F_R = R_d W\left[\int_0^{\phi_n} s^+ d\phi + \int_{\phi_n}^{\phi_e} s^- d\phi\right]$$

$$T_R = R_{wr} R_d W\left[\int_0^{\phi_e} s\phi\, d\phi + \frac{t_e h_e - t_x h_x}{2R_d}\right]$$

$$\int_0^{\phi_n} s^+ d\phi = \frac{0.003788}{6}(660.53 + 4\times 801.22 + 979.16) = 3.0585$$

$$\int_{\phi_n}^{\phi_e} s^- d\phi = \frac{(0.0117 - 0.003788)}{12}(979.16 + 4\times 837.15 + 2\times 727.36 + 4\times 641.93 + 574.85)$$
$$= 5.8846$$

$$\int_0^{\phi_e} s d\phi = \int_0^{\phi_n} s^+ d\phi + \int_{\phi_n}^{\phi_e} s^- d\phi = 3.0585 + 5.8846 = 8.9431$$

$$\int_0^{\phi_n} s^+ \phi d\phi = \frac{0.003788}{6}(0 + 4\times 1.5493 + 3.7867) = 0.0063032$$

$$\int_{\phi_n}^{\phi_e} s^- \phi d\phi = \frac{(0.0117 - 0.003788)}{12}(3.7867 + 4\times 4.8690 + 2\times 5.6479 + 4\times 6.2356 + 6.7042)$$
$$= 0.043651$$

$$\int_0^{\phi_e} s\phi d\phi = \int_0^{\phi_n} s^+ \phi d\phi + \int_{\phi_n}^{\phi_e} s^- \phi d\phi = 0.0063032 + 0.043651 = 0.049954$$

The yield stress curve is used to obtain line (xv) from line (xii) and equations s^+ and s^- to give s in lines (xiii) and (xiv). $1 - \frac{t_x}{\sigma_x}$ is equal to 0.87998 and $1 - \frac{t_e}{\sigma_e}$ to 0.86463. Multiplication of it by ϕ gives the next two lines.

Simpson's rule is used to evaluate the integrals, $\int_0^{\phi_e} s d\phi$ and $\int_0^{\phi_e} s\phi d\phi$. Both are evaluated separately either side of the neutral point and the two components added.

Then

$$F_R = R_d W \int_0^{\phi_e} s\,d\phi = R_d W \left[\int_0^{\phi_n} s^+ d\phi + \int_{\phi_n}^{\phi_e} s^- d\phi \right] = 0.7346 \times 1.224 \times 8.9431 = 8.0412\ MN.$$

$$T_R = R_{WR} R_d W \left[\int_0^{\phi_e} s\phi\, d\phi + \frac{t_e h_e - t_x h_x}{2R_d} \right] \quad (\textit{When both tensions are ignored})$$

$= 0.3 \times 0.7346 \times 1.224 \times (0.049954+0) = 0.013475$

$= 13.48\ kN.m$ (Both rolls 26.96 $kN.m$)

$$T_R = R_{WR} R_d W \left[\int_0^{\phi_e} s\phi\, d\phi + \frac{t_e h_e - t_x h_x}{2R_d} \right] \quad (\textit{When both tensions are applied})$$

$= 0.3 \times 0.7332 \times 1.224 \times (0.049954+0.006126)$

$= 0.01513\ MN.m$ (Both rolls 30.26 $kN.m$)

- The approximated roll force, $F_R = 8.0412\ MN.$
- The approximated torque, $T_R = 30.26\ kNm.$

- The real calculated roll force, $F_E = 8.009\ MN.$
- The real calculated torque, $T_E = 26.925\ kNm.$

The error in the calculated value of roll force $= \frac{F_E - F_R}{F_R} \times 100\ per\ cent = 0.4\ per\ cent$

The error in the calculated value of roll torque $= \frac{T_E - T_R}{T_R} \times 100\ per\ cent = 11.02\ per\ cent$

At the beginning of this calculation the deformed roll radius was calculated from the experimental roll force. When the theory is used to predict the values of rolling force and torque, the experimental rolling force is not known and one obtains consistent values of F_R and $R_d R$ by the procedure described in this section.

The calculations in this Appendix are tedious. The authors are attempting to find a analytical method of calculating roll force and torque similar to that described earlier in Bland and Ford (1948) for the "tension" and "no-tension" case, respectively.

The following Table A-1 is the result of calculation by Simpson's Rule based on Bland and Ford approach to validate the model. In comparison to real calculation value, error per cent is less than 10%. Thus, two methods are still useful for estimating rolling force.

At stand 4 of the tandem cold rolling mill (0.4 to 0.3*mm*)

Table A-1: Calculation of Rolling Force (Based on BSL Specifications)

	Exit point 1	Point 2	Neutral Point 3	Point 4	Point 5	Point 6	Entry point 7
h [*mm*]	0.3000	0.3028	0.311	0.3249	0.3443	0.3694	0.4000
ϕ_n	-	-	0.0039	-	-	-	-
L	0	-	-	-	-	-	0.0086
(i) ϕ [*radians*]	0 (Appr.)	0.0019	0.0039	0.0058	0.0078	0.0097	0.0117
(ii) $\sqrt{\frac{R_d}{h_x}}\phi$	0 (Appr.)	0.0957	0.1914	0.2879	0.3844	0.4809	0.5774
(iii) $\arctan\left(\sqrt{\frac{R_d}{h_x}}\phi\right)$ [*radians*]	0 (Appr.)	0.0954	0.1892	0.2803	0.3669	0.44825	0.5236
(iv) $H_e = 2\sqrt{\frac{R_d}{h_x}}\arctan\left(\sqrt{\frac{R_d}{h_x}}\phi_e\right)$	0 (Appr.)	9.4489	18.7288	27.7567	36.3353	44.3794	51.8416
(v) $H_e - H$	-	-	33.113	24.085	15.506	7.4622	0
(vi) μH	0 (Appr.)	0.1889	0.3746	-	-	-	-
(vii) $\mu(H_e - H)$	-	-	0.6623	0.4817	0.3101	0.1491	0
(viii) $e^{\mu H}$	1 (Appr.)	1.208	1.4544	-	-	-	-
(ix) $e^{\mu(H_e - H)}$	-	-	1.9392	1.6188	1.3636	1.161	1
(x) $R\phi^2$	0	2.749e-6	1.099e-5	2.487e-5	4.433e-5	6.937e-5	0.0001
(xi) $h = h_x + R\phi^2$ [*mm*]	0.3	0.303	0.311	0.325	0.344	0.369	0.0004
(xii) Percentage deformation $\frac{h_f - h}{h_f} \times 100\%$ [*per cent*]	70	69.89	65.89	65.82	65.68	64.93	60
(xiii) Pressure s^+ at exit $s^+ = \frac{\sigma h}{h_x}\left(1 - \frac{t_x}{\sigma_x}\right)e^{\mu H}$ [*MPa*]	660.53	801.22	979.16	-	-	-	-
(xiv) Pressure s^- at entry $s^- = \frac{\sigma h}{h_e}\left(1 - \frac{t_e}{\sigma_e}\right)e^{\mu(H_e - H)}$ [*MPa*]	-	-	979.16	837.15	727.36	641.93	574.85
(xv) Yield Stress k [*MPa*]	749.88	747.24	739.45	726.74	709.66	688.78	664.85
(xvi) $s^+\phi$ [*MPa*]	0 (Appr.)	1.5493	3.7867	-	-	-	-
(xvii) $s^-\phi$ [*MPa*]	-	-	3.7867	4.8690	5.6479	6.2356	6.7042
(xviii) Strain $\ln(h_e) - \ln(h_{ept\ or\ xpt})$	0.3322	0.3217	0.2906	0.2402	0.1731	0.0920	0
(xix) Speed [*m/s*]	20.7331	20.5448	20.0000	19.1459	18.0639	16.8392	15.5498
(xx) Strain rate $\dot{\varepsilon}_{gap}$ [*1/s*]	1861.37	1829.6	1732.07	1587.29	1412.95	1227.85	1047.02
F_E [*MN*]	-	-	5.2323	3.6396	2.268	1.067	0
F_X [*MN*]	0 (Appr.)	1.2652	2.8143	-	-	-	-

Torque calculation result is not shown in this table as the effect of torque on mill stability is ignored.

Based on the Bland and Ford Approach (Simpson's rule)

Roll Flattening Ratio : $\frac{R_d}{R_{WR}} = \frac{0.7346}{0.3} = 2.4487$

$F_R = 8.0412MN, \quad F_H = 31.1kN, \quad F_V = 8.04MN$

Based on the Bland and Ford Approach (Real value)

Roll Flattening Ratio : $\frac{R_d}{R_{WR}} = \frac{0.7332}{0.3} = 2.444$

$F_R = 8.01MN, \quad F_H = 30.997kN, \quad F_V = 8.009MN$

APPENDIX B: JOURNAL BEARING IN THE BACKUP ROLL

B-1. Fluid Film (Vance et al., 2010)

The primary requirement for hydrodynamic lubrication is that sufficient lubricant exists between the shaft journal and the bearing at all times. The formation of an oil whirl to lift the shaft journal is dependent on the speed (relative speed between the shaft and the bearing), load (weight of the rotor or any additional side loads, or gear loads, or side loads due to misalignment), and the oil viscosity of the lubricant.

These parameters are combined and presented by the ZN/P curve shown in Figure. B-1. This is also known as the Stribeck curve. This curve describes the three particular regimes while the system accelerates to operating speed or decelerates from the operating speed to standstill conditions. These regimes are dry friction, where surface contact between the asperities of the shaft and the bearing exist; mixed lubrication regime, or boundary friction; and full hydrodynamic lubrication, or fluid friction, where a thin film exists between the shaft and the bearing, which supports the static and dynamic loads in the rotating shaft.

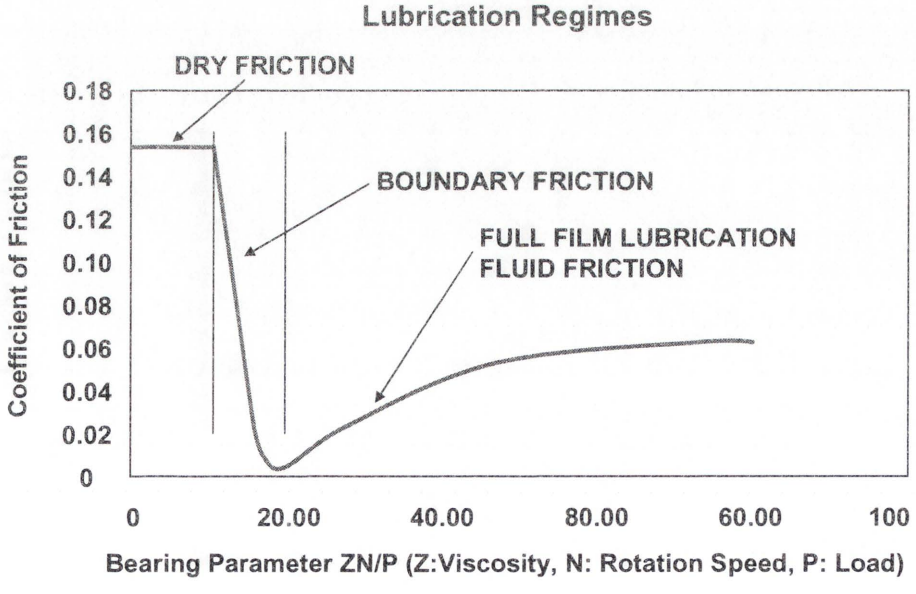

Figure B-1: The ZN/P curve and the three lubrication regimes (Vance et al, 2010)

The exaggerated regimes in the fluid film bearings are graphically represented in Figure. B-2 as the shaft accelerates from standstill to steady state condition under load. The full hydrodynamic regime has the direct influence on the dynamic characteristics of the system as it speeds up from stand still to possibly pass through one or more critical speeds on its way to reaching the design operation speed.

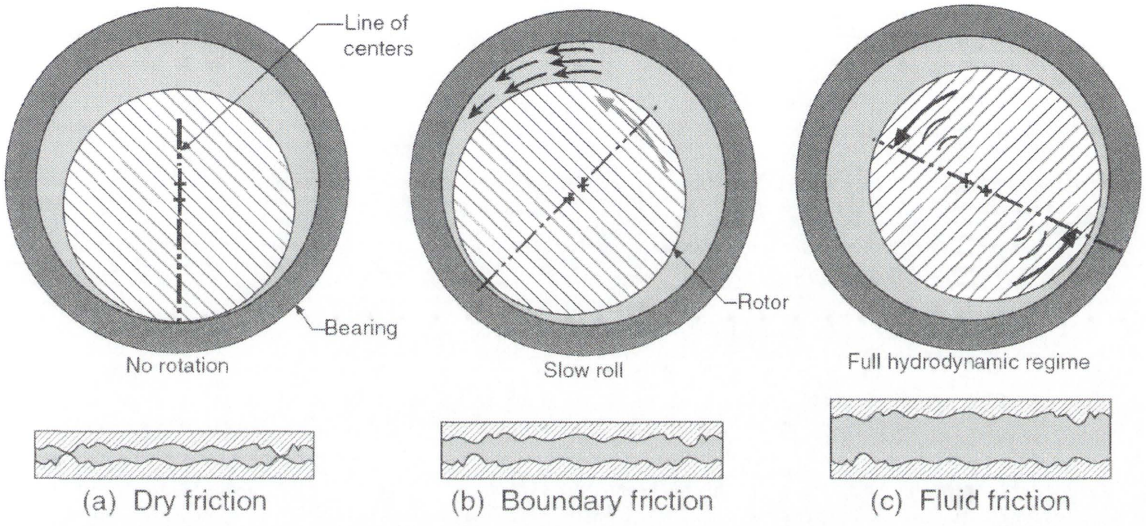

Figure B-2: Three lubrication regimes in fluid film journal bearing (Vance et al, 2010)

B-2. Equations of Motion

For a rigid rotor with a m mass supported by two symmetric bearings as shown in Figure. B-3. If excitation forces F'_{BH} and F'_{BV} are acted at the bearing center, the equations of motion for the rotor can be written as follows:

$$m_{BH}\ddot{x}_{BH} = F_{HCH} - F'_{JBH} \tag{B.1}$$

$$m_{BH}\ddot{y}_{BH} = -F_{HCV} + F'_{JBV} - W_{BH} + F_{HCf} \tag{B.2}$$

$$m_{BR}\ddot{x}_{BR} = F'_{JBH} - F'_{H} - F_{fc}\cos(\beta - \phi_n) \tag{B.3}$$

$$m_{BR}\ddot{y}_{BR} = F'_{JBV} + F'_{V} - W_{BR} - F_{fc}\sin(\beta - \phi_n) \tag{B.4}$$

In practical use of journal bearings, the linearised bearing forces are defined as:

$$F'_{JBH} = k_{xx}\Delta x + k_{xy}\Delta y + c_{xx}\Delta\dot{x} + c_{xy}\Delta\dot{y} \tag{B.5}$$

$$F'_{JBV} = k_{yx}\Delta x + k_{yy}\Delta y + c_{yx}\Delta \dot{x} + c_{yy}\Delta \dot{y} \tag{B.6}$$

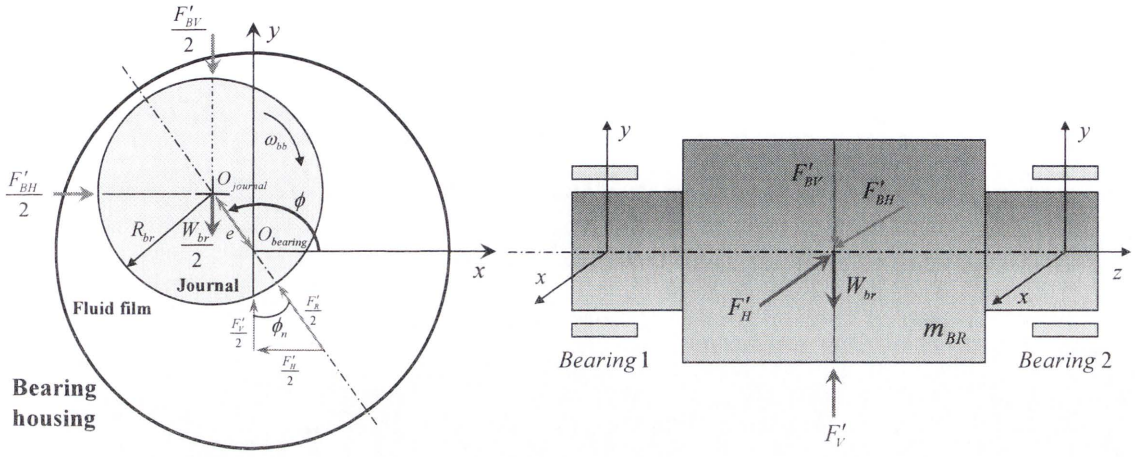

Figure B-3: A rigid rotor-bearing system for the upper backup roll

As shown in Figure B-3, if a rolling mill system is vibrating owing to the strip oscillation - unbalancing displacements resulted from the reaction force between two work rolls under the specific rolling condition - the relative displacement of the backup roll can be defined by the difference between the displacements of the backup roll and bearing housing chock. From this assumption, the relative position between the rotor and bearing housing can be defined as follows:

$$\Delta x = x_{BR} - x_{BH} \text{ and } \Delta y = y_{BR} - y_{BH} \tag{B.7}$$

where x_{BR} and y_{BR} are the position of the rotor and x_{BH} and y_{BH} the position of the bearing housing chock. The mill frame is considered fixed to the ground so that its motion is assumed to be zero and can be neglected.

Based on the given bearing parameters, initial conditions have been determined from the well known journal bearing theories by Rezvani and Hahn (1993) and Adiletta et al. (1996). Table B-1 shows the calculated results to validate the journal bearing model used in this study. For the rotational direction and the ratio of the bearing length to the diameter, it is found force calculations by Rezvani approach are more consistent than those compared to Adiletta approach.

Table B-1: Bearing Oil-Film Force Calculation Results for the Short Bearing Solution (L/D =0.5) and Long Bearing Solution (L/D=1.0), respectively

		Eccentricity	Rotational Speed (*rad/s*)	F_H (*N*)	F_V (*N*)
Short Bearing Assumption	Adiletta	0.7339	29.586 (CCW)	-1.423e^6	-9.369e^6
	Rezvani	0.7339	29.586 (CCW)	-1.423e^6	-9.369e^6
	Adiletta	0.7339	29.586 (CW)	-8.472e^6	-4.245e^6
	Rezvani	0.7339	29.586 (CW)	+1.424e^5	+9.367e^6
Long Bearing Assumption	Adiletta	0.7339	29.586 (CCW)	-7.116e^5	-4.684e^6
	Rezvani	0.7339	29.586 (CCW)	-7.116e^5	-4.684e^6
	Adiletta	0.7339	29.586 (CW)	-4.2362e^6	-2.122e^6
	Rezvani	0.7339	29.586 (CW)	+7.116e^5	+4.684e^6

APPENDIX C: TAPERED ROLLER BEARING IN THE WORK ROLL

C-1. Tapered Roller Bearing

The work roll supports high load resulted from the strip deformation and is supported by the tapered roller bearing which effectively relieve the stress in the shaft. Due to its complexity and different results depending on assumptions, it has not fully verified with other models. However, in this study, axial deflection of the roller is ignored as it is adequately supported by two-row or four-row tapered roller bearing so that axial force cancels out. Figure C-1 shows the single-row tapered roller bearing and the resulting stiffness matrices are combined considering spring combination. For more detailed derivation, refer to Lim (1989).

In order to validate Lim's approach simulations have been performed to compare the translational stiffness coefficients of the bearing matrix with the published analytical and experimental results (Gargiulo, 1980).

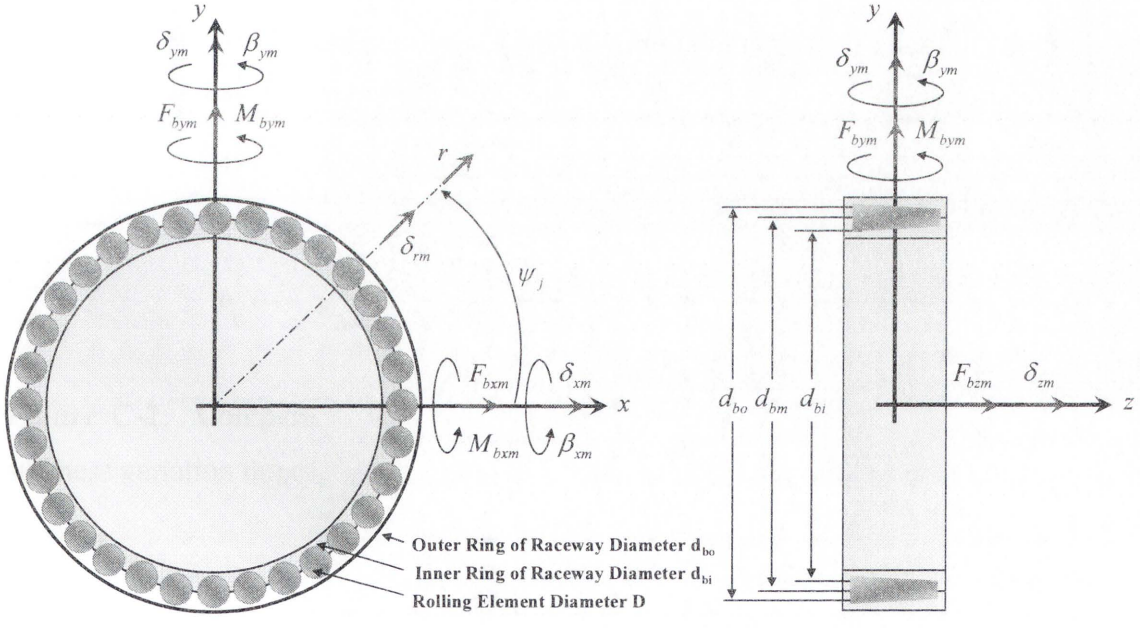

Figure C-1: Tapered roller bearing in the work roll (Rolling element bearing)

Table C-1 show the parameters used for validation with Gargiulos's formula and Figure C-2 displays the radial stiffness variation depending on the radial deflection. Note that in this study, axial deflection and thrust force have been ignored to simplify the complex tapered roller bearing model.

Table C-1: Parameters of the roller bearing used for parametric study

Parameters	Value
Load deflection exponent, n	10/9
Load deflection constant, K_n $[MN/m]$	300
Number of rolling elements, Z	50
Radial clearance, C_{wb} $[\mu m]$	50
Pitch radius, r_j $[mm]$	188.25
Rolling element angle, α_0 $[deg]$	15
Rotational speed, ω_{wb} $[RPM]$	133.33 (CCW)

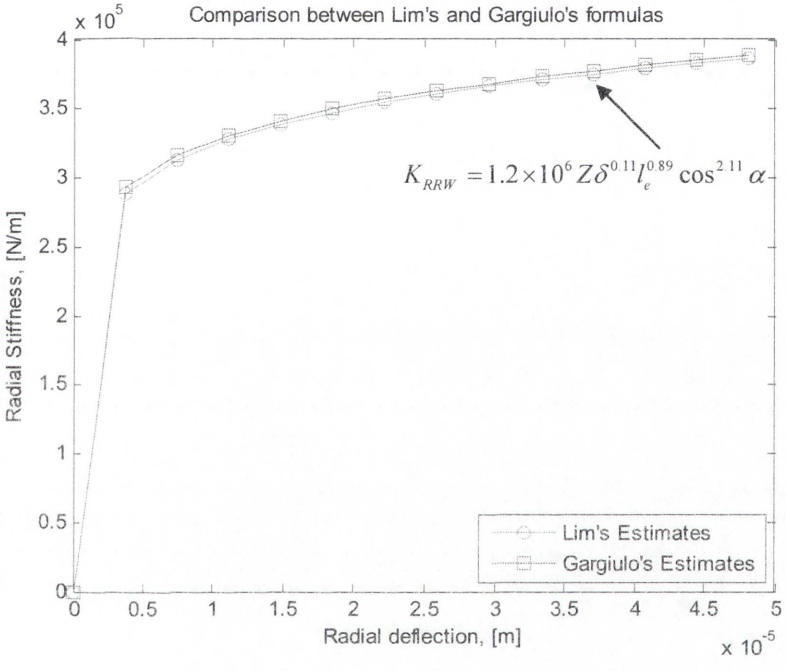

Figure C-2: Comparison between Lim's approach and Gargiulo's formulas (Radial stiffness variation depending on radial deflection)

REFERENCES

Adiletta, G., Guildo, A.R., Rossi, C., 1996. Chaotic motions of a rigid rotor in short journal bearings. Nonlinear Dynamics. 10, pp. 251-269.

Alexander, J.M., 1955. A Slip Line for the Hot Rolling Process. Proc. Inst. Mech. Eng. 168, pp. 1021-1030.

Alexander, J.M., Brewer, R.C., Rowe, G.W., 1988. Manufacturing Technology, Vol. 2, Ellis Horwood Ltd.

Anand, L., 1993. A Constitutive Model for Interface Friction. Computational Mechanics. 12, pp. 197-213.

Arimura, T., Kamata, M., Saito, M., 1970. An Analysis of the Dynamic Behavior of Tandem Cold Mills. Automatica. Vol. 6, pp. 601-607.

Azushima, A. 1978. Characteristics of Lubrication in Cold Sheet Rolling, in Lubrication Challenges in MetalWorking and Processing. In: Proceedings of the First International Conference, IIT. Research Institute, Chicago, IL, USA, June 7-9, pp. 1-7.

Azushima, A., Miyagawa, M., 1984. Evaluation of Lubricity and Anti-Seizure Property of Lubricant in Cold Sheet Rolling: An Investigation into Friction and Lubrication in Cold Rolling IV. J. JSTP 25 (285), pp. 915-920.

Barus, C., 1893. Isotherms, Isopiestics and Isometrics Relative to Viscosity. The American Journal of Science. 45, pp. 87-96.

Bay, N. 1987. Friction Stress and Normal Stress in Bulk Metal-Forming Processes. Journal of Mechanical Working Technology. Vol. 14, pp. 203-223.

Belli, P., Bittanti, S., De Marco, A., 2004. On the Origin of Torsional Vibrations in Hot Rolling Mills and a Possible Remedy. Journal of Dynamic Systems, Measurement, and Control. Vol. 126, pp. 811-823.

Bland, D.R., Ford, H., 1948. The calculation of roll force and torque in cold strip rolling with tensions. Proc. Inst. Mech. Eng. 159, pp. 144-163.

Bowden, F.P., Tabor, D., 1954. The Friction and Lubrication of Solids Part I. Clarendon Press, Oxford, Part II.

Chang, D., 1994. An Advanced Slab Analysis of the Strip Rolling Process. Ph.D. Thesis, Northwestern University, Evanston, Illinois.

Chefnuex, L., Fischbach, Jean-Paul., Gouzou, Jacques., 1984. Study and industrial control of chatter in cold rolling. Iron and Steel Engineer. pp. 17-26.

Chen, Y., Liu, S., Shi, T., Yang, S., Liao, G., 2002. Stability Analysis of the Rolling Process and Regenerative Chatter on 2030 Tandem Mills. Proc. Instn. Mech. Engrs. Part C: Journal of Mechanical Engineering Science. Vol.216, pp. 1225-1235.

Cheng, Y.Q., Zhang, Hui., Chen, Z.H., Xian, K.F., 2008. Flow Stress Equation of AZ 31 Magnesium Alloy Sheet During Warm Tensile Deformation. Journal of Materials Processing Technology. Vol.208, pp. 29-34.

Dowson, D., 1979., History of Tribology. Longmans/Green, London, New York.

Farley, T.W.D., Rogers, S., and Nardini, D., 2006. Understanding Mill Vibration Phenomena., Proceedings of the Conference: Vibration in Rolling Mills, Institute of Materials, Londeon, UK, 9th November 2006.

Farley, T.W.D., 2006. Rolling Mill Vibration and its Impact on Productivity and Product Quality. Innoval Technology Ltd. Banbury, OX16 1TQ, UK

Farley, T.W.D., 2006. Mill Vibration Phenomena during Cold Rolling. Innoval Technology Ltd.

Freshwater, I.J., 1996. Simplified Theories of Flat Rolling – I: The Calculation of Roll Pressure, Roll Force and Roll Torque. Int. J. Mech. Sci. Vol. 38, No.6, pp. 633-648.

Freshwater, I.J., 1996. Simplified Theories of Flat Rolling – II: Comaprison of Calculated and Experimental Results. Int. J. Mech. Sci. Vol. 38, No.6, pp. 649-660.

Ginzburg, Vladimir. B., 1985. Basic Principles of Customized Computer Models for Cold and Hot Strip Mills. Iron Steel Eng. 62, pp. 21-35.

Gronostajski, Z., 2000. The Constitutive Equations for FEM Analysis. Journal of Materials Processing Technology. Vol. 106, pp. 40-44.

Gargiulo, E.P., 1980. A simple way to estimate bearing stiffness", Machine Design. Vol. 52, pp. 107-110.

Gohar, R., 1974. A Numerical Method of Obtaining the Deformed Shape of the Roll in the Cold Rolling Process. Int. J. Mech. Sci. Vol. 16, pp. 249-258.

Harris, Tedric.A., Kotzalas, Michael. N., 2007. Advanced Concepts of Bearing Technology 5th Edition, CRC Press, Taylor & Francis Group.

Hitchcock, J.H., 1935. Roll Neck Bearings, Appendix I-II-III, in ASME Report of Special Research Committee, New York, pp. 33-52.

Holmes, R., 1960. The vibration of a rigid rotor on short journal bearings. J. Mech. Eng. Sci. 2(4), pp. 337-341.

Hu, Pei-Hua., Zhao, Huyue., Ehmann, K.F., 2001. Fifth-Octave-Mode Chatter in Rolling. Proc. Instn. MEch. Engrs. PART B: JOURNAL OF ENGINEERING MANUFACTURE. Vol.215. pp. 797-809.

Hu, Pei-Hua., Zhao, Huyue., Ehmann, K.F., 2006. Third-Octave-Mode Chatter in Rolling, Part 1: Chatter Model. Proc. Instn. MEch. Engrs. PART B: JOURNAL OF ENGINEERING MANUFACTURE. Vol.220, pp. 1267-1277.

Hu, Pei-Hua., Zhao, Huyue., Ehmann, K.F., 2006. Third-Octave-Mode Chatter in Rolling, Part 2: Stability of a Single-Stand Mill. Proc. Instn. MEch. Engrs. PART B: JOURNAL OF ENGINEERING MANUFACTURE. Vol.220, pp. 1279-1292.

Hu, Pei-Hua., Zhao, Huyue., Ehmann, K.F., 2006. Third-Octave-Mode Chatter in Rolling, Part 3: Stability of a Multi-Stand Mill. Proc. Instn. MEch. Engrs. PART B: JOURNAL OF ENGINEERING MANUFACTURE. Vol.220, pp. 1293-1303.

Huyue Zhao, 2008. Regenerative Chatter in Cold Rolling. Ph.D. Thesis, Northwestern University, Evanston, Illinois, USA

Johnson, Gordon.R., Cook, William.H., 1983. A Constitutive Model and Data for Metals Subjected to Large Strains, High Strain Rates and High Temperatures. Proceedings of the Seventh International Symposium on Ballistics, Hague, The Netherlands, 541–547.

Johnson, Robert.E. and Qi, Quan. 1994. Chatter Dynamics in Sheet Rolling. Int. J. Mech. Sci. Vol.36, No.7, pp. 617-630.

Jortner, D., Osterle, J.F., Zorowski, C.F., 1960. An Analysis of Cold Strip Rolling. Int. J. Mech. Sci. Pergamon Press Ltd. Vol. 2, pp. 179-194.

Khonsari, M.M., Chang Y.J., 1993. Stability boundary of non-linear orbits within clearance circle of journal bearings. J. Vib. Acoustics, 115, pp. 303-307.

Khonsari, M.M., Booser, E.R., 2001. Applied tribology: bearing design and lubrication. New York, NY: Wiley.

Kimura, Yukio., Sodani, Yashuhiro., Nishiura, Nobuo., Ikeuchi, Naoki., Mihara, Yutaka., 2003. Analysis of Chatter in Tandem Cold Rolling Mills. ISIJ International. Vol.43. (1), pp. 77-84.

Kudo, H., 1960. Some Analytical and Experimental Studies of Axi-Symmetric Cold Forging and Extrusion-II. Int. J. Mech. Sci. Pergamon Press Ltd. Vol. 2, pp. 102-127.

Kudo, H., 1961. Some Analytical and Experimental Studies of Axi-Symmetric Cold Forging and Extrusion-II. Int. J. Mech. Sci. Pergamon Press Ltd. Vol. 3, pp. 91-117.

Lee, D., Zaverl, F.J.R., 1982. Neck Growth and Forming Limits in Sheet Metals, Int. J. Mech. Sci. Vol. 24, No. 3, pp. 157-173.

Lenard, J.G., Lim, L.S., 1984. Study of Friction in Cold Strip Rolling. Journal of Engineering Materials and Technology. Vol. 106, pp. 139-146.

Lenard, J.G., 1992. Friction and Forward Slip in Cold Strip Rolling. Tribology Transactions. Vol. 35, 3, pp. 423-428.

Lenard, J.G., Malinowski, Z., Pietrzyk, M., 1992. Comparison of the Predictive Capabilities of Mathematical Models of the Flat Rolling Process. Journal of Materials Processing Technology. Vol. 34, pp. 85-92.

Levanov, A.N., 1997. Improvement of Metal Forming processes by Means of Useful Effects of Plastic Friction. Journal of Materials Processing Technology. 72, pp. 314-316.

Lim, T.C., 1989. Vibration transmission through rolling element bearings in geared rotor systems. Ph.D. Thesis, The Ohio State University, Columbus, Ohio 4320, USA.

Lim, T.C., 1990. Vibration transmission through rolling element bearings, Part I: Bearing Stiffness Formulation. J. Sound and Vibration. 139(2), pp. 179-199.

Lin, Y.J., Suh, C.S., Langari, R., Noah, S.T., 2003. On the Characteristics and Mechanism of Rolling Instability and Chatter. Transaction of the ASME. Vol.125, pp. 778-786.

Lin, J.F, Huang, T.K, Hsu, C.T., 1991. Evaluation of Lubricants for Cold Strip Rolling. Wear. 147, pp. 79-91.

Malvern, Lawrence.Earl., 1969. Introduction to the Mechanics of a Continuous Medium. Ch. 6 Section 6.5 and 6.6, Prentice-Hall, Englewood Cliffs, NJ.

Matsui, K., Matsushita, T., Takatsuka, K., Yamaguchi, Y., 1984. Evaluation of Lubricants for Rolling of Aluminium Sheet and Foil. Advanced Technology Plasticity. 1, pp. 247-252.

Matthews, D.L., Yuen, W.Y.D., 2006. Minimising Skidding in Cold Rolling. Proceedings of SEAISI 2006 Conference, Cebu, Phillippines, 15-17 May, pp. 1-13.

Meehan, Paul. A., 2002. Vibration Instability in Rolling Mills: Modelling and Experimental Results. Journal of Vibration and Acoustics. Vol.124, pp. 221-228.

Nadái, A., 1931. Plasticity. McGraw-Hill. New York.

Orowan, E., and D.I., 1943. The calculation of roll pressure in hot and cold flat rolling. Proc. Instn. Mech. Engrs. 150, pp. 140–167.

Paton, D.L., Critchley, S., 1985. Tandem Mill Vibrations: Its Causes and Control. Iron and Steel Making. pp. 37-43.

Pawelski, Oskar, Rasp, Wolfgang., Friedewald, Klaus., 1986. Application of the theory of rolling to rolling in the case of mill vibrations. Steel Research 57, No. 8, pp. 373-376.

Prakash, R.S., Dixit, R.M., Lal, G.K., 1995. Steady-State Plane-Strain Cold Rolling of a Strain-Hardening Material. Journal of Materials Processing Technology, Vol. 52, pp. 338-358.

Prandtl, L., 1923. Zeitschrift für angewandte Mathematic und Mechnik. Vol.3, p.401.

Qiu, Z.L., Yuen, W.Y.D., Tieu, A.K., 1999. Mixed-Film Lubrication Theory and Tension Effects on Metal Rolling Processes. Transaction of the ASME. Vol. 121, pp. 908-915.

Ramsberg, W., Osgood, W.R., 1941. Determination of Stress-Strain Curves by Three Parameters. Technical Note No. 503, National Advisory Committee on AeroNautics, NACA.

Rasmussen, J.R. Kim., 2003. Full-Range Stress-Strain Curves for Stainless Steel Alloys. Journal of Constructional Steel Research. Vol.59, pp. 47-61.